

1-1-2014

Influence of Coastal Processes on Speleogenesis and Landforms in the Caribbean Region

Patricia Kambesis

Follow this and additional works at: <https://scholarsjunction.msstate.edu/td>

Recommended Citation

Kambesis, Patricia, "Influence of Coastal Processes on Speleogenesis and Landforms in the Caribbean Region" (2014). *Theses and Dissertations*. 2706.
<https://scholarsjunction.msstate.edu/td/2706>

This Dissertation - Open Access is brought to you for free and open access by the Theses and Dissertations at Scholars Junction. It has been accepted for inclusion in Theses and Dissertations by an authorized administrator of Scholars Junction. For more information, please contact scholcomm@msstate.libanswers.com.

Influence of coastal processes on speleogenesis and landforms in the Caribbean Region

By

Patricia N. Kambesis

A Dissertation
Submitted to the Faculty of
Mississippi State University
in Partial Fulfillment of the Requirements
for the Degree of Doctor of Philosophy
in Earth and Atmospheric Sciences
in the Department of Geosciences

Mississippi State, Mississippi

May 2014

Copyright by
Patricia N. Kambesis
2014

Influence of coastal processes on speleogenesis and landforms in the Caribbean Region

By

Patricia N. Kambesis

Approved:

John E. Mylroie
(Director of Dissertation)

Renee M. Clary
(Committee Member)

Brenda L. Kirkland
(Committee Member)

Arthur N. Palmer
(Committee Member)

Michael E. Brown
(Graduate Coordinator)

R. Gregory Dunaway
Professor and Dean
College of Arts & Sciences

Name: Patricia N. Kambesis

Date of Degree: May 17, 2014

Institution: Mississippi State University

Major Field: Earth and Atmospheric Sciences

Major Professor: John E. Mylroie

Title of Study: Influence of coastal processes on speleogenesis and landforms in the Caribbean Region

Pages in Study: 236

Candidate for Degree of Doctor of Philosophy

Evolution of rocky coastlines is controlled by littoral, biological and fluvial processes. Resultant landforms are overprinted and/or new ones formed as a result of changes in sea level caused by glacioeustasy and/or local tectonics. On carbonate coasts, chemical erosion in the form of karstification takes on a dominant role. Type of karstification is an important factor in understanding carbonate coast evolution and landform development so it is critical to identify type of karstification. In this research, fractal indices were used to distinguish cave and thus karstification type. It was determined that fractal indices effectively differentiated cave types and the indices were used to distinguish cave types at study sites on Barbados, the ABC Islands (Aruba, Bonaire, Curaçao) and the Caribbean coast of the northeast Yucatan peninsula, Mexico. This research evaluated caves located in the phreatic, epiphreatic and vadose zones of the northeast coast of Quintana Roo, Mexico to determine the relationship between the caves and to coastal processes. Three distinct coastal landforms associated with caves on the study sites were evaluated to quantify and model the interplay of littoral, fluvial and karstic processes and cave and karst development. On Barbados, the combination of

surface fluvial processes, and mixing-zone and fluvial-karstic dissolution, resulted in the formation of gullies. Some gullies contained caves in their bounding walls and/or served as points of recharge to fluvial caves. Bokas of the ABC islands are distinctive geomorphic structures that formed from the interplay of fluvial, littoral and mixing zone karstification. The morphology of the bokas was a function of dominant geomorphic process. The caletas of the Yucatan Caribbean were formed by karstification processes that also produced features with mixing-zone-like morphologies but with fluvio-karstic function. The results of this research expand the Carbonate Island Karst Model (CIKM), which explains eogenetic dissolutional processes and landforms on small carbonate islands, to one that includes carbonate islands of all sizes, and carbonate continental coasts.

Keywords: Coastal karst, caves and fractals, gully, boka, caleta,

DEDICATION

This work is dedicated to my father, Peter Kambesis, who always told me to be fearless in whatever I chose to do.

ACKNOWLEDGEMENTS

I would like to acknowledge my advisor extraordinaire, Dr. John Mylroie who first put the notion in my head of pursuing a PhD and for ultimately guiding me through the whole process – I will never be bitter! Many thanks to my committee members: Dr. Brenda Kirkland for her insights on all things carbonate, Dr. Renee Clary for her great comments and advice (and a shared appreciation for shoes!) and Dr. Art Palmer, who took time away from his busy research schedule to be a fabulous mentor and personal cave science guru.

I want to express great appreciation to my fellow classmates and colleagues who helped with the fieldwork and data compilation required for this dissertation: Joan Mylroie for always being the voice of reason and giving the best compass; Jon Sumrall for his willingness to pull a survey tape into the smallest of spaces; Erik Larson for always reminding us that the numbers don't lie; Jeanne Lambert Sumrall for keeping us all smiling; Athena Nagel for pushing the tightest of places; Ryan Travis for great field assistance; Nicole Ridlen for her enthusiasm for caving and life in general; Jason Polk for all of his spot-on advice; Eli Winkler for moral support and a gung ho caving attitude; Mike Lace for surveying and making maps of lots of small caves.

Special thanks go to Jim Coke for his help, input and discussions on the great underwater caves of Quintana Roo, and to the Quintana Roo Speleological Survey for

providing important data and information. Parts of this dissertation would not have happened without that support.

Extra extra thanks to Peter Sprouse and the many cavers of Pamuul Grotto for surveying and providing data and maps of the “dry” caves of Quintana Roo, an important part of this dissertation.

Financial support for this work was provided by Cave Research Foundation and the National Speleological Foundation.

TABLE OF CONTENTS

DEDICATION	ii
ACKNOWLEDGEMENTS	iii
TABLE OF CONTENTS	v
LIST OF TABLES	ix
LIST OF FIGURES	xi
CHAPTER	
I. INTRODUCTION	1
1.1 Overview	1
1.2 The Carbonate Island Karst Model	2
1.3 Sea Level Changes and Marine Oxygen Isotope Stages	6
1.4 Research Topics	8
1.4.1 Morphometric Analysis of Cave Patterns using Fractal Indices	10
1.4.2 Geologic controls on the development of caves of Quintana Roo, Mexico	12
1.4.3 Coastal re-entrants on carbonate coasts	15
1.5 Section summary	16
II. MORPHOMETRIC ANALYSIS OF CAVE PATTERNS USING FRACTAL INDICES	20
2.1 Abstract	20
2.2 Introduction	21
2.3 Overview	25
2.3.1 Landscapes, landforms and fractal morphometry	25
2.3.2 Cave patterns, cave types, and fractal morphometry	27
2.3.3 Euclidean versus Fractal Geometry	29
2.3.4 Fractal Indices	31
2.3.4.1 Fractal Dimension	32
2.3.4.2 Lacunarity	33
2.4 Methods	35
2.4.1 Data acquisition and image processing	35

2.4.2	Statistics	37
2.5	Results.....	38
2.5.1	Descriptive statistics	38
2.5.2	Statistical tests.....	38
2.6	Discussion.....	40
2.6.1	Analysis of descriptive statistics.....	40
2.6.2	Analysis of statistical tests.....	42
2.6.2.1	Analyses of fractal indices between all cave types.....	42
2.6.2.2	Analyses of fractal indices between specific cave types pairs.....	43
2.6.3	Regression analysis.....	45
2.7	Summary	46

III. THE GEOLOGIC CONTROLS ON THE DEVELOPMENT OF
CAVES WITHIN THE PHREATIC, EPIPHREATIC, AND VADOSE
ZONES ON THE NORTHEAST COAST OF QUINTANA ROO,
MEXICO.....62

3.1	Abstract.....	62
3.2	Introduction.....	63
3.3	Overview.....	64
3.3.1	Geography.....	64
3.3.2	Stratigraphy.....	65
3.3.3	Structural geology.....	67
3.3.4	Hydrology and aquifer dynamics.....	68
3.3.5	Cenotes and dry sinkholes	72
3.3.6	Caletas and crescent-shaped beaches.....	73
3.3.7	Caves of Quintana Roo	74
3.4	Methods.....	74
3.4.1	Cave survey/inventory/cartography	75
3.4.2	Digital data analysis.....	75
3.4.3	Morphometric Analysis of caves and karst.....	76
3.5	Results.....	76
3.5.1	Structural orientation and cave passage depth analysis	76
3.5.2	Collapse feature distribution (cenotes and dry sinkholes)	77
3.5.3	Springs and related discharge features.....	78
3.5.4	Cave distribution and density.....	78
3.5.5	Cave morphology analysis.....	79
3.5.6	Hydrologic observations	80
3.6	Discussion.....	81
3.6.1	Cave passage orientation and distribution	82
3.6.2	Cave passage morphology	84
3.6.3	Vertical development of passages.....	86
3.6.4	Multiphase cave development.....	88
3.7	Summary	89

IV.	A INFLUENCE OF KARSTIC, FLUVIAL, AND LITTORAL PROCESSES ON THE DEVELOPMENT OF REENTRANTS AND ASSOCIATED FEATURES OF ROCKY CARBONATE COASTS.....	112
4.1	Abstract.....	112
4.2	Introduction.....	113
4.3	Overview.....	114
4.3.1	Gullies of Barbados.....	114
4.3.1.1	Site Description.....	119
4.3.1.2	Geologic setting.....	120
4.3.2	Bokas of the ABC Islands.....	124
4.3.2.1	Site Description.....	126
4.3.2.2	Geologic setting.....	126
4.3.3	Caletas of northeast Quintana Roo, Mexico.....	130
4.3.3.1	Site Description.....	131
4.3.3.2	Geologic setting.....	132
4.4	Methods.....	135
4.5	Results.....	138
4.5.1	Gully Results.....	138
4.5.2	Boka Results.....	140
4.5.3	Caleta Results.....	141
4.6	Discussion.....	143
4.6.1	Gullies.....	143
4.6.2	Bokas.....	147
4.6.2.1	Boka types.....	147
4.6.2.2	Boka distribution.....	147
4.6.2.3	Boka origin.....	148
4.6.3	Caletas.....	152
4.7	Summary.....	154
V.	CONCLUSIONS.....	191
5.1	Fractal indices as a measure of cave morphology.....	191
5.2	Geologic controls on the development of caves within the phreatic, epiphreatic and vadose zones on the northeast coast of Quintana Roo, Mexico.....	195
5.3	Influence of karstic, fluvial, and littoral processes on the development of reentrants and associated features on rocky carbonate coasts.....	200
5.3.1	Gullies Summary.....	200
5.3.2	Bokas summary.....	202
5.3.3	Caleta summary.....	203
5.4	Epilogue.....	205

REFERENCES	207
------------------	-----

APPENDIX

A. DATA TABLES	222
B. CAVE MAPPING STANDARDS.....	232
B.1 Quintana Roo Cave Mapping Project Standards	233
B.2 Cave Research Foundation Survey Standards	234

LIST OF TABLES

2.1	Comparison of Euclidean and fractal geometries	47
2.2	Descriptive statistics – Fractal dimension for cave types	47
2.3	Descriptive statistics - Lacunarity for cave types	48
2.4	Kruskal-Wallis One Way Analysis of Variance on Ranks test.....	48
2.5	Student-Newman-Keuls Method – Fractal Dimension.....	48
2.6	Friedman Repeated Measures Analysis of Variance on Ranks	49
2.7	Student-Newman-Keuls Method - Lacunarity.....	49
2.8	Regression Analysis of Fractal dimension versus Lacunarity	49
3.1	Fractal dimension for a selection of underwater and vadose zone caves	90
4.1	Geomorphic zones of Barbados	156
4.2	Summary of geographical statistics for the ABC Islands	157
4.3	Summary of mapped gully segments by geomorphic zone	157
4.4	Results of fractal analysis of stream caves versus gully caves	157
4.5	Summarized BMI ranges and percentages of boka types for each island.....	158
4.6	Results of fractal morphometric analyses on some of the caves of the ABC islands	158
4.7	Morphometric Analysis (fractal) for select underwater caves.....	158
A.1	Fractal Indices for flank margin caves.....	223
A.2	Fractal Indices for continental hypogene caves	224
A.3	Fractal Indices for allogenic stream caves	225
A.4	Fractal indices for littoral caves.....	226

A.5	Fractal indices for tafoni	227
A.6	Morphometric data for bokas of Aruba	228
A.7	Morphometric data for bokas of Bonaire.....	229
A.8	Morphometric data for bokas of Curaçao	230
A.9	Morphometric data for caletas	231

LIST OF FIGURES

1.1	Carbonate Island Karst Model	18
1.2	Marine Isotope Stages (MIS5 and 7 shown) and sea level versus time.....	19
1.3	Overview map of field sites	19
2.1	Cave pattern at mixing corrosion zone	50
2.2	Cave patterns classification.....	51
2.3	Koch Snowflake, one of the earliest fractal curves to be described.	52
2.4	Box counting method.....	52
2.5	Examples of lacunarity	53
2.6	Sliding box counting method.....	54
2.7	Lacunarity values from the sliding box counting method	54
2.8	Box plots summarizing descriptive statistics for fractal indices.....	55
2.9	Hypogene cave fractal indices and morphological examples	56
2.10	Flank margin cave fractal indices and morphological examples	57
2.11	Allogenic stream cave fractal indices and morphological examples	58
2.12	Littoral cave fractal indices and morphological examples	59
2.13	Tafoni fractal indices and morphological examples	60
2.14	Scatterplots of fractal dimension vs. lacunarity for different cave types.....	61
3.1	Study area on the northeast coast of Quintana Roo, Mexico	90
3.2	Stratigraphy of the Yucatan peninsula, Mexico.....	91
3.3	Stratigraphy of the northeast coast of Quintana Roo, Mexico.....	92

3.4	Ridge and swale plane of the northeast coast of Quintana Roo, Mexico	93
3.5	Structural features of the Yucatan peninsula	93
3.6	Collapsed sinkhole in a vadose zone cave in Quintana Roo, Mexico	94
3.7	Caleta and crescent shaped beach	94
3.8	Azimuth rose diagrams from regional cave data	95
3.9	Rose diagrams on inclination.....	95
3.10	Frequency distribution on depth for vadose zone caves relative to modern sea level	96
3.11	Frequency distribution of underwater cave depths relative to modern sea level.....	96
3.12	Deepest cave sections in the Quintana Roo region – Hoyo Negro (-60m),	97
3.13	Deepest cave sections in the Quintana Roo region – Blue Abyss (-70m)	98
3.14	Deepest cave sections in the Quintana Roo region – The Pit(-119m)	99
3.15	Cenote distribution from Sian Ka’an Reserve to Akumal	100
3.16	Cenote distribution in Playa del Carmen area.....	101
3.17	Distribution of coastal springs of northeast Quintana Roo	102
3.18	Cave distribution and density of underwater and vadose zone caves.	103
3.19	Coastal maze passages of Cenote Abejas section of Sistema Sac Actun	104
3.20	Map of Cueva Camaras.....	105
3.21	Anastomotic cave passage development.....	105
3.22	Complex mazes associated with cenotes.	106
3.23	Map of Hell’s Gate Section of Sistema Sac Actun	107
3.24	Map of Grotte des Aluxes	108
3.25	Water flow in underwater and vadose-epiphreatic zone caves.....	109

3.26	Flank margin caves of the Tulum area.....	109
3.27	Map of Yax Muul section of Sistema Sac Actun.....	110
3.28	Cave passage development on the northeast coast of Quintana Roo, Mexico	111
4.1	Site map of study area.....	159
4.2	Gullies of Barbados.....	160
4.3	Geologic and geomorphic features of Barbados.....	161
4.4	Geomorphic zones of Barbados	161
4.5	Mt. Brevator Cave, a typical flank margin cave of Barbados.....	162
4.6	Animal Flower Cave, a typical hybrid cave of Barbados	163
4.7	Harrison’s Cave, a typical stream cave of Barbados	164
4.8	Sinkhole distribution and density on Barbados	165
4.9	Site map of the ABC Islands (Aruba, Bonaire, Curaçao).....	166
4.10	Typical boka on Curaçao	166
4.11	Hybrid caves that result from littoral erosion of flank margin caves	167
4.12	General geologic maps of the ABC Islands.....	168
4.13	Study site maps in Quintana Room, Mexico	169
4.14	Stratigraphy of the northeast coast of Quintana Roo, Mexico.....	169
4.15	Structural features of the Yucatan peninsula	170
4.16	Boca measurements and ratios used to quantify boka morphology.....	170
4.17	Boca morphologies on the ABC Islands.....	171
4.18	Method for measuring caletas.....	172
4.19	Gully drainage system of Barbados	173
4.20	Major Watersheds of Barbados.....	173
4.21	Location of stream caves of Barbados	174

4.22	Flank margin caves in some of the gullies of Barbados.	175
4.23	Gullies that contain caves, Barbados	176
4.24	Boka distribution on Curaçao	177
4.25	Boka distribution on Aruba.....	178
4.26	Boka distribution on Bonaire	179
4.27	Distribution of coastal springs/caletas	180
4.28	Caleta morphologies of the northeast coast of Quintana Roo.....	181
4.29	Distribution of caletas and crescent-shaped beaches on the Yucatan Caribbean.....	182
4.30	Structural trends of caletas and crescent-shaped beaches.....	183
4.31	Distribution of caves, springs/caletas and beaches	184
4.32	Model for cave development within gullies of Barbados	185
4.33	Boka development is a function of reef terrace width	186
4.34	Model I for development of a fluvially dominated boka	187
4.35	Models II and III for development of littoral and littoral/fluvial boka	188
4.36	Caves associated with Caleta Xel Ha.....	189
4.37	Model for development of a linear caleta	190

CHAPTER I

INTRODUCTION

1.1 Overview

The evolution of rocky coastlines is driven by the continuous action of waves, tides and winds that mechanically break down the rock. More subtle but still important are the effects of biological activity in contributing to coastal erosion. From the landward side come the effects of fluvial processes that interact with the littoral environment. Chemical erosion is also recognized, to a degree, as an erosive agent on rocky coasts. When the rocky component is carbonate in composition, chemical erosion takes on a more dominant role in the form of karstification that exposes the coastal zone to dissolutional denudation. The Carbonate Island Karst Model (CIKM) has been the preeminent guide that explains the genesis and morphology of eogenetic dissolutional processes and features on small carbonate islands (see Mylroie and Mylroie 2013 for the latest version). The model is effective enough to be expanded to explain eogenetic karstification in more complex coastal settings, which is the one of the topics of this research.

Young tropical carbonate islands display a unique hydrology that involves the interaction of a freshwater lens and saline water, and are classified as eogenetic karst because of their diagenetically young bedrock, near horizontal attitude, and close proximity to their marine depositional environment. The term eogenetic, as defined by

Choquette and Pray (1970), is one of a series of three time-porosity stages that occur during the evolution of porosity of carbonate rocks; eogenetic refers to the time of early burial, mesogenetic to the time of deeper burial, and telogenetic associated with the erosion of long-buried carbonates. Vacher and Mylroie (2002) put forth the term *eogenetic karst* to refer to a land surface and associated porosity system developing in rocks that are undergoing eogenetic, meteoric diagenesis. This term differs from eogenetic karren which is used to describe small-scale carbonate bedrock etching. (For a full review, see Taboroši et al., 2004 or Taboroši and Kázmér, 2013).

The close proximity of eogenetic carbonates to their marine depositional environment assures that for sloping carbonate ramps, small changes in global sea level result in significant changes in sub-aerially exposed zones (Mylroie and Carew 1995). Vacher and Mylroie (2002) contend that island size and thus catchment size control the nature of cave development on carbonate islands. This was subsequently demonstrated by Larson (2014). The current model of carbonate island evolution, the Carbonate Island Karst Model, or CIKM (e.g. Mylroie and Mylroie 2007; 2013) explains the development of karstic features on small islands dominated by eogenetic carbonates. Small islands were the basis for this initial work because of the spatial constraints small size placed on observed karst features.

1.2 The Carbonate Island Karst Model

The Carbonate Island Karst Model (CIKM) has been the preeminent guide that explains the genesis and morphology of eogenetic dissolutional features on small carbonate islands (see Mylroie and Mylroie 2013 for the latest version). The evolution of the Carbonate Island Karst Model began with the advent of the flank margin cave (FMC)

model (Myroie and Carew 1990) that was developed to explain cave genesis in the Bahamas. The model was eventually expanded to Isla de Mona (Puerto Rico) in the Caribbean and subsequently the Mariana Islands of the western Pacific. The FMC model proposed a type of cave development very different from the models used to explain the genesis and morphology of caves that occur in continental interiors: continental cave types are epigene and hypogene. Epigene caves form in direct association with local surface hydrology and as a result of solutional aggressiveness derived from surface or near surface processes (Palmer 2007). Hypogene caves occur in environments that are completely decoupled from surface hydrology and from *acids* that originate deep beneath the surface (Palmer 2007). Some cave researchers (e.g. Palmer 2007) classify flank margin caves as hypogene because they contain morphological features that resemble those typical of hypogene caves and form in environments that some do not consider to be directly tied to surface hydrology. The classification of flank margin caves is still a topic for debate (Klimchouk et al. 2014).

Myroie and Carew (1990) described coastal cave morphology of caves on small carbonate islands as typified by large chambers with many ramifying passages that interconnect. The chambers are wider than high with undulatory wall surfaces, and bedrock pillars are common. Inland trending passages typically terminate in blind bedrock walls. Features common to many continental epigene caves, such as obvious points of surface recharge and discharge, wall scallops, and fluvially-derived sediments, are not detected in flank margin caves. (Fluvial sediments can appear after the cave is breached and captures local surface runoff.) The FMC model explains this type of cave morphology and cave development within the context of island hydrogeology, which

involves the interaction of a freshwater lens with saltwater of marine origin. According to the FMC model, dissolution of bedrock occurs at the distal margin of a freshwater lens at the dissolutionally aggressive interface between the freshwater lens and underlying saline water (the halocline or mixing zone) (Mylroie and Carew 1990). The cross section of the freshwater lens decreases at the lens margin, causing an increase in flow velocity, and interchange of reactants and products at the lens margin (Raeisi and Mylroie 1995). Organic material, which by decay can either produce additional CO₂, or drive anoxia and H₂S production, can be trapped at the density interface of the top of the freshwater lens and at the halocline. This enhances the dissolutional potential of the water (Mylroie and Mylroie 2007).

In the late 1990's, fieldwork conducted in Guam and the adjacent Mariana Islands encountered a geologic setting that was quite different than those observed in the Bahamas and Isla de Mona (Mylroie and Jenson 2000). The rocks were older, not exclusively carbonate, and the islands more tectonically complex. This scenario resulted in allogenic recharge, which sank at the contact between carbonate and non-carbonate rocks forming recharge and discharge features similar to those on continents (Mylroie and Jenson 2000). The complex geology expressed in Guam necessitated a more comprehensive interpretation of cave and karst development. The field work in Guam and additional work on Saipan expanded the FMC model into the more comprehensive Carbonate Island Karst Model (CIKM)(Figure 1.1), and brought together the various components that controlled cave and karst development on carbonate islands (Mylroie and Jenson 2000, Mylroie et al. 2001, Mylroie and Mylroie 2007, 2011, 2013). The most recent specifics of CIKM are summarized as follows:

1. A lens of meteorically derived freshwater is buoyantly supported by saline water that has infiltrated the coastal bedrock. At the interface between fresh- and saline water, mixing of the two waters forms a brackish layer with renewed dissolutional capability, though both the seawater and freshwater are themselves initially saturated with respect to CaCO_3 (Plummer 1975).
2. The elevation of the freshwater lens tracks sea level, so the lens and its associated dissolutional environments can migrate as a result of glacioeustasy or local tectonics. Both processes can operate rapidly in terms of geologic time.
3. On a global scale, coastal limestones are predominantly eogenetic or diagenetically immature. Primary features, such as depositional porosity and initial allochem geochemistry, are commonly unaltered (Vacher and Mylroie 2002).
4. The shape and distribution of the freshwater lens and the chemistry of freshwater recharge is controlled by the configuration of the carbonate rocks relative to adjacent non-carbonate lithology. This results in four basic conditions, featured here as islands to present simple end members of the carbonate coastal condition:
 - a. Simple Carbonate Island (Fig. 1.1A)—Carbonate rocks are the only lithology present within the recharge and discharge field of the freshwater lens. Recharge is entirely autogenic and the freshwater flow regime is solely controlled by the properties of the carbonate rock
 - b. Carbonate-Cover Island (Fig. 1.1B)—Carbonate rocks only, are exposed at the surface and recharge is entirely autogenic. Non-carbonate rocks occurring in the subsurface may partition or distort the freshwater lens. Turbulent conduit

flow may develop that is perched in the vadose zone on the contact between carbonate and non-carbonate rocks.

- c. Composite Island (Fig. 1.1C)—Carbonate and non-carbonate rocks are exposed at the surface, producing autogenic and allogenic recharge to the freshwater lens. The lens is partitioned and distorted, and turbulent conduit flow develops in the vadose zone at the carbonate/non-carbonate contact.
- d. Complex Island (Fig. 1.1D) —Carbonate and non-carbonate rocks are interrelated by syndeposition and/or tectonic structures. Partitioning, perching, and confining of the freshwater lens are possible.

The island categories as listed above illustrate idealized models. In actuality, islands may display many of the presented characteristics with transitional forms (Mylroie and Mylroie 2013). The most effective use of the above categories is to classify portions of islands or carbonate coasts by the category that best describes the local conditions (Mylroie and Mylroie 2013).

To address karstic features on uplifted regions of island interiors that resemble epigene continental karst, Vacher and Mylroie (2002) made the distinction between *island karst* versus *karst on islands*. Island karst forms as per the CIKM, whereas karst on islands develops in uplifted regions of island interiors and has many of the characteristics of epigene karst in continental interiors (Mylroie and Mylroie 2007).

1.3 Sea Level Changes and Marine Oxygen Isotope Stages

Global sea level has varied throughout geologic time and is attributed to eustatic and/or isostatic effects. Eustatic sea level variations result from changes in the volume of water in the oceans, which is strongly affected by the size of the icecaps (Sidall et al.

2006). Sea-level is also a function of the geometry of the ocean basins that changes on time scales of millions of years and is associated with plate tectonics (Lambeck and Chappell, 2001).

On the Quaternary time scale in the Caribbean region, sea level variations are the result of the global effects of glacioeustasy and local tectonics. The uplifted reef terraces of Barbados and the ABC islands are a function of their proximity to the Caribbean plate boundary. However, a comparison of elevation and age of the Upper Pleistocene rocks on Yucatan's northeast coast to other similar-age areas in the tectonically quiescent Bahamas indicate that there has been very little vertical displacement of this area since the last Pleistocene high stand of 125,000 years ago (Szabo 1978).

Eustatic effects on sea level are determined using proxy records based on oxygen isotope variations in deep-sea sediments, dated shorelines and coral reefs, and reconstructions of past ice sheets (Lambeck and Chappell, 2001). The events differentiated in isotope sequences are termed Marine Isotope Stages (MIS) to distinguish them from those identified from ice cores or speleothem sequences (Gibbard 2007). Marine oxygen-isotope stages are alternating warm and cool periods in the Earth's paleoclimate. The numbering system used to identify the stages start from the present (MIS1) and go backwards in time. Glacial events are assigned even numbers and interglacial events are given odd numbers. Lower case letters indicate sub-stages. For example, MIS5 is divided into interglacial sub-stages 5a, 5c and 5e and glacial sub-stages are 5b and 5d (Gibbard 2007). Figure 1.2 shows a graph of MIS5 and MIS7 and sea level, versus time.

1.4 Research Topics

The objective of this research is to further expand the current model on eogenetic karst development (CIKM) on small islands to any size carbonate island and to carbonate continental coastlines, with specific focus on the coastal landforms influenced by karst processes.

The topics addressed in this research included:

1. **Morphometric analysis of cave patterns using fractal indices:** This research investigated improved morphometric indices for quantitatively identifying and comparing coastal cave types and other cave types. A variety of caves occur on carbonate coasts and it is critical to be able to differentiate them in order to understand which processes are affecting a coast.
2. **Geologic controls on caves currently located within the vadose and epiphreatic zones of an eogenetic carbonate continental coast:** This investigation compared the characteristics and controls on the development of submerged phreatic conduits and vadose-epiphreatic zone caves. Both of these features have formed within an extensive coastal carbonate aquifer. These comparisons served to provide a better understanding of karstification within the mixing zone environment of an eogenetic carbonate continental coast.
3. **Influence of karstic, fluvial, and littoral processes on the development of reentrants and associated features on rocky carbonate coasts:** This research addressed the development of coastal reentrant models to explain

coastal features formed by a combination of karstic, littoral, and fluvial processes and overprinted by the effects of sea level change.

The field sites for this study include a variety of eogenetic islands (Barbados, Aruba, Bonaire, Curaçao), and an eogenetic continental coast (northeast coast of Quintana Roo, Mexico) (Figure 1.3).

If there is a limitation to the CIKM it is that its original emphasis was on small carbonate islands, as the spatial limits helped constrain possible interpretations for observed karst phenomena. However, CIKM has been successfully used to describe flank margin cave development in telogenetic island settings such as New Zealand (Myroie et al. 2008), and on Cres Island, Croatia (Otoničar et al. 2010).

Carbonate coast environs on all size islands and on continents display a variety of landforms and features that result from a combination of karstic, littoral, and depending on local geology, fluvial processes. These may include coastal reentrants (any type of indentation in a coastline), collapse features, and coastal springs and related features. Depending on coastal geology, the island categories ascribed to small islands by the CIKM may manifest singly, or in combination on larger carbonate islands and carbonate coastlines. This results in cave development environments ranging from freshwater/saltwater mixing zones, to allogenic/autogenic recharge cave systems, to pseudokarst in the form of littoral, mechanical, and tafoni caves (Myroie and Myroie 2011). In order to better address karst and cave development on carbonate islands of all sizes and on carbonate continental coastlines, the Carbonate Island Karst Model could be expanded to the Carbonate Coastal Karst Model. It is hoped that the topics addressed in this research can facilitate that transition.

1.4.1 Morphometric Analysis of Cave Patterns using Fractal Indices

An important tool in the study of carbonate coasts is the use of quantitative morphometric analyses to distinguish between the different caves types indigenous to the coastal environment (e.g. Waterstrat et al. 2010). Descriptive cave passage morphology has traditionally been used to distinguish phreatic, vadose, and polygenetic cave passage genesis. Mylroie and Carew (1990) (Figure 2.1) qualitatively described laminar recharge and its relationship to cave morphology in the coastal setting. Palmer (1991, 2007, 2011) used hydrologic recharge and structural properties of bedrock to predict descriptive morphology based on the physical layout of caves and the relationship of cave passages (Figure 2.2). Quantitative morphologic description of cave passage layout (Mylroie 2008) has shown promise for differentiating cave types in carbonate coastal environments. Morphometric differentiation between coastal caves types was based on work by Roth (2004) who related geometric analysis of flank margin caves of the Bahamas to cave development processes.

Subsequent studies employed morphometric analyses based on similar parameters as per Roth (2004), to determine if these parameters could differentiate between cave types (Stafford et al. 2006, Owen 2007, Lace 2008, Waterstrat et al. 2010). Some deviations were made from Roth's methods in that additional parameters were measured (e.g. entrance width, interior width, and inland extent). Recent attempts at morphometric analysis using these methods have proven to be problematic because of inconsistencies between measured parameters within morphometric datasets, non-reproducibility of statistical results, insufficient sample size, and exploration bias (Curl 2011, Mixon 2011, Waterstrat et al. 2011).

The biggest issue with traditional cave morphometry is that even though three-dimensional data are available, the focus is on morphology in two dimensions (Myrloie 2008), though there have been some efforts to use three-dimensional cave data in morphometric analysis. Labourdette et al. (2007) utilized three-dimensional data from the map of a Bahamian flank margin cave for conceptual modeling. In the interior continental setting Filipponi et al. (2009) used the three-dimensional geometry of complex cave systems in order to calculate statistical evidence of inception horizons, and thus relating geological setting to hydrogeologic boundary conditions.

As with other shapes and forms in nature, cave patterns are heterogeneous and display self-similar irregular and fragmented geometries which by definition make them fractals. As a consequence, the use of Euclidean-based metrics alone to define and characterize caves may actually be a limitation in morphometric analyses. Fractal indices have been used to characterize individual cave morphologies and spatial distributions (Curl, 1986; Lavery 1987, Florea and Wicks 2001). There has been limited work on the use of fractal modeling of conduit networks (Jeannin et al. 2007, Filipponi et al. 2009)

The questions addressed in this section of the research on “Morphometric Analysis of Cave Patterns using Fractal Indices” are as follows:

1. Do coastal caves have distinct morphological characteristics that can be quantified with fractal analysis?
2. Can a set of fractal indices differentiate cave types?
3. Can quantitative cave morphometry as determined by either Euclidean and/or fractal geometries be correlated with cave/karst formational processes?

This initial part of the research explored the fractal nature of cave morphology using pattern recognition techniques. The goal was to ascertain if fractal geometry provides a viable means of describing cave dimensions and morphology, and to determine if there is any predictive utility of fractal indices. The fractal indices used for this research were fractal dimension, which quantifies the complexity of a pattern, and lacunarity, which quantifies the texture (homogeneous versus heterogeneous) of a pattern. The results of this study showed that fractal indices can quantitatively distinguish cave types though caution is urged to always consider geologic context.

1.4.2 Geologic controls on the development of caves of Quintana Roo, Mexico

In all karstic systems, regional hydrology and resultant cave type vary with mode of recharge, catchment size, rock/water interaction, and hydrodynamics. Cave passage distribution, morphology, and density are controlled by hydrogeology, nature of recharge, source of aggressiveness, lithology, and structure (Palmer 1991, 2007, 2011). In the eogenetic coastal setting, the overall hydrologic regime is affected by eustatic sea-level fluctuations and/or local tectonic sea-level change, and can result in extensive polygenetic caves that have developed in different elevation tiers. The caves may be overprinted by features associated with turbulent and/or laminar flow as well as littoral processes. The dissolutional processes that form coastal caves can also impact the morphology of the associated coastline (e.g. Kambesis and Coke 2013).

Vacher and Mylroie (2002) suggested that the size of an island, and thus catchment size, controls the nature of cave development on carbonate islands. Small islands have a very large perimeter to area ratio, and meteoric catchment is easily discharged to the sea as laminar flow, creating classic flank margin cave conditions.

However, as islands (and carbonate platforms) grow larger via carbonate accretion and/or decreases in sea level, island area increases by the square, with only a linear increase in perimeter. Meteoric catchment increases faster than the available discharge perimeter, and laminar flow paths become longer and much less efficient. Under these conditions, Vacher and Mylroie (2002) predicted that conduit flow becomes sustainable for island drainage, and can support the development of integrated turbulent flow cave systems with flank margin caves limited to coastal areas between conduit discharge points.

Interestingly, Vacher and Mylroie (2002) stated, in their description of eogenetic cave types, that submerged linear phreatic cave systems of the Bahamas and the Bermuda platform as observed by cave divers are relict features unrelated to current groundwater conditions. Larson (2014) has shown that the area to perimeter ratio of an island is not the control; instead, it is island size, which results in an increase of the water budget and directly causes sustainable conduit flow. Submerged linear phreatic cave systems that are characteristic of the Yucatan carbonate coast study site as described below, do appear to be very much related to current groundwater conditions.

The northeast coast of the Yucatan peninsula consists of an eogenetic carbonate coastline with a complex regional hydrology that has resulted in the formation of an extensive conduit-drained aquifer (Beddows 2004, Smart et al. 2006). On the northeast coast in Quintana Roo State, Mexico, more than 1170 km of submerged cave passages within 223 cave systems have been documented (Quintana Roo Speleological Survey (QRSS) 2013). In addition to the underwater caves systems, over 115 km of cave passages have been surveyed within 100+ cave systems currently located within the vadose zone and between the vadose and phreatic zones (i.e. epiphreatic zone), as well as

relict flank margin caves located in eolianites along the coast (Kelly et al. 2006). North, south and west of this extensive block of cave development, the density of cave passages appears to notably decrease (QRSS 2013).

The objective of the Quintana Roo research was to identify the geological controls that resulted in the formation of caves currently located within the vadose and epiphreatic zones of an eogenetic carbonate continental margin, and to determine their relationship to the extensive array of submerged cave systems.

The questions addressed in this section of research on “Geologic controls on the development of caves within the vadose and epiphreatic zones on the Northeast Coast of Quintana Roo, Mexico” are:

1. What factors control cave passage orientation and distribution of caves in the study area?
2. What causes the variations of cave passage morphology and passage density with distance from the coast?
3. What is the relationship between caves currently located in the vadose zone and epiphreatic zone, and the extensive, hydrogeologically active network of underwater cave systems that are prevalent in the region?
4. Is the decrease in cave passage density between the Puerto Morelos-Muyil block and adjacent areas a function of difficult land access and cave exploration bias, or due to changes in geological boundary conditions?

Determination of geological controls, and geomorphic relationships were accomplished by fracture analysis of cave passage trends; morphometric analysis of cave systems and cave passages using Euclidean and fractal-based indices; quantification of

relationship of topographic surface to cave elevation, and of elevations of distinct tiers of cave development; identifying stratigraphic horizons and structures that display cave and karst development.

1.4.3 Coastal re-entrants on carbonate coasts

Coastal development on rocky carbonate islands and continental coastlines is affected by littoral processes in the form of waves, tides and winds that erode them and form distinct landforms (Bird 2008). When rivers interact with coastlines, sediments are transported, deposited, and reworked by littoral processes to form depositional features; the mixing of fluvial and marine waters results in physiochemical variations at the interface of both water types (Huggett 2007). Karst processes subject carbonate coastlines to additional erosive agents that expose the coastal zone to dissolutional denudation.

The research on coastal reentrants and related forms focused on karst-related features of erosive carbonate coastlines of the Caribbean region whose rocky component consists of fossil reef structures. Features of the fossil reef structures included coastal reentrants, a variety of caves, distinct collapse features some of which are associated with the reentrants, and distinct coastline morphologies. The locations of many of these features or combinations of them, and distinctive coastal morphologies, occur within the study sites for this research which include:

1. The island of Barbados
2. The windward side of the ABC Islands (Aruba, Bonaire, and Curaçao)
3. The northeast coast of Quintana Roo, Mexico

Though Barbados and the ABC Islands are classified as composite islands as per CIKM, the form and function of their coastal reentrants and associated features have a completely different character due to the differences in local geological conditions.

The questions addressed in the final research section “Influence of karstic, fluvial, and littoral processes on the development of reentrants and associated features on rocky carbonate coasts” are listed as follows:

1. What are the morphological characteristics and distributions of coastal reentrants and related features on fossil reef structures of carbonate islands, and on carbonate continental coasts?
2. What influence does coral reef ecology have on the initial development of fluvially-related coastal reentrants, and do those reentrants pre or post-date the reef terraces in which they form?
3. Are distinct cave and feature types associated with the different types of coastal reentrants?
4. How do fluvial processes interact with karstification on fossil reef structures?
5. Can the origin and character of coastal reentrants and related features be incorporated into a broader model that addresses cave and karst development on carbonate islands of all sizes, and on carbonate continental coasts?

1.5 Section summary

The objectives of this research included improving morphometric analyses for quantitatively identifying and differentiating coastal cave types using fractal geometry;

identifying geological controls on the development of caves currently located in the vadose and epiphreatic zones within a mixing-zone environment of a carbonate continental coastline, and determining the relationship of those caves to the phreatic caves of the region; development of coastal reentrant models to explain eogenetic coastal karst features formed by a combination of karstic, littoral, and/or fluvial processes. The ultimate goal of this research was to expand the Carbonate Island Karst Model to the Carbonate Coastal Karst Model in order to encompass coastal karst and cave development on all types and sizes of carbonate islands and carbonate continental coasts.

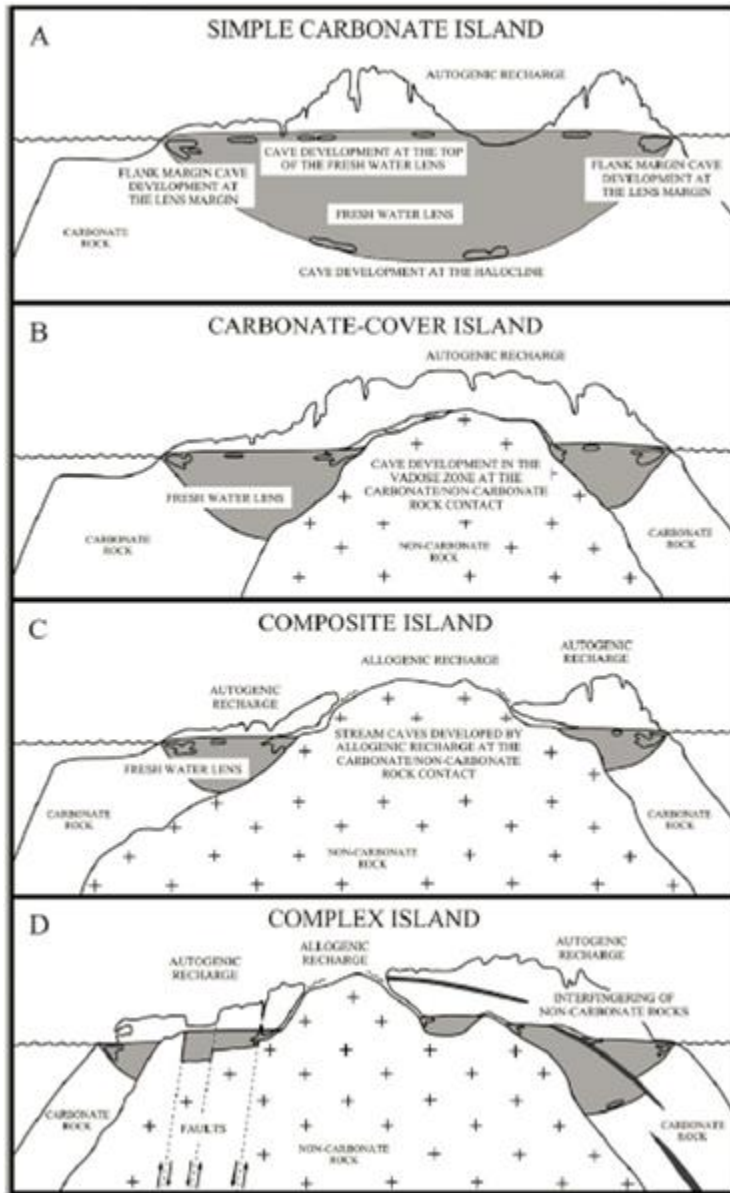
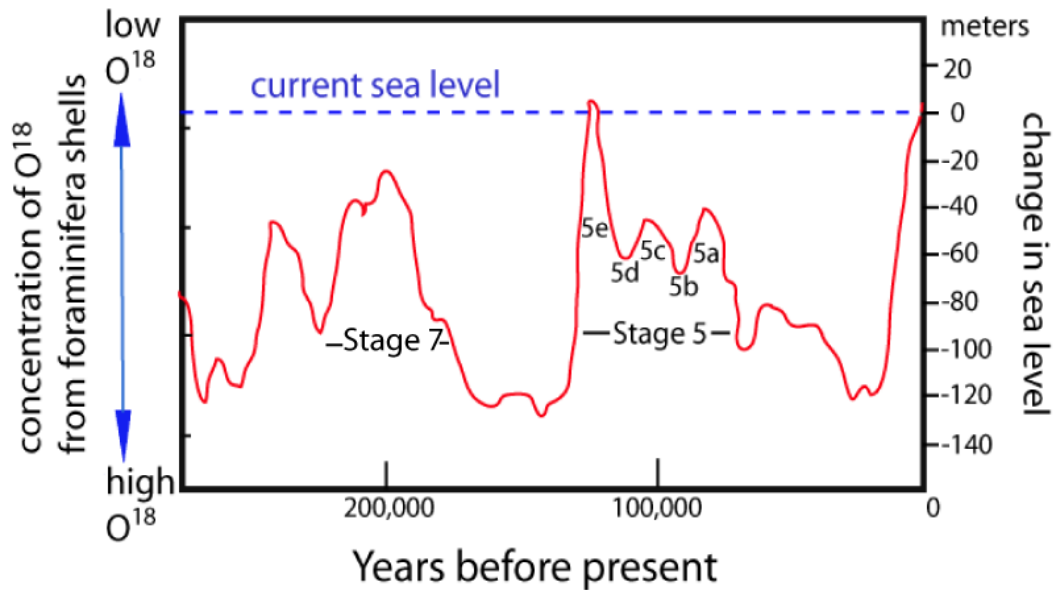


Figure 1.1 Carbonate Island Karst Model

From Mylroie and Mylroie 2007. (A) Simple carbonate island, (B) Carbonate cover island, (C) Composite island, (D) Complex island

Late Pleistocene and Holocene Sea-level Curve



data modified from CLIMAP isotopic data summarized from Imbrie and Imbrie 1986

Figure 1.2 Marine Isotope Stages (MIS5 and 7 shown) and sea level versus time



Figure 1.3 Overview map of field sites

Study sites: Barbados, Aruba, Bonaire, Curaçao and the northeast coast of Quintana Roo, Mexico.

CHAPTER II

MORPHOMETRIC ANALYSIS OF CAVE PATTERNS USING FRACTAL INDICES

2.1 Abstract

Cave type and morphology are controlled by hydrogeologic and geologic factors, so by inverse analogy, cave type and morphology could be used to determine the hydrologic and geologic conditions under which caves developed. Euclidian metrics have traditionally been used to quantify and compare cave morphologies even though caves have irregular and complex shapes. Caves have been shown to possess characteristics that identify them as fractals within certain ranges, so the use of Euclidean-based metrics alone to define and characterize them may be a limitation in morphometric analyses. Other factors that limit full morphometric analyses of caves include focus on two-dimensional cave data as these are typically what are available, and exploration bias as cave exploration and documentation are limited to spaces that are humanly passable, epitomizing the subjective nature of anthropogenic-based measurements. This research ascertained that fractal geometry provided a viable means of describing and comparing cave dimensions and morphology. The fractal indices used were fractal dimension, which quantifies the complexity of a pattern, and lacunarity, which quantifies the texture (homogeneous versus heterogeneous) of a pattern. Fractal indices were calculated for cave patterns of different genetic varieties including allogenic stream caves, continental mixing zone (hypogene) caves, flank margin caves, littoral caves, and tafoni. The

quantitative morphological distinctions in cave patterns as identified by fractal dimension and lacunarity, proved to be statistically significant. The implications of this result are that cave morphometry as defined by fractal indices could be used to augment the identification of geological and hydrological controls on the development of caves and cavernous permeability. However, any interpretation based on fractal indices must be made within the constraints of the natural system that holds the fractal object.

2.2 Introduction

An important tool in the study of cave morphology is the use of quantitative morphometric analyses to distinguish between the different caves types indigenous to the various geologic conditions (e.g. Waterstrat et al. 2010). Mylroie and Carew (1990) (Figure 2.1) qualitatively described laminar recharge and its relationship to cave morphology in the coastal setting. Palmer (1991, 2007, and 2011) used recharge and structural properties to predict cave morphology (Figure 2.2). Quantitative morphologic description of cave passage layout has shown promise for differentiating cave types in carbonate coastal environments (Mylroie 2008).

As with other shapes and forms in nature, cave morphologies are heterogeneous and display to some degree, self-similar, irregular and fragmented geometries which by definition make them fractals (Curl 1986). As a consequence, the use of Euclidean-based metrics alone to define and characterize cave patterns may be a limitation in morphometric analyses. Fractal dimension is an index used as a numerical measure of an object's complexity (surface roughness) and reflects its scale invariance. It describes how an object occupies space, and is related to the complexity of its structure. Sample independence or scale invariance measures have a physical significance since the average

of their spatial means does not depend on the scale (or dimension of space) over which they are averaged (Klinkenberg 1992). Theoretically, scale invariance or fractal measures allow extrapolations from properties observed at one scale to properties of scale that have not been observed (Gilbert 1989). Fractal indices have been used to characterize individual cave morphologies and spatial distributions (Curl, 1986; Lavery 1987, Florea and Wicks 2001), and there has been work on the use of fractal modeling of conduit networks (Jeannin et al. 2007, Filipponi et al. 2009).

This research explored the fractal nature of cave morphology as described by fractal indices. The goal was to ascertain if fractal geometry provided a viable means of describing and comparing cave dimensions and morphology. The fractal indices used for this study were fractal dimension, which quantifies the complexity of a pattern, and lacunarity, which quantifies the texture of a pattern (homogeneous versus heterogeneous). Fractal indices were calculated for cave patterns of different genetic varieties including allogenic stream caves, continental mixing zone (hypogene) caves, flank margin caves, littoral caves, and tafoni.

The quantitative morphological distinctions in cave patterns as determined in this study, proved to be statistically significant so the implications are that cave morphometry as defined by fractal indices could be used as an identifier for types of geological and hydrological controls on the development of caves and cavernous permeability. However, any interpretation based on fractal indices must be made within the constraints of the natural system that holds the fractal object.

Caves potentially have unique morphometric signatures that could be used to differentiate them, e.g. flank margin caves versus littoral caves. In order to determine if

caves types have a unique set of morphometrics, it is necessary to review morphometric tools used in the analysis of landforms in general.

Within the context of geomorphology, morphometry is defined as the measurement and mathematical analysis of the configuration of the Earth's surface and of the shape and dimensions of its landforms (Bates and Jackson 1987). Evans (1972) proposed that morphometry was the most important tool in obtaining quantitative analysis of landscape features. Some of the first usages of morphometry were for the analysis of fluvial systems (Horton 1945), in the analysis of topographic maps (Strahler 1952), and quantifying drainage features (Strahler 1957). With extensive use of computers, the availability of digital datasets, and the development of computer algorithms for their spatial analysis, morphometry provided quantitative descriptors of geometry and topology of geomorphologic features, assisted in the determination of physical laws of patterns, scaling, complexity and variability of geological structures, and provided numerical indexes that could be correlated with physical parameters of practical interest. (Ganas et al. 2005, Pardo-Iguzquiza et al. 2011).

Morphometric parameters and indices serve multiple purposes in the study of caves, cave systems, and karst landscapes. Morphometric indices based on the ratios of simple dimensional measurements of caves have been used in the statistical analysis of large databases collected in regional speleological inventories in the attempt to recognize different geomorphic populations of caves (Piccini 2011). They have been used descriptively to identify specific types of caves (Waterstrat et al., 2010), to correlate morphometric indices with hydraulic behavior (Glennon 2001), for inverse modeling of karstic networks (Pinault et al. 2004), to characterize degree of karstification, and in

comparisons of karst systems (Pardo-Iguzquiza et al. 2011). Pardo-Iguzquiza et al. (2011) and Piccini (2011) provide extensive reviews of morphometric techniques and indices used in the morphometric analysis of karst landscapes, cave systems and individual caves.

Morphometric analyses have been used in the study of surficial expressions of karst such as networks of polygonal karst (Williams 1972), dolines and other karstic depressions (Day 1984, Denizman 2003), cockpit karst landscapes (Lyew-Ayee et al. 2007, Huang and Day 2013), and karren and other features of bedrock sculpturing (White and White 2000). Morphometric analyses using parameters measured from cave maps have been applied to differentiate and identify types of caves or groups of caves (Roth 2004, 2006, Frumkin and Fischhendler 2005, Stafford et al. 2006, Labourdette et al. 2007, Lace 2008, Waterstrat et al. 2010,) and to quantify features within caves (Curl 1974, Rice-Snow et al. 1996).

In the study of individual caves and caves systems, Curl (1966) recognized the effect of exploration bias on morphometric analysis. He used the term *proper cave* to describe a void that is large enough for human entry and *proper entrance* for ones that are naturally humanly passable. This is an important consideration when attempting to describe caves from a morphological perspective as there needs to be a clear definition of what is meant by the term “cave” (Curl 1966, Piccini 2011). Exploration bias is a critical constraint in cave morphometry because those sections of a cave that are humanly enterable are only part of the entire network of underground voids. As a consequence conventional morphometric analyses of caves or cave systems can only be directly applied to those sections of cave that are humanly passable. To overcome this,

morphometric analyses must either take into account a large population of caves of a specific karst area to get a statistically significant description of cave development and/or use indices that are scale independent such as fractals (Curl 1966, Piccini 2011). Curl (1986) was the first to attempt to quantitatively describe cave geometry based on fractal properties. Curl (1986) stated

At the very least, a fractal analysis of cave geometry works toward eliminating the present anthropomorphism of cave studies, where caves are defined frequently as only 'enterable by humans,' thereby implicitly limiting their study (p. 782).

2.3 Overview

2.3.1 Landscapes, landforms and fractal morphometry

According to Goodchild (1982), landforms have fractal characteristics within certain ranges of scales. As a result, fractal geometry can provide useful reference standards for landform analysis, and variations in fractal indices may reflect the processes, geologic structures and time that have influenced the development of landforms at different scales (Mark and Aronson, 1984; Lam and De Cola, 1993). Fractal geometry, which deals with natural shapes and patterns, has been applied to various aspects of morphometric analysis of karst landscapes and landforms.

In regional cave studies using large cave survey databases, Curl (1964, 1966) recognized that the distribution of cave lengths approximates a power law when *entranceless* caves are used in the distribution. He noted that cave length is a scale invariant parameter associated with self-similar fractals (Curl 1986). This parameter makes it possible to estimate the number, length or volume of *non-proper* caves (not humanly passable) in a region (Curl 1966). Badino (2001) did a similar study by

comparing cave lengths and vertical extent of caves on a worldwide basis. He found the power law similarly demonstrated with cave lengths, but determined that vertical extent did not share that characteristic. Badino (2001) attributes this to the average karstic limestone thickness.

Kusumayudha and Zen (2000) correlated the fractal dimension of different parts of the Oyo River (Indonesia) to fractal dimensions of underlying cave rivers and suggested that they were directly proportional.

Maramathis and Boudouvis (2006) determined the fractal dimension of a coastal karstic spring in Crete via a deterministic mathematical model using MODKARST, part of the USGS suite of groundwater modeling computer programs, and related it to the existence of a power law relating the aggregate cross-section of seawater conduits to the water table elevation.

Verbovšek (2007) related the fractal analysis of cave lengths in a large regional database of Slovenian caves to tectonic and hydrogeological setting based on cave density and distribution.

Fractal indices have been used along with other morphometric parameters to study the morphology and karstic evolution of individual cave systems. Finnesand and Curl (2009) used fractal dimension to determine the distribution of cave passage sizes in Tjoarvekrajgge Cave, the longest cave in Norway. Fractal dimension was among the suite of morphometrics used to analyze Okshola-Kristihola Cave System in Norway (Skoglund and Lauritzen 2010).

2.3.2 Cave patterns, cave types, and fractal morphometry

An important objective of morphometric cave studies has been to identify and differentiate genetic categories of caves and to use that information in studying the evolution of karst systems. Since cave type and morphology are determined by hydrogeologic and geologic factors, by inverse analogy, cave type and morphology could be used to determine the hydrologic and geologic conditions under which the caves developed. Mylroie and Carew (1990) used qualitative morphology to relate laminar recharge to coastal cave morphology (Figure 2.1). Palmer (1991, 2007, and 2011) was most successful in relating cave morphology to hydrology (Figure 2.2). Though he did not use morphometrics *per se*, he was qualitatively able to relate types of groundwater recharge and the structural character of the bedrock to cave patterns.

The “holy grail” of cave morphometric studies is to be able to quantify cave morphologies and relate the results to speleogenetic processes. To that end researchers, have used ratios of various parameters (length, width, area, and perimeter) measured and/or calculated from plan view cave maps to statistically differentiate cave types, with limited success. Roth (2004) established a series of morphometric parameters based on measurements from plan view cave maps to classify various Bahamian coastal caves. Stafford et al. (2006) employed maximum cave width vs. maximum cave entrance width to graphically differentiate cave morphologies on Tinian (Mariana Islands). Lace (2008) used similar methods to characterize coastal cave types in Puerto Rico and Waterstrat et al. (2010) used these parameters to differentiate between coastal dissolutional caves, littoral caves, and tafoni. The limitation to most of these methods is that they are best used for small to medium sized caves (less than a few kilometers in extent) with limited

vertical development, and with relatively simple morphologies. The other limitation is that the data were measured from plan view maps which are problematic in the study of features that are three-dimensional in nature, which all humanly passable caves are.

Curl (1986) took a different approach to measuring cave parameters, specifically length. He devised an elegant technique which included the survey line used to map the cave. His method filled the cave (via computer) with spherical-shaped linked modular elements (LME) that touched each other and the nearest walls of the cave. A LME that was the size of the distance to the nearest wall (lesser of the measured passage dimensions) was placed at each survey station. The distance between stations was occupied with more LMEs. The “length” of the cave was then determined by summing all sizes of the LMEs. The anthropocentric nature of the data (that which could be mapped by humans) gave a lowest LME size of 0.6 meters which Curl called the *proper modulus*. Curl (1986) determined that the statistical distribution of LME sizes were hyperbolic, thus exhibiting power law characteristics, and as a consequence were fractal in nature.

In other studies of individual caves based on the LME method, Curl (1986) was able to calculate the fractal dimension (the property of how an object fills space) and to estimate cave volume by assuming that the self-similarity extended to zero size. Coupling this with information from the known distribution of proper cave lengths in various regions, Curl (1966) was able to calculate that in limestone regions of Pennsylvania, there is a total of 2.1×10^7 cubic meters of cave space, 37% of which has a modulus below 1.0 meter, and 14% of which has a modulus below 1.0 centimeter. These results illustrated the utility of fractal geometry versus methods based only on Euclidean geometry.

The limitations of using the LME method in cave morphometrics is reiterated by Curl (1999) who noted that the method does not really settle the matter of measuring cave length and emphasized the subjective nature of anthropomorphic-based measurements.

Despite the uncertainty of how to actually interpret fractal indices, with enough contextual data, fractal geometry may be of use in characterizing natural phenomena, i.e. spatial objects, and processes in time, more adequately than by traditional Euclidian geometry. Fractal geometry has proven a useful tool in quantifying the structures of a wide range of idealized and naturally occurring objects. The range of application extends from pure and applied mathematics, to medicine, and through the natural and social sciences (Goodchild 1982, Plotnick et al. 1996, Melo 2007).

2.3.3 Euclidean versus Fractal Geometry

In Euclidean geometry, objects are composed of points, lines and polygons. More complex objects include planes, spheres, rectangular volumes, arcs, cylinders, etc. These objects can be classified as having an integer dimension which is its topological dimension. This also applies to Euclidean measures such as the circumference of a circle, a curve, or the boundary of any object. A line has one-dimensional topology because one number uniquely defines any point on it. Defining a point on a two-dimensional surface can be uniquely represented by two numbers and this is typically accomplished by gridding the surface and measuring two distances along the grid lines. The volume of a solid object is three-dimensional on the same basis as above; it takes three numbers to uniquely define any point within the object.

Mathematically describing the topological dimension in Euclidean geometry is a function of an object's change in size as the linear dimension increases (or decreases).

For example, if a three-dimensional object is scaled, the volume increases by the cube of the scale factor. The relationship between dimension D, linear scaling L and the resulting increase in size S is given as:

$$S=L^D \quad 2.1$$

In order to calculate topological dimension, the equation is rewritten as:

$$D=\text{Log}(S)/\text{Log}(L) \quad 2.2$$

The equation results in an expression for topological dimension depending on how the size of the object changes as a function of linear scaling. In Euclidian geometry, the value of D is an integer depending on the actual geometry of the object (point = 1, versus line = 2, versus cube = 3).

In mathematics and in nature, there are morphologies that do not conform to integer-based dimensionality (Bourke 1991). The dimensions of those forms have a value that exceeds their topological dimension and is actually between it, and is referred to as the fractal dimension. These are geometries that lie in a plane but if they are linearly scaled by a factor L, the area does not increase by L-squared but by some non-integer amount. These are fractals. The classic Koch Snowflake (Figure 2.3) has a fractal dimension of 1.2619. The fundamental differences between Euclidian and fractal geometry are summarized in Table 2.1.

A fractal is defined as a rough or fragmented geometric shape that can be subdivided into parts, each of which is approximately a reduced-size copy of the whole (Veena et al. 2009). The term fractal, originally coined by Benoît Mandelbrot (1983), has its root from the Latin *fractus* meaning “broken” or “fractured”. The defining properties

of fractals are self-similarity and scaling, either in an exact geometric sense or in a statistical sense (Klinkenberg 1992). Fractals in nature differ from mathematically-derived fractals in that the former exhibit fractal behavior over limited space and time scales whereas the latter display infinite self-similarity and scaling. (Bassingthwaight et al. 1994).

2.3.4 Fractal Indices

Mandelbrot (1983) noted that two fractals with different morphologies may have the same fractal dimension. As a consequence, fractal dimension alone does not provide a unique morphological specification. But there are other fractal indices that are complementary to fractal dimension that can be extended to the description of the spatial distribution of fractals and these were considered in this research. Lacunarity, which characterizes the *gappiness* of a fractal, and is a measure that provides more detail about the homogeneous versus heterogeneous “texture” of a fractal, can be used as a complement to fractal dimension (Melo 2007). Though fractal dimension is most commonly used in fractal and pattern analysis and recognition, lacunarity is also used though not as commonly (Plotnick 1996). Both indices are used in the fields of medicine, dentistry, and in physical and natural sciences (Plotnick 1996, Melo 2007).

There is one more fractal index that has seen very limited use in fractal analysis called succolarity. This fractal index description, as explained by Mandelbrot (1983), is that succolating fractals include filaments that would have allowed percolation. Mandelbrot (1983) does not offer any means of determining succolarity. Melo (2007) described succolarity as the percolation degree of an image, i.e. how a given fluid can

flow through the image. Though Melo (2007) presented a theoretical approach for calculating succolarity; this index was not be utilized for this research.

It is important to keep in mind for all fractal indices that they are descriptive in nature rather than an indicator of genesis or function, i.e. they are measures of the morphologic property of an object. Any interpretation based on fractal indices must be made within the constraints of the natural system that holds the fractal object.

2.3.4.1 Fractal Dimension

Fractal dimension is an index used as a numerical measure of an object's complexity (surface roughness) and reflects its scale invariance. It describes how an object occupies space and is related to the complexity of its structure. Sample independence or scale invariance measures have a physical significance since the average of their spatial means does not depend on the scale (or dimension of space) over which they are averaged (Klinkenberg 1992). Theoretically, scale invariance or fractal measures allow extrapolations from properties observed at one scale to properties of a scale that have not been observed (Gilbert 1989).

There are a number of different methods to calculate fractal dimension including similarity dimension (Mandelbrot 1993), Hausdorff dimension (Grassberger 1981, Falconer 1990), box counting dimension (Block et al. 1990, Falconer 1990), information dimension (Falconer 1990), correlation dimension (Addison 1997, Weisstein, 2006), and pointwise and average pointwise dimension (Addison 1997). This research used the box counting dimension (fixed and sliding) to calculate fractal dimension and lacunarity. Fractal dimension was calculated using FRACTAL© version 3.4.7 (the

software author provided a one-year usage license for this study), and lacunarity values were generated using ImageJ plug-in FracLac, developed by the National Institute of Health, to work with digital images. The fixed-box counting method application was for calculating fractal dimension and the sliding-box method for determining lacunarity.

The box counting method for determining fractal dimension, originally called the Minkowski–Bouligand dimension (Falconer 1990) is conducted with image processing software which can use either a binarized or grayscale digital image of the object to be analyzed. The object is covered with just enough boxes (N) of size δ (δ^2 for squares, δ^3 for cubes) to completely encompass it. The values for N and δ are used in the following equation which calculates the fractal dimension D:

$$D = \left[\lim_{\delta \rightarrow 0} \frac{\log(N\delta)}{\log(1/\delta)} \right] \quad 2.3$$

As an example, (Figure 2.4A), a digital image is covered with a grid of size δ and the number of boxes (N) that covers the image is counted ($N\delta$). A second, finer grid is placed on the image and the process is repeated. The number of iterations is determined by the user. By Equation 2.3, fractal dimension = $\log(69/29/\log 2) = 1.25$. The values for $\log(N\delta)$ are plotted against $\log(1/\delta)$ (Figure 2.4B) and a straight line joins the plotted values. The slope of that line is the fractal dimension $D = 1.25$.

2.3.4.2 Lacunarity

Lacunarity is a measure of the *gappiness* or homogeneous versus heterogeneous texture of an object. The root of the word is from the Latin lacuna, which translates to “lake” or “gap”. Lacunarity is a complement to fractal dimension and it can improve the textural description of a fractal (Rauch 2007). The property of lacunarity is a function of

the distribution of gaps (or holes) within the fractal. According to Mandelbrot (1983), a fractal is said to be lacunar if the gaps that it contains are large. Fractals with large gaps may also be translationally or rotationally invariant (Plotnick et al. 1996) (Figure 2.5 A-D).

Just as there are different ways to calculate fractal dimension, the same holds for lacunarity. For this study, lacunarity was calculated with the sliding box scanning method utilized by FracLac which is a plug-in for ImageJ image processing software. The application bases its analysis on pixel distribution that is obtained from sliding box scanning (Figure 2.6) at different box sizes and grid orientation. This method differs from the fixed-box method (Figure 2.4B) used for fractal dimension where the image is sampled only once. Sliding-box scanning averages the pixels per box as opposed to just counting the number of pixel-containing boxes as is done for fixed-box scanning. The equation for lacunarity calculation is

$$\lambda_{\epsilon g} = CV_{\epsilon g} = (\sigma/\mu)^2_{\epsilon g} \quad 2.4$$

where λ is lacunarity, CV = coefficient of variation (standard deviation/mean), σ is the standard deviation and μ is the mean for pixels per box at size ϵ in a box count at orientation g .

The value for lacunarity is calculated using the pixel distribution that is defined by the number of pixels in each ϵ -sized box in the grid. The lacunarity for each grid of size ϵ is then calculated from the standard deviation, σ , and mean, μ , for pixels per box. Consequently, there is a λ value for each ϵ in each series of grid sizes in each g , grid orientation, in a set of grid orientations. FracLac graphs the data ($\ln\lambda$ vs. $\ln\epsilon$) (Figure 2.7),

and can distill all of the data into one value for lacunarity and does so by summarizing data over all grid orientations, i.e. the mean of the means for the image.

Degree of lacunarity is used to characterize the texture of a fractal. A high lacunarity means that the fractal is texturally heterogeneous (Mandelbrot 1983). Fractals with small gaps (and low lacunarity) are classified as homogeneous (Melo 2007). Along with the lacunarity index, descriptors of fractal texture (gappiness, heterogeneity, homogeneity, and translational or rotational invariance) can be used as modifiers to differentiate fractals that have the same fractal dimension.

2.4 Methods

The indices of fractal dimension and lacunarity were calculated for a set of known types of caves with varying morphologies. Karstic (dissolutional) and pseudokarstic caves were included in this study. The karstic caves included allogenic stream caves, continental hypogene caves, and flank margin caves. The cave types analyzed in this research occur in a variety of geographical locations and geological environments. The pseudokarst cave types used in this study were littoral caves from the Channel Islands of California and the Bahamas, and tafoni that were exclusively from Quaternary eolianites of the Bahamas.

2.4.1 Data acquisition and image processing

The baseline data for this research were digital cave survey data, and cave maps whenever digital data were not available. A variety of caves of known type were processed in order to determine characteristic fractal dimension and lacunarity for cave

types. Tables A.1-A5 of Appendix A list the cave types and sample sizes used for this study.

All survey data were processed with COMPASS data reduction software which generates text-based data files, line plots (two and three-dimensional) in plan and profile, and 3D-shapefiles. COMPASS is shareware software, produced by Larry Fish, which processes and plots cave survey data and exports data in a variety of file formats. Hard copy cave maps were scanned and digitized using the COMPASS application Map-to-Data that creates COMPASS data files from the digitized data. Cross sections, profiles, and known vertical extent were used to augment vertical data on digitized maps.

Processed COMPASS data were plotted and displayed on the COMPASS plot viewer. Data from caves with a vertical extent of less than 20 meters were exported from the viewer in grayscale as 3D shapefiles. Caves with vertical extent of greater than 20 meters were sliced into vertical layers or stacks of equal value (depending on vertical extent of cave), and each layer exported as a grayscale bitmap image for compilation by the image processing software. This was done within the Compass Viewer using the “Set Complex: Exclude by Depth” function.

Three software packages were utilized for image processing. ArcScene10.2® was used to produce 3D grayscale image files from the caves with less than 20 meters of vertical extent. Fractal dimension was calculated using FRACTAL© version 3.4.7 which can process individual grayscale bitmap files or stack-series files. Lacunarity was calculated with ImageJ plug-in FracLac, a freeware developed by National Institute of Health. FracLac calculates lacunarity from the same file formats used to determine fractal dimension.

FRACTAL© version 3.4.7 and FracLac analyze digital images using box-counting and sliding-box-counting functions. FRACTAL© version 3.4.7 calculates a fractal dimension value (as per equation 2.3) and also provides exportable raw data used to generate log-log plots. ImageJ generates a distilled value for lacunarity (as per Equation 2.4) and also provides the raw data used in lacunarity calculations. Data resolution for both fractal indices were recorded to 10^{-4} in order to capture subtle variations between cave-type morphology.

2.4.2 Statistics

Fractal dimension and lacunarity values were exported to Sigmaplot™ for descriptive statistics and for statistical analyses. The Shapiro-Wilk test was run on the data sets to test for normality. Because the data did not pass normality testing, non-parametric analyses were used. For fractal dimension, the Kruskal-Wallis One-way Analysis of Variance by Ranks was the statistical test used to determine if there were statistically significant differences in fractal dimension between cave types. The Friedman Repeated Measures Analysis of Variance on Ranks method was used to test statistical significance of difference of data for lacunarity. To compare specific cave types to each other the Student-Newman-Kuels method was used for both fractal indices.

Linear regression analyses was conducted on the data set in order to determine if there was a relationship between lacunarity (dependent variable) and fractal dimension (independent variable).

2.5 Results

. Fractal dimension and lacunarity data were analyzed descriptively and with statistical tests, and the results are listed in the following sections.

2.5.1 Descriptive statistics

Descriptive statistics for fractal dimension data are summarized in Table 2.2, and displayed in Figure 2.8A via box plots for cave types. Table 2.3 summarizes descriptive statistics for lacunarity data and Figure 2.8B shows box plots for cave types and lacunarity.

Examples of cave morphologies along with fractal indices were compared and summarized in Figures 2.9-2.13. Each figure shows a range of actual cave morphologies from simplest to most complex for both fractal dimension and lacunarity.

2.5.2 Statistical tests

Statistical analyses of fractal dimension and lacunarity data were conducted in order to determine if these morphometric parameters could differentiate cave type. The data were tested for normality using the Shapiro-Wilk test to a threshold of $p < 0.050$. The analysis showed that the data were not normally distributed.

The statistical test used to compare fractal dimension for cave types was the Kruskal-Wallis One-way Analysis of Variance by Ranks whose parametric equivalent is the one-way analysis of variance test (ANOVA). The Kruskal-Wallis test is a non-parametric method that tests if samples originate from the same distribution and compares two or more samples that are independent. The results, summarized in Table

2.4, indicated that the differences in the median values among the cave types are greater than would be expected by chance and that the difference is a statistically significant ($P = <0.001$).

In order to test which groups were different from each other and how different they were, the post hoc Student-Newman-Keuls method was used to determine variation between specific pairs of cave type. The results are displayed in Table 2.5. The test showed that there is a significant difference in fractal dimension between cave types.

Analyses were conducted on lacunarity for the different cave types. The data were tested for normality using the Shapiro-Wilk test with a threshold of $p < 0.050$. The analysis showed that the data were not normally distributed. The statistical test used to compare lacunarity for cave types was the Friedman Repeated Measures Analysis of Variance on Ranks test whose parametric equivalent is the one-way analysis of variance test (ANOVA). This is a non-parametric method that tests if samples originate from the same distribution, and compares two or more samples that are independent. The results, summarized in Table 2.6, indicated that the differences in the median values among the cave types are greater than would be expected by chance and that the difference is statistically significant ($p = <0.001$).

As with fractal dimension, the post hoc Student-Newman-Keuls method was used to determine variation between specific pairs of cave types and the results are shown in Table 2.7. With the exception of hypogene versus littoral caves, all other pairs of cave types tested to be statistically different.

Regression analyses were run for fractal dimension (independent variable) versus lacunarity (dependent variable). Figure 2.14 shows a series of graphs illustrating the

results of the regression analyses for each cave type. These data are listed in Table 2.8. The only cave type that showed a relationship between fractal dimension and lacunarity were allogenic stream caves.

2.6 Discussion

According to Palmer (2007), cave type is determined by the interplay of mode and scale of recharge, and the structural characteristics of the rock (Figure 2.2). The focus of this research was to ascertain if cave types could be distinguished with fractal indices, to determine the relationship of those indices, and to attempt to describe the values within the geologic and hydrologic context of the cave types. Results of data analyses are explained in the following sections.

2.6.1 Analysis of descriptive statistics

Descriptive statistics for fractal dimension for different cave types are summarized in Tables 2.4A. Hypogene caves have the largest range of values for fractal dimension which is to be expected for the morphologies of a cave type with a diversity of recharge modes (H₂S oxidation zones, rising thermal water, deep mixing zones) operating over regional hydrologic scales. Figure 2.9 displays this variety of form though it does not illustrate the vertical component of the caves due to the limitations of two-dimensional representations. Lacunarity range in hypogene caves ranks third among the 5 cave types. The maze nature of hypogene caves, can result in textures that approach appearing homogeneous.

Allogenic stream caves (Figure 2.11) rank second in fractal dimension range though considerably lower than hypogene caves. Allogenic stream caves have two modes

of recharge (sinking streams and sinkholes) that operate over local hydrologic conditions though they do form across the same spectrum of structural rock characteristics as hypogene caves. They rank highest in lacunarity values and overall range of lacunarity values which is attributable to the linear nature of the cave pattern, which increases in heterogeneity as the pattern complexity increases. Exceptions to the linearity of allogenic stream caves are commonly caused by floodwater mazes at restrictions or breakdown, and/or in their multi-level development due to changes in base level which adds a vertical maze component to their morphology.

Littoral caves (Figure 2.12) rank third in fractal dimension range and are fourth in lacunarity range. The narrow fractal dimension and lacunarity ranges expressed in this analysis may be a result from using samples from only two geographic sites (Channel Islands, California and the Bahamas). The caves from both of those reasons did not vary greatly in pattern appearance. This may be a function of development restricted to coastal zones though the rock types did from strictly carbonates in the Bahamas to a wider range of rock types on the Channel Islands. Flank margin caves (Figure 2.10) came in fourth in fractal dimension range and second in lacunarity range. They have a narrow range of pattern types because their formation is restricted to the coastal environment.

Tafoni that formed in Quaternary eolianites of the Bahamas (Figure 2.13) were the least variable in morphology as indicated in the fractal indices. The conditions under which they form are restricted to those areas subject to wind erosion but out of the reach of sea spray (Owen 2013).

2.6.2 Analysis of statistical tests

An important question in this study was whether or not each cave type had a characteristic range of fractal indices and if so, whether the differences between cave types were statistically significant. Statistical tests compared fractal dimension (Table 2.5A) and lacunarity (Table 2.5B) of all five cave types. In order to test degree of difference between groups, the post hoc Student-Newman-Keuls method was used to determine variation between specific pairs of cave types and the results are summarized in Tables 2.6A and 2.6B).

2.6.2.1 Analyses of fractal indices between all cave types

The most morphologically complex caves are continental hypogene caves and the highest values for fractal dimension occurred in the hypogene group. These caves form three-dimensional mazes that give high fractal dimension values i.e. high measure of object complexity. However, lacunarity values are low because high density cave passage cave patterns express a homogeneous textural appearance.

The fractal dimension values for flank margin caves ranked directly below hypogene caves. Flank margin caves can have very complex footprints, but they are typically much less developed in vertical extent than hypogene caves or stream caves. However, their lacunarity values are higher than those of hypogene caves because the mazes they form are not as three-dimensionally dense and therefore more heterogeneous in texture.

Allogenic stream cave fractal dimensions are less than flank margin caves but well above littoral caves. In nature, allogenic stream caves are very linear though they can have complex local patterns as stated above. Their linearity is what makes for a less

complex three-dimensional pattern. However, their linearity also gives much higher lacunarity values than the other cave types i.e. the cave morphologies are more heterogeneous.

Caves with the lowest fractal dimension and lacunarity are littoral caves and tafoni respectively. This was reflected in the data, with tafoni caves having the lowest values for fractal dimension and littoral caves just a little bit higher. There is some degree of latitude in terms of littoral cave morphologies because of wave energy versus configuration of the coastline and variations in rock structure and lithologies. Tafoni had the lowest fractal index values because of their restricted geologic and geographic location i.e. the sample groups was exclusively from quaternary eolianites from the Bahamas. Their simple morphology also gives them a very homogeneous morphological texture.

2.6.2.2 Analyses of fractal indices between specific cave types pairs

In order to test which groups are different from each other and how different they were, the post hoc Student-Newman-Keuls method, was used to determine variation between specific pairs of cave type and the results are summarized in Tables 2.6.

Fractal dimension between pairs is summarized in Table 2.6A. Hypogene and flank margin caves ranked the closest in fractal dimension in terms of similarity in morphology. Though both cave types formed in very different geologic conditions and diagenetic maturity of the rock is telogenetic in the former versus epigenetic in the latter, both cave types are initially formed by mixing zone corrosion so their overall morphologies are similar.

Hypogene caves versus tafoni showed the biggest difference in fractal dimension morphology. In nature, their modes of genesis are distinctly different with hypogene caves formed by mixing-zone corrosion and tafoni by mechanical erosion. Hypogene caves are karstic whereas tafoni are classified as pseudokarst (Owen 2013).

Flank margin caves and littoral caves ranked significantly different in terms of fractal dimension. Flank margin caves form by mixing zone corrosion whereas littoral caves formed by mechanical erosion which also makes them pseudokarstic. It should be noted that flank margin caves that have been exposed to erosion by wave energy may become overprinted by littoral erosion and can be confused with littoral caves.

The data show that littoral caves and tafoni have the second most similar fractal dimension morphology and their q value (mean difference and variance) is much higher than that of hypogene and flank margin caves.

Lacunarity is compared between specific cave types in Table 2.6B. Allogenic stream caves and tafoni showed the biggest difference in lacunarity and hence texture, with allogenic stream caves having a very heterogeneous morphological texture versus tafoni which are very homogeneous. Allogenic stream caves form by turbulent flow recharge and the origin of the Bahamian tafoni is from wind erosion (Owen 2013).

The lacunarity of hypogene and littoral caves show similar low values of lacunarity and the tests indicate that they cannot be effectively differentiated within the existing data set. Both cave types originate from vastly different geologic conditions, but the low lacunarity value of hypogene mazes result from their dense passage configuration that gives them a homogeneous morphologic texture. The low lacunarity value of littoral caves results from their very simple morphology which also expresses as homogeneous

morphological texture. This situation illustrates the value of using two independent fractal indices to describe cave type. Hypogene caves will display high fractal dimension and low lacunarity. Littoral caves will display very low fractal dimension and low lacunarity.

Allogenic stream caves, flank margin caves and littoral caves compared more closely in terms of lacunarity than other types.

2.6.3 Regression analysis

Regression analyses were done in order to determine if there is a relationship between fractal dimension and lacunarity. These data are summarized in Table 2.7 and illustrated in Figure 2.14. The only cave type where fractal dimension and lacunarity showed a strong relationship was in allogenic stream caves, which gave an r^2 of 0.85. All other cave types showed no indication of relationship between these two parameters.

The allogenic stream cave data set contains cave patterns formed by recharge processes (recharge via sinking streams and sinkholes) that are very similar so the patterns they produce are also similar. This may account for the strong relationship between fractal dimension and lacunarity values. The overall pattern trend shows that the more complex the fractal dimension, the more heterogeneous its pattern and this is mirrored in the regression analysis.

The continental hypogene cave regression analysis gave an r^2 of 0.258. The lack of relationship between the two parameters may be because the regression analysis was comparing a mix of recharge-resultant textures instead of comparing textures within specific recharge types (H_2S oxidation zones, rising thermal water, deep mixing zones). Specific recharge mode is not identified in the continental hypogene data set so it is

currently not possible to test if each recharge mode has a subset of characteristic fractal indices.

Flank margin caves show no relationship between fractal dimension and lacunarity ($r^2=0.0159$). This may be due to two factors: the coastal location of the flank margin cave and the degree of development. Flank margin caves form at the distal end of a freshwater lens which tracks the edge of a carbonate coast. Freshwater lens morphology will vary depending on its location with respect to linear sections of the coast versus irregular sections like at embayments or changes in coastline trend. The flank margin cave morphology will reflect lens morphology. Flank margin cave footprint can vary from configurations that parallel a linear coast, to ones that wrap around a coast of changing trend. Early in the development of flank margin caves they form as small dissolutional voids which, through time, enlarge and join with other voids (Labourdette et al. 2006). The lack of linear relationship between flank margin cave fractal dimension and lacunarity may be similar to that of hypogene caves i.e. subtle differences in recharge configurations.

2.7 Summary

The results of this research indicate that fractal indices have the potential to be effectively used to describe cave morphologies and to quantitatively distinguish cave types. The results were successfully analyzed within the geological, hydrological, and geographical contexts in which the cave types were formed.

However there are a number of limitations to this study. All of the caves used were known entities with respect to types, so there may be sampling bias in terms of cave selection. Littoral cavers were limited to cave data from two locations: Channel Islands,

California USA, and the Bahamas. Tafoni analyzed were exclusively from Bahamian Quaternary eolianites. Tafoni occur in a wide-range of rock types on a world-wide scale. Sampling size for each cave type was the minimum necessary for statistical analyses (30 from each cave type). The data set did not include caves formed from diffuse discharge, network mazes, or anastomotic mazes. The larger cave systems analyzed in this research were treated as mono-fractals whereas it may have been more appropriate to analyze them as multi-fractals. It is currently uncertain if relevant comparisons can be made between mono- and multi- fractals and more analysis is necessary to make that determination.

Table 2.1 Comparison of Euclidean and fractal geometries

Properties of Euclidean vs. Fractal Geometry	
Euclidean geometry	Fractal geometry
Describes simple shapes (points, lines, polygons)	Can describe geometries found in nature (irregular shapes)
Based on characteristic size or scale and a few characteristic sizes or length scales i.e. radius of a circle, length of a side of a cube	No specifically defined size or scale, are self-similar and independent of size or scaling
Can be defined by a simple equation	Defined by algorithm

Modified from Falconer 1990

Table 2.2 Descriptive statistics – Fractal dimension for cave types

Cave type	Range	Maximum	Minimum	Mean	Median	25%	75%
Hypogene	0.466	2.754	2.288	2.438	2.398	2.338	2.456
Allogenic stream	0.191	2.298	2.107	2.209	2.208	2.174	2.253
Littoral (sea caves)	0.187	2.200	2.012	2.075	2.071	2.037	2.096
Flank margin	0.177	2.460	2.238	2.359	2.357	2.328	2.389
Tafoni	0.079	2.079	2.000	2.018	2.010	2.001	2.029

Table 2.3 Descriptive statistics - Lacunarity for cave types

Cave type	Range	Maximum	Minimum	Mean	Median	25%	75%
Allogenic stream	10.156	11.975	1.816	4.763	4.667	2.678	5.918
Flank margin	3.098	3.257	0.158	1.879	1.951	1.059	2.749
Hypogene	2.188	2.625	0.437	1.218	1.178	0.739	1.561
Littoral (sea caves)	1.212	1.424	0.212	0.972	1.072	0.768	1.266
Tafoni	0.530	0.632	0.112	0.264	0.249	0.226	0.277

Table 2.4 Kruskal-Wallis One Way Analysis of Variance on Ranks test

Differentiating Cave Types by Fractal Dimension				
Group	N	Median	25%	75%
Flank margin caves	30	2.357	2.325	2.392
Continental hypogene caves	30	2.398	2.337	2.470
Allogenic stream caves	30	2.208	2.171	2.254
Tafoni	30	2.010	2.001	2.030
Littoral caves (sea caves)	30	2.071	2.036	2.097

H = 133.277 with 4 degrees of freedom. (P = <0.001)

Table 2.5 Student-Newman-Keuls Method – Fractal Dimension

Comparisons between cave types by fractal dimension			
Cave types	Comparison of ranks	q	P<0.05
Hyp vs. Taf	3235.500	13.597	yes
Hyp vs. Lc	2455.500	12.888	yes
Hyp vs. St	1532.500	10.710	yes
Hyp vs. Fmc	329.000	3.439	yes
Fmc vs. Taf	2906.500	15.255	yes
Fmc vs. Lc	2126.500	14.861	yes
Fmc vs. St	1203.500	12.582	yes
St vs. Taf	1703.000	11.902	yes
St vs. Lc	923.000	9.659	yes
Lc vs. Taf	780.000	8.154	yes

Fmc: flank margin; Hyp: continental hypogene; St: stream; Taf: tafoni; Lc: littoral (sea cave)

Table 2.6 Friedman Repeated Measures Analysis of Variance on Ranks

Differentiating Cave Types by Lacunarity				
Group	N	Median	25%	75%
Flank margin caves	30	1.951	1.058	2.770
Continental hypogene caves	30	1.178	0.731	1.620
Allogenic stream caves	30	4.677	2.639	5.927
Tafoni	30	0.249	0.225	0.278
Littoral caves (sea caves)	30	1.072	0.731	1.273
Chi-square=96.773 with 4 degrees of freedom. (P = <0.001)				

Table 2.7 Student-Newman-Keuls Method - Lacunarity

Comparisons between cave types by lacunarity			
Cave types	Comparison of ranks	q	P<0.05
St vs. Taf	116.000	13.395	yes
St vs. Lc	73.000	10.324	yes
St vs. Hyp	68.000	12.415	yes
St vs. Fmc	43.000	11.103	yes
Fmc vs. Taf	73.000	10.324	yes
Fmc vs. Lc	30.000	5.477	yes
Fmc vs. Hyp	25.000	6.455	yes
Hyp vs. Taf	48.000	8.764	yes
Hyp vs. Lc	5.000	1.291	no
Lc vs. Taf	43.000	11.103	yes

Fmc: flank margin; Hyp: continental hypogene; St: stream; Taf: tafoni; Lc: littoral (sea cave)

Table 2.8 Regression Analysis of Fractal dimension versus Lacunarity

Cave Type	r ²
Continental hypogene caves	0.253
Flank margin caves	0.016
Littoral caves (sea caves)	0.004
Tafoni	0.002
Allogenic stream caves	0.850

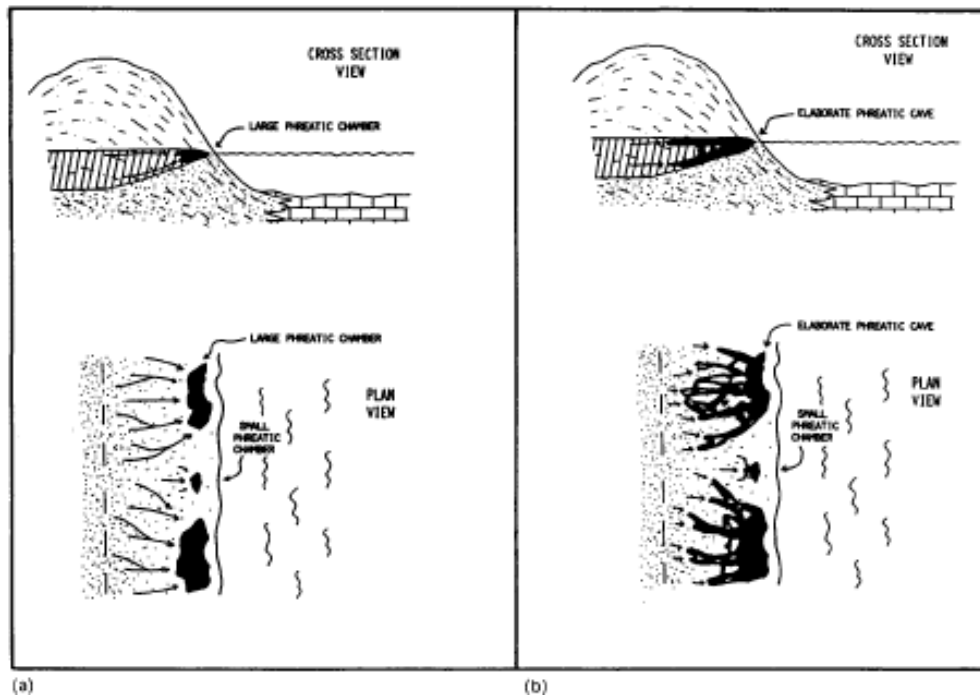


Figure 2.1 Cave pattern at mixing corrosion zone

From Mylroie and Carew 1990

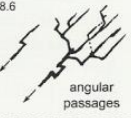
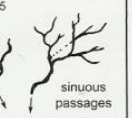
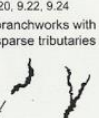
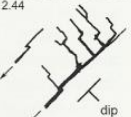
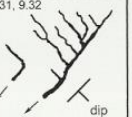


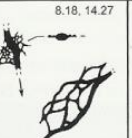

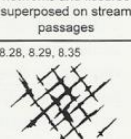
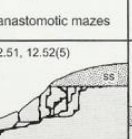
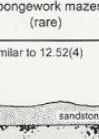

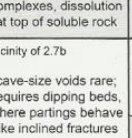
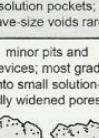
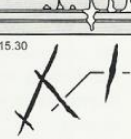
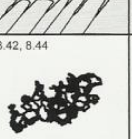

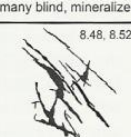
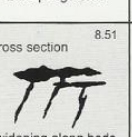

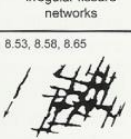
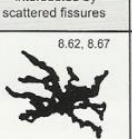
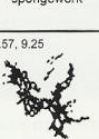
		GENERAL CAVE PATTERN	STRUCTURAL CHARACTER OF ROCK			
			fractures	bedding-plane partings	intergranular pores	
RECHARGE TYPE	KARST DEPRESSIONS	Branchwork stream passages, usually in multiple tiers. Also single-passage stream caves. Vadose passages trend mainly down the dip. Passages are sinuous in bedded rocks, angular in highly fractured rocks.	gentle dip 8.6 	8.5 	9.20, 9.22, 9.24 branchworks with sparse tributaries 	
			steep dip 2.44 	9.31, 9.32 	may disperse into non-traversable openings 	
	DIFFUSE	sinking streams (great discharge fluctuation)	Crude branchworks and single-passage stream caves, with network or anastomotic diversions and flood-water injection features. Some are formed along stream banks, swamps, or lakes	8.16, 8.17, 8.21, 8.22 	8.18, 14.27 anastomotic mazes 	8.19 spongework mazes (rare) 
		through overlying or underlying insoluble rock	Extensive networks, shaft-canyon systems, or porosity zones, according to rock structure. Caves concentrate just below the base of the insoluble rock	8.28, 8.29, 8.35 	12.51, 12.52(5) shaft and canyon complexes, dissolution at top of soluble rock 	similar to 12.52(4) solution pockets, cave-size voids rare 
	HYOGENIC	into porous or fractured soluble rock	Epikarst and shallow networks in fractured rock, formed by dispersed recharge to all fissures. Rudimentary spongework in porous rock.	2.12, 8.26 epikarst 	vicinity of 2.7b cave-size voids rare; requires dipping beds, where partings behave like inclined fractures 	minor pits and crevices; most grade into small solutionally widened pores 
		coastal or deep mixing zones	Spongework and crude ramifying caves in porous coastal limestones. Networks and single fissures in deep mixing zones.	15.30 scattered fissures, many blind, mineralized 	8.42, 8.44 2-D spongework 	2.58, 8.41 spongework, crude ramifying caves 
		rising thermal water usually mixed with shallow water	Irregular fissure networks. Widening along bedding is possible, but with fissures below. Spongework in porous rock.	8.48, 8.52 irregular fissure networks 	cross section 8.51 widening along beds intersected by scattered fissures 	15.25 spongework 
		sulfuric acid in H ₂ S oxidation zones	Irregular networks, 2-D and 3-D spongework. Scattered large rooms may be present. Fissures commonly extend into floors. Some contain active streams.	8.53, 8.58, 8.65 networks, some isolated fissures 	8.62, 8.67 ramifying patterns and 2-D spongework 	8.57, 9.25 3-D spongework, ramifying patterns 

Figure 2.2 Cave patterns classification

Cave patterns classified by recharge type and the structural character of the bedrock in which the cave formed. From Palmer 2007

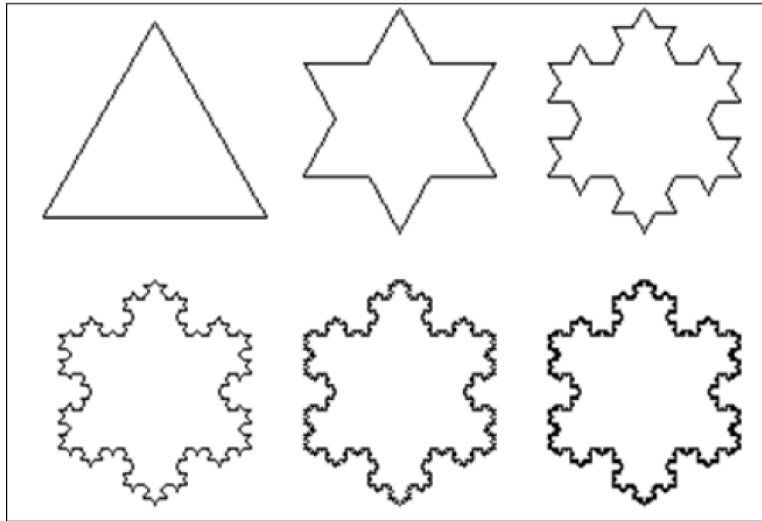


Figure 2.3 Koch Snowflake, one of the earliest fractal curves to be described.

From Addison 1997

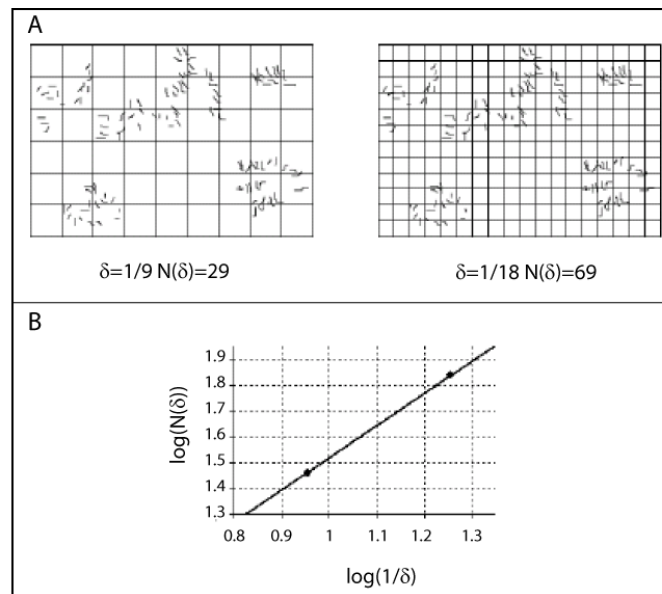


Figure 2.4 Box counting method

(A) Different sized grids (boxes) are used to measure the occurrence of pixels in each grid box. (B) illustrates the log-log plot of number of boxes vs. resolution of boxes. The fractal dimension is the slope of the line between the two points. After Falconer 1990

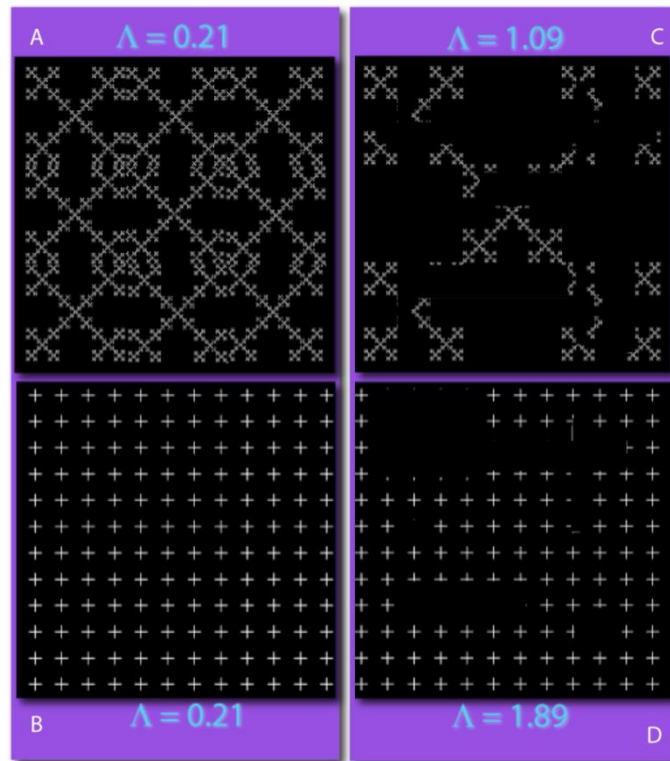


Figure 2.5 Examples of lacunarity

(A) is similar to (B) as both have the same number of black and white pixels in terms of homogeneity and translationally and rotationally invariant patterns as reflected in the equal value for lacunarity. (C) and (D) display a greater variation (are more heterogeneous) and since they have irregular gaps are not rotationally or translationally invariant. This invariance is reflected in their lacunarity values. It is not visually obvious that (D) has greater lacunarity than (C). From ImageJ FracLac User's Manual 2012.

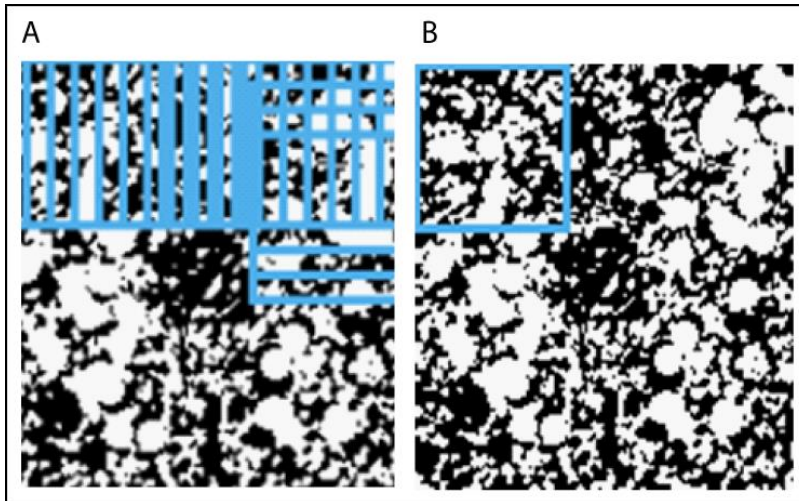


Figure 2.6 Sliding box counting method

(A) Sliding box counting method versus fixed box counting method (B). From ImageJ FracLac User's Manual 2012

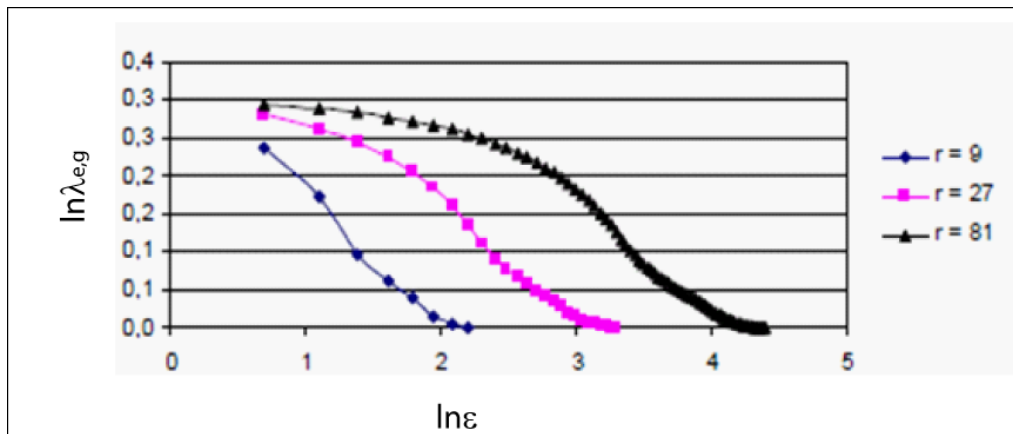


Figure 2.7 Lacunarity values from the sliding box counting method

Graph of $(\ln \lambda$ vs. $\ln \epsilon)$ at three resolutions ($r=9, 27, 81$). Lacunarity is calculated using the pixel distribution (number of pixels in each box). The lacunarity for each grid of size ϵ is then calculated from the standard deviation, σ , and mean, μ , for pixels per box. There is a λ value for each ϵ in each series of grid sizes in each g , grid orientation, in a set of grid orientations. FracLac graphs the data $(\ln \lambda$ vs. $\ln \epsilon)$. The software can distill all of the data into one value for lacunarity and does so by summarizing data over all grid orientations i.e. the mean of the means for the image (Mere 2007).

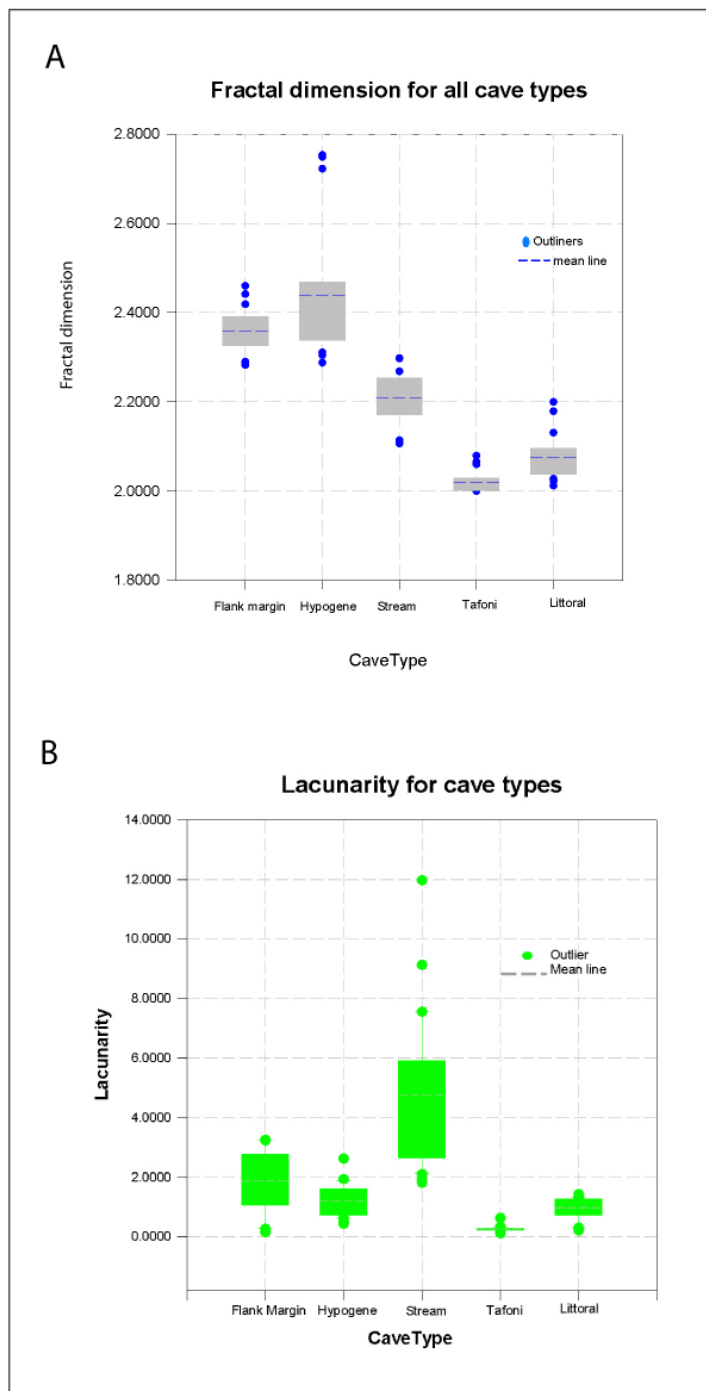


Figure 2.8 Box plots summarizing descriptive statistics for fractal indices
 Descriptive statistics for (A) fractal dimension, (B) lacunarity

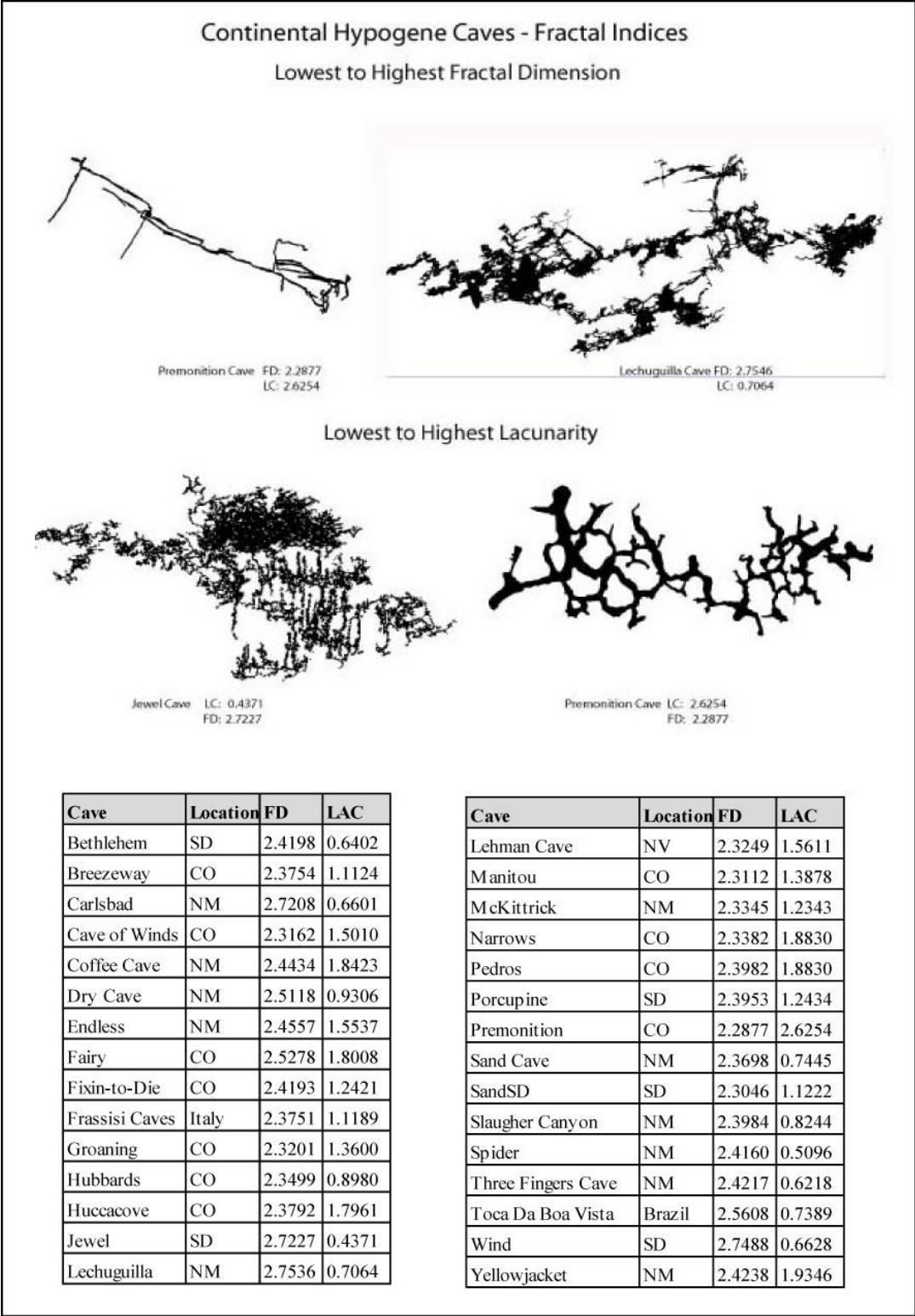


Figure 2.9 Hypogene cave fractal indices and morphological examples

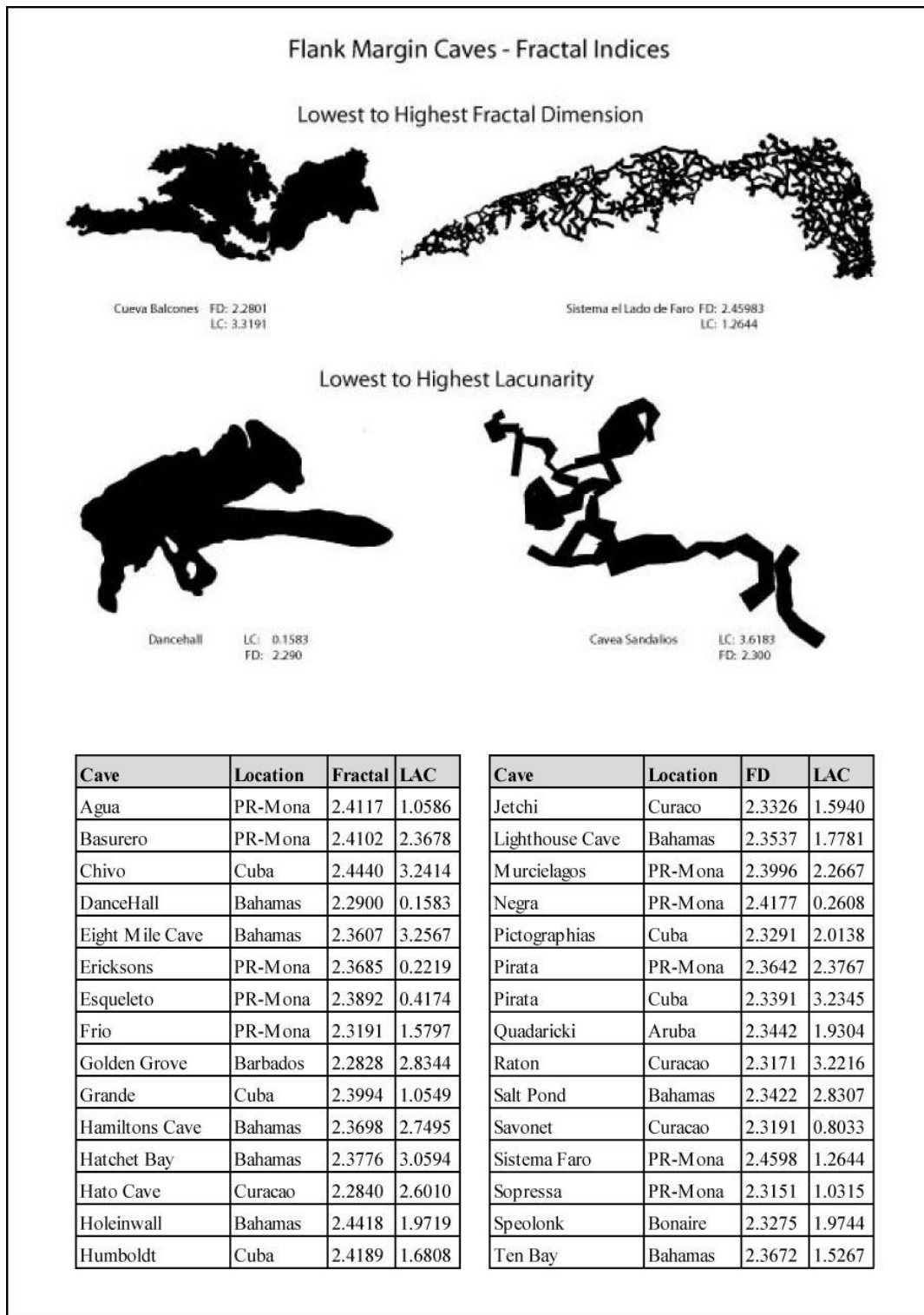


Figure 2.10 Flank margin cave fractal indices and morphological examples

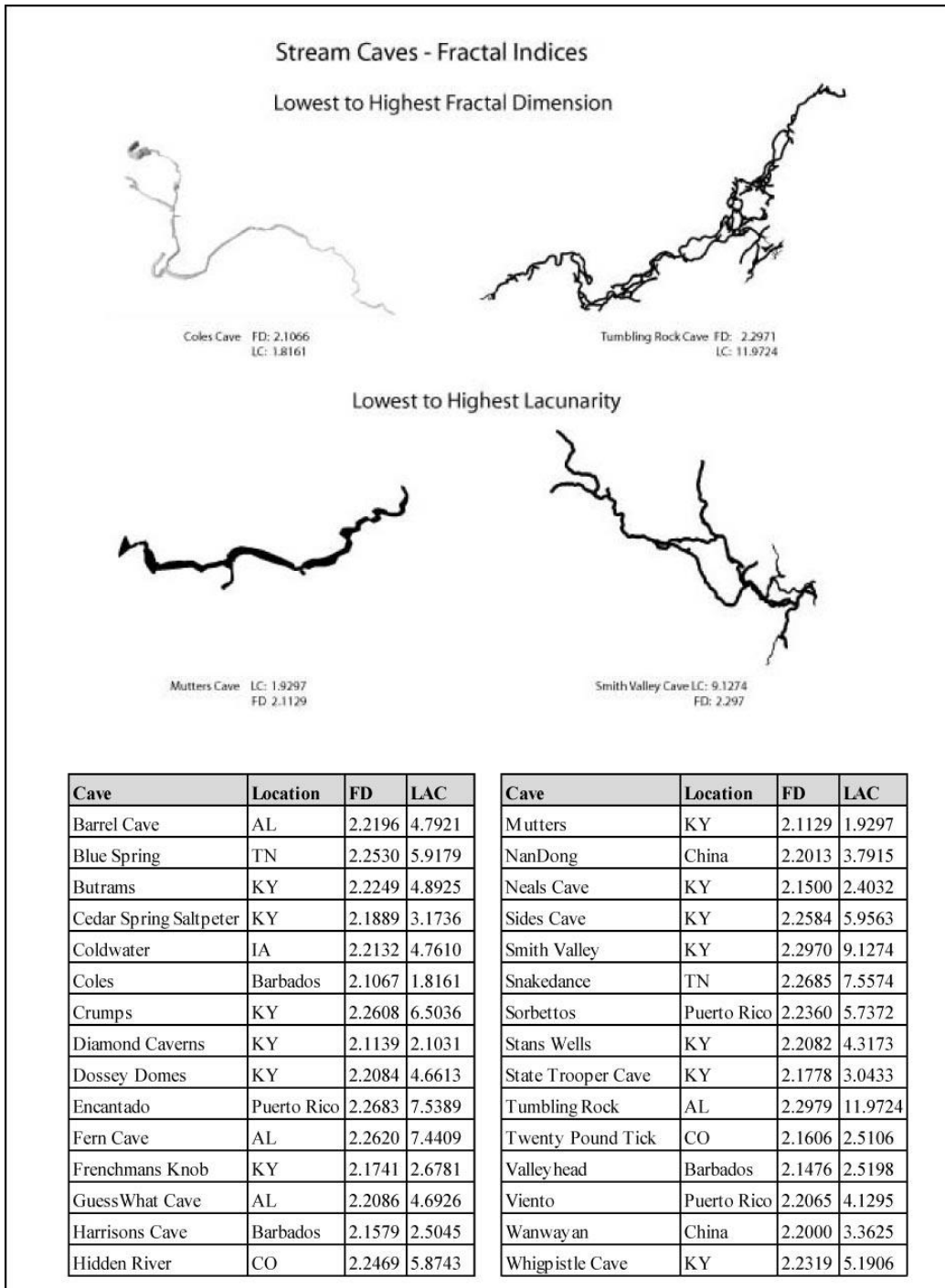


Figure 2.11 Allogenic stream cave fractal indices and morphological examples

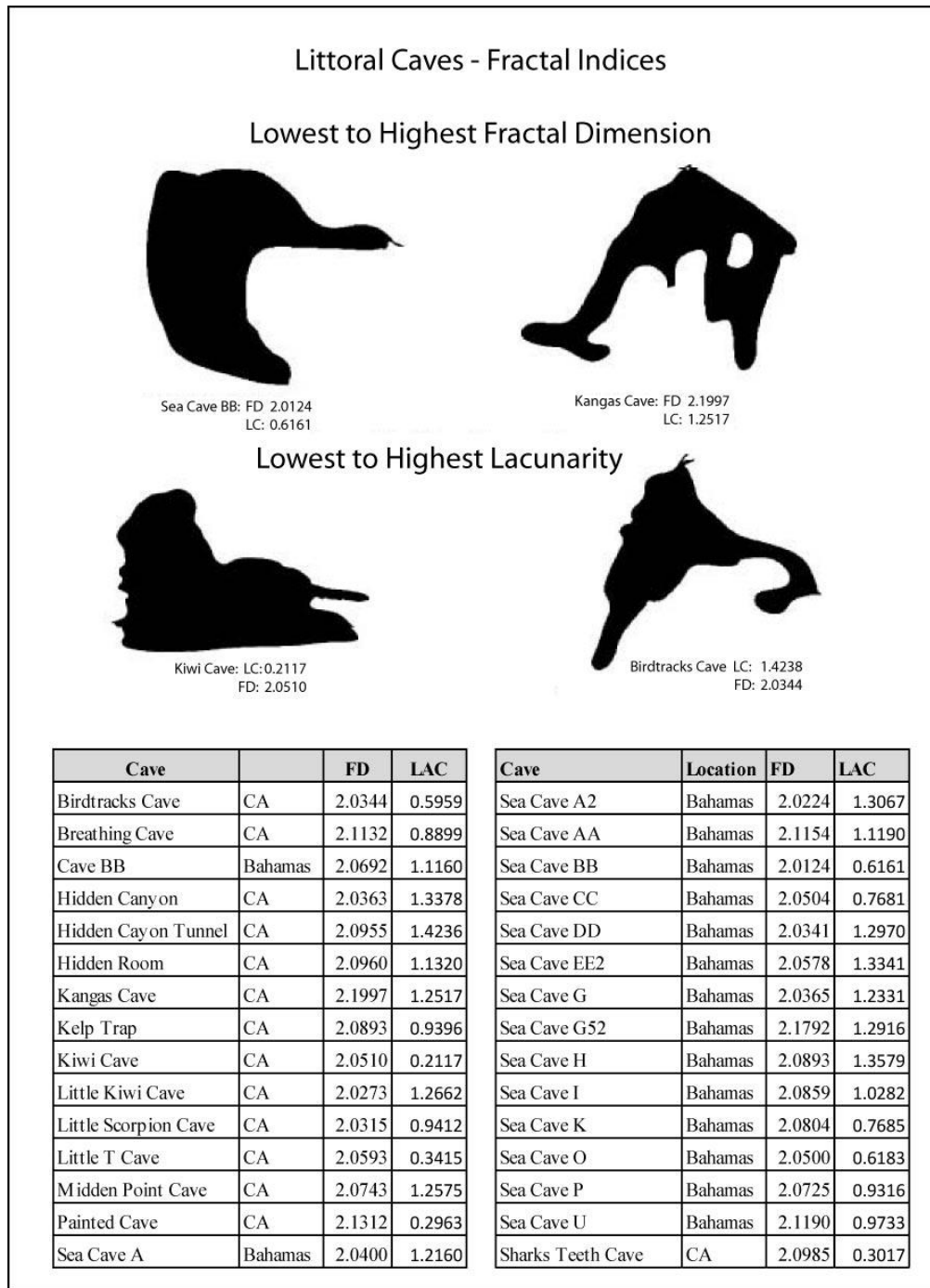


Figure 2.12 Littoral cave fractal indices and morphological examples

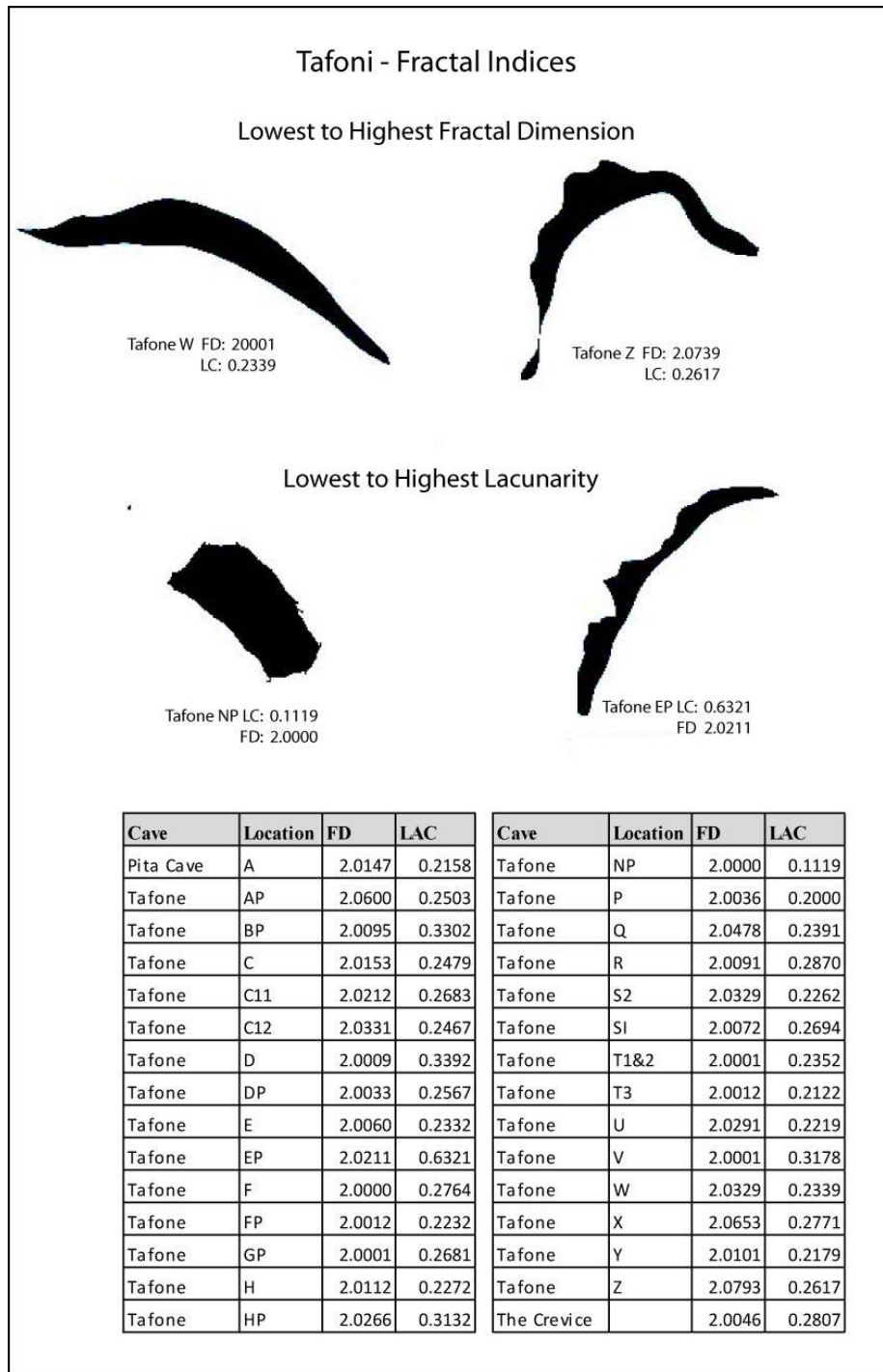


Figure 2.13 Tafoni fractal indices and morphological examples

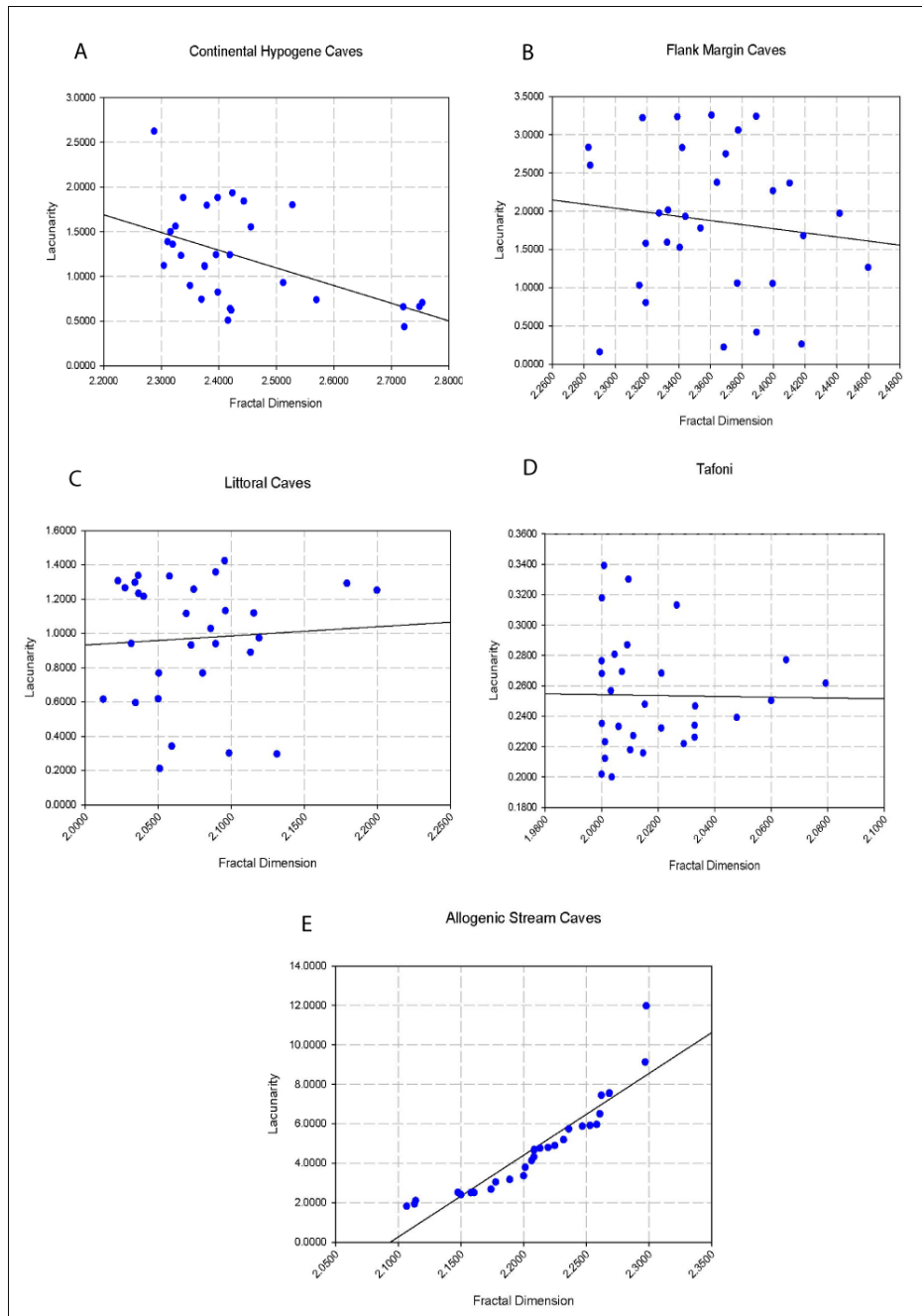


Figure 2.14 Scatterplots of fractal dimension vs. lacunarity for different cave types

(A): continental hypogene, (B): flank margin, (C) littoral (sea caves), (D) tafoni, (E) allogenic stream caves

CHAPTER III
THE GEOLOGIC CONTROLS ON THE DEVELOPMENT OF CAVES WITHIN THE
PHREATIC, EPIPHREATIC, AND VADOSE ZONES ON THE NORTHEAST
COAST OF QUINTANA ROO, MEXICO

3.1 Abstract

The northeast coast of the Yucatan peninsula within the state of Quintana Roo, Mexico, is an example of a carbonate coastline with a complex regional hydrology that has resulted in the formation of an extensive, density stratified, conduit-drained aquifer. Exploration and mapping of the extensive conduits (underwater cave systems) have been ongoing since the mid-1980s and there is a large dataset that describes their character and extent. All caves in the region are not submerged and some occur in the vadose-epiphreatic zone of the aquifer. Exploration and documentation of the vadose and epiphreatic-zone caves are still in early stages so there is a considerable amount of exploration bias in the existing data. This research compared the features and characteristics of the underwater caves with those caves located within the vadose-epiphreatic zone. Though there are a few striking exceptions, both groups of caves displayed two different morphologies: inland cave passages follow a northwest trend and form linear, anastomosing conduits that are perpendicular to the coast. Cave passages at or near the coast and within beach ridges consist of rectilinear mazes that parallel the coast and/or the beach ridges. Analyses of cave data and maps indicate that cave system

configuration and passage morphology are influenced by regional and local structures as well as stratigraphy. Passage morphologies are also influenced by local conditions such as ceiling collapse or speleothem development both which may result in stream diversion. Comparison and analyses of the underwater caves with the vadose-epiphreatic zone caves of the region indicated that they share the same characteristics with the exception of elevation and location with respect to the coast. The vadose-epiphreatic zone caves occur at slighter higher elevations than the submerged caves and are absent in areas less than a kilometer from the coast. The very similar morphologies of both groups of caves indicate that the vadose-epiphreatic zone caves formed from the same processes as the underwater caves i.e. mixing-zone corrosion. This strongly suggests that the vadose-epiphreatic zone caves formed when sea level was higher during MIS5e and became stranded in the vadose zone when sea levels subsequently dropped. A more comprehensive understanding of cave development was accomplished by the study of all caves in the region regardless of their position with respect to sea level.

3.2 Introduction

The state of Quintana Roo, Mexico, located along the northeast coast of the Yucatan peninsula (Figure 3.1), consists of an eogenetic carbonate coast whose complex regional hydrology has resulted in the formation of an extensive conduit-drained aquifer (Beddows 2004, Smart et al. 2006). On the Caribbean coast of Quintana Roo between Puerto Morelos and Muyil over 1170 km of submerged cave passages within 275 cave systems have been documented (QRSS 2014). In addition to the underwater cave systems are caves that currently reside in the vadose-epiphreatic zone of the aquifer as well as flank margin caves located in eolianites along the coast near Tulum (Kelly et al.

2006). North, south and west of this extensive block of cave development, the density of cave passages appears to notably decrease.

Scientific work within the underwater caves requires advanced technical skills in open circuit diving and/or rebreather technology. Time limits and the technical logistics of cave diving constrain the scientific work that can be accomplished in underwater caves. The caves currently located within the vadose-epiphreatic zones, henceforth referred to as vadose zone caves, are easily accessed using standard speleological exploration techniques and are not subject to the time or technical constraints of cave diving. Knowledge of their locations, distribution, morphology, and passage density is evolving since these features are in the process of being documented. This study compares the characteristics of the underwater and vadose zone caves in order to further the understanding of both.

3.3 Overview

3.3.1 Geography

The Yucatan peninsula is the aeri ally emergent part of the greater Yucatan Platform; a carbonate platform with a surface area of 300,000 km² (Bauer-Gottwein et al. 2012). The low-elevation, heavily karstified peninsula encompasses over half of the total platform surface area, and divides the Gulf of Mexico from the Caribbean Sea. The Campeche Bank is the western submerged part of the platform and extends 200 km northwest into the Gulf of Mexico at depths of less than 200 m. The eastern submerged bank extends up to 10 km from the Caribbean shoreline with a 400-meter loss of elevation into the Yucatan Basin east of Cozumel (Beddows 2003). Platform asymmetry is due to down-faulting that has led to the development of fracture zones parallel to the

Caribbean coast (Beddows 2004). The peninsula has been tectonically quiescent since the late Pleistocene (Weidie 1985) so major variations in sea level are solely attributed to glacioeustasy.

The climate of the Yucatan peninsula is tropical with distinct wet and dry seasons (Kottek et al. 2006). The average annual temperature is 26°C, with a range in monthly averages between 23–29°C (Beddows 2004). May to September is the hot, rainy season and October to April is the relatively cooler, dry season. There is a significant east–west precipitation gradient across the peninsula (Neuman and Rahbek 2007). The Caribbean coast is the wettest side with >1500 mm of precipitation per year (Gonzalez-Herrera 2002).

Regional-scale evapotranspiration (ET) on the Yucatan as determined from simple water-balance equations, field measurements, and remote sensing is approximately 17% of mean annual precipitation (Lesser 1976, Back 1985, Thomas 1999, Bauer-Gottwein et al. 2012).

ET is spatially variable across the peninsula with higher ET along the coasts and lower ET in the less densely vegetated and much drier northwest part of the peninsula (Bauer-Gottwein et al. (2012).

3.3.2 Stratigraphy

The stratigraphy of the Yucatan Peninsula is comprised of limestones, dolomites and evaporites overlying a basement of igneous and metamorphic rocks (Weidie 1985). The platform interior is composed of Eocene-Paleocene rocks surrounded by Miocene-Pliocene deposits, grading to and underlying Quaternary-age strata at the coasts (Ward 1997, 2003) (Figure 3.2). The eastern peninsular coastline consists of a 10-km band of

off-lapping carbonates that was deposited during interglacial sea-level high stands in the Pleistocene (Ward 1985).

The coastal carbonates have been divided into Upper, Middle, and Lower Pleistocene units comprised of marine and non-marine sequences (primarily eolianites) that accumulated in shelf margin, reef, and back reef facies during interglacial high stands (Ward 1985), and separated by unconformities indicative of exposure and erosion of the platform surface on marine retreat (Lauderdale et al. 1979, Rodriguez 1982) (Figure 3.3). Marine sequences include beach, near shore and lagoonal strata, and coral-reef limestone; non-marine rocks consist of eolianites, freshwater lacustrine carbonate mudstone, and caliche (Ward 2003). Underlying the Pleistocene strata are Miocene-Pliocene carbonate rocks (Richards and Richards 2007).

A narrow ridge and swale plain of Upper Pleistocene limestone located five to ten meters above present sea level, characterizes the northeast coast of Quintana Roo between Cancun and Tulum (Ward and Brady 1979) (Figure 3.4). Ridge crests are one to five meters above the swales, and are spaced 50 to 200 meters apart, paralleling the modern coastline (Ward 2003). There are as many as 20 ridges at the widest part of the plain but they all coalesce south of Akumal (Beddows 2003). The Middle Pleistocene unit, which is 150 km long, up to 4 km wide and 3-10 m thick, underlies the beach-ridge plain, and is exposed at the surface as a low-relief karst plain due west of it (Ward 2003). East of the beach-ridge plain are Upper Pleistocene barrier-reef limestones.

Lithological changes in reef facies reflect the different environments of deposition of a reef structure and these differences are typically related to distance from the coastline that was active at the time of deposition.

3.3.3 Structural geology

The state of Quintana Roo is within the Eastern Block-Fault district that extends from Cape Catouche on the northeast coast, to the Yucatan's border with Belize (Figure 3.5). It is one of five physiographic regions of the Yucatan peninsula which are defined by the influence of prominent fracture or lineament systems (Isphording 1974). The two main faults/lineaments in Quintana Roo are the Holbox Lineament Zone and the Rio Hondo Fault Zone.

The Holbox Lineament Zone (HLZ), originates at the northeastern coast of the peninsula and continues south to within 10 km of the coast inland from Tulum, trending N 5°E to N 10E (Bauer-Gottwein et al. 2012). The HLZ is expressed on the surface by the alignment of polje-like depressions that seasonally fill with water making narrow, aligned swamps (Weidie 1978). Remote sensing data indicate that development of regional dissolution features were strongly influenced by the lineament zone and result in high permeability and groundwater drainage (Southworth 1985, Tulaczyk et al. 1993). High subsurface electrical conductivity values relative to surrounding areas were detected in the vicinity of Tulum and were interpreted to indicate increased porosity and permeability associated with the faulting (Bauer-Gottwein et al., 2012).

The Rio Hondo fault zone (RHFZ) consists of a series of northeast trending (N30-32E) normal faults and has been identified as the on-shore continuation of an extensive horst and graben fault block system located off the southern Caribbean coast of Quintana Roo (Weidie 1985). This observation is supported by seismic data that confirms the fault system aligns sub-parallel to the southern Caribbean coast (Bauer-Gottwein et al. 2012). Surface expression of the RHFZ is seen in the alignment of shallow lakes, coastal bays,

and the orientation of Cozumel which is identified as a horst block (Lesser and Weidie 1988). Interpretation of synthetic aperture radar (SAR) remote-sensing images suggest that the Rio Hondo fault system extends northwards and intersects with the Holbox fracture zone in the vicinity of Tulum (Gondwe et al. 2010).

A well-defined fracture trend (N50-60W) has been identified along the entire coast indicating that fractures control the inland development and extent of coastal features such as caletas (lagoons) and crescent-shaped beaches (Weidie 1978). A second set of fractures with a trend of N30-40E parallels the coast and influences the lateral extent of coastal features. Weidie (1978) noted that the fracture sets may form an orthogonal system that is genetically related to the RHFZ. He observed changes in fracture trend along the Caribbean coast and speculated the existence of a conjugate fracture system.

The location of coastal discharge features, caletas, and crescent-shape beaches correlate with areas of maximal fracturing (Weidie 1978). The existence of extensive underwater conduits that display northwest and southeast trends support the idea that linear dissolution corridors are developed along the extensive fracture and lineament zones that occur in northeast Quintana Roo (Tułaczyk et al. 1993).

Structural heterogeneities within the aquifer include bedding planes, fissures and fractures, some of which are dissolutionally enlarged to conduits via mixing zone corrosion (Worthington et al. 2000, Smart et al. 2006).

3.3.4 Hydrology and aquifer dynamics

The coastal karst aquifer of Quintana Roo is unconfined and recharged by precipitation from extensive inland areas north of Akumal for cave systems north of that

area, and from the west near Muyil for the underwater cave systems in the vicinity of Tulum (Kambesis and Coke 2013). The aquifer responds to short term conditions such as heavy rains, barometric pressure, tides, and ocean density, which, supports the hypothesis that base flow originates far inland from the coast (Neuman and Rahbek 2007).

The northeast coast of Quintana Roo receives approximately 2.5×10^6 m³/yr of marine inflow from the Caribbean Sea resulting in a density-stratified aquifer where a thin meteoric-derived freshwater lens floats on the denser saline water (Lesser 1980). Separating the fresh from saline water is the halocline, which is a density and temperature transition zone that serves as a hydrochemical mixing zone. Freshwater and saltwater flow is decoupled at the halocline which is thickest near the coast but decreases inland to a sharply defined boundary (Beddows 2003, 2004). The mixing zone responds to several factors including conduit cross section, turbulence from conduit discharge, and tidal pumping, although the effects of the latter diminish inland (Beddows 2004).

Hydrological field research by Beddows (2004) has documented two types of saline flow on the Caribbean coast: a shallow two-way flow that corresponds to tidal frequency (up to >9 km inland), and a continuous incursion of sea water at a range of 5 to 45 m in depth. Saline inflow is tidally modulated; the deep saline flows occur continuously regardless of mean sea level and tidal change.

From the coastline proper to 0.4 km inland, the halocline gradient is steep and is accounted for by the low hydraulic conductivity of the area due to restricted size of conduits (Beddows 2004). For the zone >0.4 km to 10 km inland, the depth to the halocline is shallower than predicted by the Ghyben-Herzberg principle (GHP) especially in areas of high conduit density. In those zones the high permeability of the conduits

truncate the depth to the mixing zone because freshwater is quickly removed, causing an upward flow of saline water from below the freshwater lens (Beddows 2004). For distances greater than 10 km from the coast, the depth to the halocline does seem to follow the Ghyben-Herzberg model (Neuman and Rahbek 2007).

Mixing zone corrosion is accepted as the main mechanism for conduit development in the eogenetic aquifer of the Yucatan Caribbean (Beddows 2004, Smart et al. 2006). In the submerged caves, this hypothesis is supported by the observation that the vertical location of caves in the region is either directly associated with the position of the halocline or is above it, between 10 to 25 meters below current sea level (Beddows 2004, Smart et al. 2006). Other mechanisms that may contribute to conduit development include microbially mediated reactions associated with processes involving sulfates, and reoxidation of sulfide to produce sulfuric acid that may also drive dissolution (Stoessel et al. 1993). These processes can also occur in sediments derived from surface runoff via cenotes (Smart et al. 2006).

Gulley et al. (2013) put forth an alternate model for cave formation in eogenetic karst aquifers. They hypothesized dissolution occurs when water flows from aquifer regions with low PCO_2 into regions with higher PCO_2 . The increase in PCO_2 comes from fractures connecting the soil zone to water tables and water flowing from regions of low PCO_2 into regions of high PCO_2 . This condition dissolves CO_2 from the atmosphere, reduces pH, and dissolves limestone. They posited that simple geochemical models demonstrate small gradients in PCO_2 along flow paths are an order of magnitude more efficient at dissolving limestone than mixing of vadose and phreatic water.

The Pleistocene strata have a primary matrix porosity of 14-23% (Harris 1984). The structural heterogeneities, high matrix porosity, and the existence of conduits make for a triple porosity aquifer. The matrix acts as storage for 97% of the aquifer but contributes very little to the flow; flooded conduit systems with very little storage capacity (3%), link inland recharge to springs on and just off the Caribbean coast accounting for at least 99% of the freshwater flux to the sea (Worthington et al. 2000, Beddows 2004). The submerged conduits increase aquifer transmissivity as evidenced by hydrodynamic response to changing hydrological boundary conditions with 84% of the 30 cm amplitude semi-diurnal tidal signal transmitted to free water surfaces in cenotes at 1 km inland, and 39% at cenotes 6 km inland (Beddows 2003).

Aquifer discharge of groundwater to the Caribbean Sea is via a network mesh of conduits of varying size from tens of millimeters in width to humanly enterable passages that can range up to 80 meters in width (QRSS 2013). Beddows (2004) gave a crude estimate of coastal discharge within the 80 km section of Caribbean Yucatan coast in her study area to be 2.3×10^7 m³/year per kilometer of coast.

Though hydraulic gradient data are sparse on the peninsula, measurements range from 7mm/km (Neuman and Rahbek 2007) on the northwest side of the peninsula to 58mm/km to 130mm/km inland of the eastern coast, and near the coast south of Playa del Carmen, respectively (Moore et al. 1992, Beddows 2004). On a global scale, such nearly flat gradients are the lowest known in comparison to other karst areas (Ford and Williams 2007). The extremely low gradient and its value ranges are attributed to local and regional depressions in the water table caused by numerous conduits that locally attract groundwater flow (Ford and Williams 2007). Conduit density in the Tulum to Xel Ha

area has been calculated to be $>4\text{km}/\text{km}^2$ (Beddows et al. 2007a). In the current state of underwater cave exploration and survey of conduits in the Tulum area, cave lengths are not necessarily being extended, but rather that the gaps between known systems are decreasing as more passage is discovered (and hence the conduit density is increasing).

Though there is an absence of flow indicators (scallop) in the underwater caves of the region, cave divers report strong water flow within many of the underwater passages and the observed occurrence of dunes of white silt along the perimeter of cave passages, indicating turbulent flow (Coke personal communication 2013).

Though precise vertical control is lacking on the peninsula overall, the elevation in Quintana Roo is about 30 m or less above sea level with local relief of 5 m but rarely exceeding 10 m. Lack of surface drainage features coupled with minimal vertical control make it impossible to identify individual drainages basins (Beddows 2004). Instead, sub-regional distinctions have been made based on fault zones and subtle variations in surface topography (Lesser and Weidie 1988).

3.3.5 Cenotes and dry sinkholes

Cenotes are near-circular, water-filled sinkholes that intersect the groundwater table. There are two types of cenotes; pit cenotes and collapse cenotes (Neuman and Rahbek 2007). Pit cenotes are common to most areas of the Yucatan peninsula with the exception of Campeche State and the central Serrita de Ticul (Coke 2009). Profiles of pit cenotes show bell-shaped vertical shafts that may extend 100 m below the water table (Beddows et al. 2007) They formed by dissolution of deep strata that collapse to the surface from past sea-level fluctuations. It is rare for pit cenotes to display extensive

horizontal cave passage development though there are some exceptions, but the conduits are not very extensive (Beddows 2004).

Collapse cenotes are predominant in the study area and are distinctly different from the typical pit cenote in that they form by mechanical collapse of the ceilings of shallow phreatic cave systems when buoyant support is lost as a result of low sea levels (Beddows et al. 2007b). Cenote density above the extensive underwater cave systems of Quintana Roo is about one cenote for every 300 meters of cave passage (Neuman and Rahbet 2007).

Dry sinkholes (Figure 3.6) are extremely common in the high density cave block between Puerto Morelos and Muyil. These features have the same origin as the collapse cenotes that serve as portals to underwater cave systems. The dry sinkholes access cave passages currently within the vadose zone.

3.3.6 Caletas and crescent-shaped beaches

Significant groundwater discharge to the Caribbean Sea occurs via springs and small discharge vents associated with submerged phreatic conduits. An inventory of coastal discharge features documented in Chapter IV of this student documented 20 coastal springs and numerous small outflows and seeps. Coastal inlets (or lagoons) called caletas are narrow coves that extend inland for up to several hundred meters and are associated with larger coastal springs (Back et al. 1979) (Figure 3.7). Caletas form where discharging freshwater conduits mix with saltwater at their seaward margins causing an increase in local dissolution and inducing conduit collapse that migrates inland to form a cove (Beddows 2004). As dissolution continues to act on the caleta limestone and weakening it by solution channels, they becomes more vulnerable to mechanical erosion

by wave action (Back et al.1979). As the inlet opening widens, waves have greater access to the caleta walls which eventually erode to form a crescent shaped beach (Back et al. 1979) (Figure 3.7). Caletas and crescent-shaped beaches are an example of coastal reentrants produced by dissolution that characterize some carbonate coasts (e.g. Stafford et al. 2004, Kambesis et al. 2012).

3.3.7 Caves of Quintana Roo

Since the 1980s, the Caribbean coast of Quintana Roo, Mexico has been the focus of intense underwater cave exploration. Cave divers have documented an extensive series of linear, phreatic interlinked and anastomosing conduits within a 110 km block of coastline that extends from Puerto Morelos south to Muyil on the northern boundary of the Sian Ka'an Biosphere Reserve, and inland from eight to twelve km from the coast, which is near the eastern boundary of the Holbox Lineament Zone (Smart et al. 2006). This zone of cave development corresponds to the 10-12 km band of Pleistocene carbonates that rim the Caribbean Yucatan coast from Cancun to Tulum and beyond. In addition to the underwater caves systems are caves that currently reside in the vadose-epiphreatic zone of the aquifer as well as flank margin caves located in eolianites along the coast near Tulum (Kelly et al. 2006). North, south and west of this extensive block of cave development, the density of cave passages appears to notably decrease.

3.4 Methods

Field work in the study area consisted of mapping, inventorying and geo-locating caves and karst related features. Data were transformed to digital cave maps volumetric plots, and shapefiles for morphometric analysis. Existing maps were scanned in order to

be included in the analyses. Following are the documentation methods and analyses used for this study.

3.4.1 Cave survey/inventory/cartography

Caves were mapped using cave survey protocols as summarized in Appendix B.1. Instruments for cave mapping included Suunto compass/clinometer, and laser-range finders (with fiberglass tape backup). Garmin GPSMAP CSX 60 hand held GPS units were used for geo-referencing cave entrance locations, sinkhole collapses and coastal discharge features (datum to NAD 83 UTM) that were added to a karst feature inventory of the area. Each location was recorded to a 3-meter radius using the unit's location averaging function. Coastal features that could not be accessed in the field were assessed via remote sensing applications.

WALLS V2-B8 by David McKenzie, a freeware cave data reduction/plotting program distributed by the Texas Speleological Survey, was used to reduce and plot survey data to scalable vector format (SVG) for analysis and map production, and to export shapefiles for use in ArcGIS™. WALLS data are easily transferable to COMPASS files.

Survey notes were scanned, and along with SVG line plots, imported into Adobe Illustrator® (a professional drawing program) for manuscript map production.

3.4.2 Digital data analysis

Digital data sets from underwater and vadose zone caves were used to generate a series of rose diagrams for passage azimuth and inclination. Frequency plots made from

the vertical component of the survey datasets were made to show cave passage development with respect to current sea level.

3.4.3 Morphometric Analysis of caves and karst

Cave maps and cave-feature locational data were projected on satellite imagery in order to quantify distribution and density of cave passages and cave features.

Morphometric comparisons of underwater and vadose zone caves at the system and passage level were conducted by direct comparisons of cave maps and from calculating fractal dimension, which measured passage complexity.

A significant number of maps of vadose- zone caves were available for use in this research. Though 1170 km of survey has been conducted in the underwater caves of the study area, most remain as line plots with no passage detail. This reflects the difficulty in detailed data collection during the high-risk activity of cave diving. A small portion of the data is detailed enough and has been transformed to data-rich cave maps. Sistema Sac Actun, which is the longest cave in Mexico and second longest in the world, does have detailed enough maps for morphometric analysis. Because of its great extent, it served as a type example of underwater caves with which to make comparisons for this study.

3.5 Results

3.5.1 Structural orientation and cave passage depth analysis

Separate sets of rose diagrams for azimuth and inclination, based on regional survey data for the vadose zone and underwater caves were generated for structural analysis. The azimuth diagrams (Figure 3.8) for vadose zone and underwater based on

regional data display a strong northwest-southeast component to cave passage development though there appears to be a stronger east-west component in the underwater caves. The inclination rose diagrams (Figure 3. 9) are very similar for both data sets.

Frequency distribution graphs were generated to display regional vertical development with respect to sea level. The vadose zone caves (Figure 3.10) obviously show vertical development above sea level; three dominant elevation zones are 2, 4 and 8 meter above sea level. The underwater caves (Figure 3.11) show predominant vertical development at the following depths: -15m to -21m, -11m to -14m, and at -6m to -8m. In the underwater cave dataset three sections of significantly deep cave development have been documented by cave divers at Hoyo Negro, Aktun Hu (-60m) (Figure 3.12), Blue Abyss, Nohoch Nah Chich (-70m) (Figure 3.13), and The Pit- Dos Ojos (-119m)(Figure 3.14). Significant cave depth has also been documented in submerged cave passages located less than 200 meters from the coast (Bordignon personal communication 2014).

There is some passage development noted above sea level for the underwater caves at elevations 0-8 m and this area is located within Sistema Sac Actun. It is not certain if the tendency for minimal vadose zone passages above underwater caves is a typical characteristic of underwater caves in general, or if it is an expression of exploration bias that favors the documentation of underwater caves over dry cave.

3.5.2 Collapse feature distribution (cenotes and dry sinkholes)

The karst feature inventory shows the distribution of cenotes (water filled collapsed sinkholes) and dry collapsed sinks leading to vadose zone cave passages. Sub-sections of the inventory are displayed in Figures 3.15 and 3.16 and show the distribution

of cenotes and dry sinkholes in the Tulum and Playa del Carmen areas are synonymous with cave entrances in the region.

3.5.3 Springs and related discharge features

Coastal discharge vents (springs) are displayed in Figure 3.17. A total of 20 springs have been documented in the area but numerous smaller vents that are currently undocumented discharge offshore. Crescent-shaped beaches, which are features associated with caletas, were also documented and analyzed.

3.5.4 Cave distribution and density

Cave passage development on the northeast coast of Quintana Roo occurs between Muyil and Puerto Morelos and up to 12 km inland (Figure 3.18). Within this area 1170 km of underwater passages have been documented in 275 discrete caves (Figure 3.18). Of those, 8% contain sections in the vadose zone. The highest density of underwater cave occurs between Muyil and Akumal and cave density within this 430 km² area is 2.7km/km². Cave density in the 45 km² block containing Ox Bel Ha is 5.2 km/km². The cave density of Sistemas Sac Actun and Dos Ojos which occur within a 108 km² block is 2.9km/km². These particular cave systems have an inland extent of up to 9 kilometers and continuous passages have been documented to connect to coastal discharge points

The greatest concentration of caves located within the vadose-epiphreatic zone occurs in the area between Akumal and Playa del Carmen and extending 7 km inland (Figure 3.18). Over 115 km of cave passages have been surveyed in 114 cave systems and 4% of those caves contain epiphreatic passages. Within this 234 km² area, cave

density is 0.5 km/km². Sistema Pool Tunich is the most extensive at 38 km, followed by Sistema Sac Muul (11 km) and Sistema Dos Arboles (8 km) (QRSS 1013).

3.5.5 Cave morphology analysis

Cave maps revealed that there are two types of cave passage morphologies in the region. Caves that are less than a kilometer from the coast display high-density rectilinear mazes that parallel the coast on a northeast-southwest trend. The cave passages that make up the mazes are low and horizontal, almost canyon-shaped in places, and are interspersed with fissure-controlled chambers. They are devoid of speleothems, and coated with clay-like silt. The limestone is very friable and in places can be unstable. Passages in the Cenote Abejas section of Sistema Sac Actun display this morphology (Figure 3.19). Exploration was very difficult in this section of cave due to the unstable nature of the bedrock and silt which compromises visibility (Coke personal communication 2013). There are currently no vadose zone caves within 500 meters of the coast however there are vadose zone caves with the near-coast morphology. Cueva Camaras (Figure 3.20) is a vadose zone maze cave located in a beach ridge less than two kilometers from the coast. A notable exception to the coastal passage morphology “rule” is Sistema Ox Bel Ha; the inland trend of large, linear anastomotic passages continues all the way to the coast.

The other type of passage morphology characteristic in the region occurs in caves or cave segments located a kilometer or more from the coast. These caves display a distinct linear pattern and elliptical passage morphology. Passages tend to average up to 10 meters in width though they can be of greater size. They are anastomotic in configuration and run perpendicular to the coast on a northwest-southeast trend.

Speleothems are common in both the underwater and vadose-epiphreatic zone caves. Sistema Dos Arboles (Figure 3.21), a vadose-epiphreatic zone cave and Maya Blue, part of Sistema Ox Bel Ha (Figure 3.21b), exemplify this type of passage development.

Cave maps show the anastomotic mazes to occur near entrances and in association with upper level passages. Cenote Balancanche, an underwater cave (Figure 3.22A), has 10 collapse cenotes located within a 0.6 km² zone of anastomosing passages. Sistema Pool Tunich (Figure 3.22B), a vadose zone cave, also shows anastomotic development near cenote entrances.

Some sections of maps that appear to show anastomotic passage development but are showing two levels of passage that overlie each other. The Hell's Gate section (Figure 3.23) in the Nohoch Nah Chich region of Sac Actun shows overlying upper level passages that appear to be part of the same maze, but in actuality exist on two levels. There are no upper level passages in the vadose-epiphreatic caves of the region.

Fractal dimension was calculated for the cave footprints of a selection of underwater and vadose zone caves and are summarized in Table 3.1. The fractal dimension values fall between those characteristic of the higher range of values for flank margin caves and the mid-range values for hypogenic maze caves.

3.5.6 Hydrologic observations

Many of the caves located in the vadose zone are completely dry. Cueva Camaras (Figure 3.20) is an example of a cave within a beach ridge, which is located 2 kilometers from the coast at an elevation of 10 meters above sea level. Cave development within the ridge occurs at approximately 6 meters above sea level. Vadose zone caves that are located a kilometer or more from the coast contain epiphreatic sections that can contain

pools of water or may be inundated wall-to-wall with water, both which respond to daily tidal pulses. Grotte Aluxes (Figure 3.24) is an example of a near-coast beach ridge cave (1 km from the coast; cave developed at 0-1 meter above sea level) and contains shallow and epiphreatic zones that respond to tidal pulses. The vertical extent of Sistema Pool Tunich ranges from 6-8 meters above sea level through below sea level. The cave, which ranges up to 7 km inland, contains dry, epiphreatic, and phreatic sections.

Though there is an absence of flow indicators (scallops) in the underwater caves of the region, cave divers report strong water flow within many of the underwater passages and the observed occurrence of dunes of white silt along the perimeter of cave passages, indicating turbulent flow (Coke personal communication 2013) (Figure 3.25A). The northern sections of Sistema Pool Tunich located 7 km from the coast (Figure 3.25B) contain areas where turbulent flow is documented in sections of cave passages that extend to the local water table. Daily tidal pulses have been observed in vadose-epiphreatic zone caves along the coast such as Grotte Aluxes.

3.6 Discussion

Exploration bias has to be considered when making comparisons between the underwater and vadose zone caves of Quintana Roo. This concern is most evident in Figure 3.18, which shows the distribution of underwater versus vadose zone caves. What is not immediately obvious from this graphic is that exploration and documentation of underwater caves has been ongoing since mid-1980, whereas exploration and detailed documentation of equal focus did not begin in the vadose zone caves until 2008. The underwater caves and vadose-epiphreatic zone caves of northeast Quintana Roo share

many characteristics though there are some subtle differences which do not detract from the relationship of the two cave types but rather support it.

3.6.1 Cave passage orientation and distribution

The major structural orientation and inclination of the underwater and vadose-epiphreatic zone caves are very similar though the underwater caves seem to have more E-W development. This may be an artifact of comparing 1170 km versus 115 km of cave survey rather than any real differences in orientation or it may be related to topography as the dry caves are restricted to high ground areas whereas the flooded caves are not.

Tułańczyk et al. (1993) suggested that fissure or joint controlled networks were the initial precursors to the dissolutional conduits that currently drain to the coast. Due to the limited lateral extent of fissure controlled passages (Kambesis and Coke 2013), it is also possible that there is no structural control on incipient passages but rather that coastward hydraulic gradient resulted in the development of sub parallel passages that randomly intersected. This bears some similarity to the development of flank margin caves as random dissolutional voids that randomly connected to form larger voids (Labourdette et al. 2007). However, cave passages with a strong linear N30°E trend and located less than 200 meters from the coast, have recently been discovered. The passages parallel the coast with a lateral extent of 4 km (personal communication Bordignon 2014) and may be related to the extensive horst and graben fault block system located off of the coast of Quintana Roo that was described by Weidie (1985). This suggests that initial conduit development did occur along regional joint and/or fault trends and that the anastomotic pattern of passage development is a secondary imprint due to local geological conditions.

There are no significant vadose zone caves located less than a kilometer from the coast though small flank margin caves are found in eolianites located on the coast in the Tulum area (Kelly et al. 2006) (Figure 3.26). Because of the small size of the flank margin caves, they do not display the typical morphology of more extensive flank margin caves, e.g. ramiform or spongework with cross-linked chambers. However, they do display the large width to low height ratio of chambers that reflect the form of the distal margin of a freshwater lens. The elevation of the Tulum flank margin caves and breakdown at their entrance areas suggest that the caves initially formed without entrances and were ultimately exposed by erosion and coastline retreat.

There is major underwater cave development near the coast and cave divers report the zone to be devoid of speleothems, with friable and unstable walls, and a lot of sediment. These are all the symptoms of very young limestone units. Beddows et al. (2007a) identified the near-coast environment as the active mixing zone and location of the youngest Pleistocene limestones, with the least overprinting by other processes.

Significant vadose zone cave development occurred in the beach ridges of the study area and the cave passages in those areas are characterized by low, rectilinear mazes, similar to passages actively forming at the coast today (Figure 3.20). Based on the flank margin caves that have been documented in the coastal area at Tulum, (Kelley et al. 2006), it is possible that the caves in the beach ridges may have initiated as flank margin caves but became incorporated in the regional hydrology when sea levels rose.

The distribution of underwater versus vadose zone cave passages as presented in Figure 3.18 needs to consider the distorting perspective of exploration bias. As vadose zone cave exploration continues, more vadose zone caves will be found though their

extent may not compare to that of the underwater caves. Connections are also likely between the vadose zone and underwater caves via the epiphreatic sections.

3.6.2 Cave passage morphology

As noted in Section 3.5.5, there are two types of cave passage morphologies in the region. Cave that are less than a kilometer from the coast display northeast-southwest trending high-density rectilinear mazes that parallel the coast. These passages can have either elliptical or fissure dominated cross sections. Cave passages located greater than a kilometer from the coast display a northwest-southeast trending linear pattern with predominantly elliptical cross sections. The morphological differences of cave passages from coastal to inland configuration may in part be caused by changes in lithology where Holocene to Pleistocene age carbonates transition to older, more consolidated ones and cave passages are contained within more massive and stable bedrock. For example, at distances of 3 to 6 km from the coast, the southern and northern arms of Sistema Sac Actun at Naval and Nohoch Nah Chich respectively encounter Neogene rocks (Coke 2009). Lateral branching of passages still occurs but the number of passages is limited to just one or two primary discharge tunnels; secondary passages are small in dimension and length and typically end in impassible tubes or cracks that discharge freshwater (Coke 2009).

An exception to the near-coast morphology of many of the caves along the coast is observed in Sistema Ox Bel Ha, which displays the passage characteristics of an inland cave in its sections all the way to the coast (Coke 2009). The spring vents of Sistema Ox Bel Ha appear to be located in an older paleo-coastline section than caves to the northeast. The distribution of caletas, which are common northeast of Ox Bel Hall, drop

to practically none in the Ox Bel Ha coastal vicinity. This is support for the idea of a change in geologic boundary conditions south of Tulum.

The karst inventory has identified hundreds of cenotes, i.e., sinkhole collapses, in the study area. The anastomosing configuration of the inland cave passages may in part be influenced by regional structure, but local conditions may also play a very significant role. Cenotes form as a function of the removal of buoyant support when water drained from formerly submerged cave passages causes collapse. Extensional fractures that formed as a result of ceiling collapses make for zones of weakness that result in more extensive areas of underground breakdown. Groundwater flow would find new routes around the breakdown and the multiple diversions would result in anastomosing passage configurations. The 600-meter wide collapse zone displayed in Cenote Balancanche (Figure 3.22a) strongly influences the morphological pattern of surrounding cave passage. In Sistema Pool Tunich, the five entrances on a circular trend in Figure 3.22b are the result of a large, circular surface collapse that may have initiated the formation of the complex maze characteristic of the area. Other factors that influence cave patterns because they affect water flow include sediment and speleothem occlusion.

Smart et al. (2006) proposed that coastal caves of Quintana Roo were intermediary between continental stream caves and flank margin caves. However, the fractal indices calculated for ten select caves in the study area classified them as intermediate between flank margin caves and hypogene caves (Table 3.1) . This reflects that continental hypogene caves and the caves of Quintana Roo both form by mixing zone corrosion which results in similar morphologies. However the Quintana Roo caves function as a drainage system related to surface hydrology versus hypogene caves whose

hydrology is not directly related to surface drainage. Turbulent flow has been documented in both the underwater caves and in sections of the vadose-epiphreatic zone caves that are deep enough to encounter the local water table. Fractal dimension is a means of classifying cave morphologies for descriptive and comparative purposes. It does not dictate process, though morphologies can suggest possible processes as demonstrated by the above analysis.

3.6.3 Vertical development of passages

The vadose zone caves of the region range from being completely dry to containing sections that are epiphreatic. Water levels (or lack of water), within the vadose-epiphreatic zone caves of the region are a function of the cave's location with respect to sea level. Though vadose-epiphreatic zone caves closest to the coast typically contain water, inland caves may also contain water, have underwater sections, or connect to more extensive underwater systems depending on their elevation with respect to sea level. When cave development is greater than 2 meters above sea level, passages are typically dry. Passages that are located 0-2 meters above sea level have a combination of passages that are completely dry to those that contain pools or wall-to-wall water passages which respond to daily tidal pulses. Sections of caves that occur below the water table may contain underwater segments or may connect to more extensive underwater caves.

The submerged cave passages of northeast Quintana Roo are fairly shallow in terms of world depth standards. In historic Sac Actun, passage depths range from <2 to up to 20 meters; Nohoch Nah Chich region depth ranges span from 2-6 and 8-15m and 16-20; Actun Hu region from 5-10m; and Dos Ojos region at 5-10m and 14-20m.

However, there are three notable exceptions that all occur within the Nohoch Nah Chich-Aktun Hu-Dos Ojos regions of Sistema Sac Actun. These areas require advanced cave diving techniques and equipment, and mixed gases.

Hoyo Negro (Figure 3.12) is a breakdown-floored pit within the Actun Hu region with a depth of 60 meters. The Blue Abyss (Figure 3.13) is an underwater vertical shaft with a depth of 71 meters and has been explored to a breakdown maze at the base of the shaft. “The Pit” in Dos Ojos (Figure 3.14) is a steeply descending breakdown-floored passage that begins at a cenote entrance and leads to a series of large breakdown-floored chambers, giving that section of cave a depth of 119 meters. The deep sections of Sistema Sac Actun are in saltwater and hint at the existence of deeper levels of cave development which are mostly unknown. Water samples collected in The Pit were analyzed to be chemically identical to nearby marine water (Barton 2001). There are reports of large holes along the walls of the modern barrier reef at depths of 100 meters that could potentially lead to deep levels of cave development, formed when sea level was over a hundred meters lower than it is today (Barton 2001). Deep cave passages (>50 meters) have recently been documented near the coast though they have not yet been studied in any great detail (Bordignon 2014).

Smart et al. (2006) suggested that dissolution could occur in the salt-water-occupied deeper zones of the cave. Beddows (2004) documented an increase in temperature with depth in The Pit and Blue Abyss (approximately 2°C/100m). Though these waters are typically saturated with respect to calcium carbonate minerals, forced advection could cool the water and result in undersaturated water that could dissolve limestone in the deep saline zone (Smart et al. 2006).

Vertical development in the vadose zone caves is all above current sea level though some elevations push above the 6-meter sea level high mark of MIS5e. These areas are where the survey line was run between the surface and down into a cenote which means those elevations can be attributed to progradational collapse rather than anomalous glacioeustasy.

3.6.4 Multiphase cave development

The low hydraulic gradient of the Yucatan peninsula means that water levels within Quintana Roo cave systems track sea level. The current location of the halocline and the vertical distribution of cave passages indicate that the cave systems have undergone multiple phases of development. The existence of air-filled cave passages above water filled passages, such as Yax Muul (Figure 3.27) and multilevel areas such Hells Gate, both in the Nohoch Nah Chich region (Figure 3. 23) attest to the relationship of sea level to cave passage development.

The elevation of the limestones containing the vadose zone caves indicate that they formed when sea level was higher than today which would likely be MIS5e. In order to create subareial exposure to form a freshwater lens, there had to be a drop in sea level during MIS5e. Carew and Mylroie (1999) discussed a mid-MIS5e low stand for similar situations in the Bahamas. When sea level dropped post MIS5e, the caves that formed during that time were stranded in the vadose zone.

Figure 3.28 illustrates the multiple phases of cave development in the Quintana Roo study area and the relationship between the underwater caves and those occurring in the vadose-epiphreatic zone.

3.7 Summary

Cave system configuration and passage morphology are influenced by regional structure and/or stratigraphy but are also the result of local conditions such as ceiling collapse or speleothem development, both which may result in stream diversion. Multi-level passages in underwater caves can produce an anastomosing pattern in plan view maps. There are no upper level passages within the vadose zone caves.

Cave system configuration is predominantly linear anastomosing conduits for passages that trend perpendicular to the coast on a northwest trend. Cave passages within beach ridges have a rectilinear maze form and follow the trend of the beach ridges. Cave development also parallels the coast on a northeast trend. There are no vadose zone caves located less than a kilometer from the coast.

The caves located within the vadose-epiphreatic zone were developed in limestones deposited during MIS5e and formed by mixing zone dissolution during lower sea levels within MIS5e. The caves were stranded in the vadose zone with subsequent lowering of sea level post-MIS5e.

The vadose-epiphreatic zone caves share the same characteristics with the underwater caves of the region in terms of cave system and passage morphology, origin, genesis and continued development. A more comprehensive understanding of cave development in the region has been accomplished by analyzing and comparing the underwater and vadose-epiphreatic zone caves.

Table 3.1 Fractal dimension for a selection of underwater and vadose zone caves

Underwater	Fractal Dimension	Vadose-Epiphreatic	Fractal Dimension
Sistema Sac Actun	2.5083	Sistema Pool Tunich	2.3953
Sistema Ox Bel Ha	2.6049	Sistema Sac Muul	2.3668
Dos Pisos	2.3781	Dos Arboles	2.3901
Sand Crack	2.3579	Fallen Fig	2.2973
Sistema Camilo	2.3727	Cueva Camaras	2.3876

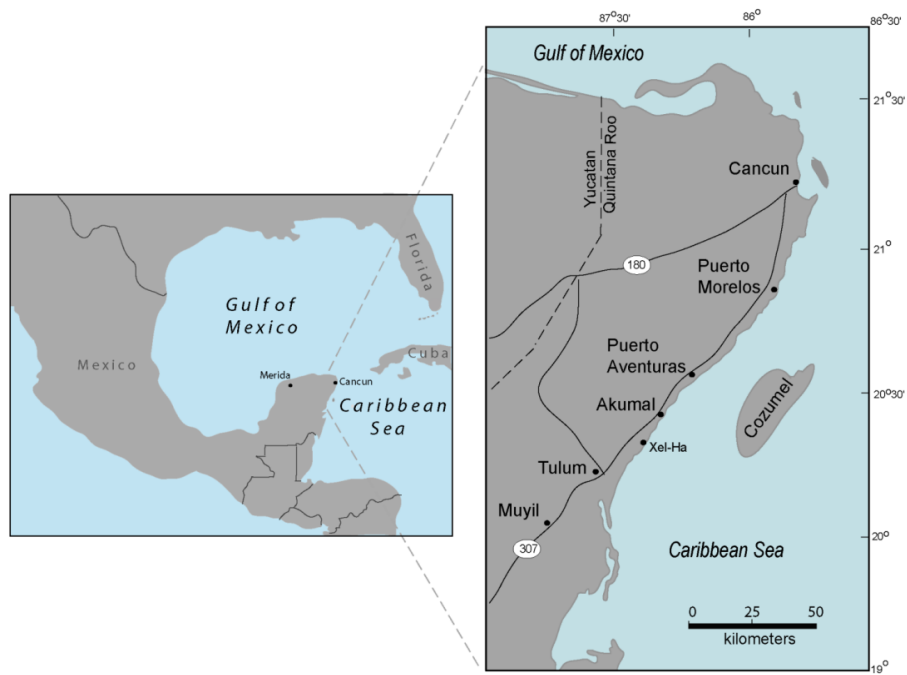


Figure 3.1 Study area on the northeast coast of Quintana Roo, Mexico

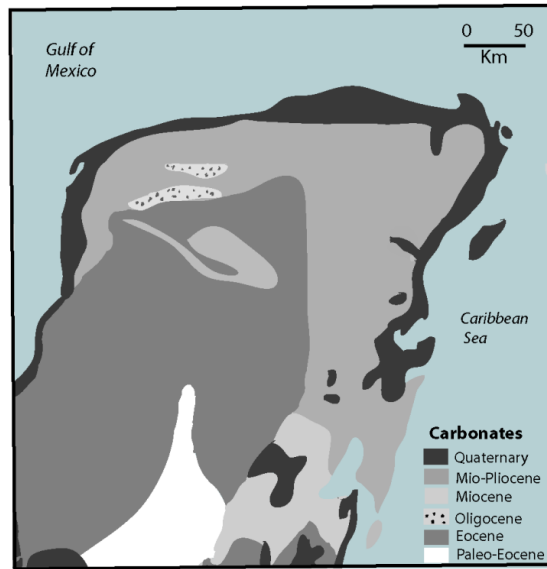


Figure 3.2 Stratigraphy of the Yucatan peninsula, Mexico

Modified from Ward 1985

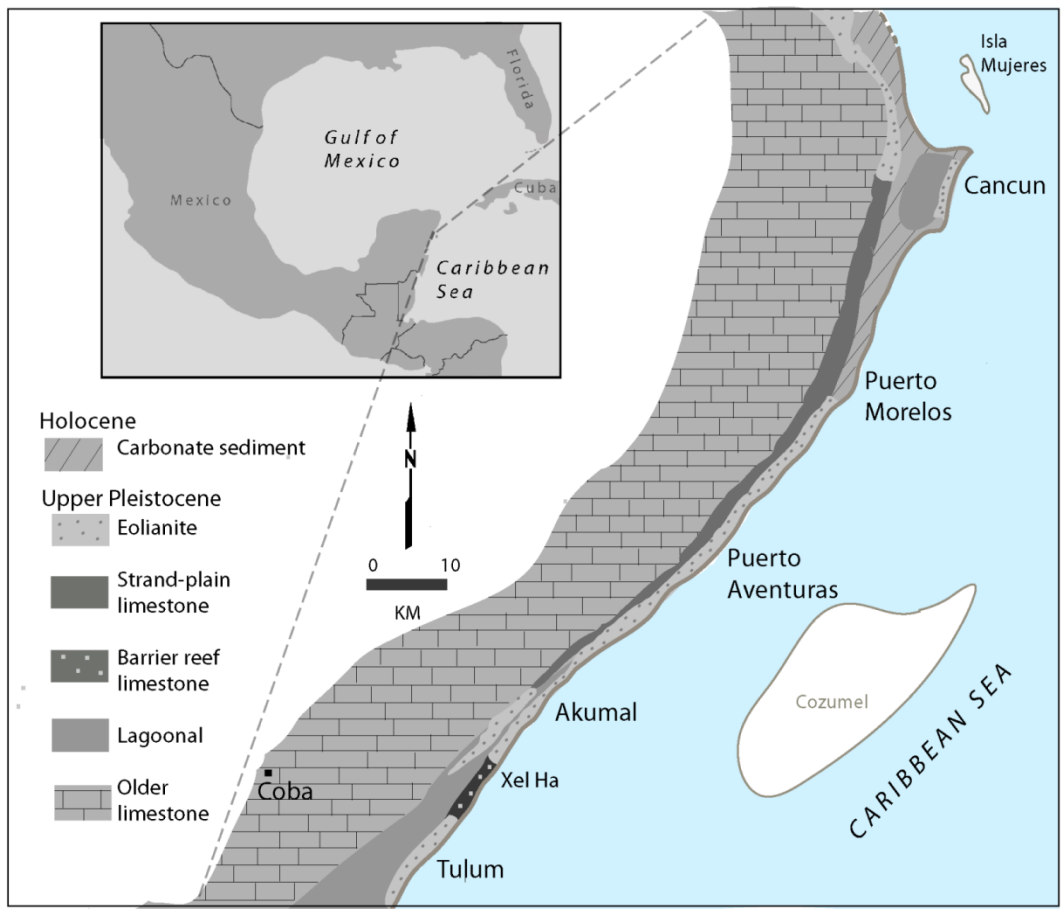


Figure 3.3 Stratigraphy of the northeast coast of Quintana Roo, Mexico

Modified from Ward 1985

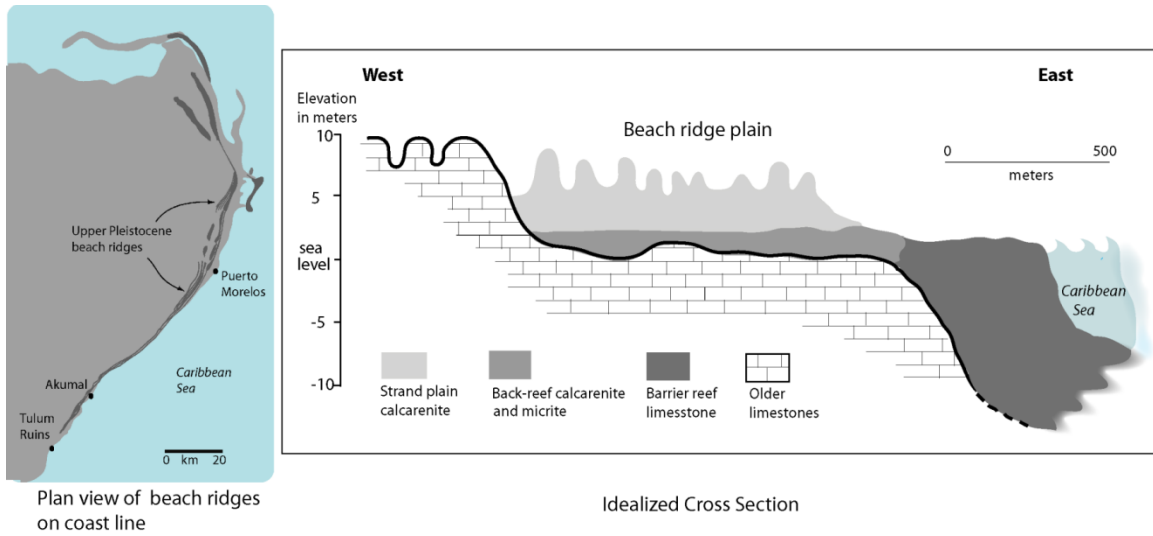


Figure 3.4 Ridge and swale plane of the northeast coast of Quintana Roo, Mexico

Modified from Ward 1985

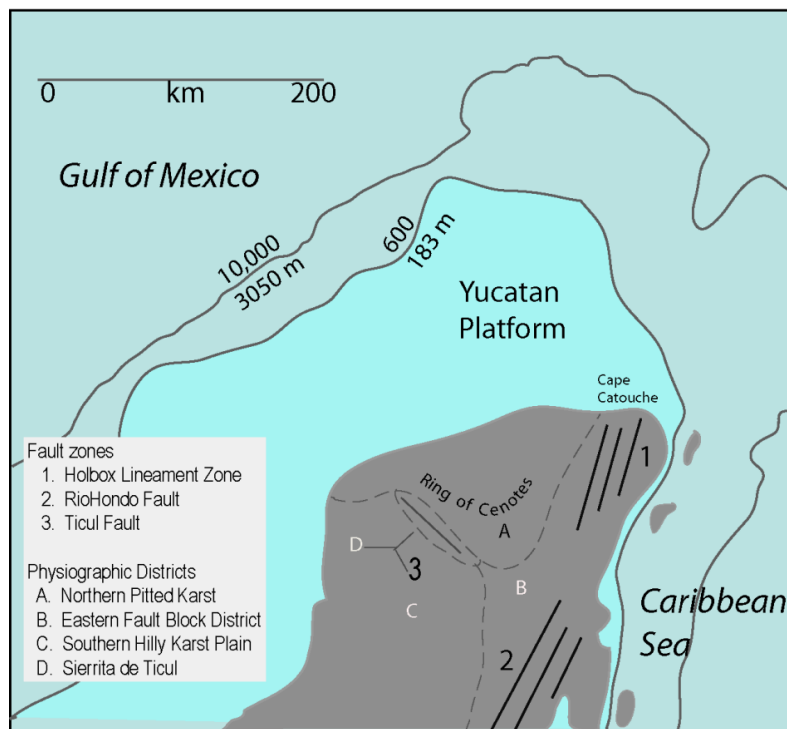


Figure 3.5 Structural features of the Yucatan peninsula

Modified from Beddows 2003



Figure 3.6 Collapsed sinkhole in a vadose zone cave in Quintana Roo, Mexico

Photo: Dave Bunnell

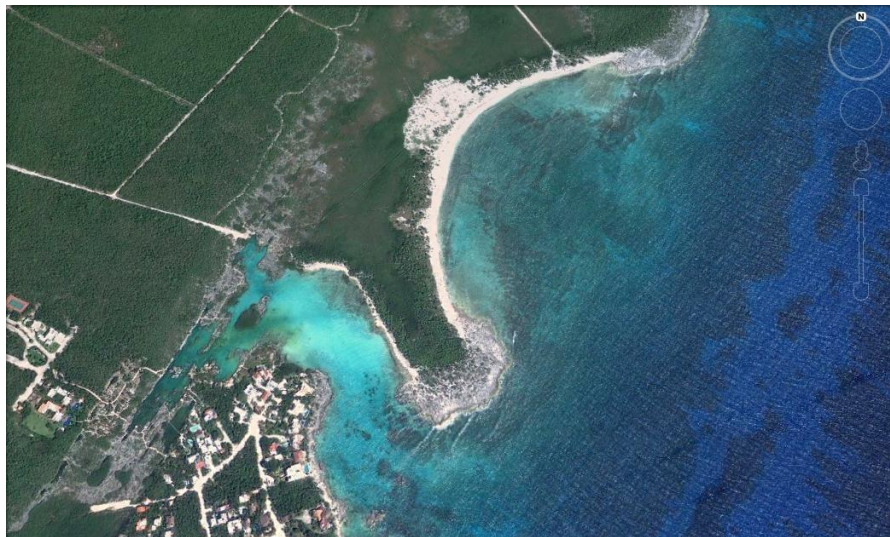
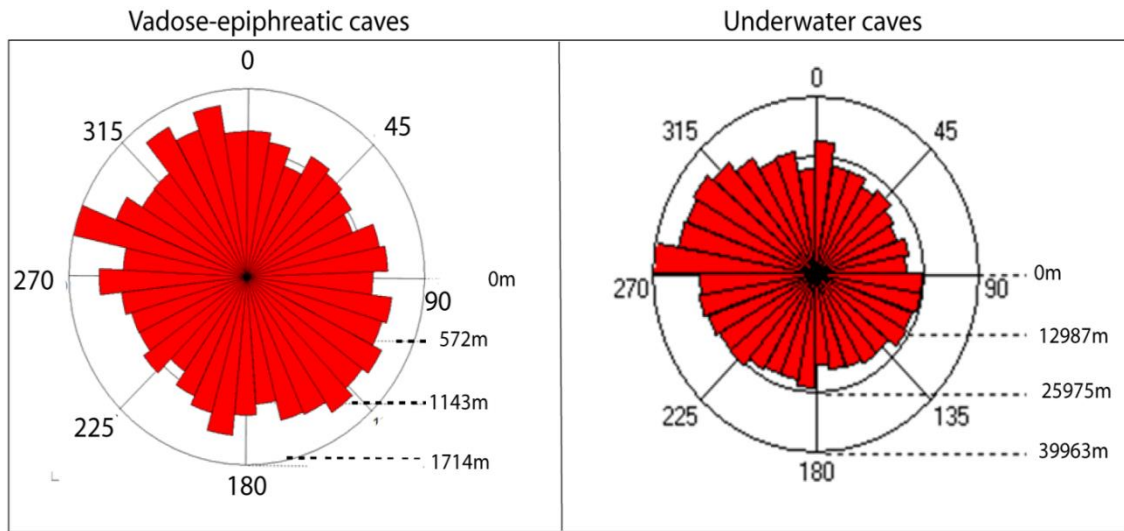


Figure 3.7 Caleta and crescent shaped beach

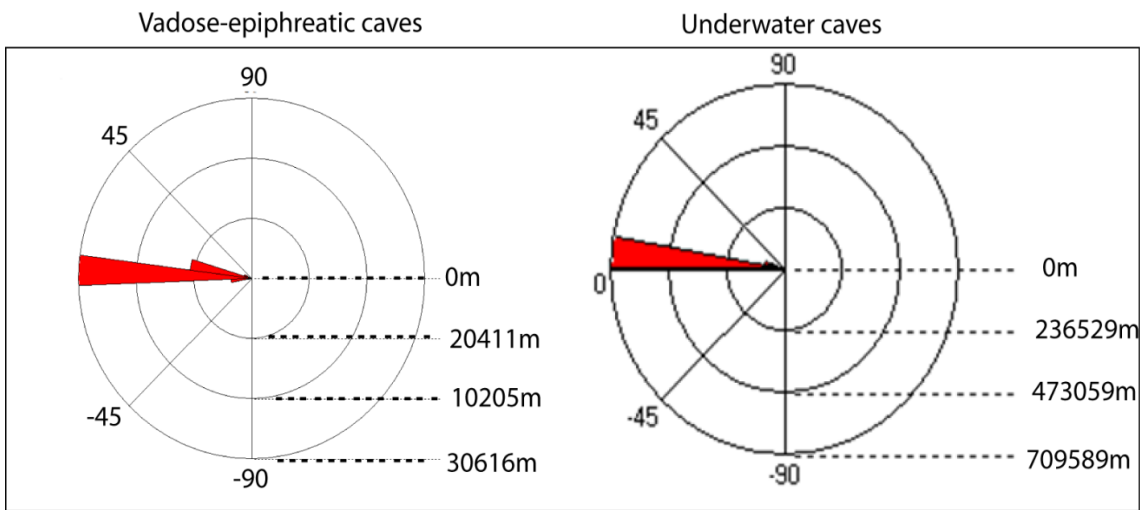
Feature on the left is Caleta Yalku; feature on the right is a crescent-shaped beach. Image from Google Earth



Azimuth Rose Diagrams

Figure 3.8 Azimuth rose diagrams from regional cave data

From regional cave survey data of vadose-epiphreatic zone and underwater caves (Data for underwater caves: QRSS 2013)



Inclination Rose Diagrams

Figure 3.9 Rose diagrams on inclination

From regional cave survey data of vadose-epiphreatic zone and underwater caves. Data for underwater caves: QRSS 2013

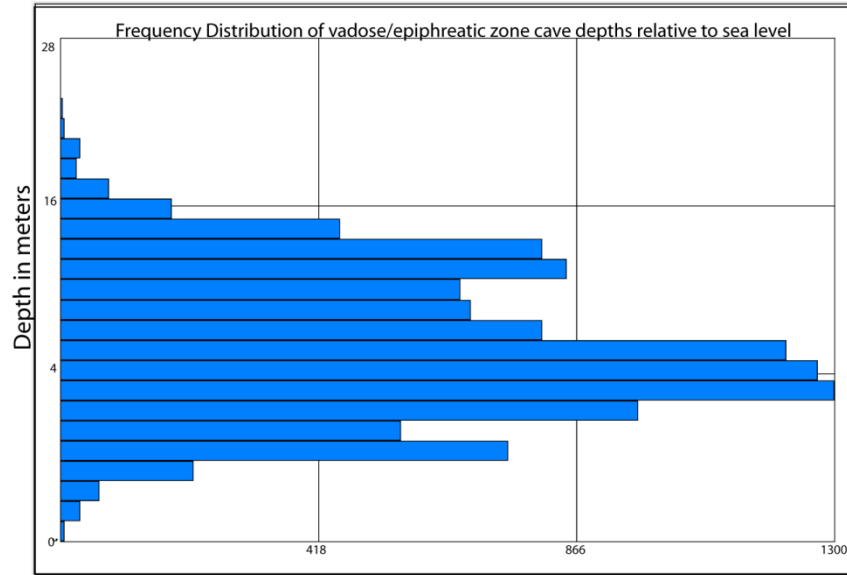


Figure 3.10 Frequency distribution on depth for vadose zone caves relative to modern sea level

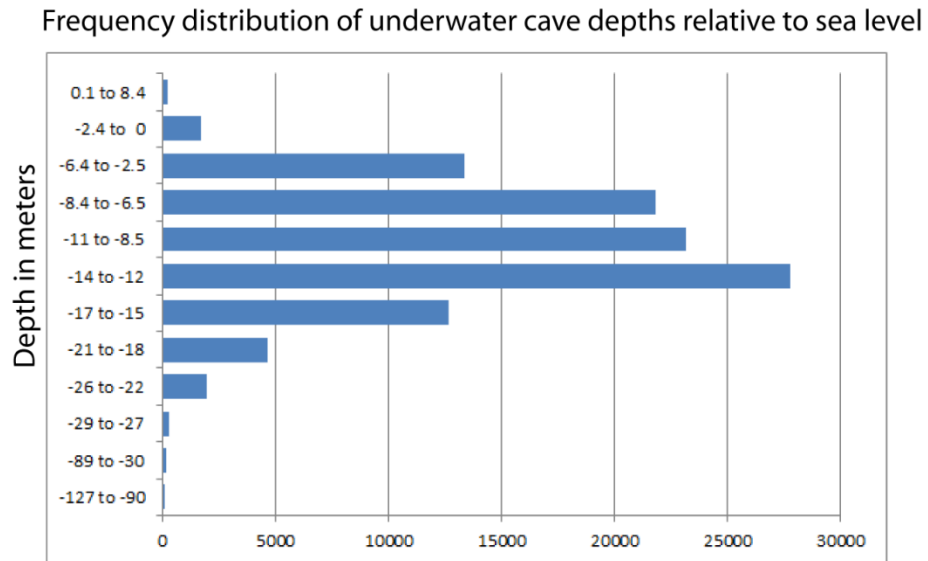


Figure 3.11 Frequency distribution of underwater cave depths relative to modern sea level

Data source: QRSS 2013

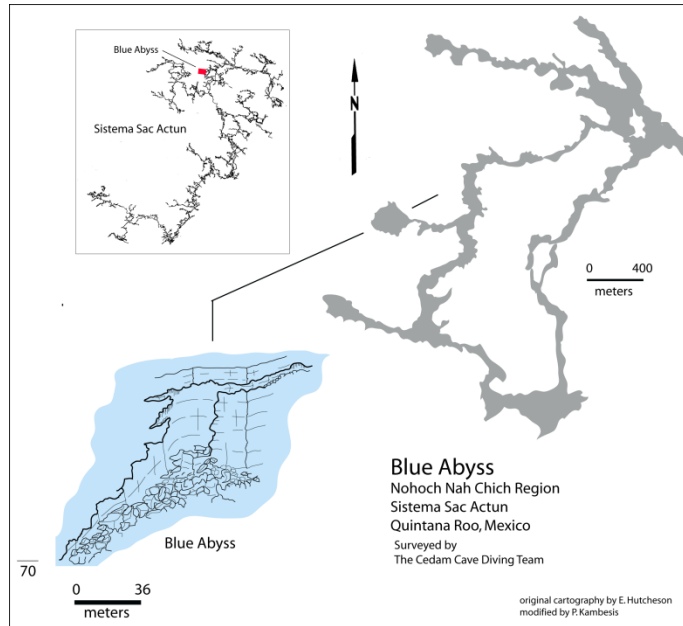


Figure 3.13 Deepest cave sections in the Quintana Roo region – Blue Abyss (-70m)

Located in Nohoch Nah Chich region of Sistema Sac Actun

Cartography: E. Hutcheson, modified by P. Kambesis

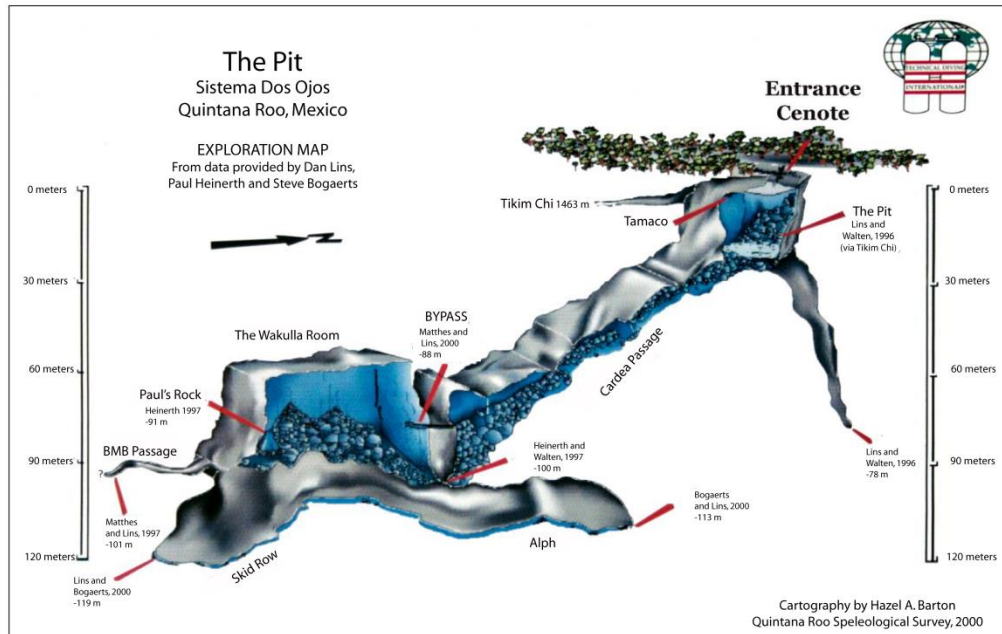


Figure 3.14 Deepest cave sections in the Quintana Roo region – The Pit(-119m)

Located in Dos Ojos region of Sistema Sac Actun

Cartography: H. Barton

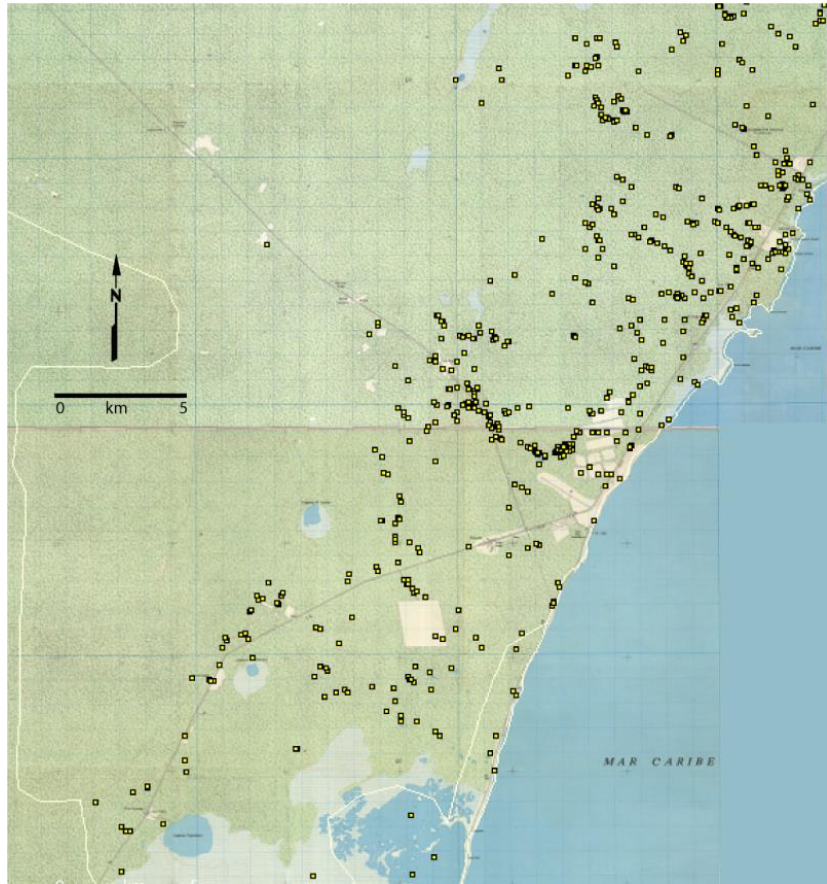


Figure 3.15 Cenote distribution from Sian Ka'an Reserve to Akumal



Figure 3.16 Cenote distribution in Playa del Carmen area

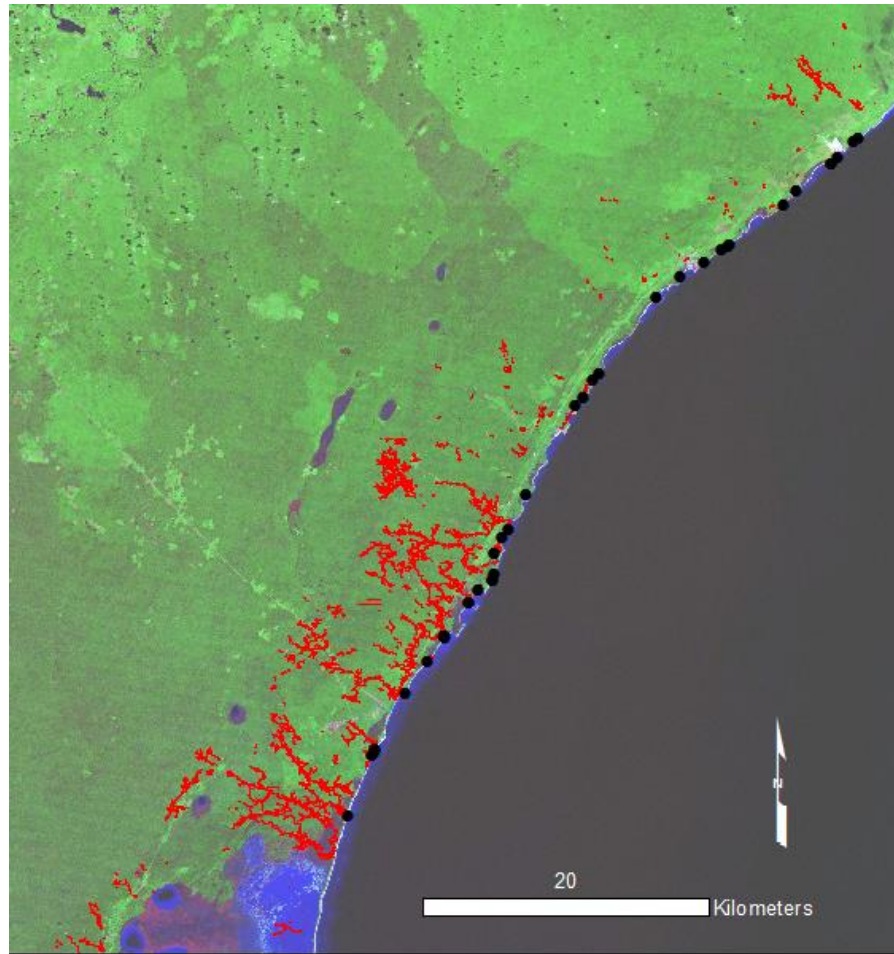


Figure 3.17 Distribution of coastal springs of northeast Quintana Roo

Black dots are costal springs; Red lines are cave systems. Cave data source: QRSS 2013

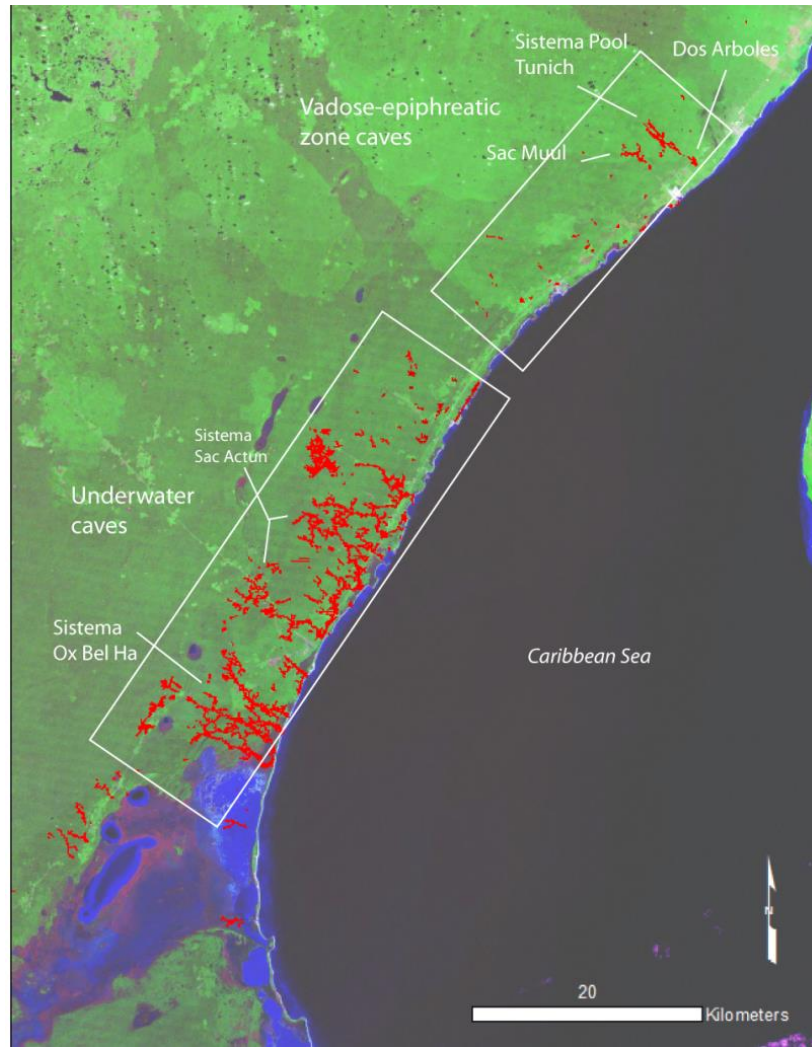


Figure 3.18 Cave distribution and density of underwater and vadose zone caves.

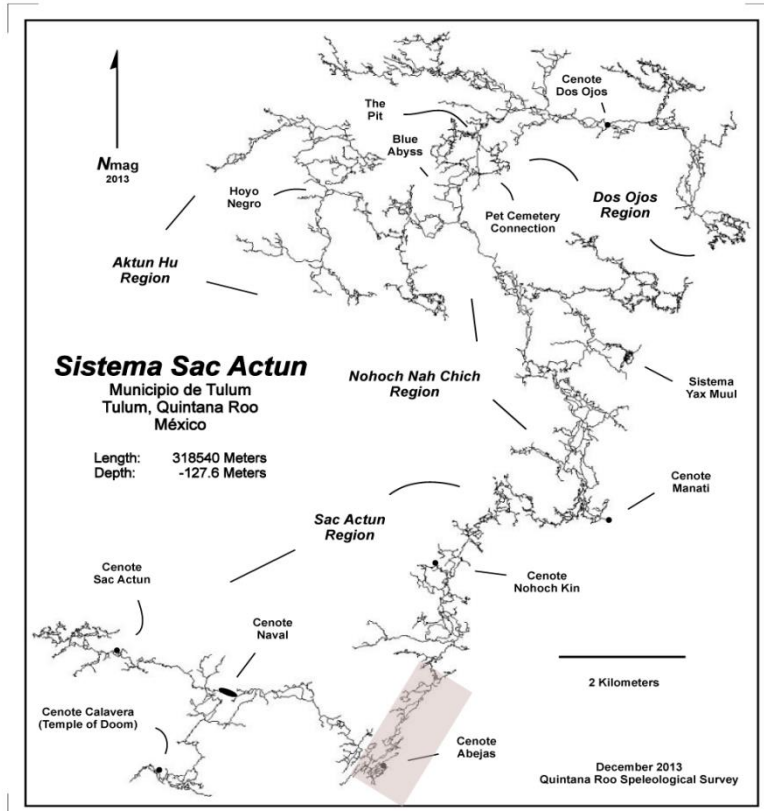


Figure 3.19 Coastal maze passages of Cenote Abejas section of Sistema Sac Actun

Highlighted area shows the northeast trending maze passages of the Cenote Abejas section – Sistema Sac Actun, the second longest cave in the world and longest cave in Mexico. The passages of this section of cave parallel the coast. Northwest trending passages are fracture controlled, anastomosing in configuration and located perpendicular to the coast (QRSS 2013)

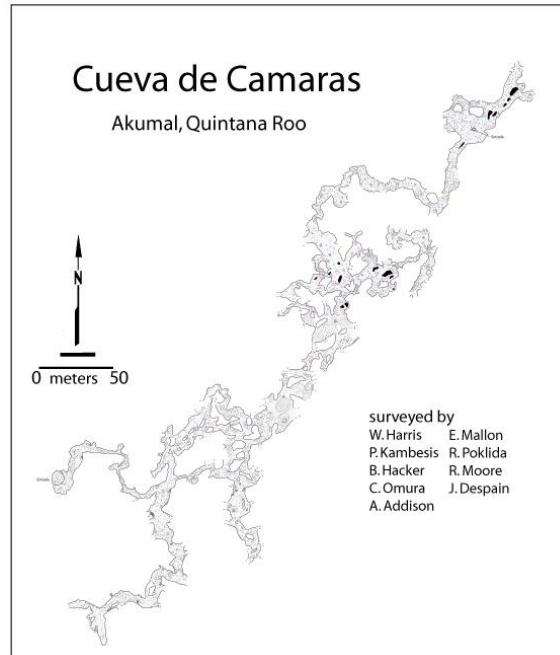


Figure 3.20 Map of Cueva Camaras

This cave is a rectilinear maze cave formed within a beach ridge located 2.5 km from the coast. Cartography: Aaron Addison

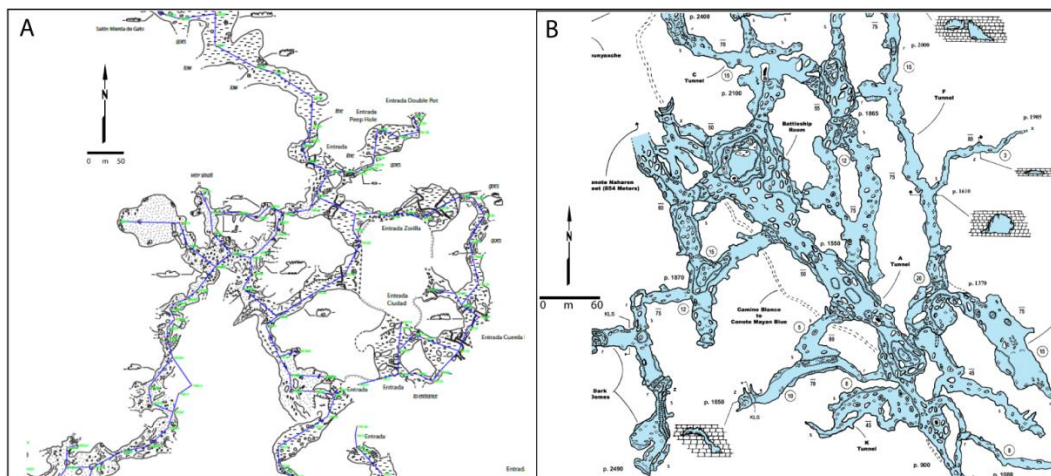


Figure 3.21 Anastomotic cave passage development

(A) Segment of Dos Arboles (located in vadose zone), (B) section of Sistema Ox Bel Ha (underwater) that display northwest trending anastomotic passages. Cartography: Dos Arboles, Sprouse and Kambesis; Ox Bel Ha, James G. Coke IV.

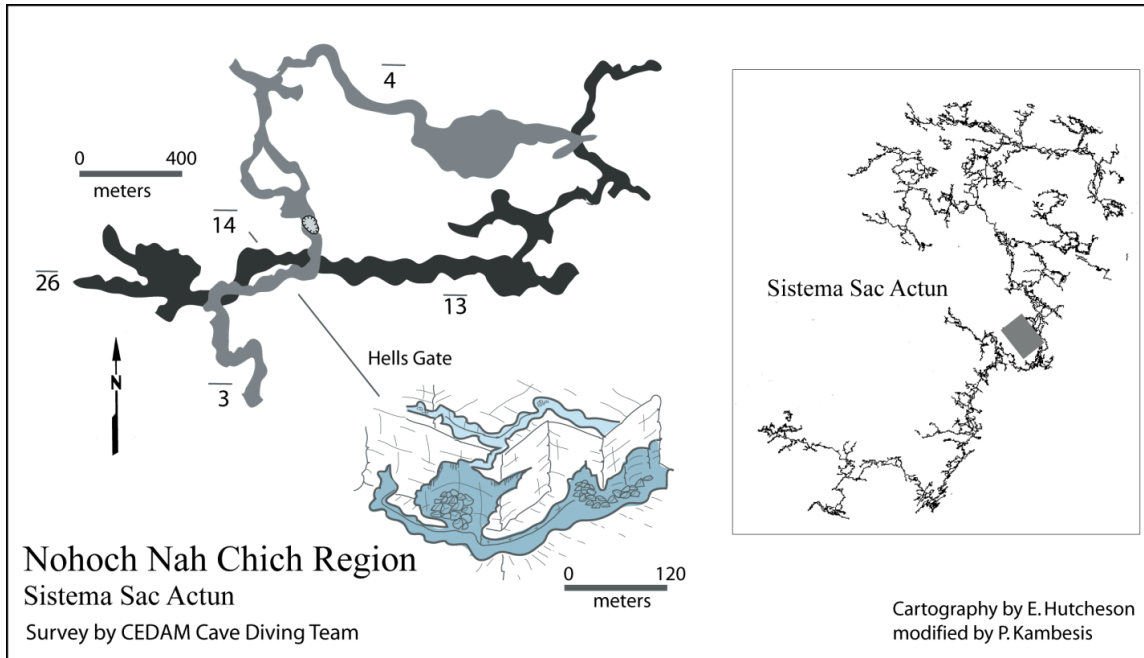


Figure 3.23 Map of Hell's Gate Section of Sistema Sac Actun

Superposition of upper and lower level passage development,
 Cartography: E. Hutcheson, modified by P. Kambesis

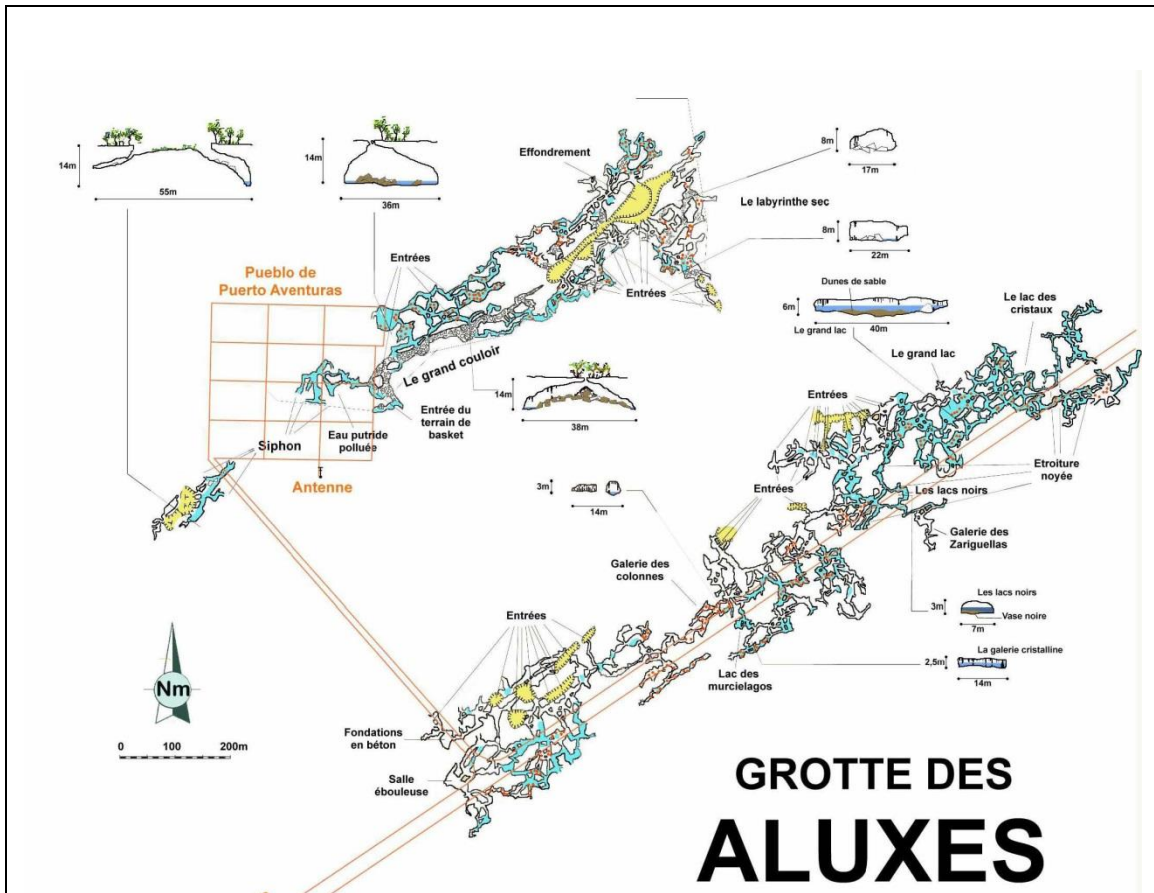


Figure 3.24 Map of Grotte des Aluxes

Grotte des Aluxes is formed in beach ridge located 1 km from the coast with sections that extend into the epiphreatic zone. Cartography: C. Thomas

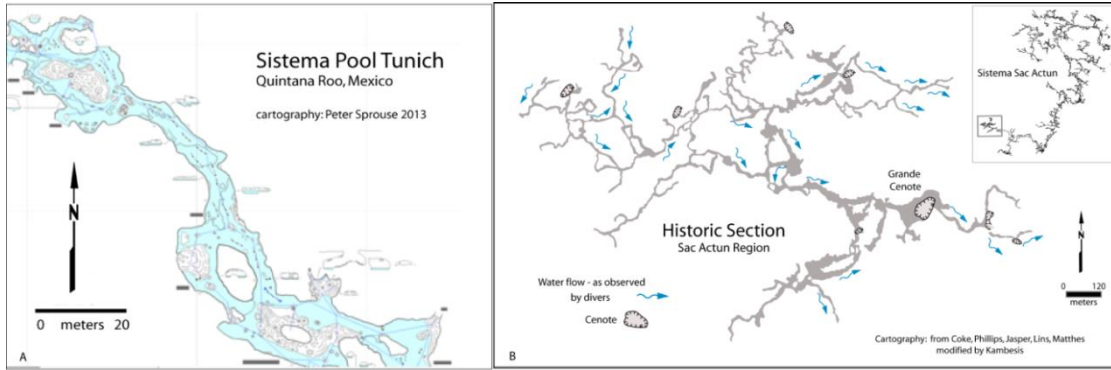


Figure 3.25 Water flow in underwater and vadose-epiphreatic zone caves

(A) Water flow documented in the northern most reaches of Sistema Pool Tunich, Cartography, P. Sprouse; (B) Water flow as reported by cave divers in Sistema Sac Actun, Cartography Coke, Phillips, Jasper, Lins, and Mathes, modified by Kambesis

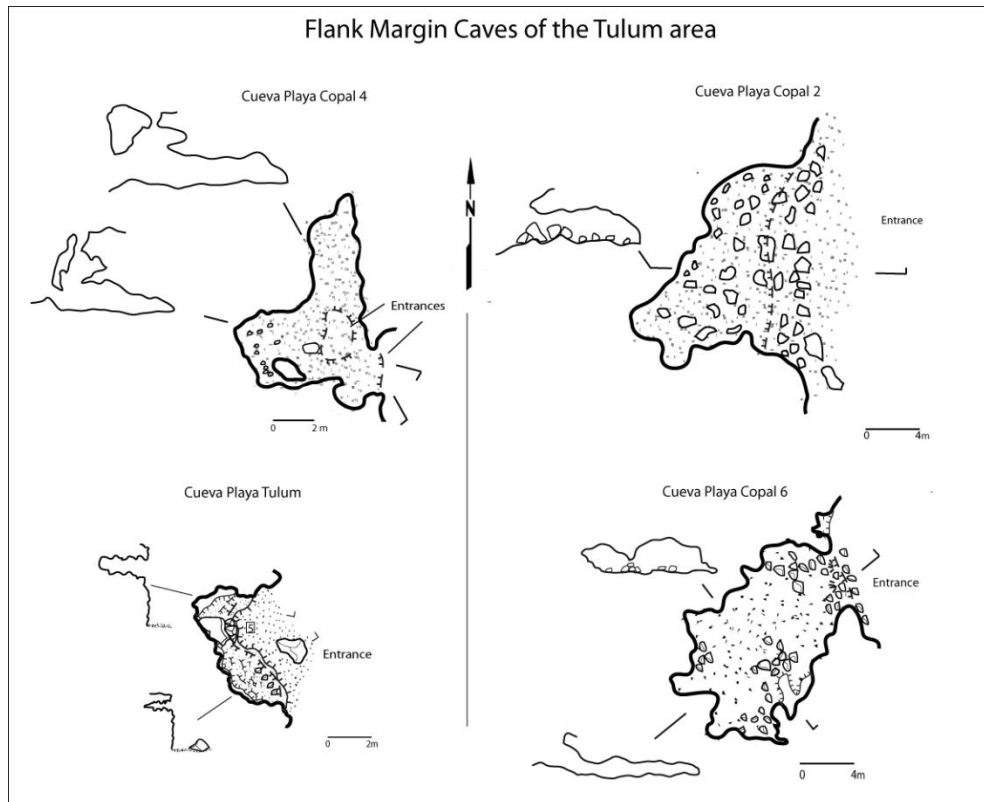


Figure 3.26 Flank margin caves of the Tulum area

Cartography: P. Kambesis

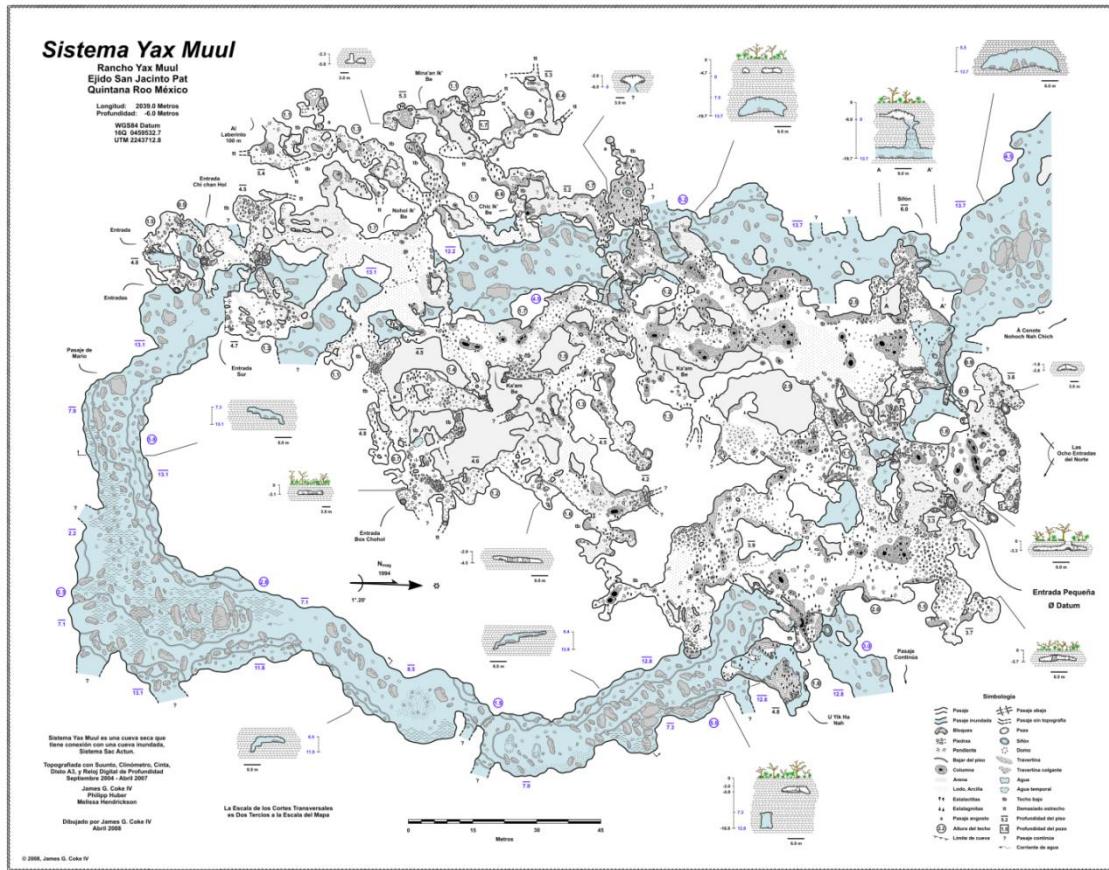


Figure 3.27 Map of Yax Muul section of Sistema Sac Actun

Map shows the relationship between underwater and vadose zone cave passages typical of the study area. Cartography: James G. Coke IV

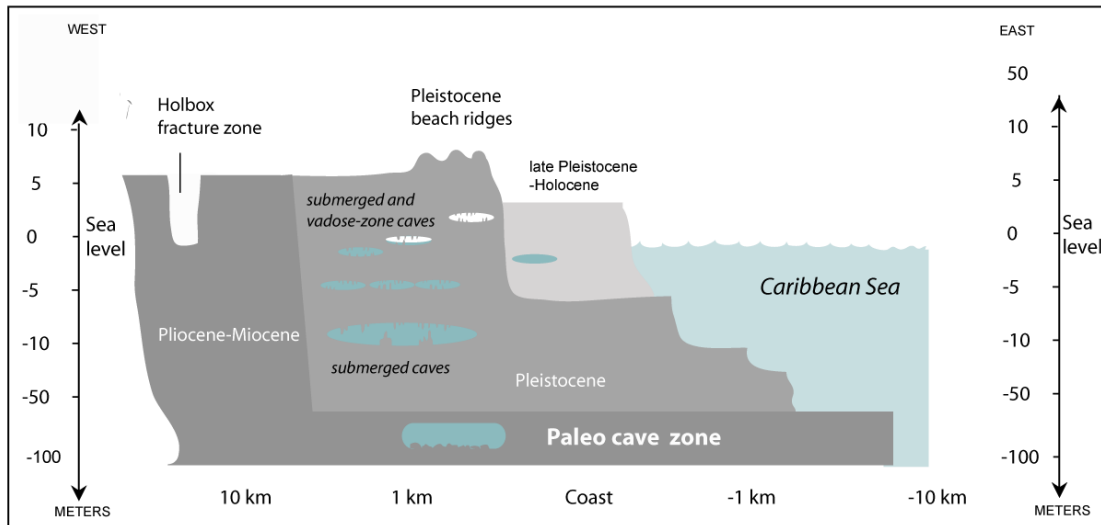


Figure 3.28 Cave passage development on the northeast coast of Quintana Roo, Mexico
 Modified from Richards and Richards (2009)

CHAPTER IV

A INFLUENCE OF KARSTIC, FLUVIAL, AND LITTORAL PROCESSES ON THE DEVELOPMENT OF REENTRANTS AND ASSOCIATED FEATURES OF ROCKY CARBONATE COASTS

4.1 Abstract

Coastal re-entrant features on rocky carbonate coasts form as a result of fluvial and/or littoral processes and are further modified by karstification and changes in sea level. The gullies of Barbados are examples of fluvial features that were karstified during sea level high stands and that are currently being affected by fluvial karstification. The bokas of the ABC islands have formed from a combination of fluvial, littoral, and karst processes that act on the windward side of the islands. Coastal mixing-zone dissolution is the sole mode of karstification. Flank margin caves which are a hallmark of this type of karstification can be found in the walls of many of the bokas and likely formed during past sea-level high stands. On the modern coast, littoral erosion is exposing flank margin caves that are eroding to form natural bridges, blow holes and coastal collapse features. Karstification is also evident in the older reef terraces located inland from the modern coast. Caletas, located in the major eogenetic aquifer of the northeast coast of Quintana Roo, are formed by mixing zone corrosion and the prograding collapse of cenotes. Crescent-shaped beaches are associated with caletas and result from a combination of karstic and littoral processes.

4.2 Introduction

Coastal development of islands and continents with carbonate coastlines is affected by littoral processes in the form of waves, tides and wind that erode them and form distinct landforms (Bird 2008). When rivers interact with coastlines, strata are eroded and sediments reworked by littoral processes, and the mixing of fluvial and marine waters results in physiochemical variations at the interface between water types (Huggett 2007). Karst processes subject carbonate coastlines to additional erosive agents that expose the coastal zone to dissolutional denudation.

This research focused on karst-related coastal features formed on carbonate coastlines of the Caribbean region (Figure 4.1) whose rocky component consists of Pleistocene age fossil reef terraces. Re-entrant features addressed in this study include gullies (dry valleys), bokas and caletas (the latter two are shallow coastal inlets). Associated with these features are caves, collapse features, and distinct coastline morphologies. The geographic locations of many of these features or combinations of them, and distinctive coastal morphologies occur within the study sites for this research which include Barbados, the windward side of the ABC Islands (Aruba, Bonaire, and Curaçao) and the northeast coast of Quintana Roo, Mexico. The origin and development of these features were influenced by a combination of coral reef ecology, coastal processes, fluvial drainage, and karstification. The purpose of this research is to characterize the interactions of these processes and their resulting features.

4.3 Overview

4.3.1 Gullies of Barbados

The island of Barbados is riddled with many dry valleys locally called gullies (Figure 4.2). The features are of variable lengths and depths and are located on the moderate to steep slopes of all parts of the island. The limestone gullies drain toward the northern, western, and southern coastlines and resemble a network of narrow creek beds in the interior highlands, merging progressively to fewer and wider channels down slope and seaward (Machel et al. 2012). The gradient of most gullies is on average 2° and valley depths can range up to ~30 m (Fermor 1972). Gullies are dry most of the year and may contain small ephemeral streams. During heavy precipitation the gullies can be inundated with fast-flowing floodwaters. Some of the gullies contain cave remnants along their perimeters (Machel et al. 2012).

The origin of the gullies of Barbados has been a controversial topic (Schomburgh 1848, Tricart 1968; Fermor 1972, Machel 1999, Mylroie et al. 2010; Machel et al. 2012). The occurrence of speleothems at cave entrances along many gully walls, along with large boulders that lie scattered along the floors of some gullies, suggest an origin from stream cave dissolution and subsequent roof collapse (Machel 1999).

Speed (2012), who differentiated gullies into fluvial and karst-affected channels, proposed that the latter were surface expressions of subsurface drainage networks formed at the base of the limestone unit. He suggested that groundwater collected in subterranean conduits that converged downstream. As the conduits enlarged in their down-gradient flow along the contact between carbonate and non-carbonate strata, they collapse and widened creating channels that prograded to the surface along downslope trajectories. He

supported this idea with the observation that large rocks at the bottoms of karst-affected channels were too coarse (5-10 m diameter) to have been moved by stream flow. In addition, he posited that fluvial down cutting would produce deep gorges that cut through the limestone and into the nonresistant bedrock—a condition that is not observed—and thus he suggested that gullies must have evolved by some other process.

An alternate model proposed by Machel et al. (2012) suggested that gullies may have formed from downward erosion from surface drainage followed by flooding of the valleys during glacioeustatic sea-level rise. The cave segments observed in gully walls did not originate from subsurface streams but may be remnants from mixing zone dissolution that formed flank margin caves. Glacial eustasy, tectonic uplift, and erosion widened the gullies and exposed the caves. Tufa speleothems are common in the entrance areas of the eroded caves.

Barbados has been classified into four major geomorphic zones as proposed by Speed (2012) with slight modification for this research (Table 4.1). The zones include the Terraced Flank (Zone I), the Central Highlands (Zone II), the Windward Slope (Zone III) and the Scotland District (Zone IV).

Zone IV, the oldest zone and referred to by Speed (2012) as foundation rock, consists of strata that make up an accretionary prism complex consisting of terrigenous turbidites and gravity flow deposits that are interbedded with hemipelagic and pelagic radiolarites of Eocene age (Speed 1990). Emplacement of tectonic diapirs consisting of a combination of organic mud and mud matrix likely continues today and may be responsible for the elevation of Barbados above the rest of the accretionary prism (Speed, 1990). Overlying the Eocene rocks are flat-lying Miocene chinks, marls and radiolarites

of the Oceanics Group (Senn 1946). The chalks form a regional aquitard that is missing in but a few, relatively small locations around the island (Machel et al. 2012). The major geomorphic agent in this zone is fluvial erosion (Speed 2012).

Zone III is a north-south trending belt that forms the windward retreating margin of Zones I and II (Speed 2012). It is composed of an active landward escarpment and a hummocky gullied apron formed from the retreat of the escarpment. The apron trends seaward and is underlain by landslide deposits indicating that mass wasting is the major geomorphic process in this zone (Speed 2012).

Zone II is an elevated rolling plain that ranges in elevation from 340 meters at Mt. Hillaby, to 130 meters on the northern side of the island with a limestone thickness that varies between 50 and 130 meters (Speed 2012). The zone has been heavily karstified as evidenced by numerous sinkholes and caves. The zone is underlain by the oldest limestone unit on the island that may range from Pleistocene (Banner et al. 1994) to early Pleistocene at 700 ka (Speed 2012). The oldest parts of this limestone unit were deposited during a very early episode in the island's development and formed as an extensive, low bank which covered the entire island (Speed 2012). The zone is bordered by ancient sea cliffs (the Second High Cliff) except on its eastern margin where it is bounded by Zone III. The entire unit unconformably overlies the foundation rock. This limestone unit differs from the younger units of Zone I by its greater thickness and diagenetic maturity (Speed 2012). A combination of karstic and fluvial processes, along with normal faulting, are the main geomorphic agents in this zone (Speed 2012).

Zone I extends from Zone II and the Second High cliff to the modern coastline and encompasses the northern, western and southern slopes of the island. Uplift has resulted

in stair-stepping marine terraces and erosion has produced a hummocky, gullied terrain on which the marine terraces have been heavily degraded. This zone also displays karst features. Zone I is underlain by Pleistocene limestone units (0 to 70 meters in thickness) that are younger in age and much less diagenetically mature than those that make up Zone II (Speed 2012). The geomorphic processes that formed this zone are three-fold: deposition of limestone and erosion that produced the stepped terraces during tectonic uplift, karstification, and subaerial erosion by running water that degraded the terraces (Speed 2012).

The hydrology of Barbados is controlled by the contact between the Pleistocene reef limestones which forms an unconfined aquifer, and the underlying Miocene chalk which dips toward the sea and forms a regionally extensive aquitard (Senn 1946; Banner et al. 1990). Autogenic recharge enters the limestone aquifer at discrete points and makes its way to the contact between the Pleistocene limestones and underlying Miocene chalk. Groundwater travels along the contact via turbulent flow until it reaches a point where the aquitard is below sea level (Kambesis and Machel 2013). The groundwater forms as a wedge-shaped freshwater lens overlying saltwater that has intruded into the aquifer. The fresh-saltwater interface makes a dissolutionally aggressive mixing zone that can form phreatic voids within the hosting limestone (e.g., flank margin caves, Figure 4.5). The lens varies in thickness from 4 meters on the west coast to greater than 50 meters on the southeast section of the island (Speed 2012). Zone IV is hydrologically characterized by fluvial drainage with flow paths that go directly to the sea.

Barbados is classified as a 'composite carbonate island' according to the Carbonate Island Karst Model (CIKM) (Myloie and Myloie 2007), because non-

carbonate rocks are exposed at the surface in the northeast part of the island. The configuration of the geologic units that make up the island and their interaction with meteoric recharge and freshwater-saltwater hydrology coupled with glacioeustasy and tectonics has resulted in the formation of a variety of caves and karst features. Though flank margin caves are abundant, stream caves drain sections of Zone II and polygenetic caves occur on the terraces of Zone I and II and along the coast in Zone I. The most common type of cave on Barbados is the hybrid cave. These features are formed because hydrological conditions changed repeatedly with the interaction of glacioeustatic sea-level variations and tectonic uplift. As a result, flank margin caves are commonly exposed by wave action and cliff retreat that subjects the caves to littoral processes and overprinting to form hybrid caves (Figure 4.6).

Stream caves similar to those found in continental settings are found in Barbados (Figure 4.7). They typically occur downslope from the edge of the Scotland District in Zone II. The caves are recharged from sinkholes on the surface and from direct input of water at the upstream end of gullies (Groves 1994). The underground streams recharge the freshwater lens that is located close to the coast.

Other types of caves have also been documented on the coast including littoral, talus and fissure caves (Kambesis and Machel 2013). However, these are pseudokarstic which means they resemble dissolutional caves but are formed by different processes. Speleogenetic factors that control formation of all cave types on Barbados are a function of hydrology, chemical dissolution, mechanical erosion, mass movement, or a combination thereof.

Sinkholes are extremely abundant on Barbados. A sinkhole inventory documented 2,830 sinkholes on the island (Wandelt 2000), and Day (1983) found sinkhole abundance to be 9.47/km², with the highest density at the 100-150 meter elevation (Figure 4.8). The sinkholes of Barbados come in two forms: large inter-fluvial sinkholes located between gullies, and small shafts occurring within the gullies (Day 1983). The inter-fluvial sinkholes tend to be filled with low permeability soil that impedes infiltration of water into the aquifer, whereas the shafts act as conduits that transmit large volumes of water downward at times of heavy rain (Jones and Banner 2003).

4.3.1.1 Site Description

Barbados is located approximately 150 km east of the Lesser Antilles volcanic island arc. The major axis of the island has a 34-km north to south trend and an east-west extent of ~23 km at its widest. The topographic configuration of the island is asymmetric with its highest point of elevation on Mt. Hillaby at 340m above sea level. The northeast and western slopes have grades of 4-7% , and north, east and south slopes are at 1-3% grades. The perimeter of the island encompasses 97 km and total land area is ~431 km² (Iniss et al. 2001.) Gullies occur as radiating dry drainage channels that originate around the island's high point and trend downslope towards the coast.

Barbados currently has a humid to sub-humid tropical maritime climate with a wet season that runs from June to November/December and a dry season from December/January through May. Average precipitation varies across the island due to orographic effects (Humphrey 2004) and can range between 1,100 mm to 2,100 mm

(Iniss et al. 2001). The island lies within the path of the northeast trade winds with average monthly temperatures ranging between 21°C and 31°C, depending on the season.

Island topography is characterized by gently sloping terraces of Pleistocene carbonates (locally called Coral Rock) separated by cliffs that parallel the coasts (Figure 4.3). The Upper Coral Rock terrace has an elevation range from 180 to 240 meters above sea level, the Middle Coral Rock terrace ranges in elevation from about 60 to 90 meters, and the Lower Coral Rock terrace is only a few meters to tens of meters above sea level.

The physiography of the island is the result of glacioeustasy combined with continuous tectonic uplift of 0.5m /ky on average over the last million years and punctuated by increased rates of uplift that created the major cliffs that now border the main terraces. The cliffs are named First High Cliff and Second High Cliff (Speed 1983, Taylor and Mann 1991, Schellmann and Radtke 2004). The objective of this study was to determine the geologic controls on gully development.

4.3.1.2 Geologic setting

Barbados has been classified into four major geomorphic zones as proposed by Speed (2012) with slight modification for this research (Table 4.1). The zones include the Terraced Flank (Zone I), the Central Highlands (Zone II), the Windward Slope (Zone III) and the Scotland District (Zone IV).

Zone IV, the oldest zone and referred to by Speed (2012) as foundation rock, consists of strata that make up an accretionary prism complex consisting of terrigenous turbidites and gravity flow deposits that are interbedded with hemipelagic and pelagic radiolarites of Eocene age (Speed 1990). Emplacement of tectonic diapirs consisting of a combination of organic mud and mud matrix likely continue today and may be

responsible for the elevation of Barbados above the rest of the accretionary prism (Speed, 1990). Overlying the Eocene rocks are flat-lying Miocene chalks, marls and radiolarites of the Oceanics Group (Senn 1946). The chalks form a regional aquitard that is missing in but a few, relatively small locations around the island (Machel et al. 2012). The major geomorphic agent in this zone is fluvial erosion (Speed 2012).

Zone III is a north-south trending belt that forms the windward retreating margin of Zones I and II (Speed 2012). It is composed of an active landward escarpment and a hummocky gullied apron formed from the retreat of the escarpment. The apron trends seaward and is underlain by landslide deposits indicating that mass wasting is the major geomorphic process in this zone (Speed 2012).

Zone II is an elevated rolling plain that ranges in elevation from 340 meters at Mt. Hillaby, to 130 meters on the northern side of the island with a limestone thickness that varies between 50 and 130 meters (Speed 2012). The zone has been heavily karstified as evidenced by numerous sinkholes and caves. The zone is underlain by the oldest limestone unit on the island that may range from Pleistocene (Banner et al. 1994) to early Pleistocene at 700 ka (Speed 2012). The oldest parts of this limestone unit were deposited during a very early episode in the island's development and formed as an extensive, low bank which covered the entire island (Speed 2012). The zone is bordered by ancient sea cliffs (the Second High Cliff) except on its eastern margin where it is bounded by Zone III. The entire unit unconformably overlies the foundation rock. This limestone unit differs from the younger units of Zone I by its greater thickness and diagenetic maturity (Speed 2012). A combination of karstic and fluvial processes, along with normal faulting, are the main geomorphic agents in this zone (Speed 2012).

Zone I extends from Zone II and the Second High cliff to the modern coastline and encompasses the northern, western and southern slopes of the island. Uplift has resulted in stair-stepping marine terraces and erosion has produced a hummocky, gullied terrain on which the marine terraces have been heavily degraded. This zone also displays karst features. Zone I is underlain by Pleistocene limestone units (0 to 70 meters in thickness) that are younger in age and much less diagenetically mature than those that make up Zone II (Speed 2012). The geomorphic processes that formed this zone are three-fold: deposition of limestone and erosion that produced the stepped terraces during tectonic uplift, karstification, and subaerial erosion by running water that degraded the terraces (Speed 2012).

The hydrology of Barbados is controlled by the contact between the Pleistocene reef limestones which forms an unconfined aquifer and the underlying Miocene chalk which dips toward the sea and forms a regionally extensive aquitard (Senn 1946; Banner et al. 1990). Autogenic recharge enters the limestone aquifer at discrete points and makes its way to the contact between the Pleistocene limestones and underlying Miocene chalk. Groundwater travels along the contact via turbulent flow until it reaches a point where the aquitard is below sea level (Kambesis and Machel 2013). The groundwater forms as a wedge-shaped freshwater lens overlying saltwater that has intruded into the aquifer. The fresh-saltwater interface makes a dissolutionally aggressive mixing zone that can form phreatic voids within the hosting limestone (e.g., flank margin caves, Figure 4.5). The lens varies in thickness from 4 meters on the west coast to greater than 50 meters on the southeast section of the island (Speed 2012). Zone IV is hydrologically characterized by fluvial drainage with flow paths that go directly to the sea.

Barbados is classified as a *composite carbonate island* according to the Carbonate Island Karst Model (CIKM) (Myroie and Myroie 2007), because non-carbonate rocks are exposed at the surface in the northeast part of the island. The configuration of the geologic units that make up the island, and their interaction with meteoric recharge and freshwater-saltwater hydrology coupled with glacioeustasy and tectonics has resulted in the formation of a variety of caves and karst features. Though flank margin caves are abundant, stream caves drain sections of Zone II and polygenetic caves occur on the terraces of Zone I and II and along the coast in Zone I. The most common type of cave on Barbados, the hybrid cave, formed because hydrological conditions changed repeatedly with the interaction of glacioeustatic sea-level variations and tectonic uplift. As a result, flank margin caves are commonly exposed by wave action and cliff retreat, which subjects the caves to littoral processes, and overprinting to form hybrid caves (Figure 4.6).

Stream caves similar to those found in continental settings are found in Barbados (Figure 4.7). They typically occur downslope from the edge of the Scotland District in Zone II. The caves are recharged from sinkholes on the surface and from direct input of water at the upstream end of gullies (Groves 1994). The underground streams recharge the freshwater lens that is located close to the coast.

Other types of caves have also been documented on the coast including littoral, talus, and fissure caves (Kambesis and Machel 2013). However, these are pseudokarstic which means they resemble dissolutional caves but are formed by different processes. Speleogenetic factors that controlled formation of all cave types on Barbados are a

function of hydrology, chemical dissolution, mechanical erosion, mass movement, or a combination thereof.

Sinkholes are extremely abundant on Barbados. A sinkhole inventory documented 2,830 sinkholes on the island (Wandelt 2000), and Day (1983) found sinkhole abundance to be 9.47/km², with the highest density at the 100-150 meter elevation (Figure 4.8). The sinkholes of Barbados come in two forms: large inter-fluvial sinkholes located between gullies, and small shafts occurring within the gullies (Day 1983). The inter-fluvial sinkholes tend to be filled with low permeability soil that impedes infiltration of water into the aquifer, whereas the shafts act as conduits that transmit large volumes of water downward at times of heavy rain (Jones and Banner 2003).

4.3.2 Bokas of the ABC Islands

All coastal reentrant features located on the coasts of Aruba, Bonaire and Curaçao (Figure 4.9) are called bokas and labelled as such on maps, travel guides and in the literature. Figure 4.10A illustrates the typical morphology of a boka. Figure 4.10B shows remnants of flank margin caves that can occur in the perimeter walls of the feature. Bokas display a diversity of morphologies, distributions, and extents that indicate different origins and overprinting of processes. Associated with some of the bokas is a widespread system of fluvial valleys formed on interior Cretaceous volcanic rocks that have incised through the limestone terraces into the underlying basaltic bedrock. However, bokas also occur in areas that are not subject to fluvial drainage. Associated with both types of bokas are dissolutional and/or littoral caves, and littoral features such as natural bridges, and blowholes located on the seaward facing side of the lowest reef

terraces (Figure 4.11). Older terraces located farther inland also contain dissolutional caves.

Several origins have been proposed for bokas including one implicating tsunami activity (Scheffers 2004). Stefanic and Cornell (2011) proposed a model for boka formation indicating that they were relict and degraded karst features, formed during the post-MIS 5e sea-level low stands of the late Pleistocene, by capture of streams running off of the interior volcanic rocks. According to their model, stream capture created conduit caves at the limestone-volcanic contact. Later collapse of these caves produced rectilinear bokas, which subsequently were partially inundated by Holocene sea-level rise to produce the features observed today. This model is similar to one developed by Machel (1999) for the origin of gullies on Barbados.

An alternate model (Kambesis et al. in press) suggests that bokas did not incise the reef terraces after MIS 5e, but rather, formed syndepositionally with the reef deposition. Sediment and freshwater from interior streams prevented the formation of the reef terraces where the stream entered the sea. Seaward flow of allogenic freshwater and sediment inhibited reef growth and created a trough across the reef crest. Reef terraces formed either side of the incipient boka and uplift or eustatic sea-level drop subaerially exposed the reef crest allowing a freshwater lens to form in the reef limestones. Caves located on the incipient boka perimeter are flank margin in origin (rather than stream caves) formed due to mixing dissolution. The bokas themselves are the result of simple fluvial incision, modified today by littoral processes in their downstream ends.

None of the models on boka origin and development consider the multiplicity of form, distribution and function. It is the purpose of this research to consider those factors in boka development.

4.3.2.1 Site Description

The ABC Islands (Aruba, Bonaire and Curaçao), located 80 km north of Venezuela, are the westernmost of the Lesser Antilles island chain (Figure 4.9). The islands meet the CIKM classification of *composite carbonate island*. The tidal range for the islands is microtidal at an average value of 30 cm (Fouke, 1993). The climate shared by the islands is semi-arid with annual precipitation averaging 580 mm/year, and an average yearly temperature of 27.5°C (van Sambeek et al. 2000). Surficial discharge is via arroyos and periodic sheet wash (Westermann and Zonneveld 1956). Table 4.2 summarizes the geographic extents of all of the islands.

The xeric vegetation that is characteristic of the islands is not the result of the local climate but from the occupation and overexploitation of the land by the Spanish and Dutch settlers during the sixteenth century who cleared the native woods for human development and agriculture (Westermann and Zonneveld 1956).

4.3.2.2 Geologic setting

The ABC island chain is aligned along the crest of a 200 km-long segment of the east–west-trending Leeward Antilles ridge within the Caribbean–South America plate boundary zone. (Hippolyte and Mann 2009). The ridge is a major crustal structure of Cretaceous island arc and oceanic origin (Magnani et al. 2009) and was modified during the Cenozoic by strike-slip and convergent plate boundary motion that resulted in a series

of northwest-striking faults that separated the islands and formed steep coastlines (Gorney et al., 2006). According to Van Sambeek et al. (2000), the igneous rocks of the islands were part of a volcanic arc located on the leading edge of a tectonic plate that moved into the Caribbean from the Pacific Ocean. The island arc was thrust into the northern margin of the South American continent resulting in faulting, folding, and metamorphism as evidenced in the basement rocks. The island chain underwent significant uplift and folding during the Cretaceous through the Eocene and experienced more than 5 km of vertical displacement (Silver et al., 1975). Increased compressional stress during the Miocene uplifted the island chain into the shallow marine photic zone where carbonate reef development began (Fouke 1993). Figure 4.12A-C displays the geology of each of the islands.

Aruba basement rocks consist of basalt, dolerite, pyroclastic and volcanoclastic sedimentary rocks that make up the late Cretaceous Aruba Lava Formation (Hippolyte and Mann 2009). A tonalitic batholith was intruded in the Late Cretaceous (85 Ma) (Priem et al. 1978). These strata are unconformably overlain by the limestones of the Seroe Domi Formation of Miocene age (de Buissonje 1974).

On Curaçao the oldest rocks on the island are a 3000 m-thick volcanic-sedimentary sequence of Cretaceous–Danian age that is folded and metamorphosed to the zeolite facies (Beets et al. 1977). These units include the Curaçao Lava Formation (tholeiitic basalts), the Knip Group (silica-rich rocks and clastic sediments), and the Midden-Curaçao Formation (conglomerate, sandstone and shale), which are unconformably overlain by weakly folded limestones, sandstones and clays of Eocene

age. As with Aruba, the Miocene Seroe Domi Formation overlies these rocks (de Buissonje 1974).

Bonaire stratigraphy consists of the Albian to Coniacian-age Washikemba Formation and contains more than 5 km of submarine flows and shallow intrusions of basalt, andesite and dacite with thinner intercalations of cherty limestone (Beets et al. 1977). The 30 m thick Rincon limestone (Maastrichtian) unconformably overlies the Washikemba Formation. In the central part of Bonaire the Rincon Limestone is overlain by the Soebi Blanco Formation, a 120-meter thick fluvial sequence that is equivalent to the Danian Midden Formation of Curaçao (Beets et al., 1977). Quaternary glacioeustasy, combined with slow tectonic uplift resulted in the formation of a series of Pleistocene reef terraces that ring the coast line of all three islands. (Van Sambeek et al. 2000). The islands exemplify eroded anticlines, where the central region of each consists of weathered basalt and soil and the island perimeters are comprised of constructional reef terraces of Pleistocene age that overlie the weathered basalt (deBuissonje 1974, Hippolyte and Mann, 2009).

The Pleistocene terraces of each island, which are similar to those on Barbados (de Buissonje 1974), occur near and at the coastlines with progressively younger terraces found seaward (Alexander, 1961; Zonneveld et al, 1972; Fouke et al., 1996; Schellmann and Radtke 2004). The limestone cliffs on the windward side of the islands are divided into five distinct terraces on Curaçao and Bonaire, and three on Aruba (Alexander 1961).

Muhs et al. (2012) noted that the series of marine terraces have a stairstep type morphology with a lower terrace backed by the outer edge of the next terrace above it; though within the terrace, limestone sequences are stacked. This indicates that the

interglacial coral reef record of the ABC islands is a hybrid of those observed on uplifting versus tectonically stable coasts and is indicative of slow uplift rates alternating with rapid uplift.

Boca development occurs within the lower terrace limestone on Aruba, Bonaire and Curaçao and remnants of flank margin caves typically occur within the perimeter walls of the feature. This is the youngest and topographically lowest of reef terraces developed along the windward coasts of all three islands. The terrace attains a maximum width of 600 m on the windward side of Curaçao (Herweijer and Focke 1978) and thickness of 35m of which 2-15m is exposed above sea level (Pandolfi et al. 1999).

The lowest terrace consists of two sequences; the upper is called the Hato Unit formed during the 125,000 ka sea level high stand (MIS 5e) and the lower separated by a prominent discontinuity is the Kortelain Unit with age of up to 225,000 ka (Herweijer and Focke 1978, Schellmann et al. 2004).

Both units are made up of a barrier reef zone with *Acropora palmata* and the coralline alga *Porolithon pachydermum*, a lagoonal or back-reef zone with *Montastrea annularis sensu lato*, and *A. cervicornis*, and an inner-most lagoon dominated by *Siderastre* (de Buissonje 1974, Pandolfi et al. 1999 and Meyer et al. 2003).

The ABC island chain is classified as *composite carbonate island* as per CIKM (Myloie and Myloie 2007). Though classified as the same island type as Barbados, the relationship of the non-carbonate to the carbonates is different. In Barbados, clastics are situated at lower elevations than the carbonates adjacent to them, whereas on the ABC Islands, the igneous rocks are at higher elevation which makes for a difference in mode of recharge.

In the composite island model, both carbonate and non-carbonate rocks are exposed at the island surface allowing for autogenic and allogenic catchment. For autogenic catchment, meteoric recharge infiltrates into the carbonate rock accumulating as a lens of freshwater floating on saltwater that has permeated the island from the sea. Because the cores of the islands are non-carbonate, these areas are fluvially drained, leading to potential allogenic recharge where these streams contact the carbonates. However, to date, there is no evidence of allogenic stream caves on any of the islands. Flank margin caves are the predominant cave type on the ABC Islands and they occur in the walls of bokas, in the lower reef terrace, and in the higher reef terraces. At the lowest terrace, littoral erosion can overprint flank margin caves to form hybrid caves which are common on all three islands.

4.3.3 Caletas of northeast Quintana Roo, Mexico

Coastal inlets called caletas and crescent-shaped beaches are common on the northeast coast of the Yucatan peninsula in the state of Quintana Roo, Mexico. Caletas are narrow inlets that extend inland for a range of distances (50-700 meters) and are associated with coastal springs (Back et al. 1979). Hanshaw and Back (1984) speculated that caletas formed where discharging freshwater from conduits mix with saltwater at their seaward margins causing an increase in local dissolution and inducing conduit collapse that migrates inland to form a cove. (Their fieldwork was conducted prior to the knowledge of the extent and density of subterranean drainage.) As dissolution continued to act on the limestone, it became more vulnerable to the mechanical erosion by wave action (Hanshaw and Back 1984). As the inlet opening became wider, waves had greater

access to the caleta walls which eventually eroded to form a crescent-shaped beach (Back et al 1979).

4.3.3.1 Site Description

The state of Quintana Roo is located on the northeast coast of the Yucatan peninsula Figure 4.13A The peninsula is the aerially emergent part of the greater Yucatan Platform; a carbonate platform with a surface area of 300,000 km² (Bauer-Gottwein et al. 2012). The low-elevation, heavily karstified peninsula encompasses over half of the total platform surface area, and divides the Gulf of Mexico from the Caribbean Sea. The Campeche Bank is the western submerged part of the platform and extends 200 km northwest into the Gulf of Mexico at depths of less than 200 m. The eastern submerged bank extends up to 10 km from the Caribbean shoreline with a 400-meter loss of elevation into the Yucatan Basin east of Cozumel (Beddows 2003). Platform asymmetry is due to down-faulting that has led to the development of fracture zones parallel to the Caribbean coast (Beddows 2004). The peninsula has been tectonically quiescent since the late Pleistocene (Weidie 1985) so major variations in sea level since that time are solely attributed to glacioeustasy. The study site is between just south of Tulum to just North of Playa del Carmen (Figure 4.13B)

The climate of the Yucatan peninsula is tropical with distinct wet and dry seasons (Kottek et al. 2006). The average annual temperature is 26°C, with a range in monthly averages between 23–29°C (Beddows 2004). May to September is the hot, rainy season and October to April is the relatively cooler dry season. There is a significant east–west precipitation gradient across the peninsula (Neuman and Rahbek 2007). The Caribbean coast is the wettest side with >1500 mm of precipitation per year (Gonzalez-Herrera

2002). Evapo-transpiration (ET) is spatially variable across the peninsula with higher ET along the coasts and lower ET in the less densely vegetated and much drier northwest part of the peninsula (Bauer-Gottwein et al. 2012).

4.3.3.2 Geologic setting

The strata of the northeast coast of Quintana Roo consist of reef-related carbonates that have been divided into Upper, Middle, and Lower Pleistocene units comprised of marine and non-marine sequences (primarily eolianites) (Figure 4.14). These strata accumulated in shelf margin, reef, and back reef facies during interglacial high stands (Ward 1985), and are separated by unconformities indicative of exposure and erosion of the platform surface on marine retreat (Lauderdale et al. 1979, Rodriguez 1982). Marine sequences include beach, near shore and lagoonal strata, and coral-reef limestone; non-marine rocks consist of eolianites, freshwater lacustrine carbonate mudstone, and caliche (Ward 2003). Underlying the Pleistocene strata are Miocene-Pliocene carbonate rocks (Richards and Richards 2007).

The state of Quintana Roo is within the Eastern Block-Fault district that extends from Cape Catouche on the northeast coast, to the Yucatan's border with Belize. It is one of five physiographic regions of the Yucatan peninsula which are defined by the influence of prominent fracture or lineament systems (Isphording 1975) (Figure 4.15). The two main faults/lineaments in Quintana Roo are the Holbox Lineament Zone and the Rio Hondo Fault Zone.

The Holbox Lineament Zone (HLZ), originates at the northeastern coast of the peninsula and heads south to within 10 km of the coast inland from Tulum, trending N 5°E to N 10E (Bauer-Gottwein et al. 2012). The HLZ is expressed on the surface by the

alignment of polje-like depressions that seasonally fill with water making narrow, aligned swamps (Weidie 1978). Remote sensing data indicate that development of regional dissolution features were strongly influenced by the lineament zone and result in high permeability and groundwater drainage (Southworth 1985, Tulaczyk et al. 1993). High subsurface electrical conductivity values relative to surrounding areas were detected in the vicinity of Tulum and were interpreted to indicate increased porosity and permeability associated with the faulting (Gondwe, Technical University of Denmark, unpublished data, 2010 reported in Bauer-Gottwein et al., 2012).

The Rio Hondo fault zone (RHFZ) consists of a series of northeast trending (N30-32E) normal faults and has been identified as the on-shore continuation of an extensive horst and graben fault block system located off the southern Caribbean coast of Quintana Roo (Weidie 1985). This is supported by seismic data that confirms the fault system aligns sub-parallel to the southern Caribbean coast (Bauer-Gottwein et al. 2012). Surface expression of the RHFZ is seen in the alignment of shallow lakes, coastal bays, and the orientation of Cozumel which is identified as a horst block (Lesser and Weidie 1988). Interpretation of synthetic aperture radar (SAR) remote-sensing images suggest that the Rio Hondo fault system extends northwards and intersects with the Holbox fracture zone in the vicinity of Tulum (Gondwe et al. 2010).

A well-defined fracture trend (N50-60W) has been identified along the entire coast indicating that fractures control the inland development and extent of coastal features such as caletas (lagoons) and crescent-shaped beaches (Weidie 1978). A second set of fractures with a trend of N30-40E parallels the coast and influences the lateral extent of coastal features. Weidie (1978) noted that the fracture sets may form an

orthogonal system that is genetically related to the RHFZ. He observed changes in fracture trend along the Caribbean coast and speculated the existence of a conjugate fracture system.

The location of coastal discharge features (caletas, and crescent-shape beaches) correlates with areas of maximal fracturing (Weidie 1978). The existence of extensive underwater conduits that display northwest and southeast trends support the idea that linear dissolution corridors are developed along the extensive fracture and lineament zones that occur in northeast Quintana Roo (Tułaczyk et al. 1993).

The coastal karst aquifer of Quintana Roo is unconfined and recharged by precipitation from extensive, inland areas north of Akumal and from areas west near Muyil. The aquifer responds to short term conditions such as heavy rains, barometric pressure, tides, and ocean density, which supports the idea that base flow originates far inland from the coast (Neuman and Rahbek 2007). Aquifer discharge of groundwater to the Caribbean Sea is via a network of conduits of varying size from tens of millimeters in width to humanly enterable passages that can range up to 80 meters in width (QRSS 2014). The groundwater discharge of the Caribbean coast of the Yucatan has been estimated to be 2.3×10^7 m³/year per kilometer of coast (Beddows 2004).

The purpose of this study was to inventory and document caletas and crescent-shaped beaches and to determine their relationship with known subterranean drainage systems. Back et al. (1979) suggested that the coastal features of Quintana Roo are related to subsurface drainage but there was no knowledge at that time of extensive underwater caves systems that have been documented since the mid-1980s.

4.4 Methods

Field mapping was conducted at all sites in order to morphologically describe, inventory and survey coastal re-entrant and related features such as caves, natural bridges, blow holes, gullies, bokas, caletas and coastal springs. Feature locations were recorded with hand-held GPS units (GARMIN CSX60) and photo-documented via digital camera. Caves and other features were mapped using survey techniques as established by Cave Research Foundation standards (Appendix B.2).

Aerial photographs and satellite imagery for all field sites were obtained from the USGS remote sensing website (<http://www.usgs.gov/pubprod/aerial.html>), from the website of Instituto Nacional de Estadística et Geografía (INEGI) (<http://www.inegi.org.mx/>), and from Google Earth. Quintana Roo Speleological Survey provided supplementary hydrologic and geologic information pertaining to coastal features of Quintana Roo.

In order to analyze the gully system of Barbados, drainage networks were digitized on 1:10,000 scale geo-referenced topographic maps of Barbados, by watershed (Government of Barbados 2004), and within each watershed gullies were digitized in sections. This captured the gully systems for analysis. Other relevant information was compiled including geology, cave data, hydrology, topography and GPS locations for all features. All data were projected in UTM coordinates, WGS84.

Cave and feature locations from GPS units were downloaded to Excel and then exported to an Access database for use with a geographical information system (GIS). Cave data and related field data were processed using COMPASS data reduction software. COMPASS cave data were exported as Scalable Vector Graphics (SVG) and

shapefiles for use in Adobe Illustrator® for cartography and for GIS analysis. All data and derivative products were compiled into ArcMap® 10.2 geographical information software for analysis and cartographic rendering.

Boka field mapping was conducted on the windward sides of Aruba, Bonaire and Curaçao. Bokas were geo-referenced with hand-held GPS units. For each boka, a reference datum was established at a point midway between the terminal walls of the landward end of the feature (Figure 4.6). Azimuth of the line projected to the seaward end of the boka was recorded. Boka depths and widths were measured via survey traverse on a line perpendicular to the main axis of the boka with compass, tape and inclinometer. Boka lengths were determined either by triangulations or with hand-held GPS units, depending on the size of the feature..

In addition to numerical data, bokas were classified by relationship to surface drainage or littoral process. Fluvially influenced bokas (Figure 4.17A) were characterized by obvious connection to surface drainage and distinct rectilinearity with a long axis much greater than the width axis. Littorally-influenced bokas (Figure 4.17B) were identified as ones that were not obviously connected to a surface drainage channel, having average width and length axis that were similar in value though the width at seaward mouth was typically greater than the average width. Bokas characterized as influenced by fluvial and littoral processes showed connection to a surface channel; boka width and length dimensions were similar in value though width at seaward mouth was typically greater than average width (Figure 4.17C). The following designations were used for boka classification:

F = bokas that were dominantly influenced with surface drainage

L = bokas that appeared to be dominantly influenced with littoral processes

FL= bokas that displayed both fluvial and littoral influence

The field data were used to calibrate measurements on remote sensing images.

This allowed the remote mapping of bokas that were not documented in the field. Remote sensing parameters included boka length, maximum and minimum widths, azimuth for each boka, and vertical extent. Boka designation for computer measured features was determined from Google Earth images. Lithology of boka walls and sediment cover on boka floors were noted on field sketches and with the survey data. Caves and other coastal features were geo-referenced with hand held GPS units and mapped using Cave Research Foundation standard cave survey techniques (APPENDIX B.2). Locations of all features were added to a GIS in order to determine density and distribution of bokas and caves and to ascertain the relationship of the features.

Coastal reentrant features on all three islands vary in their size and morphology so a set of ratios was established to allow comparison of the features. These included the following:

$L / \text{width}_{\text{max}} = \text{Ar}$	Aspect ratio of length to width	4.1
$W_{\text{max}}/W_{\text{min}}=W_r$	Maximum vs minimum boka width ratio	4.2
$L/ W_r = \text{Ar}_2$	Second iteration of aspect ratio	4.3
$\text{Ar}/\text{Ar}_2= \text{BMI}$	Boka morphology index	4.4

All data were entered in an Excel spreadsheet and ratios calculated in order to determine if morphometric analysis could classify features based on the generated ratios.

For the caleta field mapping, a series of traverses were made along the coast between Tulum and Playa del Carmen (Figure 4.13b) in order to document and inventory

caletas and crescent-shaped beaches in the study area. Since much of the coast is privately owned by commercial enterprises, it was not possible to visit some sections. In those situations, features were inventoried using remote sensing maps. Cave survey data shapefiles were provided by Quintana Roo Speleological Survey in order to correlate cave systems with caletas and/or crescent shaped beaches in a GIS format. Figure 4.18 illustrates morphometric measurement of caletas and crescent-shaped beaches.

Fractal dimension was calculated for a few of the underwater cave systems of the area in order to determine how the underwater conduits of Quintana Roo compare with other caves in the study areas.

4.5 Results

4.5.1 Gully Results

The purpose of the Gully GIS was to identify the location and extent of all gullies and their related watersheds within Zones I and II and to determine their relationship to documented cave systems and other cave-related features. In order to understand the origin of gullies, it was necessary to determine their function and morphology at the drainage basin level. Table 4.3 summarizes the lengths and numbers of the mapped gully sections.

The main gully drainage network radiates asymmetrically from the island's high point at Mt. Hillaby toward the coasts (Figure 4.19A). A series of secondary gullies diverge at nearly right angles to the main gully system (Figure 4.19B).

The watersheds and gullies as mapped on the GIS are shown in Figure 4.20A. The gullies on the west coast encompassed small watersheds that drain to the sea. Gullies located on the east side of the island in Zone IV are steep sided with V-shaped valleys

and steep slopes. Watersheds are small with direct flow to the Atlantic Ocean. The south coast area is relatively flat with few distinct drainages. To the southwest the heads of gullies are at elevations between 70 and 120 m. The land surface on the north side of the island has a gentle slope and the gully systems have northeast and northwest flow paths.

The largest watershed on the island is of the Constitution River (Figure 4.20B) which has a drainage area of 55km². Gullies in the upper reaches of the watershed head from the Mt. Hillaby area. Gullies tend to be steep-sided and can have sinkholes at their bottoms. Caves formed within gully walls are common in this zone as are stream caves including Harrisons Cave and Coles Cave.

Five stream caves have been documented in the western and southern watersheds of the island (Figure 4.21) and include Springhead Cave located within the Mullens Bay watershed, Arch Cave located in the Reads Bay watershed, and Harrisons and Coles cave situated within the Constitution watershed. The longest cave on the island is Bowmanstons Cave located in the Halton watershed. It had been mapped in the early 1970s (Goddard 2007) and is reportedly 90 meters deep and 1700 meters in length. However, a map is currently not available and access to the cave is restricted. All documented stream caves are associated with a master gully and are recharged by water that flows into sinkholes, and at discrete holes in the gully.

Caves also occur in the walls of many of the gullies and they are a different type of cave than the stream caves discussed so far. They are typically small in size and extent, are ramiform in morphology, often have tufa speleothems hanging at their entrances, and are identified as flank margin caves. Saylor's Gully is an example of a gully containing a suite of flank margin caves (Figure 4.22). Fractal analysis was done on some of the gully

caves and 4 of the stream caves of the island in order to morphometrically compare cave types. Table 4.4 lists the caves for which fractal analyses were conducted.

Of the gullies identified on the GIS, 24 contain caves within the gully walls (Figure 4.23). There is likely exploration bias in these numbers as all gullies were not visited. Since they tend to be heavily vegetated, it is likely that more of the gullies contain caves within their side walls.

The gullies in Zone II are deeper than those in Zone I and have a higher concentration of caves located within gully walls. The floors of the flank margin caves can be at the same elevation as the fully floor or as observed in Jack-in-the-Box gully, they can be located up to 5-8 meters above the gully floor.

4.5.2 Boka Results

A total of 32 reentrant features were mapped during field work on the windward coasts of Aruba (7), Bonaire (5) and Curaçao (20). An additional 39 features were mapped via remote sensing (Aruba-27, Bonaire-6, Curaçao-6). Tables A.6 (Aruba), A.7 (Bonaire) and A.8 (Curaçao) of Appendix A summarize all features, measurements and ratios. The data were sorted on BMI and the numerical range for each designation is summarized in Table 4.5.

Figure 4.24 shows the distribution and density of bokas and cave features on Curaçao. Bokas (26 total) are distributed from just southeast of Watamalo to Boka Ascension, with a few small bokas occurring northeast of St. Joris Bay. Southeast of Boka Ascension, littoral caves and related features are common in the lower reef terrace. Flank margin caves occur in the lower reef terraces all along that stretch of coast as well as in the multiple reef terraces on the Hato Plain.

On Aruba, 35 bokas (Figure 4.25) have been documented from Boca Druif to just west of Boka Prins including three small bokas in the Quadiriki area. As in Curaçao, littoral caves and related features, and small flank margin caves have formed in the lowest reef terrace from Druif to Rincon. Caves have also developed in the next reef terrace up starting in the Quadariki area to Rincon and the coast due south of it.

Bokas are few on Bonaire and ten were documented on the entire windward coast of the island (Figure 4.26). Most of the boka development occurs between Malmut and Boka Oliva (a wide bay on the windward coast). Four small littoral bokas have formed on the far eastern coast between Boka Spelonk and the Washekimba estuary. A few littoral and flank margin caves have been documented along the windward coast, but most of the cave development occurs in the upper reef terraces located inland from the coast.

Fractal morphometric analyses were conducted on a selection of caves from all three island to determine cave type. Table 4.6 summarizes the results that strongly suggest that all cave development on the ABC islands are of the flank margin variety.

4.5.3 Caleta Results

A total of 30 caletas were documented from field work and from satellite imagery. Twenty-two of the caletas are directly associated with underwater cave passages that are humanly traversable to the sea (as per QRSS 2014). All of the caletas are associated with coastal springs. Distribution of caletas/coastal springs is shown in figure 4.27. Table A.9 of Appendix A summarizes morphometric data for the caletas.

Caletas display five morphologies that are illustrated in Figure 4.28A-E. Figure 4.28A shows the linear spring run morphology associated with coastal springs with points of discharge located inland, typically less than a kilometer from the coast; 26% of the

caletas inventoried display this morphology. Caletas can drain directly from or adjacent to crescent-shaped beaches (14%) and Figure 4.28B shows this phenomenon. About 20% of the documented caletas have rectangular shaped coastal reentrants (Figure 4.28C). Caletas can be directly associated with cenotes (30%) and Figure 4.28D shows this association. The remainder of the documented caletas (10%) are small coastal reentrants associated with coastal springs, and are less than 50 meters in length. They can either be circular or triangular in shape as shown in Figures 4.28E and 4.28F.

A total of 22 crescent-shaped beaches were documented and 7 of those are directly associated with coastal springs. Distribution of beaches is shown in Figure 4.29. Crescent-shaped beach development is most pronounced between Tulum to Playa del Carmen.

The structural trends of the caletas and beaches as measured for this study are summarized in Figure 4.30. The rose diagram illustrates the dominant trend of the caletas is northwest-southeast and the trend of beaches is to the northeast-southwest, normal to the direction of caleta development. Figure 4.31 shows the relationship between underwater caves, caletas, and beaches.

The caves in the study area are phreatic conduits that drain the area between the Holbox fracture zone and the coast (Kambesis and Coke 2013). Morphometric analysis of caves in the area indicates that their fractal dimension falls between the values attributed to flank margin caves and hypogene caves. (Table 4.7).

4.6 Discussion

4.6.1 Gullies

Gullies are common in all geomorphic zones of the island of Barbados. It has been suggested that the gullies formed in limestones of Zone I and II are the surface manifestation of collapsed dissolution conduits based on the occurrence of caves and associated speleothems observed in gully walls. Speed (2012) suggested that the large angular rocks that occupy many gully bottoms could not have been moved by fluvial process and are simply the upwardly prograding collapse of cave passages.

Ford and Williams (2007) indicated that the steep-walled, narrow valleys in limestone as canyons or gorges form by simple fluvial incision, rather than from cave passage collapse. They contend that surface stream flow versus underground flow is a function of allogenic recharge and/or hydraulic gradient. If stream flow on a karst surface exceeds the capacity for the karst to absorb it, the stream may maintain surface flow across the karst to the output boundary. An allogenic river with minimal elevation difference between its points of input and output will form a through-valley that incises across the karst. If there is greater vertical extent between the input and output points, an incised valley will still form if discharge remains sufficient to maintain competent surface flow. The streams located within gullies of Barbados are ephemeral. However during storm events they can fill with large volumes of fast moving flood waters, indicating that volume of infiltration of storm water exceeds the capacity of the subterranean drainage system.

A total of 705 km of gully have been documented from the GIS in Zones and I and II. However, it is highly unlikely that 705 km of collapsed cave conduits large

enough to result in the current gully configuration actually formed on the island. The recharge area of the island is not extensive enough to account for that extent and size of conduit development even when sea level was lower and island area larger.

The width of many of the gullies exceeds the width of any documented cave passages on the island. In the widest gullies, erosional collapse of gully walls would have eliminated evidence of initial cave passages. Instead, caves are observed on both sides of the walls of the widest gullies.

Ceiling collapse does happen in caves and can potentially reach the surface by progradational collapse. A cantilevered bed of rock spanning a cave passage resists gravitational stress because its strength is directly proportional to its thickness and inversely proportional to its length (White 1988). Deformation of the rock will cause microfractures that weaken the rock and cause slabs of rock to fall from the ceiling and walls. However, as a cave ceiling progrades upwards, it will tend to form a stable arch (Palmer 2007). Breakdown of cave passages can also form when a passage is first drained of water. The same principles of rock collapse that explain cave collapse can also be used to explain wall collapse from outdoor cliffs. It is likely that the large angular boulders that Speed (2012) observed in the base of gullies during his studies in Barbados were the result of the collapse of gully walls rather than progradational collapse of underlying cave passages.

Passage development in three of the five largest cave systems on the island does not directly correlate with the directional trend of any gully. The gullies follow the dip of the surface topography whereas the documented cave passages of the area follow the strike. Springhead Cave and Arch Cave are very short in length and it is not possible to

tell whether these caves are dip or strike oriented. Land use in the gullies associated with these caves (a horse ranch, and a golf course) has heavily modified the gullies so it is difficult to determine the original relationship of the caves to them. However, the lengths of Harrison's, Coles and Bowmanston's Caves (1.5, 2.5, 1.7 km respectively) are sufficient to display that conduit drainage flows along the strike rather than the dip of the rock.

The drainage pattern of the gullies on the drainage basin scale are angular and somewhat pinnate in some areas indicating that there may be structural influence on the initial development of the gully drainage pattern. Considering the geologic history of Barbados, differential uplift of the limestone coupled with unloading of the surface as strata were eroded may have resulted in fractures and fissures that were inception zones for the development of gullies. The radial configuration of gully drainage away from the rising center of the island and to the coasts is indicative of the main function of the gullies which is to drain the land surface. Once the Zone II limestone cap was breached, the mechanical action of fluvial waters cut deep drainages into the Zone IV strata and also carried ephemeral drainage to the east side of the island.

Allogenic recharge from storm events can be just as a potent an erosional agent on limestone as fluvial processes are on the siliclastic rocks of the Zone IV. Geochemical studies conducted by Groves and Meiman (2005) in the underground rivers of the Mammoth Cave System of Kentucky documented that during normal flow conditions, the underground rivers were saturated with respect to calcium carbonate minerals and very little limestone dissolution happened under normal flow. During storm events where large quantities of allogenic water quickly entered the cave system, the saturation index

of the flood waters was definitely negative and dissolution was greatest during these events. Flood waters that course through the gullies of Barbados are sufficient enough in their dissolutive capacity to dissolve surface channels into the underlying limestone. That coupled with fluvial erosion may have sculpted the gullies to their current form.

The occurrence of caves and speleothems in the walls of gullies has been cited as evidence that gullies are collapsed cave passages. However, the morphology of these caves is distinctly different from those of stream caves. Morphometric analyses using fractal dimension determined that they are flank margin caves, which are dissolutive voids that form at the interface between fresh and saline water. The speleothems that have been observed to have formed in the gully caves are tufa in nature indicative of development in the surface environment and associated with biologic activity which would have happened after the caves were exposed by erosion. Tufa speleothems are common in cliff overhangs and are not deterministic of cave origin (Taboroši et al. 2004).

Figure 4.32 illustrates a model for cave development within the gully walls. Figure 4.32A displays a pre-existing gully with intermittent drainage to the ocean. Figure 4.32B shows that sea level has risen and partially inundated the gully. Meteoric recharge puts a freshwater lens within the limestone and dissolutive voids (caves) form at the distal margin of the mixing zone between the freshwater lens and saltwater that saturates the limestone bedrock. In Figure 4.32C, sea level has dropped and the gully is exposed to surface erosion that breaches the dissolutive voids resulting in the exposure of caves in the gully walls.

4.6.2 Bokas

4.6.2.1 Boka types

The morphological characterization of the bokas of the ABC Islands as fluvially, littorally, or fluvio/littorally dominant recognized that boka development is influenced by a combination of processes including karstic ones. The characteristics and distribution of the bokas that have been studied by others on the windward northwest coast of Curaçao are not representative of all bokas on the ABC Islands.

4.6.2.2 Boka distribution

The dominant process of boka formation depends on the location and distribution of fossil reef terraces and the lateral thickness of the terraces (Figure 4.33). On the windward coasts of Aruba and Curaçao the majority of boka development occurs where the lower reef terrace is narrowest in its lateral extent (less than 300 meters) and where it abuts the igneous island core. On Curaçao, lateral thickness of the lowest reef terrace is narrowest between the northeast tip of the island near Watamula to Playa Grandi and the most pronounced fluvially-dominated bokas occur in this area (Figure 4.24). There are sections of highly degraded middle reef terrace along this stretch and fluvially dominated bokas have formed in the breaks between these segments. There is no boka development from a kilometer north of Boka Ascension, through the Hato Plain and to a kilometer north of St. Joris Bay. There is minor boka development beyond this point but only where the lower terrace abuts the volcanics.

Figure 4.25 shows boka distribution on Aruba. Bokas occur between Boka Druif and Boka Prins where the lowest terrace has a lateral extent of less than 200 meters, is in contact with the island's volcanic core, and where there are no upper reef terraces. Boka

development on Aruba is dominated by littoral type bokas (60%). Only 3% of the bokas are fluvially influenced and these occur where the lower reef terrace abuts igneous rocks of the island's core. The remainder of the island's bokas (37%) are fluvially-littorally influenced.

Bonaire (Figure 4.26) has very little boka development and this can be attributed to the fact that the island's volcanic core is much more restricted in extent than on the other islands. Multiple reef terraces are common along the coasts. The predominant origin of Bonaire bokas is littoral with 70% of all documented bokas of this type. There are 3 bokas of fluvial/littoral origin and they occur where the lower reef terrace has prograded back to the volcanic core. There are no purely fluvial bokas on Bonaire.

4.6.2.3 Boka origin

A number of ideas on the origin of bokas have been put forth by several researchers and were summarized in earlier sections. These mainly addressed the fluvially-dominated bokas located on Curaçao's northwest windward coast and suggested that all bokas share the same origin. Stefanic and Cornell (2011) presented a model of boka development where the mechanism is attributed to dissolution of cave conduits that eventually collapse, as the precursors for bokas. This is highly unlikely for several reasons. The streams that drain the landscape above the coastline are ephemeral and have likely always been. A precipitation event of enough volume and duration to cause the streams to flow would likely overwhelm the capacity of recharge features on a 200 meter-wide surface of limestone rather than result in recharging the limestone terrace. There is no evidence of conduit cave development in the bokas nor any relict or recent features that would serve as inputs of water into the limestone unit. It is more plausible that the

allogenic stream flow, which would be undersaturated with respect to calcium carbonate minerals, remained on the surface and began to dissolve limestone. That process would be augmented by mechanically weathered sediments washed down from the volcanic island core. This process is very similar to the development of Barbadian gullies.

Based on the minimum average width of all of the bokas documented in this study (33 meters) and an arbitrary height on the landward side of the feature of 2 meters, it is unlikely that there was ever enough recharge to form 200-meter segments of cave passage that averaged 33 meters in width and 2 meters in height or that all of those cave passages would have collapsed at the same time to form the 71 bokas that were documented. The core of the Stephanic-Cornell (2011) model is that the cave segments observed in gully walls were the remnants of stream caves. Morphometric analyses of the caves of the ABC islands, including those located in the walls of bokas and in higher reef terraces determined that they are flank margin caves (Table 4.6). Those located within the boka walls are degraded because of weathering and littoral erosion. Flank margin caves form at the interface between saline water and a freshwater lens making them good indicators of past sea level.

This study favors three models to address fluvially and littorally dominated bokas, and bokas that show both influences. For the fluvially dominated bokas (Model I – Figure 4.34), bokas did not incise the reef terraces after their development, but rather, formed syndepositionally with the reef development. Prior to the formation of reef terraces, the islands underwent uplift and erosion that removed 5 km of volcanic rock which would have been transported to the sea via surface streams. Surface flow would drop its sediment load once it encountered the ocean, forming deltas. The

established stream courses flowed to the sea prior to and throughout the entire Pleistocene. These established courses are evident in northeast Curaçao between the highly degraded upper reef terraces located above the lower terraces that flow to the modern bokas. Once the reefs began to form, sediment and freshwater from the interior streams inhibited the formation of the reef terraces on the deltas. Continued seaward flow of allogenic freshwater and sediment inhibited reef growth and created a trough across the reef crest. Reef terraces formed on either side of the incipient boka. Uplift or eustatic sea level drop subaerially exposed the reef crest, allowing a freshwater lens to form in the reef limestones. Small caves formed by mixing zone corrosion within the walls of the bokas. When sea levels dropped exposing the terraces to weathering and littoral erosion, wall collapse exposed the caves within the boka walls. This is evident not only in the lower reef terraces but also in the upper terraces where small, breached flank margin caves were documented on the side of one of the older reef terraces.

The occurrence of flank margin caves at two elevations in some of the fluvial bokas can be attributed to the fact that the lower reef terrace is composed of two reef terrace formations: the Hato Unit of MIS5e age and the Kortelain Unit from MIS 7. For the Kortelain Unit, the necessary subaerial exposure could have occurred during MIS 7 by tectonic uplift, to create a freshwater lens, or at the end of MIS 7, as regression occurred and perhaps paused. (Only a few thousand years are needed to make a flank margin cave, e.g. Mylroie and Mylroie 2013).

During the initial MIS 5e sea-level rise, a pause in transgression could also have placed a freshwater lens in the MIS 7 rocks. Three scenarios could create the required subaerial exposure of the MIS 5e limestones, and still maintain a freshwater lens within

those limestones. One option is a simple tectonic uplift episode(s) of a few meters during MIS 5e. A second option is a pause on the MIS 5e regression. These two options replicate those that could have worked for the MIS 7 flank margin cave speleogenesis. The final option is the much discussed mid-MIS 5e sea-level drop of a few meters. All three scenarios would create subaerial exposure of the reef to create a freshwater lens, but with sea level still high enough to place that lens within the MIS 5e limestone. The mid-MIS 5e low stand, and its possible effect on flank margin cave development, has been discussed for a similar situation in the Bahamas (Carew and Mylroie 1999).

Model II addresses littorally-influenced bokas (Figure 4.35A-E). In Figure 4.35A the carbonate bedrock of the coast is completely submerged and is intruded by sea water. Figure 4.35B shows a drop in sea level that aerially exposed the reef bedrock. Precipitation recharge accumulates as a freshwater lens within the bedrock that floats on the saltwater intrusion. The interaction of the freshwater lens and saltwater intrusion typical of coastal hydrology resulted in the formation of dissolutional voids that over time join to form flank margin caves within the island coastlines (Figure 4.35C). If sea level continues to drop, the reef bedrock is further exposed to weathering and littoral erosion and eventually the dissolutional voids (flank margin caves) are exposed on the coastline (Figure 4.35D). Wave action enlarges the voids that may eventually become bokas (Figure 4.35E).

In Model III (Figure 4.35F), as coastal erosion locally lowers the coastal land surface, the bokas begin to capture surface drainage resulting in bokas that are both fluvially and littorally influenced.

Degradation of the coast occurs not only at the coastline that is exposed to littoral processes but also meters inland as the dissolutional voids collapse forming natural bridges and blowholes.

4.6.3 Caletas

Based on geochemical studies, Back et al. (1979) determined that caletas and crescent-shaped beaches formed when coastal freshwater springs mixed with marine water causing the weakening of solution channels which made the limestone more vulnerable to wave erosion. As wave action continued to erode the coast, the caletas degraded to crescent-shaped beaches. The studies of Back et al. (1979) were done at a time when very little was known about the underwater caves that drained the peninsula

The long, linear spring-run caletas (Figure 4.28A) are all associated with well-developed cave passages and coastal springs that resurge to the surface between 300 to 700 meters inland. Examples of this are Caleta Xel Ha (700 meters long) and the series of Xel Ha underwater caves (Figure 4.36); Caleta Manati (400 meters long) is the resurgence of the Nohoch Nah Chich section of Sistema Sac Actun.

About 20% of the documented caletas appear to have a joint-controlled morphology that is expressed as rectangular shaped coastal reentrants. Structural trend, littoral processes, large discharge-volume springs that resurge directly on the coast, and dissolution at coastal springs result in distinctive caleta morphologies. Caleta Tankah (Figure 4.28C) displays a rectangular-shaped resurgence area that is over 394 meters long by 118 meters wide. This is another major resurgence for Sistema Sac Actun.

Some of the coastal springs resurge directly on the coast adjacent to and sometimes from a beach, (Figure 4.28B) such as Xunan Ha and Punto Xcace.

Underwater cave passages cannot be accessed via these and similar caletas, although they are accessed via coastal cenotes located inland from the coast. The underwater passages near those caletas consist of very, young and unstable rectilinear maze passages that are the bane of underwater exploration.

The association of caletas with cenotes indicates that caleta development may be associated with coastward progradational collapse of cenotes (Figure 4.28C). A third of all caletas along the Quintana Roo coast are in close proximity to one or more coastal cenotes.

The small circular or triangular shaped caletas are associated with smaller discharge springs that appear to be in close proximity to less extensive cave systems that have been documented near the coast. It is possible the smaller caves systems are the source of the spring discharge.

In addition to the caletas and associated springs, there are hundreds of small vents that discharge into the bays and caletas all along the coast. These features are currently undocumented.

Weidie (1978) identified a strong northwest fracture trend along the entire Quintana Roo coast that he suggested controlled the inland development and extent of coastal features. He also noted a northeast trending fracture set that parallels the coast and indicated these structures control the lateral extent of coastal features. Figure 4.30 shows that the caletas and beaches express northwest and northeast structural control.

There is very little caleta development north of Playa del Carmen. South of Tulum, caleta development is no longer apparent. However, large coastal springs resurge along the coast south of Tulum. Sistema Ox Bel Ha has humanly accessible coastal vents

but there are no obvious features analogous to caletas associated with these coastal springs. Farther south from Tulum are many coastal springs that debouche into the sea and into the large bahias (bays) characteristics of that area. The abrupt change in caleta distribution north of Playa del Carmen and south of Tulum indicates the possibility of a change in geologic boundary conditions in those areas.

Mixing-zone corrosion is an important geomorphic process for caleta development. Progradational cenote collapse may also contribute to the development of caletas, especially those with a long-linear morphology. Figure 4.37 is a model for linear morphology caleta development. In Figure 4.37A a conduit is discharging groundwater to the coast and the seaward side is subjected to mixing zone corrosion at the freshwater-saltwater interface. When sea level drops, there is a loss of buoyant support in the conduit and zones of weakness begin to develop in the ceilings (Figure 4.37B). Ceiling collapses at zones of weakness form cenotes and expose more of the conduit to both surface and littoral processes (Figure 4.37C) As sea level rises the conduits are exposed to continued dissolution and the erosive action of waves (Figure 37.D). Caleta walls collapse increasing the lateral extent of the caleta. (Figure 37.E). If the linear caletas are also considered to be associated with cenotes, then morphology of 57% of all of the Quintana Roo caletas are influenced by progradational collapse of cenotes.

4.7 Summary

Coastal re-entrants on rocky carbonate coasts form from a variety of processes that can be fluvial, littoral and/or karstic in nature. The morphology and distribution of a re-entrant feature is influenced by mode of development, local geologic controls and sea level changes. The islands of Barbados, Aruba, Bonaire and Curaçao display a diversity

of coastal re-entrants. The origin and genesis of the features vary but they share the characteristic of being influenced by karst processes associated with either coastal mixing zone dissolution, fluvio-karstic processes, or both.

The gullies of Barbados are fluvial features that were karstified during sea level high stands and are currently being affected by fluvial karstification. The bokas of the ABC islands have formed from a combination of fluvial and littoral processes that act on the windward side of the islands. Coastal mixing-zone dissolution is the sole mode of karstification on the ABC Islands. Flank margin caves which are a characteristic of this type of karstification can be found in the walls of many of the bokas and likely formed during past sea-level high stands. On the modern coast, littoral erosion is exposing flank margin caves that are eroding to form natural bridges, blow holes and coastal collapse features. Karstification is also evident in the older reef terraces located inland from the modern coast.

Caletas formed where discharging freshwater from conduits mix with saltwater at their seaward margins causing an increase in local dissolution and inducing conduit collapse that migrates inland to form a cove. As dissolution continues to act on the limestone, it becomes more vulnerable to the mechanical erosion by wave action (Hanshaw and Back 1984). Progradational collapse of cenotes may also be important for caleta development. Caletas continue to enlarge by cave passage collapse when a drop of sea level removes buoyant ceiling support. The evolution of the northeast coast of Quintana Roo, Mexico is driven by a combination of karstification and littoral processes.

Table 4.1 Geomorphic zones of Barbados

Zone	Elevation (meters)	Slope	Topography	Rock	Hydrology	Karst
I (Terraced Flank)	0-160	North, West, and South coast - 1.5° - 4.5°	Stair-stepped marine terraces, partly hummocky and gullied by river erosion	Pleistocene (75-300 ka) limestone (0-70 m thick)	Great variation in precipitation and evaporation; high infiltration; water table at 0-5 m elevation; possible conduit flow, surface runoff in large storms	Flank margin caves in gully walls and reef terraces; though possible, epigene caves not documented
II (Central Highlands)	130-340	≤2.5° to NW and SE about a central crest	Undulating, abundant sinkholes, plus river valleys, fault scarps	Pleistocene (>300 ka) limestone (50-130 m thick)	Maximum rain and minimum evaporation; high infiltration; groundwater flow to N, S and W in conduits at base of limestone aquifer; runoff in large storms	Well-developed epigene caves; flank margin caves in gully walls and reef terraces
III (Windward Slope)	0-320	East coast - 7°-10°	Receding cliffs at upper elevations, hummocky apron of landslide deposits; immature stream gullies at lower elevations	Upper realm is thick limestone at cliff-face, lower realm is landslide deposits	Large variation in rain and evaporation - elevation dependent; moderate runoff; springs emerge from fronts of landslides	non-karst
IV (Scotland District)	0-100	East coast - ≤1° in trunk channels	Deeply dissected riverine topography; steep interfluvies between low gradient floodplain	Foundation mega-unit: Miocene sedimentary strata (prism cover) unconformably overlying Paleogene Oceanic allochthon and basal complex	Large to small rainfall, low infiltration, large ephemeral runoff	non-karst
Modified from Speed 2012						

Modified from Speed 2012

Table 4.2 Summary of geographical statistics for the ABC Islands

Geographical Statistics of the ABC Islands			
Island	Aruba	Bonaire	Curaçao
Length (km)	30	40	64
Width (km)	5.5	12.5	16
Surface area (km ²)	193	288	444
Highest altitude (m)	189	241	372

Table 4.3 Summary of mapped gully segments by geomorphic zone

Gullies of Barbados by Geomorphic zones		
Zones	Length in km	Gully segments
Zones I & II	705	979
Zone IV	167	76
total	872	1055

Table 4.4 Results of fractal analysis of stream caves versus gully caves

Cave	Gully	Fractal dimension	Cave Type
Arch Cave	Apes Hill	2.1103	St
Coles Cave	Jack-in-the-Box	2.1367	St
Springhead	Springhead	2.1476	St
Harrisons Cave	Jack-in-the-Box	2.1579	St
Brontosaurus Cave	Sailors Gully	2.2754	FMC
Lucky Stars Cave	Jack-in-the-Box	2.2814	FMC
Princes Palace Cave	Broomfield	2.2925	FMC
Ha Ha Cave	Prospect Gully	2.3194	FMC

St: Stream cave FMC: Flank margin cave

Table 4.5 Summarized BMI ranges and percentages of boka types for each island

Boka origin	BMI range	Total	Aruba	Bonaire	Curaçao
Littoral dominant	<4.4- 1.3	17%	37%	70%	39%
Fluvial dominant	>0.5	42%	3%	0	42%
Fluvial and littoral	>1.30 – 0.5	41%	60%	30%	19%

Table 4.6 Results of fractal morphometric analyses on some of the caves of the ABC islands

Cave	Island	Fractal Dimension
Raton	Curaçao	2.3171
Savonet	Curaçao	2.3191
Speolonk	Bonaire	2.3275
Hato Cave	Curaçao	2.2840
Jetchi	Curaçao	2.3326
Quadaricki	Aruba	2.3442
Colossal Cave	Aruba	2.3002

Table 4.7 Morphometric Analysis (fractal) for select underwater caves

Underwater Cave	Fractal Dimension
Sistema Sac Actun	2.5083
Sistema Ox Bel Ha	2.6049
Dos Pisos	2.3781
Sand Crack	2.3579
Sistema Camilo	2.3727



Figure 4.1 Site map of study area

Image modified from Google Earth



Figure 4.2 Gullies of Barbados

Dark green linear features are the gullies on the island of Barbados Modified from Google Earth

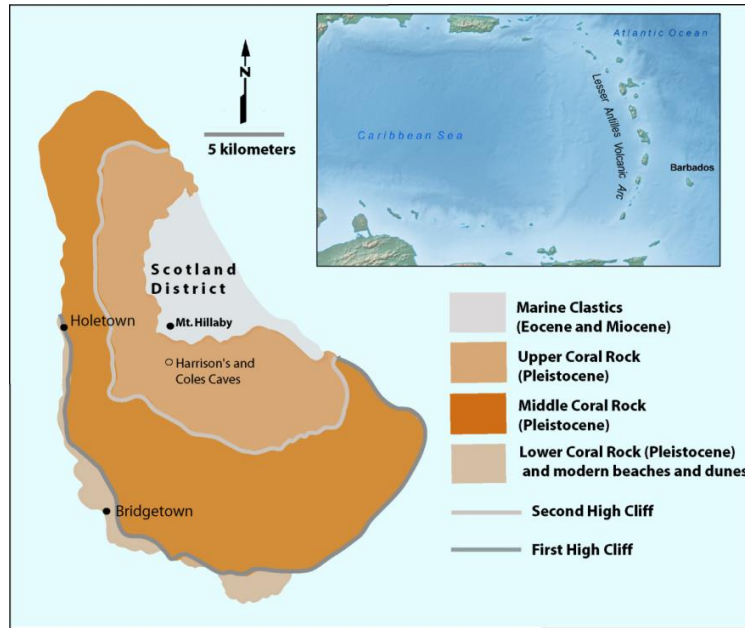


Figure 4.3 Geologic and geomorphic features of Barbados

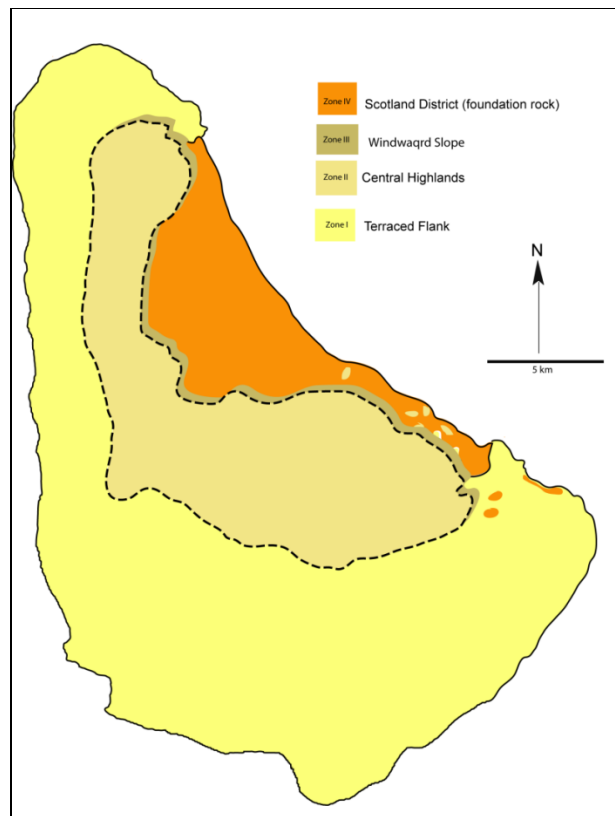


Figure 4.4 Geomorphic zones of Barbados

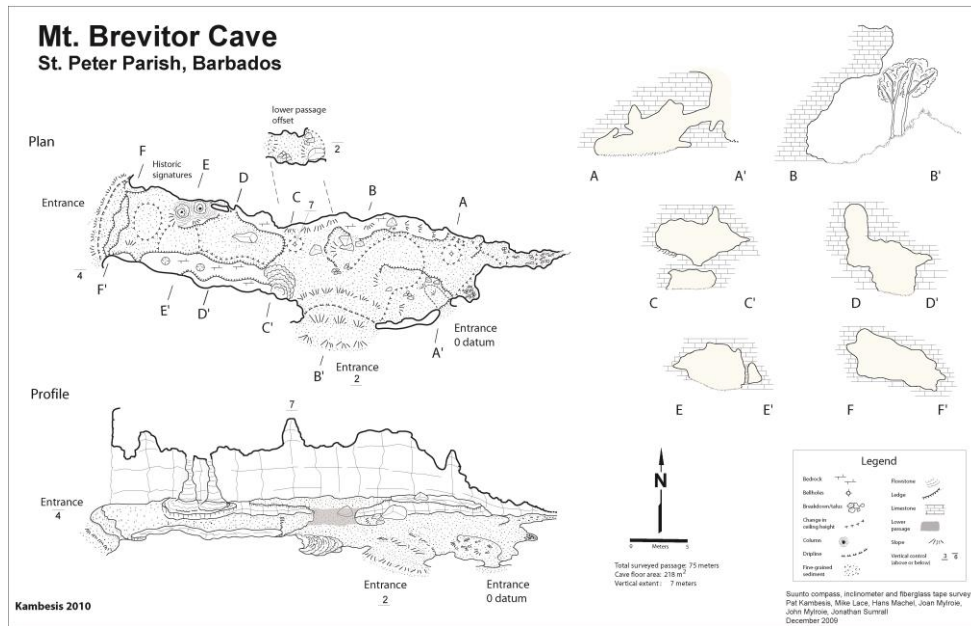


Figure 4.5 Mt. Brevator Cave, a typical flank margin cave of Barbados

Caves are located in many of the reef terraces of the island.

Cartography: P. Kambesis

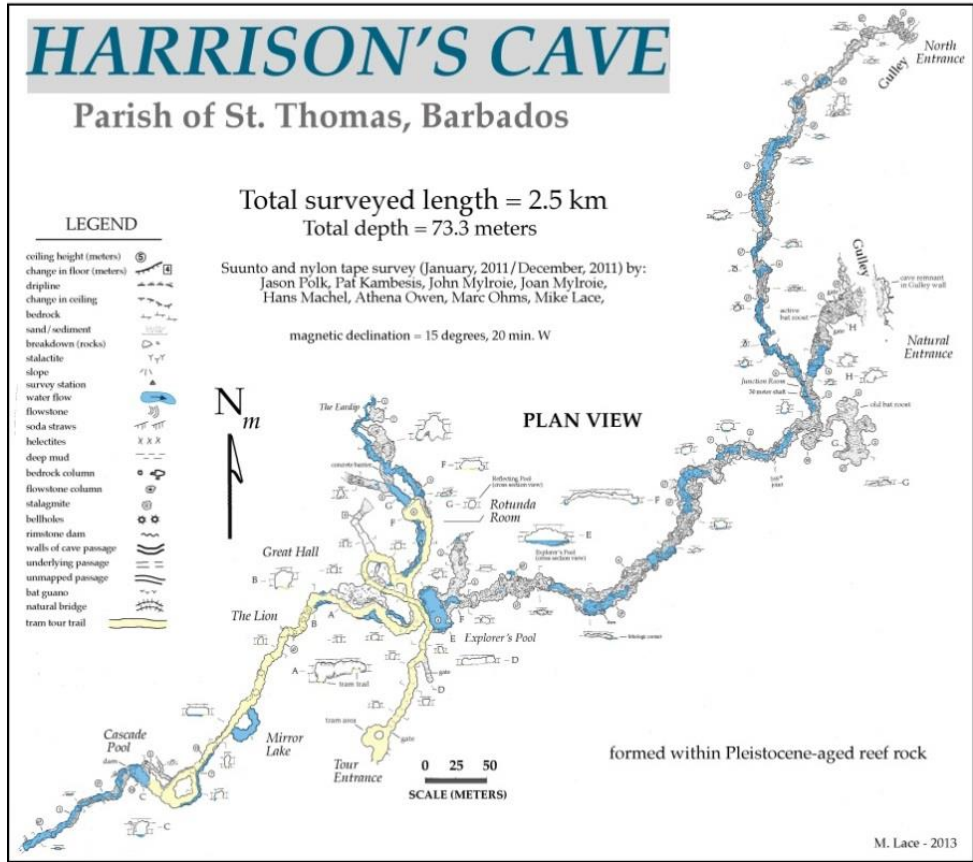


Figure 4.7 Harrison's Cave, a typical stream cave of Barbados

Harrison's Cave is currently the longest cave in Barbados and is the island's premier show cave. Cartography: Mike Lace

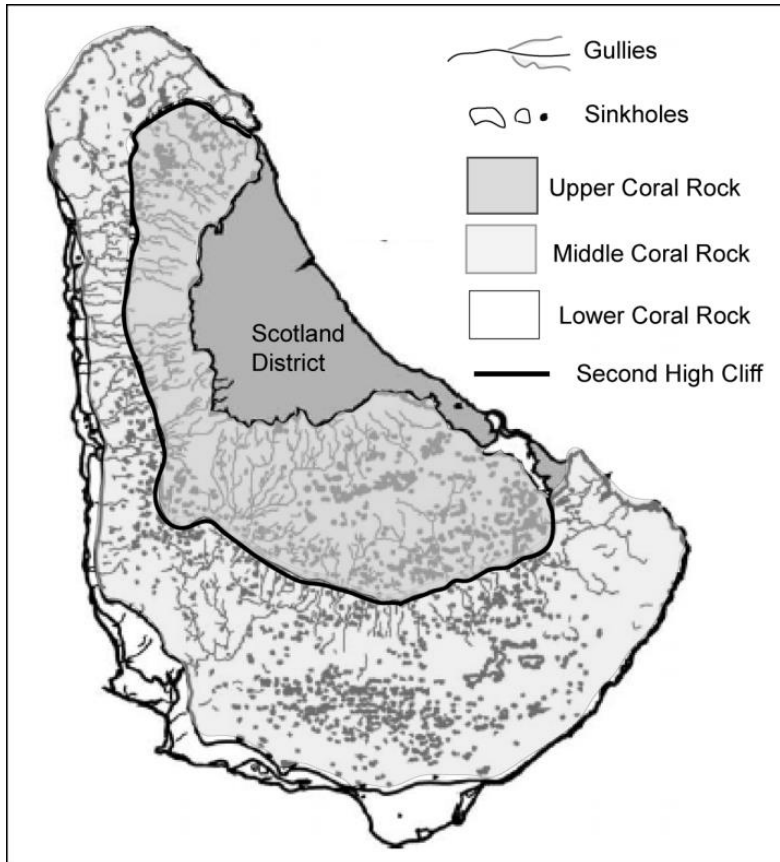


Figure 4.8 Sinkhole distribution and density on Barbados

Modified from Day 1983

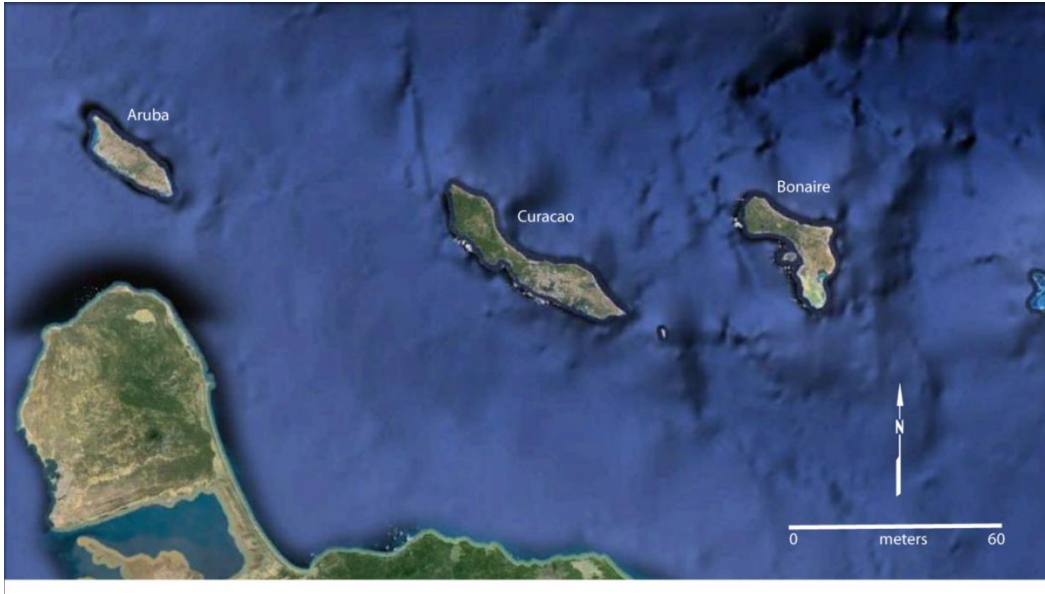


Figure 4.9 Site map of the ABC Islands (Aruba, Bonaire, Curaçao)

Image modified from Google Earth



Figure 4.10 Typical boka on Curaçao

(A) Aerial image of boka on northwest coast of Curaçao (Google Earth image), (B) Boka showing flank margin caves on the feature perimeter. Photo: J. E. Mylroie

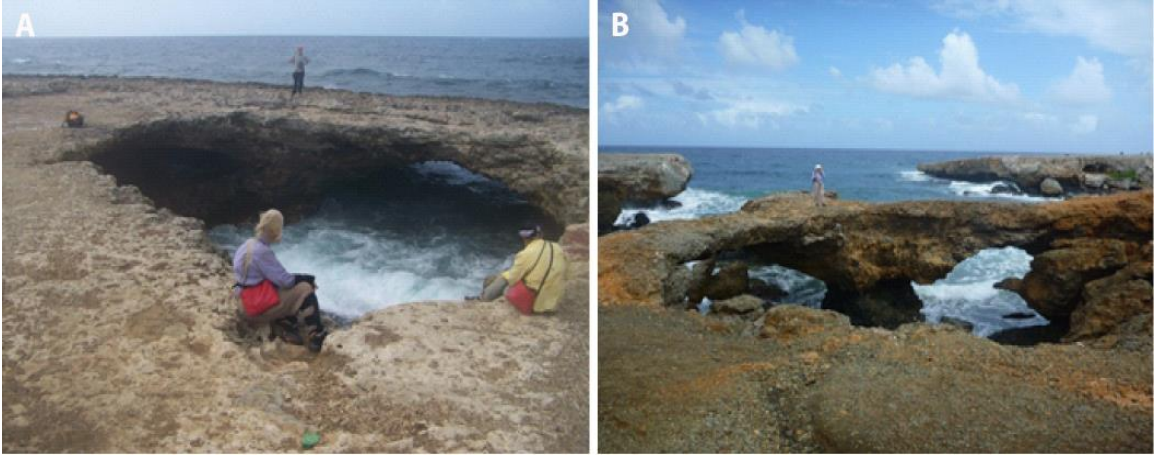


Figure 4.11 Hybrid caves that result from littoral erosion of flank margin caves Curaçao (A) and Aruba (B). Photos: J. Mylroie

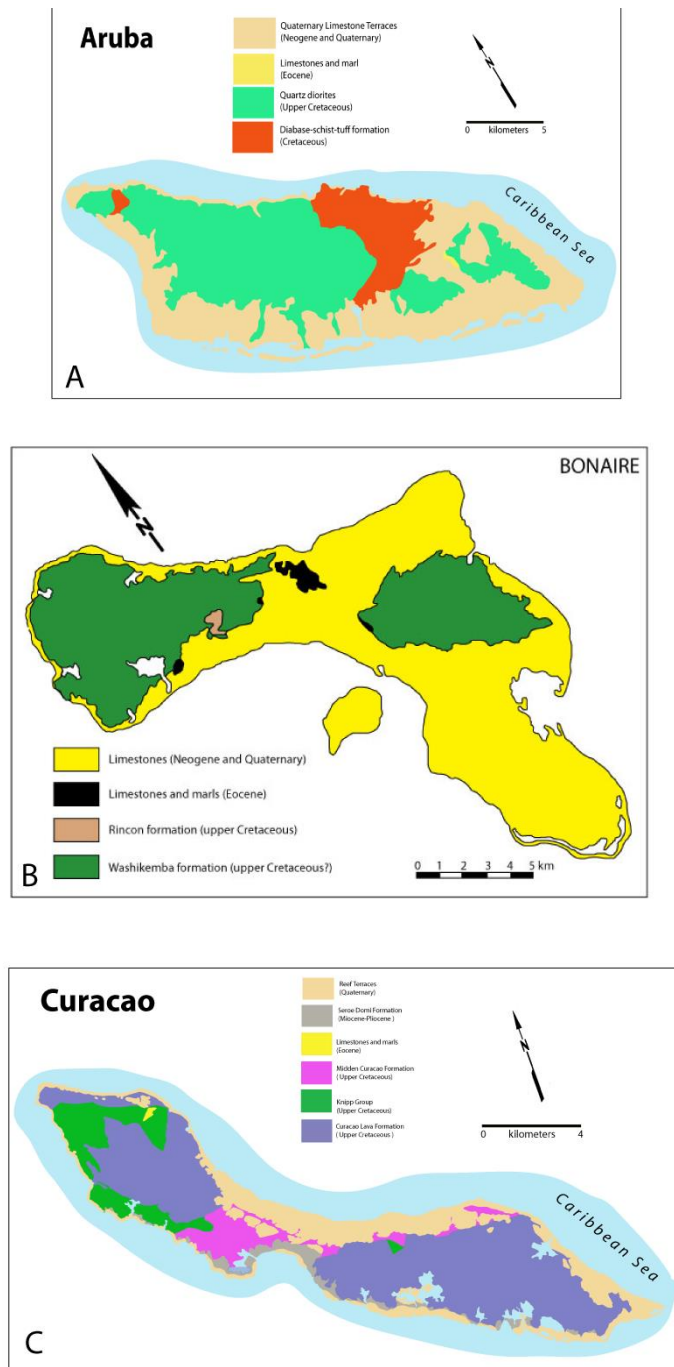


Figure 4.12 General geologic maps of the ABC Islands
Aruba (A), Bonaire (B) and Curaçao (C)

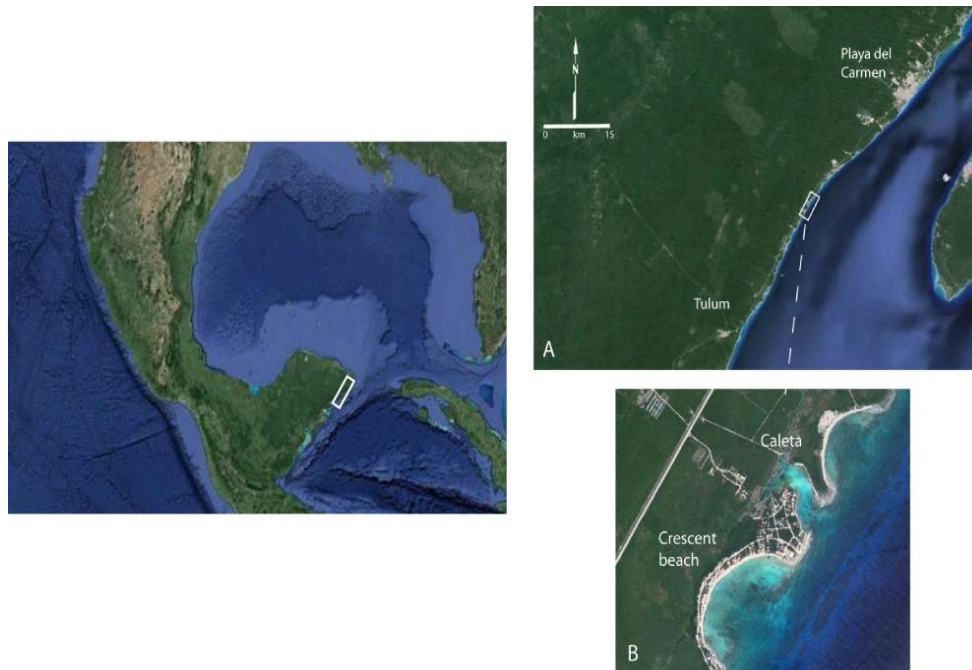


Figure 4.13 Study site maps in Quintana Roo, Mexico

Location of study sites in Quintana Roo, Mexico (A), Study site from Tulum to Playa del Carmen (B), Caleta and crescent-shaped beach (C). Images from Google Earth.

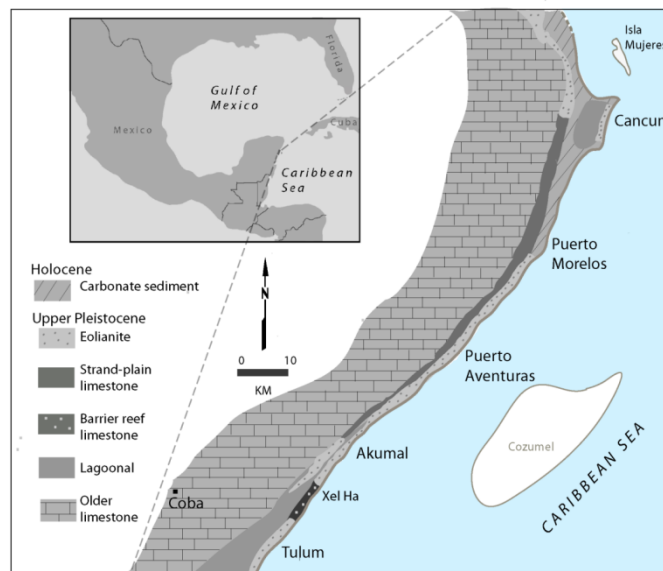


Figure 4.14 Stratigraphy of the northeast coast of Quintana Roo, Mexico

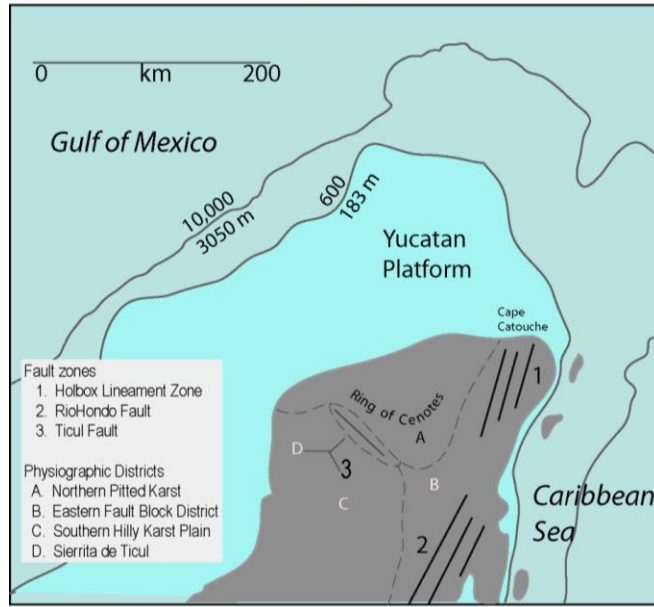


Figure 4.15 Structural features of the Yucatan peninsula



Measured parameters	★ Georeference datum	Calculated parameters
1 Length of boka (L)		Linear ratio: L/w_{max}
2 Minimum width of boka (w_{min})		Width ratio: w_{max}/w_{min}
3 Maximum width (w_{max})		Slope: VE/L
4 Vertical extent (VE)		

Figure 4.16 Boca measurements and ratios used to quantify boka morphology

Photo: H. Van Bommel

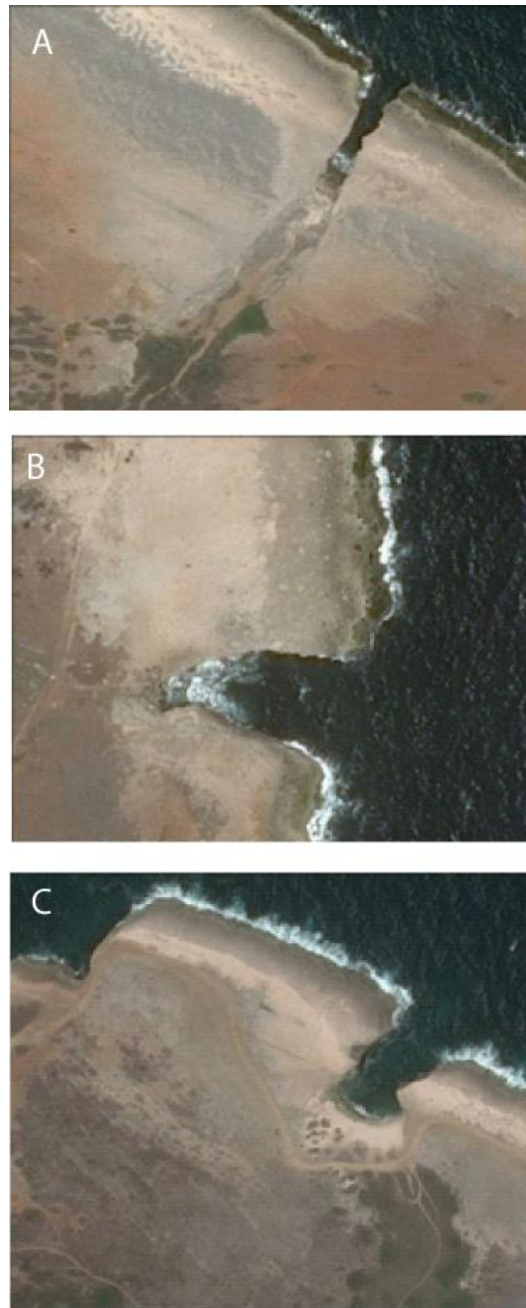


Figure 4.17 Boca morphologies on the ABC Islands

(A) Fluvially influenced boka. Note dry surface stream channel at the rear of the feature
(B) Littoral boka, no surface drainage connection; (C) Littoral/fluvial boka with dry stream channel on the bottom right. Images modified from Google Earth.



Figure 4.18 Method for measuring caletas

Image from Google Earth

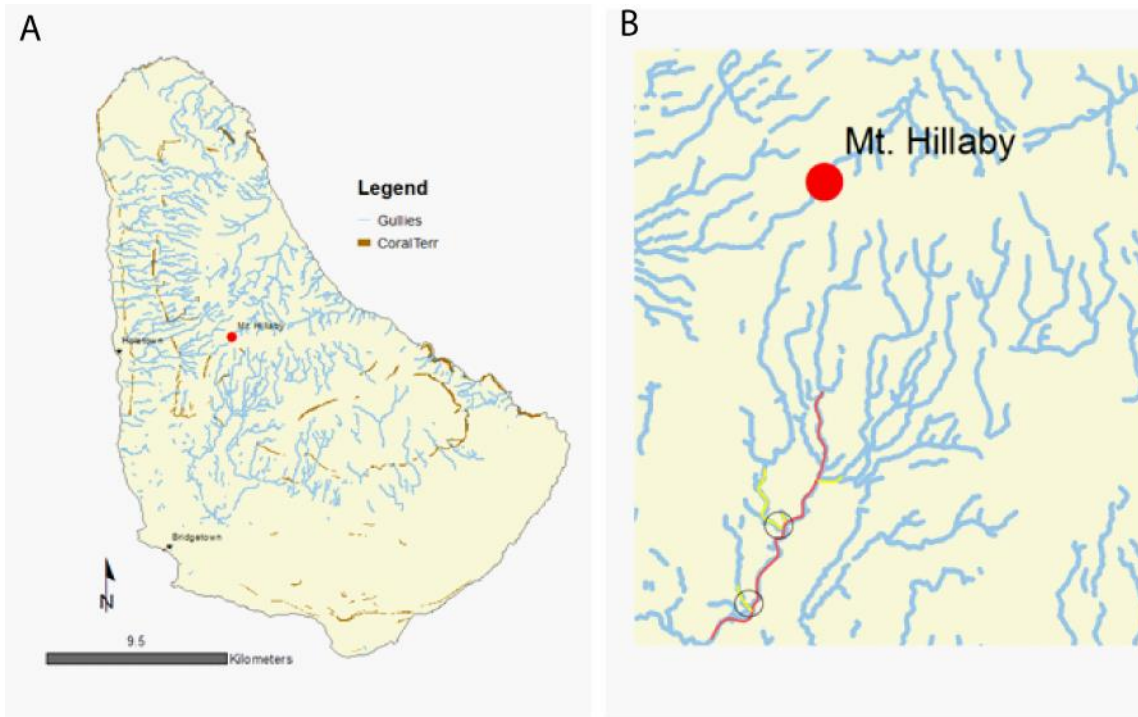


Figure 4.19 Gully drainage system of Barbados

(A) The gullies drain from the high point around Mt. Hillaby to the coasts. (B) Secondary gullies (circled) converging on a main gully network.

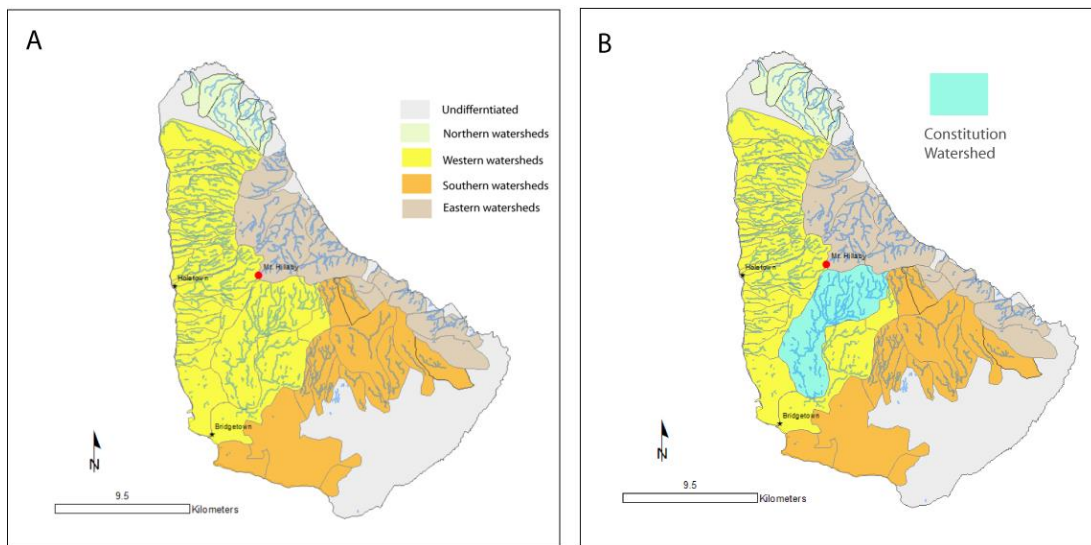


Figure 4.20 Major Watersheds of Barbados

(A) Major watersheds of Barbados. (B) Constitution Watershed, the largest on the island

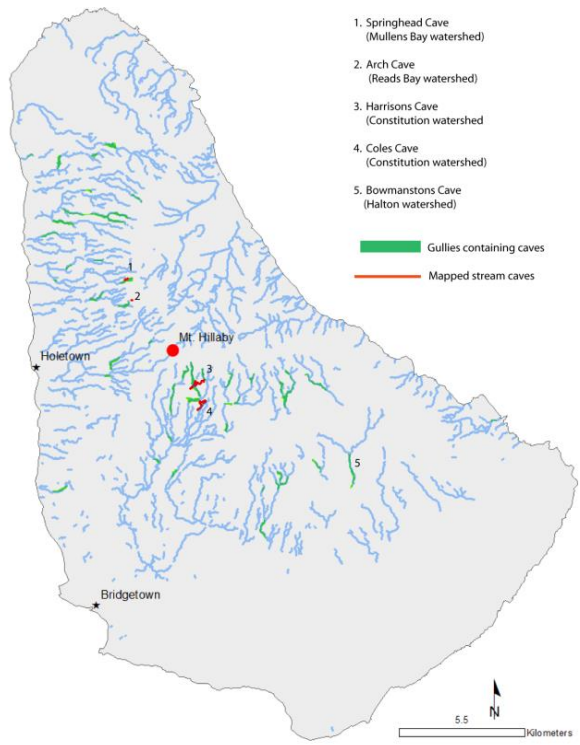


Figure 4.21 Location of stream caves of Barbados

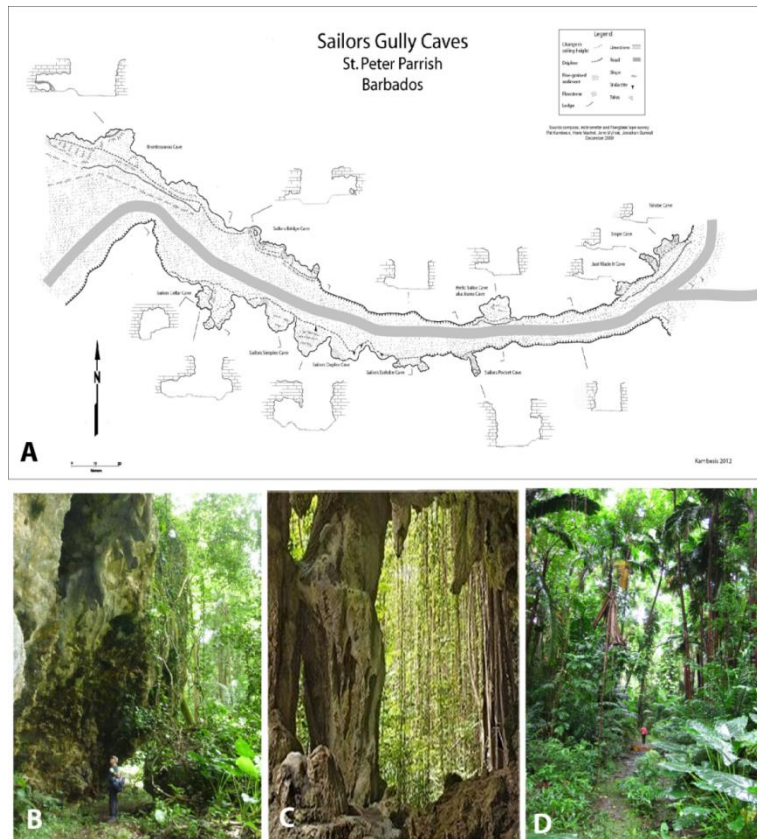


Figure 4.22 Flank margin caves in some of the gullies of Barbados.

Map of Sailors Gully (A), gully was developed for road traffic. Map shows a series of small, breached flank margin caves located along the length of the segment of gully. (B) Welchman's Gulley near Harrison's Cave. Showing typical morphology of caves which form on the perimeters of gullies. (C) Weathered calcite speleothems from a cave in Welchman's Gully. (D). Typical bottom of limestone gully. Cartography: P. Kambesis

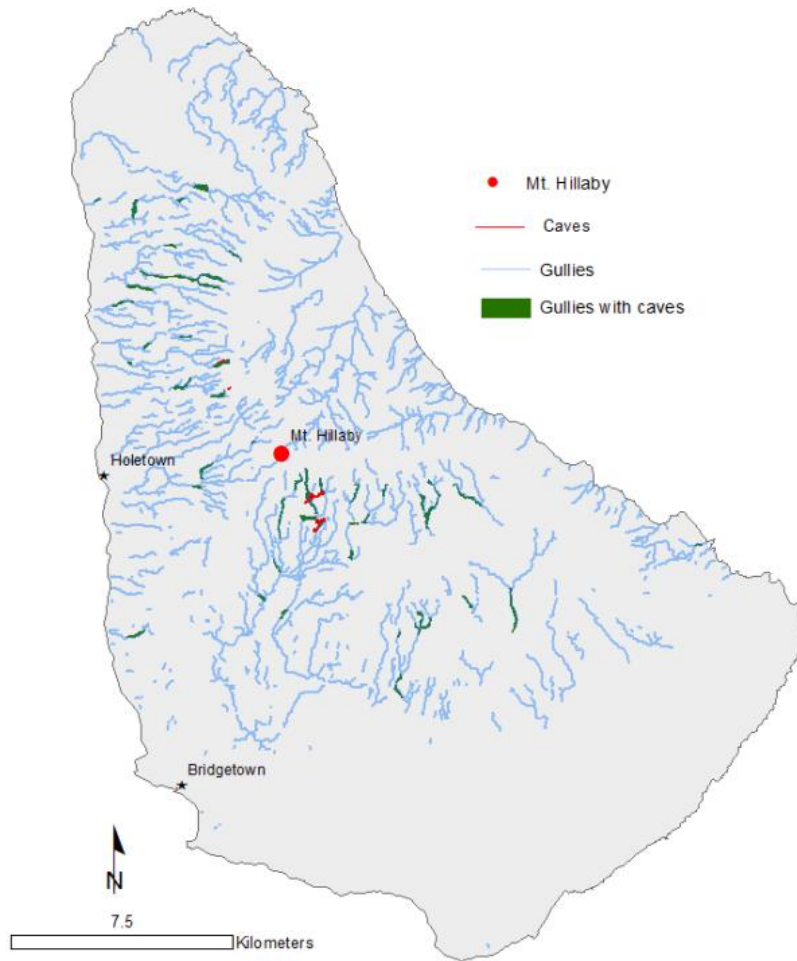


Figure 4.23 Gullies that contain caves, Barbados

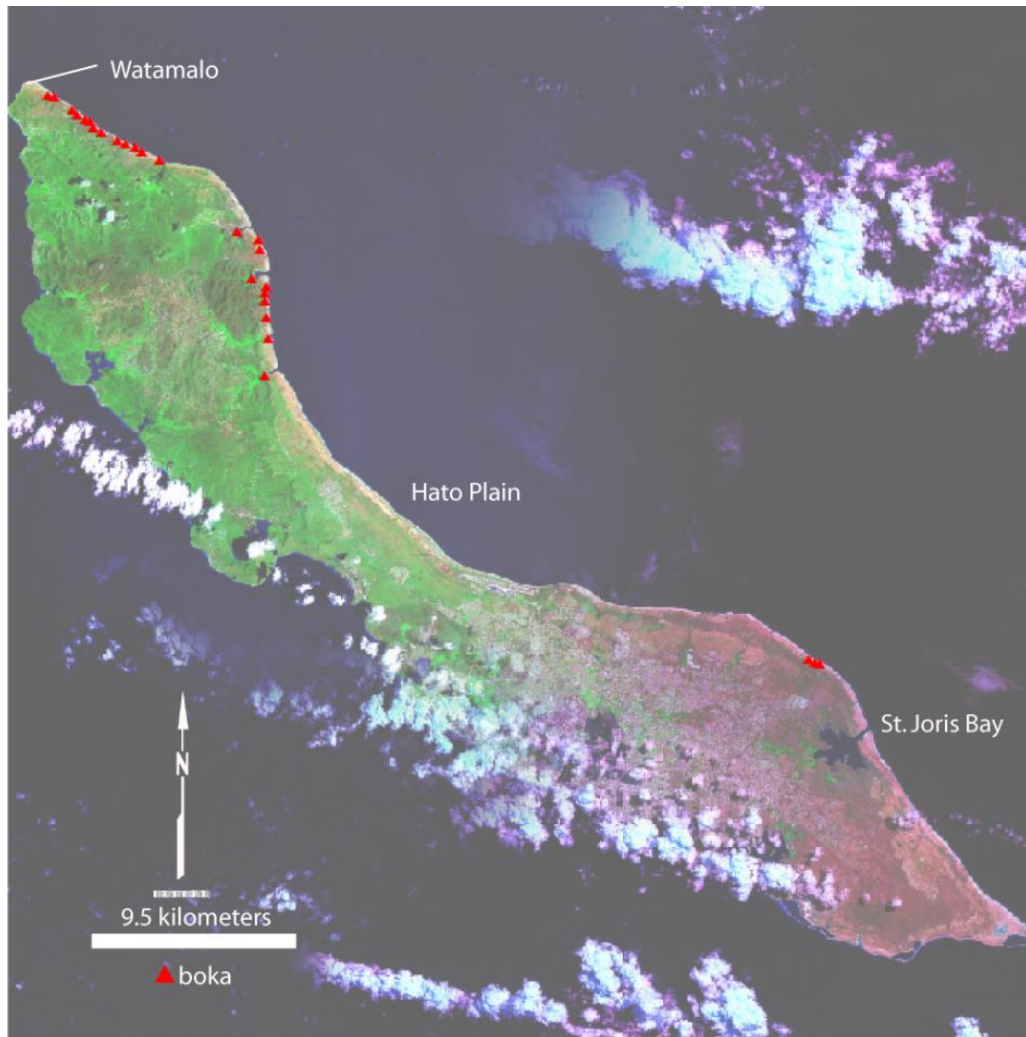


Figure 4.24 Boka distribution on Curaçao

Image source: ESRI

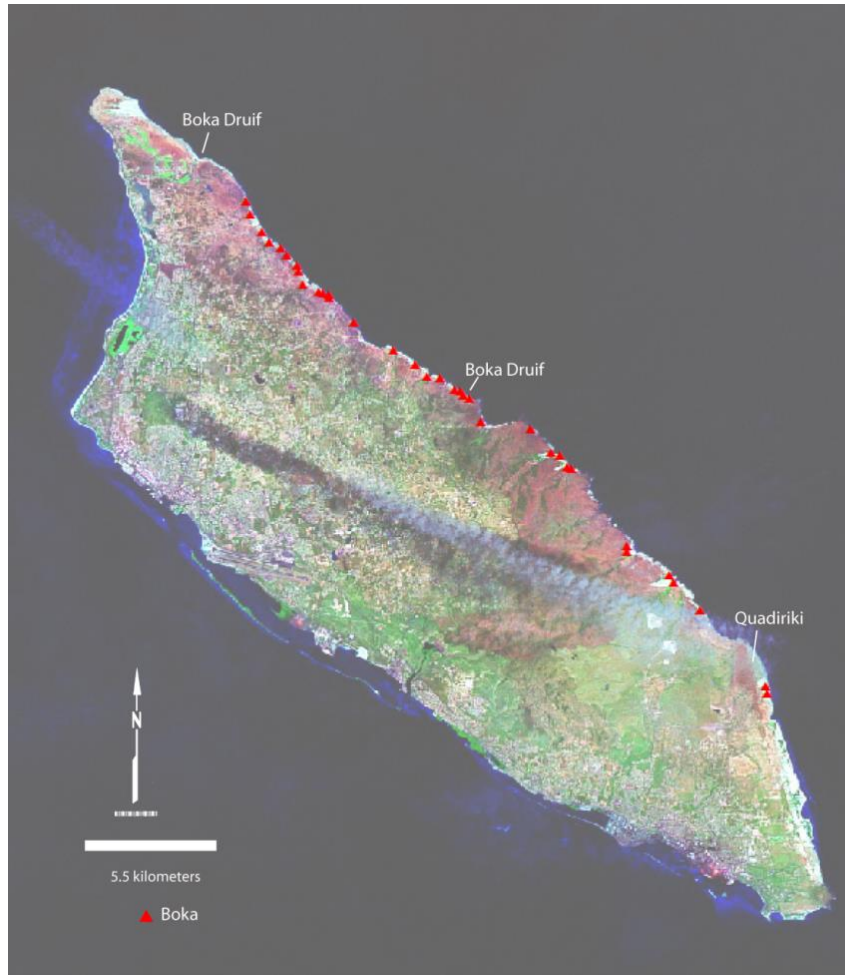


Figure 4.25 Boka distribution on Aruba

Image source: ESRI

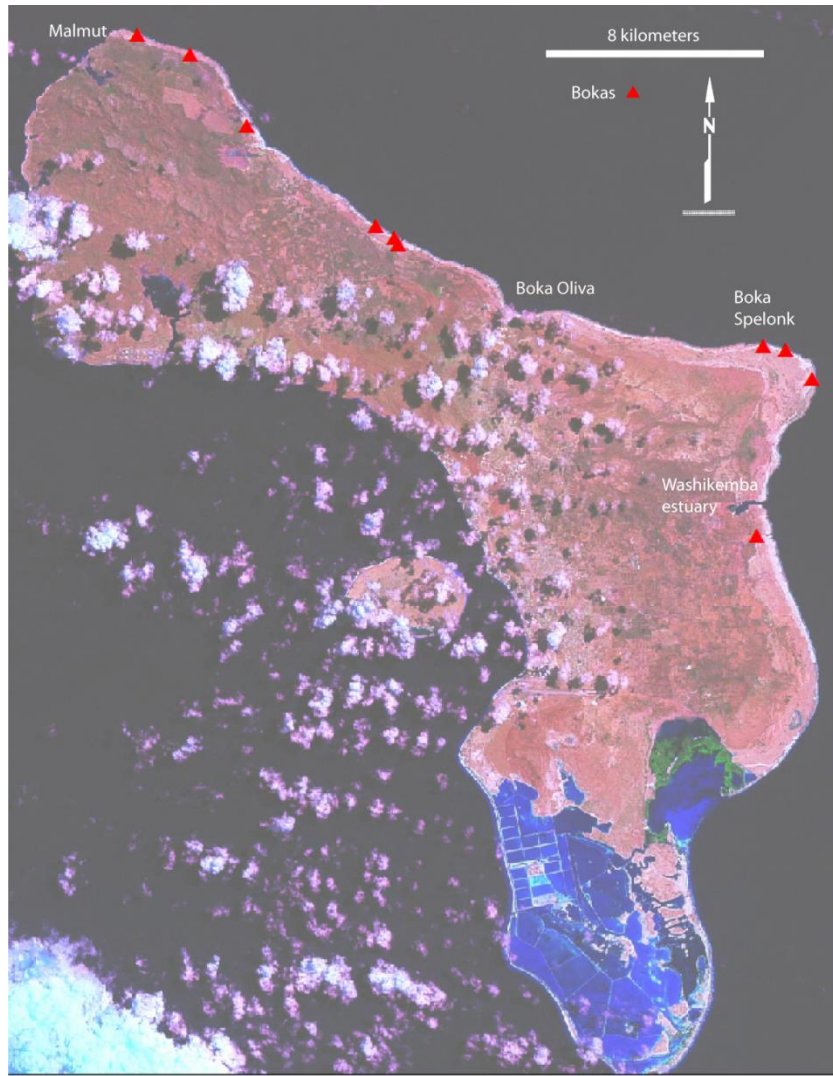


Figure 4.26 Boka distribution on Bonaire

Image source: ESRI

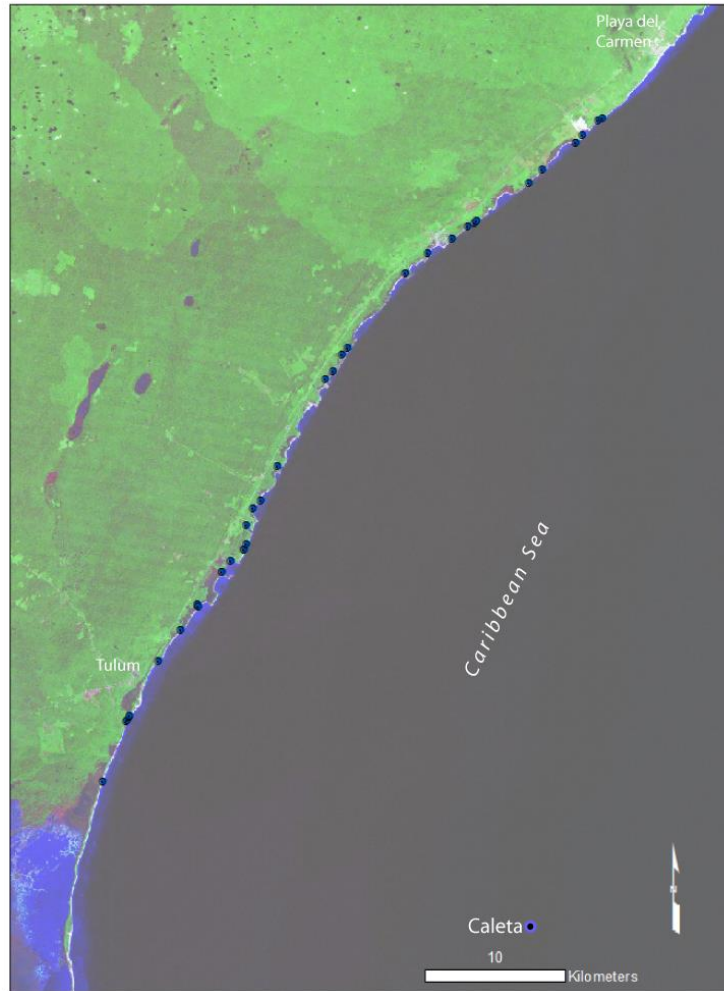


Figure 4.27 Distribution of coastal springs/caletas

Black dots are coastal springs, northeast coast of Quintana Roo, Mexico.
Image source: ESRI

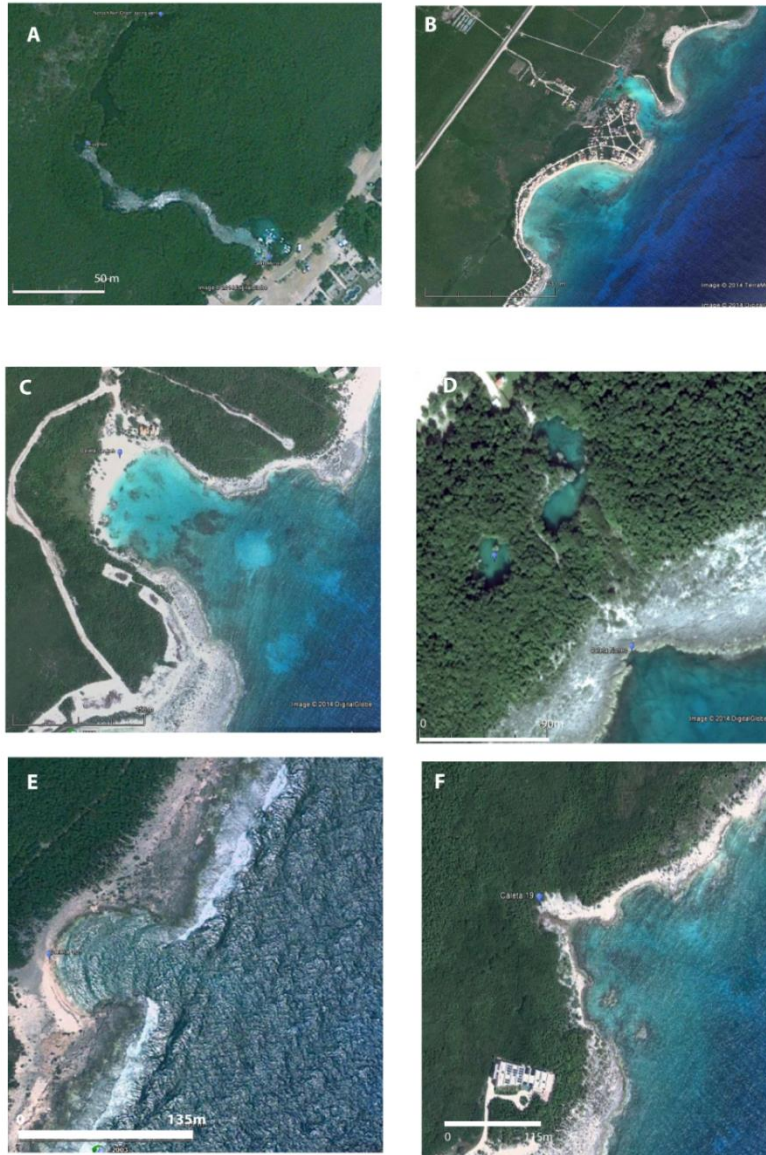


Figure 4.28 Caleta morphologies of the northeast coast of Quintana Roo

(A) shows the long-linear spring run associated with coastal springs whose points of discharge are less than a kilometer inland; 26% of the caletas inventoried display this morphology. (B) Caletas draining adjacent to crescent-shaped beaches (14%) (C) About 20% of the documented caletas take a rectangular form. (D) Caletas can be directly associated with cenotes (30%). (E) and (F) The remainder of the documented caletas (10%) are small coastal reentrants associated with coastal springs, and are less than 50 meters in length. They can either be rectangular or triangular in shape. Images from Google Earth

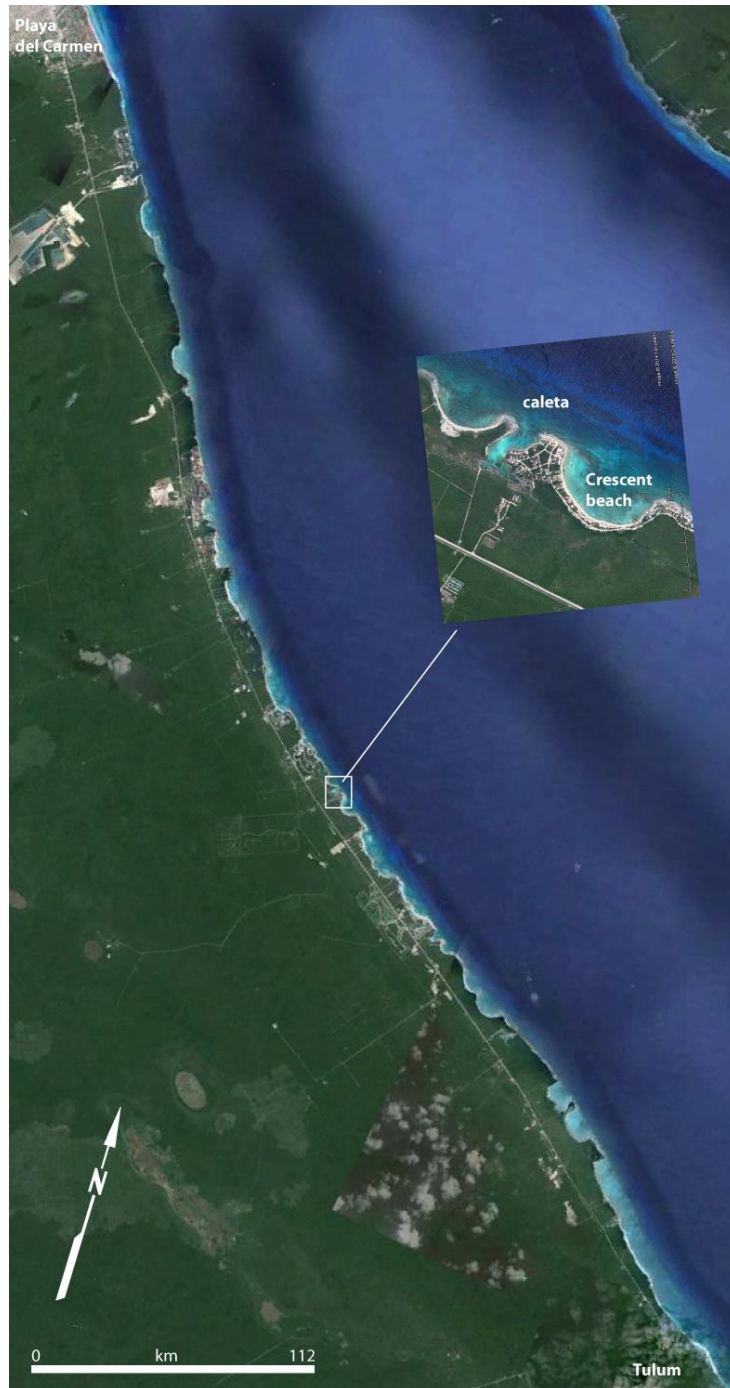


Figure 4.29 Distribution of caletas and crescent-shaped beaches on the Yucatan Caribbean

Caleta distribution diminishes at Playa del Carmen and is absent south of Tulum.
Image modified from GoogleEarth

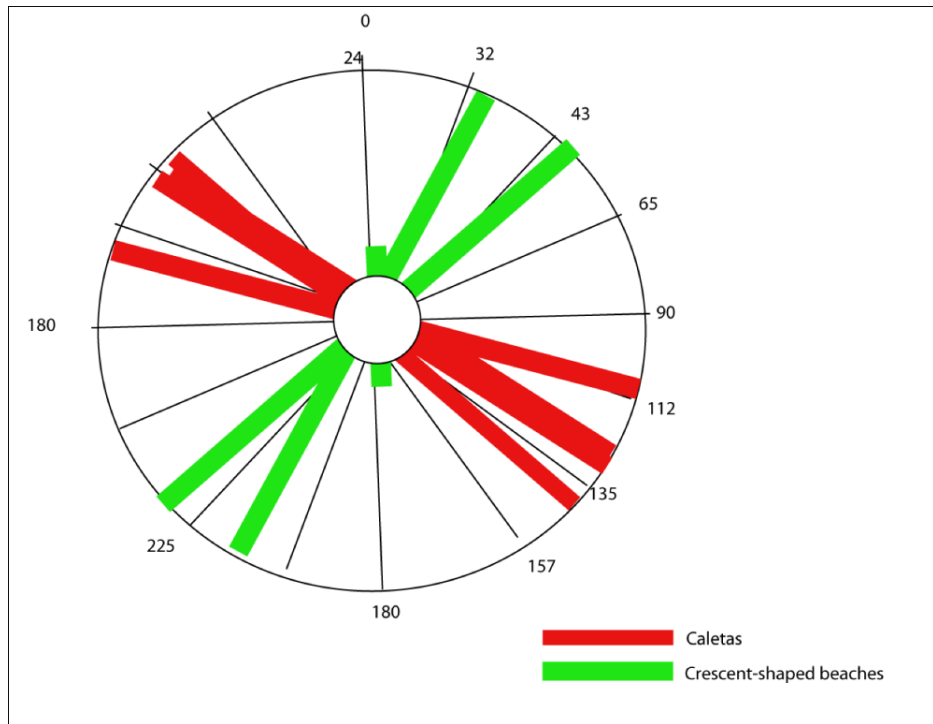


Figure 4.30 Structural trends of caletas and crescent-shaped beaches

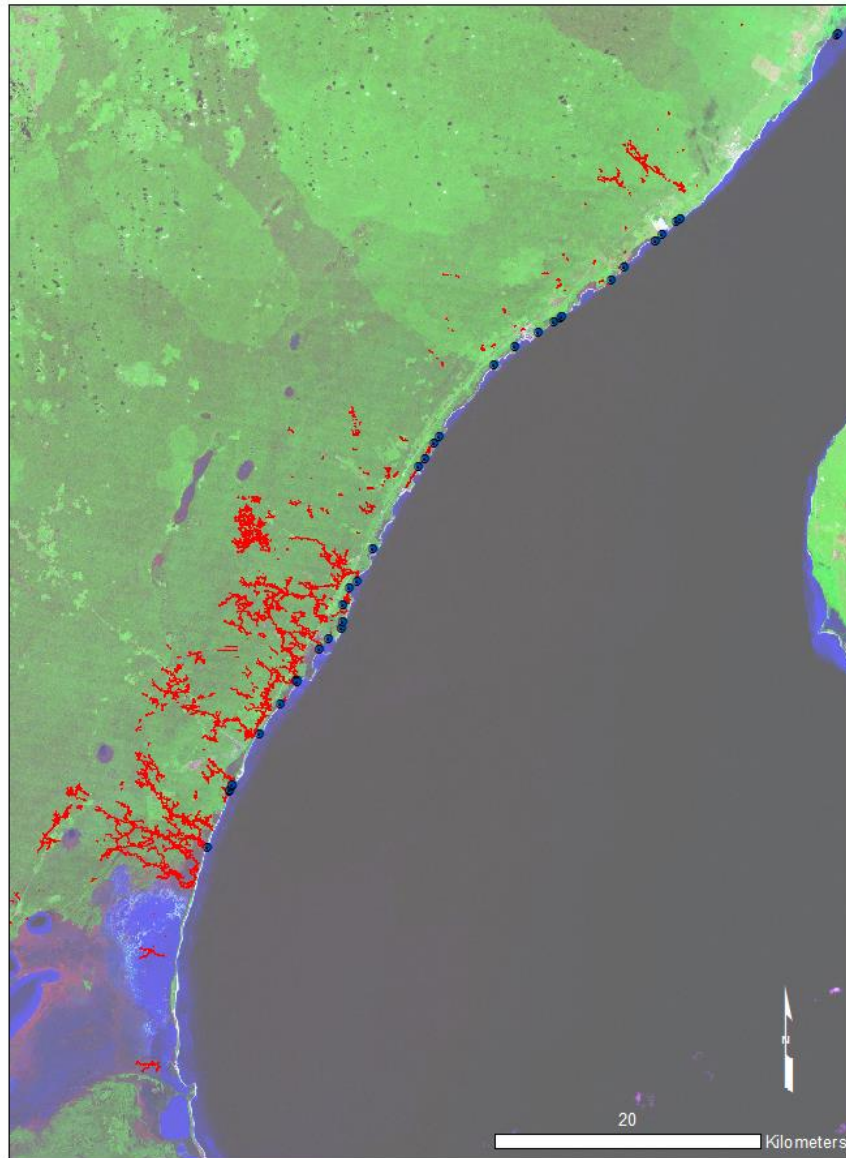


Figure 4.31 Distribution of caves, springs/caletas and beaches

Red lines are cave systems, black circles represent springs/caletas and crescent-shaped beaches. Cave data source: QRSS 2013, Image from ESRI

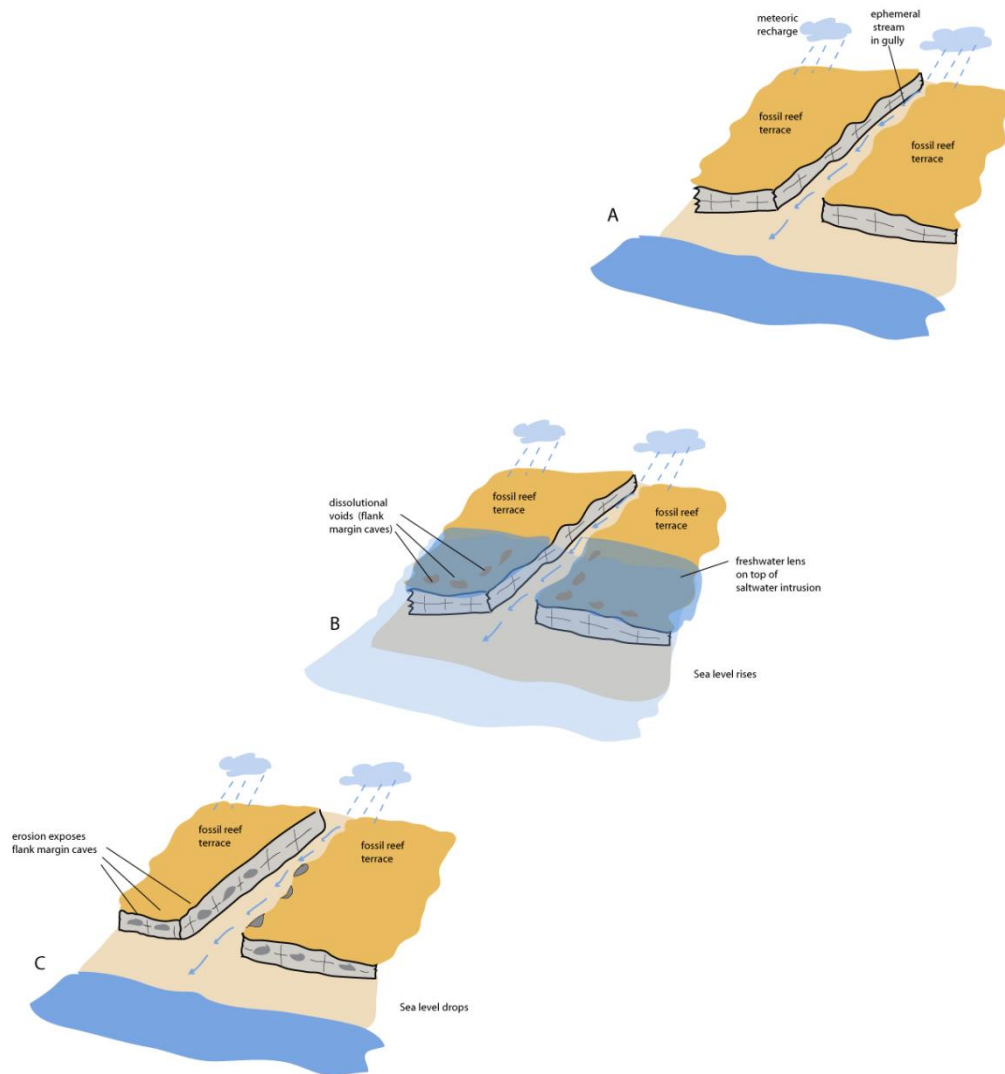


Figure 4.32 Model for cave development within gullies of Barbados

(A) Gully formed in reef terrace by intermittent streams flow. (B) Rise in sea level inundates gully. Meteoric recharge accumulates as freshwater lens floating on saltwater that saturates the bedrock. Mixing of fresh- and saltwater is dissolutionally aggressive and dissolves limestone making small flank margin caves. (C) Sea level drops, gully walls are eroded and caves are exposed.



Figure 4.33 Boka development is a function of reef terrace width

(A) is Boca Tabla and (B) is Boca Wandami, both located in Sheta Boka National Park, Curaçao. Reef terrace width is indicated with the white line.

Photo: H. Van Bommel

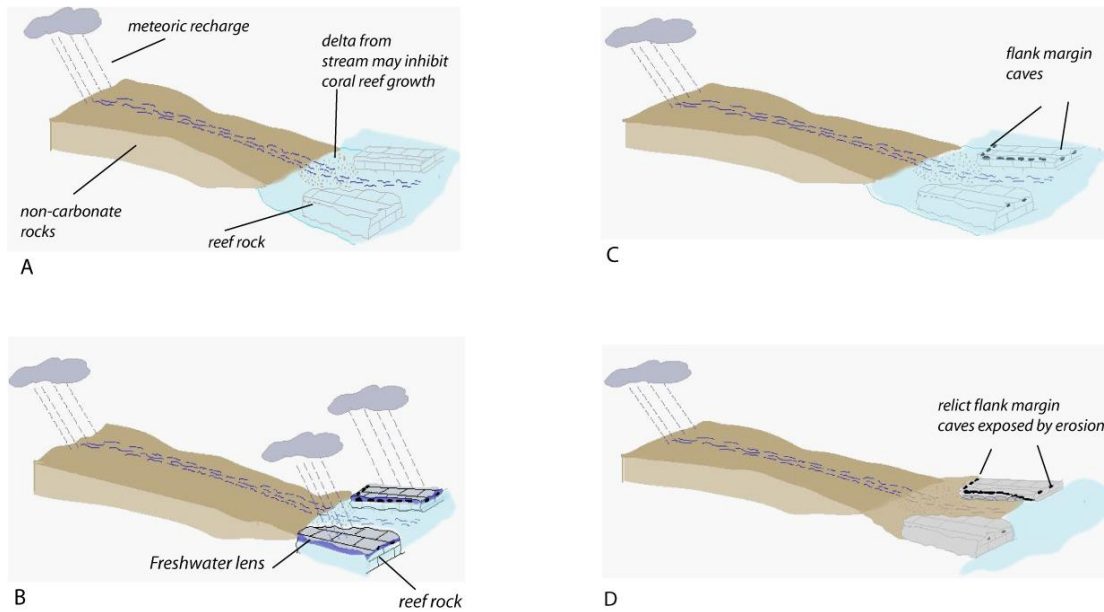


Figure 4.34 Model I for development of a fluviably dominated boka

(A) Intermittent meteoric drainage flows to the coast and inhibits coral reef growth. Sea water saturates the coral reef bedrock. (B) Sea level drops exposing the reef bedrock. Meteoric water accumulates as a freshwater lens (dark blue) and floats on the saltwater. The interface of both waters is a mixing zone that can dissolve limestone. Flank margin caves form. (C) Sea level rises, inundating the coast. (D). Sea level drops to even lower levels and exposes the reef bedrock to erosion. As the perimeter of the boka erodes due to weather or wave action, flank margin caves are exposed on the interior, landward and coastal sides of the boka.

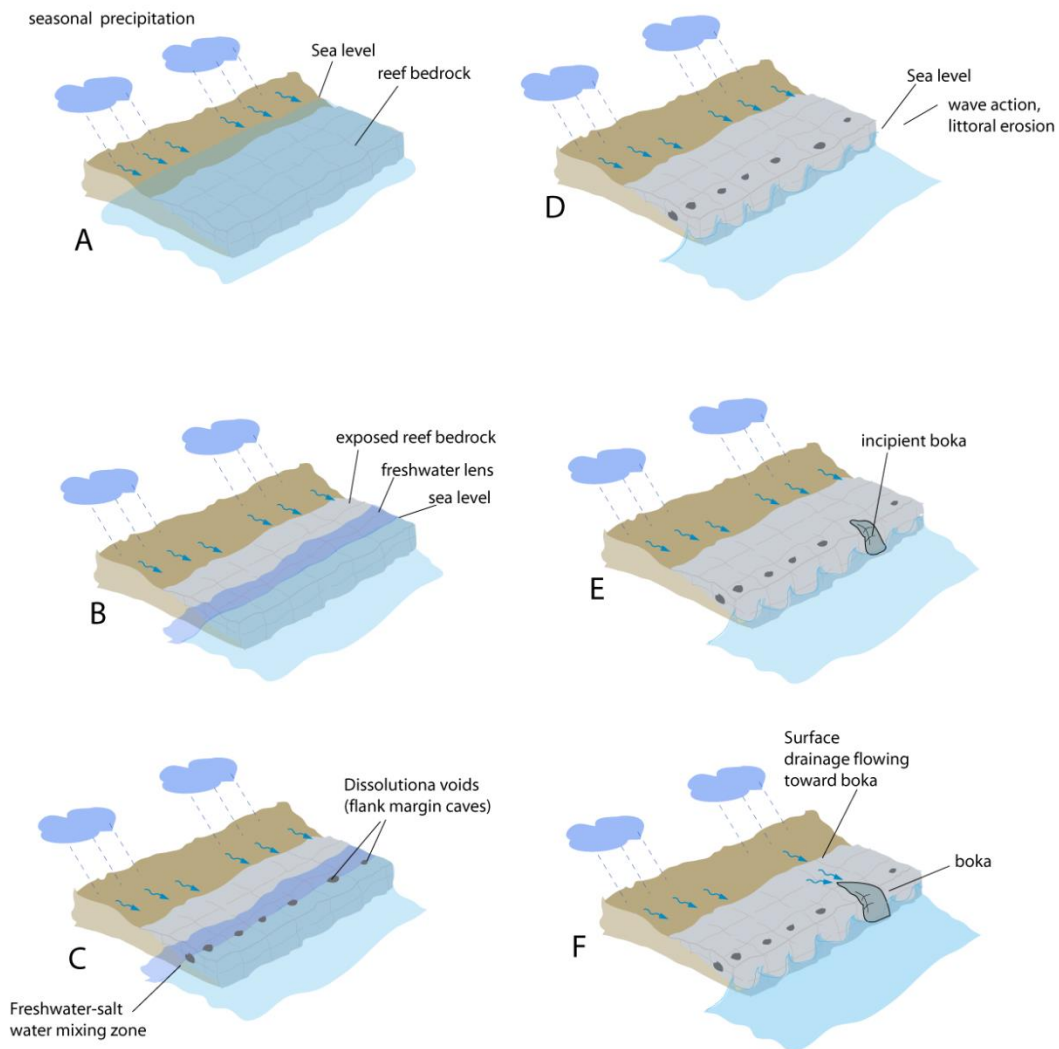


Figure 4.35 Models II and III for development of littoral and littoral/fluvial boka

(A) Sea level high stand with coral rock submerged. Sea water has intruded the bedrock
 (B) Sea level drops exposing reef bedrock. Precipitation recharge accumulates as freshwater lens within the bedrock and floats on the sea water intrusion. (C) Dissolutional voids (flank margin caves) form at the freshwater-saltwater interface. (D and E) Sea level drops and exposes the bedrock to littoral erosion and begins forming a boka (F) Weathering and littoral erosion continue to enlarge the boka. Intermittent stream flow from seasonal precipitation seeks lowest ground as it flows to the sea and connects to the boka.

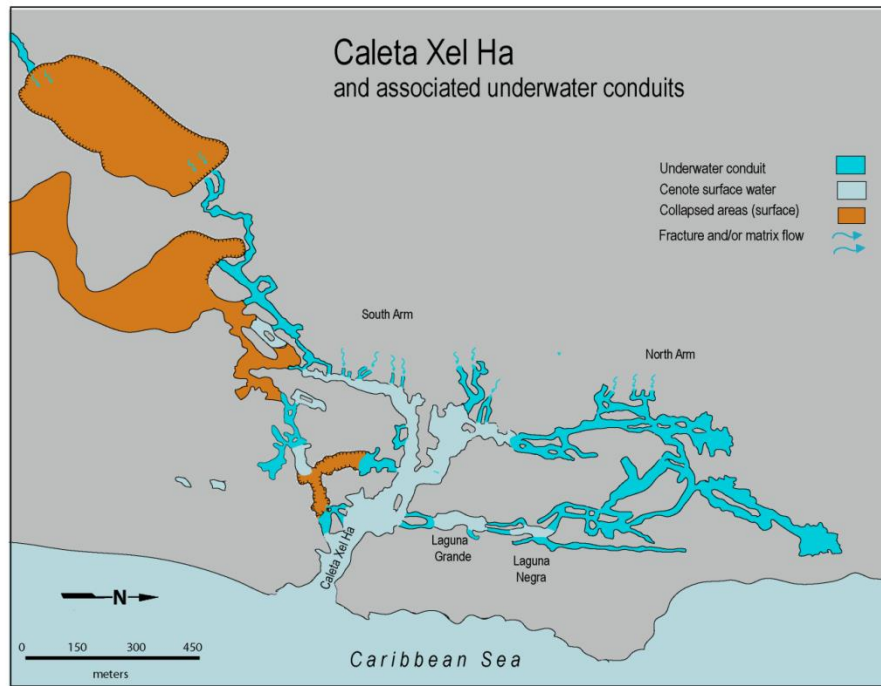


Figure 4.36 Caves associated with Caleta Xel Ha

Modified from Back et al 1979, Thomas 2005

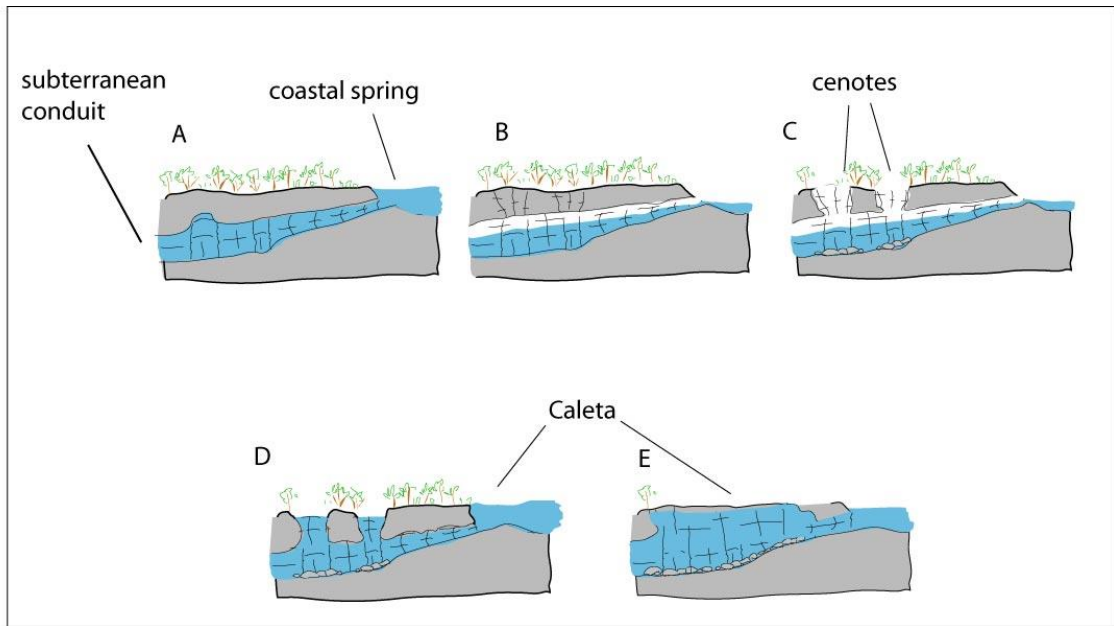


Figure 4.37 Model for development of a linear caleta

(A) Subterranean conduit discharging at the coast. (B) Drop in sea level removes some of the ceiling support and fractures develop. (C) Eventually the conduit ceiling collapses. (D) Sea level rises again exposing more of the conduit to mixing corrosion. (E) Dissolutionally weakened conduit continues coastward progradational collapse. Caleta increases in aerial extent.

CHAPTER V

CONCLUSIONS

5.1 Fractal indices as a measure of cave morphology

In this research, fractal indices were used to quantify cave type, which is indicative of mode of karstification. Fractal dimension, when reported to a precision of 10^{-4} , was able to differentiate 5 different cave types including continental hypogene caves, flank margin caves, allogenic stream caves, littoral caves and tafoni. Fractal dimension and lacunarity used together provided useful descriptive measures of cave morphology. These indices do not define process or predict outcomes but do identify cave morphologies that are characteristic of specific processes.

Continental hypogene caves can form complex three-dimensional mazes that give high fractal dimension values but low lacunarity values because high density cave passages express a homogeneous textural appearance. Continental hypogene caves have the greatest range of values for fractal dimension indicative of a cave type patterns that form from a diversity of recharge modes (H_2S oxidation zones, rising thermal water, deep mixing zones) operating over regional hydrologic scales. Regression analysis of fractal dimension versus lacunarity showed no relationship between the two parameters. It is possible the reason for this is because the analysis was comparing a mix of recharge-resultant patterns instead of comparing patterns within specific recharge types.

The fractal dimension values for flank margin caves ranked directly below hypogene caves. Flank margin caves can have very complex footprints, but they typically are much less developed in vertical extent than hypogene caves or allogenic stream caves. Their lacunarity values are higher than those of hypogene caves because the mazes they form are not as three-dimensionally dense and therefore more heterogeneous in texture. Flank margin caves rank fourth in terms of morphologic range which reflects their restriction to coastal zones and in rock types with eogenetic structural characteristics. Regression analysis shows no relationship between fractal dimension and lacunarity in flank margin caves. This may be a function of differences in the configuration of the freshwater lens which can result on morphologic textures that are both homogeneous and heterogeneous.

Fractal dimension values for allogenic stream caves were lower than flank margin caves but well above littoral caves. In nature, allogenic stream caves are very linear in form though they can have complex local patterns as stated above. Their linearity is what makes for a less complex three-dimensional pattern. Their linearity also gives much higher lacunarity values than the other cave types i.e. the cave morphologies are more heterogeneous. Allogenic stream caves rank second in range of fractal dimension values within the data sampled though considerably lower than hypogene caves. Allogenic stream caves have two modes of recharge (sinking streams and sinkholes) that operate over more local hydrologic conditions though they do form across the same spectrum of structural rock characteristics as hypogene caves. Allogenic stream caves are typically classified as epigene which means their development is closely related to surface hydrology and recharge. Exceptions to the linearity of stream caves are commonly caused

by floodwater mazes at restrictions or breakdown, and/or in their multi-level development due to changes in base level which adds a vertical maze component to their morphology. Stream caves were the only types that showed a relationship between lacunarity and fractal dimension. This may reflect their narrow range of recharge types which would give consistency in overall morphologies.

Caves with the lowest fractal dimension and lacunarity are littoral caves and tafoni respectively. There is some degree of latitude in terms of littoral cave morphologies because of wave energy versus configuration of the coastline and variations in rock structure and lithologies. Littoral caves (Figure 2.13) rank third in fractal dimension range. They are pseudokarstic i.e. not dissolutional in origin, and are restricted to coastal zones. However, they can form in a wide variety of rocks with varying structural character which may be why there appears to be no relationship between fractal dimension and lacunarity.

Tafoni had the lowest fractal index values and ranges because of their restricted geologic and geographic location i.e. the sample groups were exclusively from Quaternary eolianites from the Bahamas. Their simple morphology also gives them a very homogeneous morphological texture. This cave type displayed the smallest r^2 value from the regression analysis because there is virtually no change in lacunarity versus fractal dimension values in the data set.

The cave types with the most statistically similar morphologies were continental hypogene caves and flank margin caves. Both cave types formed in very different geologic conditions, and diagenetic maturity of the rock is telogenetic in hypogene caves

versus eogenetic in flank margin cave. However, both cave types are initially formed by mixing zone corrosion which results in similarities in their morphologies.

Hypogene caves versus tafoni displayed the biggest difference in fractal dimension morphology. In nature their modes of genesis are distinctly different with hypogene caves formed by mixing-zone corrosion and tafoni formed by mechanical erosion.

Flank margin caves and littoral caves ranked significantly different in terms of fractal dimension. Flank margin caves form by mixing zone corrosion whereas littoral caves formed by mechanical erosion. Flank margin caves that have been exposed to erosion by wave energy may become overprinted by littoral erosion and can be confused with littoral caves.

The data show that littoral caves and tafoni have the second most similar fractal dimension morphology which reflects their morphological simplicity.

In comparing lacunarity values between specific pairs of cave types, allogenic stream caves and tafoni showed the biggest difference in lacunarity. Allogenic stream caves have a very heterogeneous morphological texture versus tafoni which are very homogeneous. Allogenic stream caves, flank margin caves and littoral caves compared more closely in terms of lacunarity than other pairs.

The lacunarity values of hypogene and littoral caves show similar low values and the statistical tests indicate that they cannot be effectively differentiated within the existing data set. Though cave types originate from vastly different geologic conditions, the low lacunarity value of hypogene mazes result from their dense passage configuration that gives them a homogeneous morphologic texture. The low lacunarity value of littoral

caves results from their very simple morphology which also expresses as homogeneous morphological texture. This situation illustrates the value of using two independent fractal indices to describe a cave types. In this example, hypogene caves will display high fractal dimension and low lacunarity. Littoral caves will display very low fractal dimension and low lacunarity.

In the hypogene, flank margin and stream cave types there were some caves that had very high fractal dimensions within their type group. These caves are polygenetic which means their overall morphologies are the result of multiple stages of cave development. All caves are polygenetic to some degree but the largest cave systems show that tendency to the extreme. Polygenetic caves could also be treated as multi-fractals though it is unknown how this would affect the calculation of fractal dimension and lacunarity and if those values would be different from the values calculated in this research. That consideration was beyond the scope of this particular research.

Some caveats should be mentioned about the results of this research and use of fractal indices in order to distinguish cave type. All of the caves used in this study were known entities in terms of types so there may be a bias in sample selection. A total of 30 samples were analyzed for each cave type which is a statistical minimum for statistical testing. Fractal indices do not define process or predict outcomes but do identify cave morphologies that are characteristic of specific processes.

5.2 Geologic controls on the development of caves within the phreatic, epiphreatic and vadose zones on the northeast coast of Quintana Roo, Mexico

The underwater caves and vadose-epiphreatic zone caves of northeast Quintana Roo share many characteristics though there are some subtle differences in terms of

distribution. Exploration bias has to be considered when making comparisons between the underwater and vadose-epiphreatic zone caves of Quintana Roo as exploration and documentation of underwater caves has been ongoing since mid-1980 whereas exploration and detailed documentation of equal focus did not begin in the vadose-epiphreatic zone caves until 2008 and the data set for the latter is not as extensive as the former.

The major structural orientations and inclinations of underwater and vadose-epiphreatic zone caves are very similar. Underwater caves have a much greater depth range than vadose-epiphreatic zone caves. The vertical range of development in the vadose zone caves is above current sea level though some elevations push above the 6-meter high mark of MIS5e. These areas are where the survey line was run from the surface and down into a cenote (or vice versa) which means those elevations can be attributed to progradational collapse rather than anomalous glacioeustasy. When the depth of the vadose zone caves reaches the local water table, the epiphreatic zone is encountered and passages can contain pools of water or be inundated wall-to-wall. In some instances the epiphreatic zone may lead to phreatic passages and connect with extensive underwater caves. The 4-6 meter above sea level elevations of the vadose-epiphreatic zone caves strongly suggest that they formed during MIS5e which occurred approximately 125,000 ago when sea level was 4-6 meters higher than it is today.

In terms of distribution, there are no vadose zone caves located less than a kilometer from the coast. However, there is major underwater cave development in that zone. Cave divers report that the zone is devoid of speleothems, bedrock walls are characteristically friable and unstable, and there is lot of loose sediment (Coke 2013

personal communication, Bourignon 2014 personal communication). Beddows et al. 2007a identified the near-coast environment as the active mixing zone and location of the youngest Pleistocene limestones, with the least overprinting by other processes. There is significant vadose zone cave development in the beach ridges of the study area and the cave passages in those areas are characterized by low, rectilinear mazes, similar to passages actively forming at the coast today. It is suggested that the caves in the beach ridges may have initiated as flank margin caves but became incorporated in the regional hydrology when sea levels rose. Flank margin caves have been documented in coastal eolianites near Tulum (Kelly et al. 2006, Kambesis unpublished data). Because of the small size of these particular caves, they do not display the typical morphology of more extensive flank margin caves e.g. ramiform or sponge work with cross-linked chambers. However, they do display the large width to low height ratio of chambers that take the form of the distal margin of the freshwater lens. The elevation of the Tulum flank margin caves and breakdown at their entrance areas suggest that the caves initially developed when sea level was higher. They were formed without entrances and were ultimately exposed by erosion and coastline retreat.

The morphological differences of caves from coastal to inland configuration may be a result of lithological controls e.g. changes in lithology and/or changes in diagenetic maturity, where Pleistocene to Holocene age carbonates transition to older, more consolidated ones and cave passages are contained within more massive and stable bedrock.

An exception to the rectilinear passage morphology of most of the near coast cave sections is that of Sistema Ox Bel Ha which displays the passage characteristics of an

inland cave in its sections all the way to the coast. The discharge vents of Sistema Ox Bel Ha appear to be located in an older paleo-coastline section than caves to the northeast. The distribution of caletas, which are common northeast of Ox Bel Ha and are typically associated with coastal discharge vents, drop to none in the Ox Bel Ha coastal vicinity, though discharge vents are still common. This supports the hypothesis of a change in geologic boundary conditions south of Tulum.

Caletas do occur north of the study area (Puerto Morelos), but are not as plentiful. This may also reflect a change in geologic conditions.

The karst inventory has identified hundreds of cenotes i.e. sinkhole collapses in the study area. These features serve as entrances to the many cave systems both underwater and in the vadose zone of the study area.

Smart et al. (2006), proposed that coastal caves of Quintana Roo were morphologically intermediate between continental stream caves and flank margin caves. However, the fractal indices calculated for ten select caves in the study area classified them as overlapping between flank margin caves and hypogene caves. This reflects that continental hypogene caves and the caves of Quintana Roo both display morphologies that indicate mixing zone corrosion. However the Quintana Roo caves function as an epigene drainage system.

The anastomotic pattern of inland cave development may have been overprinted on initial fissure or joint-controlled networks (Kambesis and Coke 2013) since these have been suggested to be the precursors to the dissolutional conduits (Tułaczyk et al. 1993). Considering the limited lateral extent of fissure controlled passages, it is also possible that there is no structural control on incipient passages but rather that coastward hydraulic

gradient resulted in the development of sub-parallel passages that randomly intersected. This bears some similarity to the development of flank margin caves as dissolutional voids that randomly connect to form larger voids.

The anastomosing configuration of the inland cave passages may in part be influenced by regional structure, but local conditions also play a significant role. Ceiling collapse is a function of the removal of buoyant support when water drained from formerly submerged cave passages. Extensional fractures occurred in association with mechanical ceiling collapse, and the formation of cenotes made zones of weakness that resulted in more extensive areas of breakdown. Groundwater flow found new routes around the breakdown and the multiple diversions resulted in anastomosing passage configurations. Other factors that influence cave patterns because they affect water flow include sediment and speleothem occlusion (Smart et al. 2006).

The submerged cave passages of northeast Quintana Roo are fairly shallow in terms of world depth standards. However there are sections with depth ranges from 70 to 120 meters suggesting potentially extensive deeper cave development. Exploration at these depths, which is technically challenging, has been minimal so far.

The low hydraulic gradient of the Yucatan peninsula means that water levels within Quintana Roo cave systems track sea level. The current location of the halocline and the vertical distribution of cave passages indicate that the cave systems have undergone multiple phases of development.

5.3 Influence of karstic, fluvial, and littoral processes on the development of reentrants and associated features on rocky carbonate coasts.

Glacial eustasy during the past 200,000 years has caused significant fluctuations in sea level. High stands resulted in coral reef development on island and continental coasts, and low stands subaerially exposed carbonate coasts allowing emplacement of a freshwater lens and the initiation of karstification. Three types of carbonate coast reentrants were investigated in this study and included the gullies of Barbados, bokas of Aruba, Bonaire and Curaçao, and the caletas of the northeast coast of Quintana Roo, Mexico. The development of these features reflect a range of geomorphic agents that include a combination of fluvial, littoral, and karstic processes that operated during periods of stable and fluctuating sea levels.

5.3.1 Gullies Summary

Gullies are common in all geomorphic zones of the island of Barbados and prior studies attributed their distribution and occurrence to the formation and collapse of fluvial-type caves. A total of 705 km of gully have been documented in Zones and I and II but it is highly unlikely that 705 km of collapsed cave conduits large enough to result in the current gully configuration actually formed on the island. The recharge area of the island is not extensive enough to account for that extent and size of conduit development even when sea level was lower and island area larger.

The width of many of the gullies exceeds the width of any documented cave passages on the island. In the widest gullies, erosional collapse of gully walls would have eliminated evidence of fluvial cave passages. Instead, caves are observed on both sides of the walls of the widest gullies.

Ceiling collapse does happen in caves and can potentially reach the surface by progradational collapse. However, as a cave ceiling progrades upwards it will tend to form a stable arch (Palmer 2007). Breakdown of cave passages can also form when a passage is first drained of water. The same principles of rock collapse that explains cave collapse can also be used to explain wall collapse from outdoor cliffs. It is likely that the large angular boulders that Speed (2012) observed on the floors of gullies during his studies in Barbados were the result of the collapse of gully walls rather than progradational collapse of underlying cave passages.

Passage development in three of the five largest cave systems on the island does not directly correlate with the directional trend of any gully. The gullies follow the dip of the topography whereas the documented cave passages of the area appear to follow the strike. Because of the small sampling of known fluvial caves to date, there is not enough data to definitively determine the dominant trend of fluvial cave development.

The drainage pattern of the gullies on the drainage basin scale indicate that there may be structural influence on the initial development of the gully drainage pattern. Considering the geologic history of Barbados, differential uplift of the limestone coupled with unloading of the surface as strata were eroded may have resulted in fractures and fissures that were inception zones for the development of gullies. The radial configuration of gully drainage away from the rising center of the island and to the coasts is indicative of the main function of the gullies which is to drain the land surface. Flood waters that course through the gullies are sufficient enough in their dissolutive capacity to dissolve surface channels into the underlying limestone. That along with fluvial erosion may have sculpted the gullies to their current form.

The caves that have formed within gully walls are distinctly different from the fluvial caves of the island. The gully caves are flank margin caves and formed when higher sea levels inundated the gullies. Flank margin caves form at the interface between fresh and saline water and are reliable indicators of past sea levels. When sea levels dropped, the gullies drained of sea water and became exposed to weathering processes. The flank margin caves were exposed by erosion of the gully walls.

5.3.2 Bokas summary

The morphological characterization of the bokas of the ABC Islands as fluvially, littorally or fluvio/litorally dominant, recognized that boka development is influenced by a combination of processes including karstic ones. Dominant processes that affect boka formation depend on the location and distribution of the bokas. On the windward coasts of Aruba and Curaçao the majority of boka development occurs where the lower reef terrace is narrowest in its lateral extent (less than 300 meters) and where it abuts the igneous island core.

Bonaire has minimal boka development and this can be attributed to the fact that the island's volcanic core is much more restricted in extent than on the other islands. Multiple reef terraces are common along the coasts of Bonaire.

This research determined that the caves associated with bokas are the result of mixing-zone corrosion. Morphometric analyses of the caves determined that the caves located in the walls of the bokas are not segments of stream caves but are degraded flank margin caves.

Initial ideas on the origin of bokas mainly addressed the fluvially-dominated bokas located on Curaçao's northwest windward coast and suggested that all bokas

shared the same origin. This research showed that there is a diversity of boka morphology and origin.

5.3.3 Caleta summary

Back et al. (1979) determined that caletas and crescent-shaped beaches formed when coastal freshwater springs mixed with marine water causing the weakening of solution channels which made the limestone more vulnerable to wave erosion and thus formed caletas. As wave action continued to erode the coast, the caletas degraded to crescent-shaped beaches. An inventory of Quintana Roo caletas documented 30 features and of those 22 caletas have humanly accessible cave passages. Structural trend, littoral processes, large discharge-volume springs that resurge directly on the coast, and dissolution at coastal springs result in distinctive caleta morphologies

The long, linear spring-run caletas are all associated with well-developed cave passages and coastal springs that resurge to the surface between 300 to 700 meters inland.

About 20% of the documented caletas appear to have a joint-controlled morphology that is expressed as rectangular shaped coastal reentrants.

Some of the coastal springs resurge directly on the coast adjacent to and sometimes from a beach. Underwater cave passages cannot be accessed via these and similar caletas, although they are accessed via coastal cenotes located inland from the coast. The underwater passages near those caletas consist of very, young and unstable rectilinear maze passages that are the bane of underwater exploration.

The association of caletas with cenotes indicates that caleta development may be associated with coastward progradational collapse of cenotes. A third of all caletas along the Quintana Roo coast are in close proximity to one or more coastal cenotes.

The small circular or triangular shaped caletas are associated with smaller discharge springs that appear to be in close proximity to less extensive cave systems that have been documented near the coast. It is possible the smaller caves systems are the source of the spring discharge.

In addition to the caletas and associated springs, there are hundreds of small vents that discharge into the bays and caletas all along the coast. These features are currently undocumented.

Weidie (1978) identified a strong northwest fracture trend along the entire Quintana Roo coast that he suggested controlled the inland development and extent of coastal features. He also noted a northeast trending fracture set that parallels the coast and indicated these structures control the lateral extent of coastal features. This study documented the structural orientation of the caletas and beaches to have strong northwest and northeast orientations.

There is very little caleta development north of Playa del Carmen. South of Tulum, caleta development is non-existent, however, large coastal springs resurge along the coast south of Tulum. Sistema Ox Bel Ha, which is one of the world's longest underwater cave has three humanly accessible coastal vents but there are no obvious features analogous to caletas. Farther south from Tulum are many coastal springs that debouche into the sea and into the large bahias (bays) characteristics of that area. The diminution or absence caleta development north of Playa del Carmen and south of Tulum may indicate a change in geologic boundary conditions.

5.4 Epilogue

The Carbonate Island Karst Model (CIKM) has been the preeminent guide that explains the genesis and morphology of eogenetic dissolutional features on small carbonate islands. This research showed that the model is robust enough to be expanded to explain eogenetic karstification in more complex and larger island settings and on carbonate continental coasts such as those investigated in this research

The fractal indices developed in this research were effectively used to describe and distinguish cave types for all of the study sites and helped confirm the type of karstification. The basic tenets of CIKM were successfully used to determine mode of development for an unusual suite of small caves that in the past had been mis-identified as relict segments of stream caves. Knowledge of the mode of karstification was critical for determining the origin of the three types of coastal re-entrants studied in this research and to understand how karstification helped drive the evolution of carbonate coasts. The most complex coastal karst addressed in this research is exemplified on the northeast coast of the Yucatan peninsula where a combination of conduit flow, mixing zone corrosion and glacioeustasy have resulted in the development of one of the most extensive and significant eogenetic karst aquifers in the world. Some of the complex cave morphologies displayed in the region, especially the dense, complex mazes that occupy the many beach ridges in the area can be addressed within the scope of CIKM.

The research was able to quantitatively identify and differentiate coastal cave types using fractal geometry; identify geological controls on the development of caves currently located in the vadose and epiphreatic zones within a mixing-zone environment of a carbonate continental coastline, and determine the relationship of those caves to the

phreatic caves of the region; develop coastal reentrant models to explain eogenetic coastal karst features formed by a combination of karstic, littoral, and/or fluvial processes. The results of this research successfully expanded the Carbonate Island Karst Model to the Carbonate Coastal Karst Model. The expanded model encompasses coastal karst and cave development on all types and sizes of carbonate islands and carbonate continental coasts.

REFERENCES

- Addison, P. S., (1997), *Fractals And Chaos: An introductory course*. First Edition, Taylor and Francis, ISBN-13: 9780750304009 pp. 256
- Alexander, C.S., (1961), The marine terraces of Aruba, Bonaire, and Curaçao, Netherlands Antilles. *Annals of the Association of American Geographers* 51/1: 102-123
- Back, W., and Hanshaw, B. B., (1970), Comparison of chemical hydrogeology of the carbonate peninsulas of Florida and Yucatan, *Journal of Hydrology*, 10: 330 – 368
- Back W., Hanshaw B.B., Pyle T.E., Plummer L.N. and Weidie A.E., (1979), Geochemical significance of groundwater discharge and carbonate solution to the formation of Caleta Xel Ha, Quintana Roo, Mexico. *Water Resources Research* 15:1521–1535
- Back, W., Hanshaw, B.B., and Van Driel, J.N., (1984), Chapter 12, Role of groundwater in shaping the Eastern Coastline of the Yucatan Peninsula, Mexico. in LaFleur, R.G. (Editor), *Groundwater as a Geomorphic Agent*, Allen & Unwin, Inc., Boston pp.281-293
- Back, W., (1995), Water management by early people in the Yucatan, Mexico. *Environ Geol* 25(4):239–242
- Banner, J.L., Wasserburg, G.J., Chen, J.H., and Humphrey, J.D., (1990), Carbonate deposition, diagenesis, and hydrology on Barbados, West Indies: Uranium-series evidence: *Geological Society America Program*, 22: A88
- Barbados, Government, (2004), EPG, PDA, SEMS Gully Ecosystem Management Study: Report on the Broad-Scale Survey and Development of the GIS Database. Ministry of Housing, Lands and the Environment. 59pp.
- Bassingthwaighte, J.B., L.S.Liebovitch, and B.J.West, (1994), *Fractal physiology*. New York: Oxford University Press
- Bates, R.L., and Jackson, J., (1987), *Glossary of geology*: Alexandria, Virginia, American Geological Institute, p. 788

- Badino, G., (2001), Has Deep Karst a Fractal Behavior?, 13th International Congress of Speleology, 4th Speleological Congress of Latin American and Caribbean, 26th Brazilian Congress of Speleology, www.sbe.com.br
- Barton, H., (2001), The Pit in Dos Ojos, AMCS Activities Newsletter Number 24, p. 84-91
- Bauer-Gottwein P, Gondwe, B.N.R., Charvet, G., Marin, L.E., Robellodo-Vieyr, M. and Meresiz-Alonso G., (2011), Review: The Yucatan Peninsula karst aquifer, Mexico, *Hydrology Journal*, 19:507-524
- Beddows, P.A., (2003), Cave hydrology of the Caribbean Yucatan coast: *Association of Mexican Cave Studies Bulletin* 11, 96 p
- Beddows, P.A., (2004), Groundwater hydrology of a coastal Conduit carbonate aquifer: Caribbean Coast of the Yucatan Peninsula, México, PhD Thesis, University of Bristol, UK
- Beddows, P.A., Smart, P.L., Whitaker F.F. and Smith, S.L., (2007a), Decoupled fresh-saline groundwater circulation of a coastal carbonate aquifer: Spatial patterns of temperature and specific electrical conductivity, *Journal of Hydrology*, 346: 28-42
- Beddows, P.A., Hendrickson M.R., Webster K.H. and Kras S.M., (2007b), Mapping flooded caves from above: Surface karst inventory of the Yucatan Peninsula: 193-197
- Beets, D.J., H.J. MacGillvary & G. Klaver, (1977), Cretaceous and Early Tertiary of Bonaire. in: *Guide to the field excursions on Curaçao, Bonaire and Aruba*. 8th Caribbean Geological Conference Curaçao, 9-24 July 1977. GUA Paper of Geology 10: 18-28
- Bird, E., (2008), *Coastal Geomorphology: An introduction*, Wiley 434 p
- Bordignon, M., (2014), Personal communication
- Bourke, P., (1991), *An Introduction to Fractals*, <http://paulbourke.net/fractals/fracintro/>
- Choquette, P. W. and Pray L.C. (1970), Geologic nomenclature and classification of porosity in sedimentary carbonates: *American Association of Petroleum Geologists Bulletin*, v. 54, no. 2, p. 207-250
- Coke, J. G. IV, (2009), Yucatan Peninsula (Campeche, Yucatan, Quintana Roo) in *Caves and Karst of the USA*, eds. Palmer, A.N., and Palmer, M. V, pp. 388-390
- Coke, J. G. IV, (2013), Personal communication

- Curl, R.L., (1964), On the definition of a cave.- National Speleological Society Bull., 26, 1-6
- Curl, R.L., (1966), Caves as a Measure of Karst. - Journal of Geology, 74, 5, 798-830
- Curl, R. L., (1974), Deducing flow velocity in cave conduits from scallops, Nat. Speleo. Soc. Bull. V. 36, N2. p.1-5
- Curl, R.L., (1986), Fractal Dimensions and Geometries of Caves.- Mathematical Geology, 18, 2, 765-783
- Curl, R.L., (1999), Entranceless and Fractal Caves Revisited.- In: Palmer, A.N., Palmer, M.V., Sasowsky, I.D., eds: Karst Modeling, Special Publication 5, Karst Water Institute, Charlottesville, Virginia, p. 183-185
- Curl, R. (2011) – Comment on ‘‘Coastal Caves in Bahamian Aeolian Calcarenites: Differentiating Between Sea Caves and Flank Margin Caves Using Quantitative Morphology’’. Journal of Cave and Karst Studies, v. 73, no. 3, p. 202. DOI: 10.4311/jcks2011es0195
- Day, M. (1983), Doline morphology and development in Barbados. Annals of the Association of American Geographers 73: p. 206-219
- de Buissonje', P., (1974), Neogene and Quaternary geology of Aruba, Curaçao, and Bonaire (Netherlands Antilles). Uitgaven Natuurwetenschappelijke Studiekring voor Suriname en de Nederlandse Antillen 78, 291pp
- Denizman, C (2003), Morphometric and spatial distribution parameters of karstic depressions, Lower Suwannee River Basin, Florida. Journal of Cave and Karst Studies, v. 65, n. 1, p. 29-35
- Evans, I.S., (1972), General geomorphometry, derivatives of altitude, and descriptive statistics. In: R. J. L. Chorley (end), Spatial Analysis in Geomorphology, Methuen, London
- Falconer, K., (1990), Fractal Geometry—Mathematical Foundations and Applications. John Wiley and Sons Ltd, Chichester, pp. 288
- Fermor, J., (1972), The dry valleys of Barbados. Transactions of the Institute of British Geographers, v. 57, p. 153-165
- Filipponi, M., Jeannin, P.Y. & L. Tacher, 2009: Evidence of inception horizons in karst conduit networks.- Geomorphology, 106, 86–99
- Finnesand, T., and Curl, R. (2009), Morphology of Tjoarvekrajjge, The Longest Cave in Scandinavia, Proceedings, 15th International Union of Speleology, p 878-883

- Fish, L. CaveX, Retrieved January 2013 <http://www.fountainware.com/vrml/index.htm>
- Fish, L. COMPASS Cave Survey Software, Retrieved January 2013
<http://www.fountainware.com/compass/index.htm>
- Florea, L.J., Wicks, C.M., (2001), Solute transport through laboratory-scale karstic aquifers. *Journal of Cave and Karst Studies* 63, p 59–66
- Ford, D.C., and Williams, P.W., (2007), *Karst Hydrogeology and Geomorphology*. John Wiley & Sons Ltd., West Sussex, 562 p
- Fouke, B.W., (1993), Chronostratigraphy and Dolomitization of the Seroe Domi Formation, Curaçao, Netherland Antilles. Ph.D. dissertation, State University of New York at Stony Brook, New York, 747 pp.
- Fouke, B.W., Beets, C.J., Meyers, W.J., Hanson, G.N., and Melillo, A.J., (1996), $^{87}\text{Sr}/^{86}\text{Sr}$ chronostratigraphy and dolomitization history of the Seroe Domi Formation, Curaçao (Netherlands Antilles). *Facies*, v. 35, p. 293-320 Fouke 1978
- FracLac: <http://imagej.nih.gov/ij/plugins/fractalac/> accessed March 2013
- Frumkin, A. & I. Fischhendler, (2005), Morphometry and distribution of isolated caves as a guide for phreatic and confined paleohydrological conditions.- *Geomorphology*, 67, 457-471
- Ganas, A., Pavlidesb, S., Karastathisa, V., (2005), DEM-based morphometry of range-front escarpments in Attica, central Greece, and its relation to fault slip rates. *Geomorphology* 65, 301–319
- Gibbard, P.L., (2007), *Climatostratigraphy* In: Elias, S.A. (ed.) *Encyclopedia of Quaternary Science*. Elsevier: Amsterdam. 2819-2825
- Gilbert, L.E., (1989), Are topographic data sets fractal? *Pure Appl. Geophys*, v.131, p. 241-254
- Grassberger, P., (1981), On the Hausdorff Dimension of Fractal Attractors, *Journal of Statistical Physics*, V.26, No. 1, p. 173-179
- Glennon, J. A., (2001), Application of morphometric relationships to active flow networks within the Mammoth Cave Watershed, M.Sc. Thesis, Bowling Green: Western Kentucky University, 87 p
- Gondwe, B.R.N., Lerer S., Stisen S., Marín L., Rebolledo-Vieyra M., Merediz-Alonso, G. and Bauer-Gottwein P., (2010), Hydrogeology of the south-eastern Yucatan Peninsula: new insights from water level measurements, geochemistry, geophysics and remote sensing. *J Hydrol.* doi:10.1016/j.jhydrol.2010.04.044

- Goodchild, M. F., (1982), The fractional Brownian process as a terrain simulation model, *Modelling Simulation*, 13: 1133-1137
- Gorney, D., Escalona, A., Mann, P., Magnani, M. B., BOLIVAR Study Group, (2007), Chronology of Cenozoic tectonic events in western Venezuela and the Leeward Antilles based on integration of offshore seismic reflection data and on-land geology. *American Association of Petroleum Geologists Bulletin* 91 (5), 653–684
- Groves C., (1994), *Geology of Barbados and Harrison's Cave area: A Study of the Environmental Factors in Harrison's Cave, Barbados, West Indies*. National Speleological Foundation: 9-17
- Grove, C., and Meiman, J, (2005), Weathering, geomorphic work, and karst landscape evolution in the Cave City groundwater basin, Mammoth Cave, Kentucky, *Geomorphology*, Volume 67, Issues 1–2, Pages 115–126
- Gulley, J. D., Martin, J. B., Moore, P. J. and Murphy, J. (2013), Formation of phreatic caves in an eogenetic karst aquifer by CO₂ enrichment at lower water tables and subsequent flooding by sea level rise. *Earth Surf. Process. Landforms*, 38: 1210–1224. doi: 10.1002/esp.3358
- Goddard, R., (2007), Barbados Caves and Landslips, *Memories of Richard Goddard*, <https://barbadosfreepress.wordpress.com/2007/09/18/Barbados-caves-and-landslips-memories-of-richard-goddard/>
- Gonzalez-Herrera, R, Sanchez-y-Pinto and Gamboa-Vargas, (2002), Groundwater-flow modeling in the Yucatan karstic aquifer, Mexico, 10: 539-552
- Hanshaw B.B. & Back W., (1980) Chemical mass-wasting of the northern Yucatan Peninsula by groundwater dissolution *Geology*, 8(5): 222-224
- Harris, N.J., (1984), Diagenesis of upper Pleistocene strand plain limestones, northeastern Yucatan Peninsula, Mexico. MSc Thesis, University of New Orleans, 130 p
- Herweijer, J.P., Focke, J. W., (1978), Late Pleistocene depositional and denudational history of Aruba, Bonaire and Curaçao (Netherlands Antilles). *Geologie en Mijnbouw* 57, 177-187
- Hippolyte, J., and Mann, P., (2009), Neogene–Quaternary tectonic evolution of the Leeward Antilles islands (Aruba, Bonaire, Curaçao) from fault kinematic analysis, *Marine and Petroleum Geology*, 28 259-277
- Horton, R.E., (1945), Erosional development of streams and their drainage basins: hydrophysical approach to quantitative morphology. *Bulletin of the Geological Society of America* 56, 2 75-3

- Huang, W. and Day, M.J., (2013), Object-based image analysis for geomorphological investigation of tower and cockpit karst, Abstract, AAG Annual Meeting, Los Angeles, CA, meridian.aag.org/abstractdetail.cfm
- Huggett, R. J., (2007), *Fundamentals of Geomorphology*, second edition, Routledge, New York, 458 p
- Humphrey JD (1997) *Geology and Hydrogeology of Barbados*. In: Vacher, H., and Quinn, T. M., (eds.) *Geology and hydrogeology of carbonate islands*, *Developments in Sedimentology* 54: 381-406
- Imbrie, J., Boyle, E. A., Clemens, S. C., Duffy, A., Howard, W. R., Kukla, G., Kutzbach, J., Martinson, D. G., McIntyre, A., Mix, A. C., Molfino, B., Morley, J. J., Raymo, M. E., Shackleton, N. J., Toggweiler, J. R., (1992), On the Structure and Origin of Major Glaciation Cycles 1. Linear Responses to Milankovitch Forcing, *Paleoceanography*, Vol 7, Issue 6, pp 701-738
- Inniss V., Oderson D. and Singh A., (2001), *The Government of Barbados State of the Environment Report 2000*, GEO Barbados, United Nations Environment Programme for the Ministry of Physical Development and Environment, Barbados, 112 p
- Isphording, W.C., (1974), *Weathering of Yucatan Limestones; the genesis of terra rosas*. In: Weidie AE (ed.) *Yucatan Guidebook: New Orleans, Louisiana*, New Orleans Geological Society: 78-93
- Jeannin, P.-Y., Groves, C., Häuselaman, P., (2007), Chapter 3: Speleological investigations in *Methods in Karst Hydrogeology* edited by Nico Goldscheider and David Drew, Taylor & Francis, London. 264 p
- Jones I.C. and Banner J.L., (2003), Estimating recharge thresholds in tropical karstland aquifers: Barbados, Puerto Rico and Guam. *Journal of Hydrology*, 278:131–143
- Kambesis P.N., Mylroie J.R., Mylroie J.E., Larson E.B., Owen-Nagel A.M., Sumrall J.B. and Lace M.J. (in press), Influence of karst denudation on the northwest coast of Curaçao. 16th Symposium on the geology of the Bahamas and other carbonate regions program, Gerace Research Centre, p.34
- Kambesis, P.N., and Coke, J.G., IV, (2013). Overview of the controls on eogenetic cave and karst development in Quintana Roo, Mexico, . In Lace, M.J. and Mylroie, J. E., eds., *Coastal Karst Landforms*. Springer
- Kambesis, P. N. and Machel, H.G., (2013), Caves of Barbados, in Lace, M.J. and Mylroie, J. E., eds., *Coastal Karst Landforms*. Springer. Kambesis, P., Despain, J., Groves, C. (2013), The making of a connection: Exploration/Survey in Whigpistle Cave System, Proceedings, Mammoth Cave National Park's 10th Research Symposium, February 14-15, 2013, p. 78-81

- Karperien, A., FracLac for ImageJ.
<http://rsb.info.nih.gov/ij/plugins/fractal/FLHELP/Introduction.htm>. 1999-2013
- Kelly, K., Mylroie, J. E., Mylroie, J.R., Moore, C. M., Collins, L.R., Lica, E., Lascl, I., Roth, M. J., Moore, P.J., Passion, R., Shaw, C., (2006), Eolianites and Karst Development in the Mayan Riviera, Mexico in Davis, R.L., and Gamble, D. W., eds., Proceedings of the 12th Symposium on the Geology of the Bahamas and Other Carbonate Regions, p. 88-99
- Klimchouk, A. B, Sasowsky, I. d., Mylroie, J.E., Engle, S.A., Summers, A.S, 2014, Hypogene Cave Morphologies, Special Publication 18, Karst Waters Institute, 103p
- Klinkenberg, B., (1992), Fractals as morphometric measures: is there a relationship?, *Geomorphology*, 5 p. 5-20
- Kottek, M., Grieser J, Beck C., Rudolf, B. and Rubel F., (2006), World Map of the Koopen-Geiger climate classification updated. *Meteorol, Z.*, 15:259-263
- Kusumayudha, S., and Zen, M. T., Notosiswoyo, S.,, Gautama, R. S. (2000), Fractal analysis of the Oyo River, cave systems, and topography of the Gunungsewukarst area, central Java, Indonesia, *Hydrogeology Journal* 8 p. 271-278
- Labourdette, R., Lasclu, I., and Mylroie, J.E., Roth, M., (2007), Process-like Modeling of Flank-Margin Caves: From Genesis to burial Evolution, *Journal of Sedimentary Research*, 2007, v. 77, 0–0 Research Article DOI: 10.2110/jsr.2007.086
- Lace, M.J., (2008), Coastal cave development in Puerto Rico: *Journal of Coastal Research*, v. 24, no.2, p. 508-518.
- Lam, N.S. and De Cola, L. (eds.), (1993), *Fractals in Geography*, Englewood Cliffs, NJ: Prentice Hall
- Lambeck, K., Chappell, J., 2001. Sea level change during the last glacial cycle. *Science* 292, 679–686
- Larson, E.B., 2014, Bahamian Quaternary geology and the global carbon budget. PhD Dissertation, Mississippi State University, 142 p
- Lauderdale, R.W., Ward W.C. and Weidie A.E., (1979), Carrillo Puerto Formation of northeastern Quintana Roo, Mexico. *Gulf Coast Association of Geological Societies Transactions*
- Laverty, M., (1987), Fractals in karst. *Earth Surface Processes and Landforms* 12, p. 475-480

- Lesser, J.M., (1976), Resumendel studio geohidrologicoe hidrogeoquimicode la peninsuladeYucatan Boletin de Divulgacin Tecnica, 10: 1-11
- Lessor J.M. and Weidie A.E., (1988), Region 25, Yucatan Peninsula. In: W Back, J.S. Rosenhein and P.R. Seaber (Eds.), Hydrogeology, Geological Society of America, Boulder, Co.: 237-242
- Lyew-Ayee, P., Viles, H.A., Tucker, G.E., (2007), The use of GIS-based digital morphometric techniques in the study of cockpit karst. *Earth Surface Processes and Landforms* 32, 165–179
- Machel, H. G., Kambesis, P. N., Lace, M. J., Mylroie, J. R., Mylroie, J. E., and Sumrall, J. B., (2012), Overview of cave development on Barbados. In, Kindler, P. and Gamble, D. W., eds., *Proceedings of the 15th Symposium on the geology of the Bahamas and other carbonate regions*, p 96-106
- Machel, H.G., (1999), *Geology of Barbados: A Brief Account of the Island's Origin and Its Major Geological Features*. Barbados Museum and Historical Society, The Garrison, St. Michael, Barbados, 52 pp
- Magnani, M., B., Zelt, C.A., Levander, A., Schmitz, M., (2009) Crustal structure of the South American–Caribbean plate boundary at 67°W from controlled source seismic data, Volume 114, Issue B2, DOI: 10.1029/2008JB005817
- Maramathas, A.J., and Boudouvis A.G., (2006), Manifestation and measurement of the fractal characteristics of karst hydrogeological formations. *Advances in Water Resources* 29 p. 112-116
- Mark, D. M., and Aronson, P.B., (1984), Scale-dependent fractal dimensions of topographic surfaces: An empirical investigation with applications in geomorphology and computer mapping, *Mathematical Geology*, Vol. 16, No. 7, p. p 671-683
- Mandelbrot, B., (1983), *The Fractal Geometry of Nature*, W. H. Freeman, New York
- Melo, R. H. C. (2007), Using fractal characteristics such as fractal dimension, Lacunarity and Succolarity to characterize texture patterns on images. Master’s thesis, Federal Fluminense University. Link: http://www.ic.uff.br/~rmelo/msc_thesis.htm
- Meyer, D.L., Bries, J.M., Greenstein, B.J., Debrot, A.O.,(2003), Preservation of in situ reef framework in regions of low hurricane frequency: Pleistocene of Curaçao and Bonaire, southern Caribbean, *Lethaia* 36, 273-286
- Mixon, B., (2011), Comment on “Coastal Caves in Bahamian Eolian Calcarenes: Differentiating Between Sea Caves and Flank Margin Caves Using Quantitative Morphology”. *Journal of Cave and Karst Studies*, v. 73, no. 3, p. 202. DOI: 10.4311/jcks2011es0195

- Moore, Y. A., Stoessel, R. K., Easley, D. H., (1992), Freshwater/Sea-Water Relationship within a groundwater flow system, Northeastern Coast of the Yucatan Peninsula, *Ground Water*, Vol 30. No. 3. p.343-50
- Muhs, D. R., Pandolfi, J. M., Simmons, K.R. , Schumann, R.R., (2012), Sea-level history of past interglacial periods from uranium-series dating of corals, Curaçao, Leeward Antilles islands, *Quaternary Research* 78, <http://dx.doi.org/10.1016/j.yqres.2012.05.008>
- Myroie, J. E., and Carew, J. L., (1990), The flank margin model for dissolution cave development in carbonate platforms: *Earth Surface Processes and Landforms*, v. 15, p. 413-343
- Myroie, J.E., and Carew, J.L., (1995), Chapter 3, Karst development on carbonate islands, in Budd, D.A., Harris, P.M., and Saller, A., eds., *Unconformities and porosity in carbonate strata*, American Association of Petroleum Geologists Memoir 63, p.55-76
- Myroie, J. E., and Jenson, J., (2000), Guam and the carbonate island karst model, in Onac, B.P., and Tamas T., eds., *Karst studies and problems: 2000 and Beyond*, Proceedings of the Joint Meeting of the Friends of Karst, Theoretical and Applied Karstology, and IGCP 448, Cluf-Napoca, Romania, p. 82-86
- Myroie, J.E., Jenson, J. W. , Taborosi, D., Jocson, J.M.U., Vann, D. T., and Wexel, C., (2001), Karst features of Guam in terms of a general model of carbonate island karst: *Journal of Cave and Karst Studies*, V. 63, N.1 p. 9-22
- Myroie, J.E. and Myroie, J.R., (2007), Development of the Carbonate Island Karst Model: *Journal of Cave and Karst Studies*, v. 69, p. 59-75
- Myroie, J. E., (2008), Caves Surveys, Cave Size and Flank Margin Caves, *Compass & Tape*, Volume 17, Number 4, Issue 60
- Myroie, J.E., Myroie, J.R. & C.N. Nelson, (2008): Flank Margin Cave Development in Telogenetic Limestones of New Zealand.- *Acta Carsologica*, 37, 1, 15–40
- Myroie and Myroie, (2011), Void development on carbonate coasts: creation of anchialine habitats, *Hydrobiologia*, DOI 10.1007/s10750-010-0542-y
- Myroie J.E., and Myroie J.R. (2013) Flank Margin Caves in Carbonate Islands and the Effects of Sea Level. In: John Shroder (ed.) *Treatise on Geomorphology*, Volume 6, pp. 351-362. San Diego: Academic Press
- Neuman, B.R. and Rahbek, M. L., (2007), Modeling the Groundwater Catchment of the Sian Ka'an Reserve, Quintana Roo, *AMCS Bulletin* No. 18 pp 209

- Otoničar, B., Buzjak, N., Mylroie, J. E., and Mylroie, J. (2010), Flank Margin Cave Development in Carbonate Talus Breccia Facies: An Example from Cres Island, Croatia, *Acta Carsologica*, 39/1, pp 79–91
- Owen, A. M., (2007), *Tafoni Caves in Quaternary Carbonate Eolianites: Examples from the Bahamas*, Unpublished Master's Thesis, Mississippi State University
- Owen, A.M., (2013), *Tafoni development in the Bahamas*. In Lace, M.J. and Mylroie, J. E., eds., *Coastal Karst Landforms*. Springer
- Palmer, A. N. (1991), *Origin and Morphology of Limestone Caves*, *Geological Society of America Bulletin* V. 103, p. 1-25
- Palmer, A. N., (2007), *Cave Geology*, Cavebooks, Dayton, OH pp.454
- Palmer, A. N., (2011), *Distinction between epigene and hypogenic maze caves*, *Geomorphology* 134 p. 9-22
- Pandolfi, J.M., Llewellyn, G., Jackson, J.B.C., (1999). *Pleistocene reef environments, constituent grains, and coral community structure: Curaçao, Netherlands Antilles*. *Coral Reefs* 18, 107-122
- Pardo-Iguzquiza, E., Duran-Valsero, J., Rodriguez-Galiano, V., (2011), *Morphometric analysis of three-dimensional networks of karst conduits*, *Geomorphology* 132, p. 17-28
- Piccini, L. (2011), *Recent developments on morphometric analysis of karst caves*, *ACTA CARSOLOGICA* 40/1, 43–52, Postonja 2011
- Pinault, J.L., Deorfliger, N., Ladouche, Bakalowicz, M., (2004), *Characterization of coastal karst aquifers using an inverse modeling approach: The saline springs of Thau, southern France*, *Water Resour. Res.*, 40, W08501, doi: 10.1029/2003WR002553
- Plotnick, R.E., Gardner, R. H., Prestegard, K., Perlmutter, M., (1996), *Lacunarity analysis: A general technique for the analysis of spatial patterns*, *Physical Review E*, Volume 53, N.5, p. 5461-67
- Plummer, L.N., (1975) *Mixing of sea water with calcium carbonate ground water*. In: Whitten, E.H.T. (Ed.), *Quantitative Studies in Geological Sciences*. Geological Society of America Memoir 142. Geological Society of America, Boulder, CO, pp. 219–236
- Priem, H.N.A., Beets, D.J., Boelrijk, N.A.I.M., Heneda, E. H., Verdumen, E.A.Th., Verchure, R.H., (1978), *Rb-Sr evidence for episodic intrusion of the late Cretaceous tonalitic batholith of Aruba, Netherlands Antilles*. *Geologie en Mijnbouw* 57 (2), 293–296.

- Quintana Roo Speleological Survey website: <http://www.caves.org/project/qrss/new.htm>, accessed February 28, 2014
- Raeisi, E., and Mylroie, J. E., (1995), Hydrodynamic behavior of caves formed in the freshwater lens of carbonate islands: *Carbonates and Evaporites*, v. 10., no. 2, p. 207-214
- Rauch E., (2007), Introduction to Lacunarity. <http://www-swiss.ai.mit.edu/~rauch/lacunarity/lacunarity.html>
- Rice-Snow, S., Wicks, C.M., R. F. A. Tarhule-Lips, (1997), Detailed wall morphology of an interior flank margin cave room, Isla de Mona, Puerto Rico, *Proceedings of the 8th Symposium on the geology of the Bahamas and other carbonate regions*, James L. Carew, editor, p. 158
- Richards, D. and Richards S., (2007), Overview of the Geology and Hydrology of Coastal Quintana Roo, *AMCS Activities Newsletter*, No. 30, pp. 104-109
- Rodriguez, C. J., (1982), Petrology and diagenesis of Pleistocene limestones, northeastern Yucatan Peninsula, Mexico, MS thesis: University of New Orleans, 80 p
- Roth, M.J., (2004), Inventory and geometric analysis of flank margin caves of the Bahamas (M.S. Thesis): Mississippi State University, 117p.
(<http://sun.library.msstate.edu/ETD-db/theses/available/etd-07062004-164940/unrestricted/monica.pdf>)
- Senn, A., (1946), Geological investigations of the groundwater resources of Barbados, B.W.I.: Report of the British Union Oil Company Ltd., 123 pp
- Scheffers, A., (2004) Tsunami imprints on the Leeward Netherland Antilles (Aruba, Curaçao, Bonaire) and their relation to other coastal problems, *Quaternary International* 120 (2004) 163–172
- Schellmann G. and Radtke, U., (2004), A revised morpho- and chronostratigraphy of the Late and Middle Pleistocene coral reef terraces on Southern Barbados (West Indies). *Earth Science Reviews*, 64: 157-187
- Schombourgh, R.H., (1848), *The History of Barbados*. Longman, Brown, Green and Longmans, 722 pages: <http://archive.org/details/historybarbados00schogoo>
- Siddal, M., Chappel, J., and Potter, E.-K., (2006), Eustatic Sea Level During Past Interglacials in *The Climate of Past Interglacials*, edited by F. Sirocko et al., Elsevier, Amsterdam , pp. 75-92
- Silver, E.A., J.E. Case, H.J. MacGillavry, (1975) Geophysical study of the Venezuelan borderland. *Geol. Soc. Amer. Bull.* 86: 213-226

- Skoglund, R.O. & Lauritzen, S.E.: (2010), Morphology and speleogenesis of Okshola (Fauske, northern Norway): example of a multi-stage network cave in a glacial landscape. *Norwegian Journal of Geology*, Vol. 90, pp 123-139. Trondheim ISSN 029-196X
- Smart, P. L., Beddows, P A., Coke J., Doerr, S., Smith, A., Whitaker, F., (2006), Cave Development on the Caribbean coast of the Yucatan Peninsula, Quintana Roo, Mexico, in Harmon, R. S., and Wicks, C., eds. *Perspectives on karst geomorphology ,hydrology, and geochemistry A Tribute volume to Derek C. Ford and William B. Whiter*: Geological Society of America Special paper 404, p. 105-128
- Southworth, C.S., (1985), Application of remote-sensing data, Eastern Yucatan. In: WC Ward AE Weidie and W Back (Eds.) *Geology and Hydrogeology of the Yucatan and Quaternary Geology of Northeastern Yucatan Peninsula*. New Orleans: New Orleans Geological Society Publication:12-19
- Speed, R.C., (1983), Structure of the accretionary complex of Barbados, I: Chalky Mount .*Geological Society of America Bulletin*, v. 94, p. 92-116
- Speed, R.C., (1990), Volume loss and defluidization history of Barbados. *Journal of Geophysical Research*, 95:8983-8996.
- Speed, R. C., (2012), *Geology and Geomorphology of Barbados*, eds. C. Speed and R. Sedlock, GSA Special Paper 491, 63p.
- Sprouse (2013), unpublished standards
- Stafford, K., Mylroie, J. E., Mylroie, J. R., Jenson, J. W. and Taborosi, D., (2004), Coves and Pocket Beaches, GSA 2004 Abstract
- Stafford, K. W., Mylroie, J. E., Mylroie, J. R., Jenson, J. W., Taborosi, D., (2006), Dissolution controls related to the Carbonate Island Karst Model on tectonically active carbonate islands: Tinian and Aguijan, Commonwealth of the Northern Mariana Islands, *Proceedings of The 12th Symposium on the Geology of the Bahamas and other Carbonate Regions*, Ed. R. L. Davis and D. Gamble, p 205-218
- Stefanic, M. J., and Cornell, S. R., (2011), A multiphase model for the formation of enigmatic coastal geomorphic features of NW Curaçao; A case study of bokas from Sheta Boka National Park: *Geological Society of America Abstracts with Programs*, v.43, p.251
- Stoessel, R. K., Y. H. Moore & J. G. Coke, 1993. The occurrence and effect of sulfide oxidation on coastal limestone dissolution in Yucatan cenotes. *Ground Wat.* 31: 566–575

- Strahler, A.N., (1952), Hypsometric (area-altitude) analysis of erosional topology.- Geological Society of America Bull., 63, 11, 1117-1142
- Strahler, A.N., (1957), Quantitative analysis of watershed geomorphology.- Transactions of the American Geophysical Journal, 8, 6, 913-920
- Szabo BJ, Ward WC, Weidie AE and Brady MJ (1978), Age and magnitude of the late Pleistocene sea-level rise on the eastern Yucatan Peninsula. *Geology*, 6:513-515
- Taboroši, D., Jenson, J.W. and Mylroie, J.E. (2004), Karren features in island karst: Guam, Mariana Islands: *Zeitschrift für Geomorphologie*. N.F. 48: 369-389
- Taboroši, D. and Kázmér, M., (2013) Erosional and depositional textures and structures in coastal karst landscapes. In Lace, M.J. and Mylroie, J. E., eds., *Coastal Karst Landforms*. Springer
- Taylor FW and Mann P (1991) Late Quaternary folding of coral reef terraces, Barbados. *Geology*, 19: 103-106
- Thomas C., (1999), Aspects hydrogéologiques du Yucatan (Mexique) [Hydrogeological aspects of the Yucatan, (Mexico)]. *Karstologia* 34(2): 9–22
- Tułańczyk, S.M., Perry, E.C., Duller, C.E. and Villasuso M., (1993), Influence of the Holbox fracture zone on the karst geomorphology and hydrogeology of northern Quintana Roo, Yucatan Peninsula, Mexico. In: Beck B (ed.) *Applied Karst Geology*: Rotterdam, Balkema: 181–188
- Vacher, H.L. and Mylroie, J.E., (2002), Eogenetic karst from the perspective of an equivalent porous medium: *Carbonates and Evaporites*, v. 17, p. 182-196
- Van Sambeek, M.H.G, Eggenkamp, H.G.M, Vissers, M.J.M., (2000), The Groundwater Quality of Aruba, Bonaire, and Curaçao, *Netherlands Journal of Geosciences* 79 (4): 459-466
- Verbovšek, T., (2007), Fractal analysis of the distribution of cave lengths in Slovenia, *ACTA CARSOLOGICA* 36/3, 369-377
- WALLS http://www.utexas.edu/tmm/sponsored_sites/tss/Walls/ Accessed January 2013.
- Wandelt B. (2000), Geomorphologische Detailkartierung und chronostratigraphische Gliederung der quaternären Korallenriffe auf Barbados (West Indies) unter besonderer Berücksichtigung des Karstformenschatzes. unpublished PhD. Thesis, University of Cologne, Germany
- Ward W.C. (1997), Geology of coastal islands, northeastern Yucatan Peninsula. In: Vacher, H. L and Quinn TM (eds.) *Geology and hydrogeology of carbonate islands*, Elsevier Science Publishers: 275-298

- Ward, W.C., (1985), Quaternary geology of northeastern Yucatan Peninsula, Part 2: In: Ward WC, Weidie AE and Back, W.(eds.) Geology and hydrogeology of the Yucatan and Quaternary geology of northeastern Yucatan Peninsula: New Orleans, Louisiana, New Orleans Geological Society: 23-53
- Ward W.C. and Brady M. (1979), Strandline sedimentation of carbonate grainstones, Upper Pleistocene, Yucatan Peninsula, Mexico: AAPG Bulletin 63:362-369
- Ward WC (2003), Saltwater Intrusion & Coastal Aquifer Conference (SWICA) Field Trip to the Caribbean Coast of the Yucatan Peninsula (April):13-22
- Waterstrat, W. J., Mylroie, J. E., Owen, A. M., and Mylroie, J. R., (2010), Coastal caves in Bahamian eolian calcarenites: Differentiating between sea caves and flank margin caves using quantitative morphology: Journal of Cave and Karst Studies, v.72, p.61-74
- Waterstrat, W., J.E. Mylroie, A.M. Owen, and J.R. Mylroie (2011), – Reply to Comments on: Coastal Caves in Bahamian Eolian Calcarenites: Differentiating Between Sea Caves and Flank Margin Caves Using Quantitative Morphology. Journal of Cave and Karst Studies, v. 73, no. 3, p. 203. DOI: 10.4311/2011ES0216
- Weidie, A.E., (1978), Lineaments of the Yucatan Peninsula and Fractures of the Central Quintana Roo Coast. In: Field Trip No. 10 – Yucatan, Road Log and Supplement to 1978 Guidebook, 1982 GSA Annual Meeting, New Orleans, Louisiana: 21-25
- Weidie, A.E., (1985) Geology of the Yucatan Platform, Part 1: in Ward, W.C., Weidie, A.E., and Back, W., eds., Geology and hydrogeology of the Yucatan and Quaternary geology of northeastern Yucatan Peninsula: New Orleans, Louisiana, New Orleans Geological Society:1-19
- Weistein, E. W., Mathworld: (2006) The Web's Most Extensive Mathematics Resource, <http://mathworld.wolfram.com/West>, B.J. and W. Deering, (1994), Fractal physiology for physicists: Levy statistics. Physics Reports 246:1-100
- Westermann, J.H. & J.I.S. Zonneveld (1956), Photo-geological observations and land capability & land use survey of the Island of Bonaire (Netherlands Antilles). Koninklijk Institut voor de Tropen, Amsterdam.
- White, W.B., White, E.L., (2000), Correlation of contemporary karst landforms with paleokarst landforms: the problem of scale. Carbonates and Evaporites 10, 131–137
- Williams, P.W., (1972), Morphometric analysis of polygonal karst in New Guinea Geological Society of America Bulletin 83, 761–796

Worthington S.R.H., Ford D.C. and Beddows P.A., (2000), Porosity and permeability enhancement in unconfined carbonate aquifers as a result of solution In A.B. Klimchouk, D.C. Ford, AN. Palmer & W. Dreybrodt (Eds.), *Speleogenesis: Evolution of Karst Aquifers.* ,Huntsville, AL: National Speleological Society, Inc., pp. 463-472

Zonneveld, J. I. S., Buissonje, P. H. d. and Herweijer, J. P., (1972). Geomorphology and denudation processes. In *Guide to the Field Excursions on Curaçao, Bonaire and Aruba, Netherlands Antilles.* Natuurwetenschappelijke Studiekring voor Suriname en de Nederlandse Antillen, pp. 59-69, Utrecht, The Netherlands.

APPENDIX A
DATA TABLES

Table A.1 Fractal Indices for flank margin caves

Cave	Location	Fractal Dimension	Lacunarity
Agua	PR-Mona	2.4117	1.0586
Basurero	PR-Mona	2.4102	2.3678
Chivo	Cuba	2.4440	3.2414
Dance Hall	Bahamas	2.2900	0.1583
Eight Mile Cave	Bahamas	2.3607	3.2567
Ericksons	PR-Mona	2.3685	0.2219
Esqueleto	PR-Mona	2.3892	0.4174
Frio	PR-Mona	2.3191	1.5797
Golden Grove	Barbados	2.2828	2.8344
Grande	Cuba	2.3994	1.0549
Hamilton's Cave	Bahamas	2.3698	2.7495
Hatchet Bay	Bahamas	2.3776	3.0594
Hato Cave	Curaçao	2.2840	2.6010
Hole-in-wall	Bahamas	2.4418	1.9719
Humboldt	Cuba	2.4189	1.6808
Jetchi	Curaçao	2.3326	1.5940
Lighthouse Cave	Bahamas	2.3537	1.7781
Murcielagos	PR-Mona	2.3996	2.2667
Negra	PR-Mona	2.4177	0.2608
Pictographias	Cuba	2.3291	2.0138
Pirata	PR-Mona	2.3642	2.3767
Pirata	Cuba	2.3391	3.2345
Quadaricki	Aruba	2.3442	1.9304
Raton	Curaçao	2.3171	3.2216
Salt Pond	Bahamas	2.3422	2.8307
Savonet	Curaçao	2.3191	0.8033
Sistema Faro	PR-Mona	2.4598	1.2644
Sopressa	PR-Mona	2.3151	1.0315
Speolonk	Bonaire	2.3275	1.9744
Ten Bay	Bahamas	2.3672	1.5267

Table A.2 Fractal Indices for continental hypogene caves

Cave	Location	Fractal Dimension	Lacunarity
Bethlehem	SD	2.4198	0.6402
Breezeway	CO	2.3754	1.1124
Carlsbad	NM	2.7208	0.6601
Cave of Winds	CO	2.3162	1.5010
Coffee Cave	NM	2.4434	1.8423
Dry Cave	NM	2.5118	0.9306
Endless	NM	2.4557	1.5537
Fairy	CO	2.5278	1.8008
Fixin-to-Die	CO	2.4193	1.2421
Frassisi Caves	Italy	2.3751	1.1189
Groaning	CO	2.3201	1.3600
Hubbards	CO	2.3499	0.8980
Huccacove	CO	2.3792	1.7961
Jewel	SD	2.7227	0.4371
Lechuguilla	NM	2.7536	0.7064
Lehman Cave	NV	2.3249	1.5611
Manitou	CO	2.3112	1.3878
McKittrick	NM	2.3345	1.2343
Narrows	CO	2.3382	1.8830
Pedros	CO	2.3982	1.8830
Porcupine	SD	2.3953	1.2434
Premonition	CO	2.2877	2.6254
Sand Cave	NM	2.3698	0.7445
Sand Cave (SD)	SD	2.3046	1.1222
Slaughter Canyon	NM	2.3984	0.8244
Spider	NM	2.4160	0.5096
Three Fingers Cave	NM	2.4217	0.6218
Toca Da Boa Vista	Brazil	2.5608	0.7389
Wind Cave	SD	2.7488	0.6628
Yellowjacket	NM	2.4238	1.9346

Table A.3 Fractal Indices for allogenic stream caves

Cave	Location	Fractal Dimension	Lacunarity
Barrel Cave	AL	2.2196	4.7921
Blue Spring	TN	2.2530	5.9179
Butrams	KY	2.2249	4.8925
Cedar Spring Saltpeter	KY	2.1889	3.1736
Coldwater	IA	2.2132	4.7610
Coles	Barbados	2.1067	1.8161
Crumps	KY	2.2608	6.5036
Diamond Caverns	KY	2.1139	2.1031
Dossey Domes	KY	2.2084	4.6613
Encantado	Puerto Rico	2.2683	7.5389
Fern Cave	AL	2.2620	7.4409
Frenchmans Knob	KY	2.1741	2.6781
GuessWhat Cave	AL	2.2086	4.6926
Harrisons Cave	Barbados	2.1579	2.5045
Hidden River	CO	2.2469	5.8743
Mutters	KY	2.1129	1.9297
NanDong	China	2.2013	3.7915
Neals Cave	KY	2.1500	2.4032
Sides Cave	KY	2.2584	5.9563
Smith Valley	KY	2.2970	9.1274
Snakedance	TN	2.2685	7.5574
Sorbettos	Puerto Rico	2.2360	5.7372
Stans Wells	KY	2.2082	4.3173
State Trooper Cave	KY	2.1778	3.0433
Tumbling Rock	AL	2.2979	11.9724
Twenty Pound Tick	CO	2.1606	2.5106
Springhead	Barbados	2.1476	2.5198
Viento	Puerto Rico	2.2065	4.1295
Wanwayan	China	2.2000	3.3625
Whigpistle Cave	KY	2.2319	5.1906

Table A.4 Fractal indices for littoral caves

Cave	Location	Fractal Dimension	Lacunarity
Birdtracks Cave	CA	2.0344	0.5959
Breathing Cave	CA	2.1132	0.8899
Cave BB	Bahamas	2.0692	1.1160
Hidden Canyon	CA	2.0363	1.3378
Hidden Canyon Tunnel	CA	2.0955	1.4236
Hidden Room	CA	2.0960	1.1320
Kangas Cave	CA	2.1997	1.2517
Kelp Trap	CA	2.0893	0.9396
Kiwi Cave	CA	2.0510	0.2117
Little Kiwi Cave	CA	2.0273	1.2662
Little Scorpion Cave	CA	2.0315	0.9412
Little T Cave	CA	2.0593	0.3415
Midden Point Cave	CA	2.0743	1.2575
Painted Cave	CA	2.1312	0.2963
Sea Cave A	Bahamas	2.0400	1.2160
Sea Cave A2	Bahamas	2.0224	1.3067
Sea Cave AA	Bahamas	2.1154	1.1190
Sea Cave BB	Bahamas	2.0124	0.6161
Sea Cave CC	Bahamas	2.0504	0.7681
Sea Cave DD	Bahamas	2.0341	1.2970
Sea Cave EE2	Bahamas	2.0578	1.3341
Sea Cave G	Bahamas	2.0365	1.2331
Sea Cave G52	Bahamas	2.1792	1.2916
Sea Cave H	Bahamas	2.0893	1.3579
Sea Cave I	Bahamas	2.0859	1.0282
Sea Cave K	Bahamas	2.0804	0.7685
Sea Cave O	Bahamas	2.0500	0.6183
Sea Cave P	Bahamas	2.0725	0.9316
Sea Cave U	Bahamas	2.1190	0.9733
Sharks Teeth Cave	CA	2.0985	0.3017

Table A.5 Fractal indices for tafoni

Cave	Location	Fractal Dimension	Lacunarity
Pita Cave A	Bahamas	2.0147	Lacunarity
Tafone AP	Bahamas	2.0600	0.2158
Tafone BP	Bahamas	2.0095	0.2503
Tafone C	Bahamas	2.0153	0.3302
Tafone C11	Bahamas	2.0212	0.2479
Tafone C12	Bahamas	2.0331	0.2683
Tafone D	Bahamas	2.0009	0.2467
Tafone DP	Bahamas	2.0033	0.3392
Tafone E	Bahamas	2.0060	0.2567
Tafone EP	Bahamas	2.0211	0.2332
Tafone F	Bahamas	2.0000	0.6321
Tafone FP	Bahamas	2.0012	0.2764
Tafone G	Bahamas	2.0001	0.2232
Tafone H	Bahamas	2.0112	0.2681
Tafone HP	Bahamas	2.0266	0.2272
Tafone NP	Bahamas	2.0000	0.3132
Tafone P	Bahamas	2.0036	0.1119
Tafone Q	Bahamas	2.0478	0.2000
Tafone R	Bahamas	2.0091	0.2391
Tafone S2	Bahamas	2.0329	0.2870
Tafone S1	Bahamas	2.0072	0.2262
Tafone T1&2	Bahamas	2.0001	0.2694
Tafone T3	Bahamas	2.0012	0.2352
Tafone U	Bahamas	2.0291	0.2122
Tafone V	Bahamas	2.0001	0.2219
Tafone W	Bahamas	2.0329	0.3178
Tafone X	Bahamas	2.0653	0.2339
Tafone Y	Bahamas	2.0101	0.2771
Tafone Z	Bahamas	2.0793	0.2179
The Crevice	Bahamas	2.0046	0.2617

Table A.6 Morphometric data for bokas of Aruba

Boka	BMI	Length meters	Width meters	Width meters	Vertical Extent meters	Slope	Azimuth degrees	*	**
Aruba 5	3.69	27	36	13	4	0.15	51		L
Aruba 10	3.28	26	16	3	2	0.08	41		L
Aruba 20	2.82	31	35	11	3	0.10	56		L
Aruba 26	2.14	30	33	17	3	0.10	31		L
Aruba 22	1.85	22	23	13	5	0.23	37		L
Aruba 13	1.67	117	37	7	3	0.03	46		L
Yup	1.63	108	101	58	9	0.08	36		L
Aruba 25	1.61	35	30	16	5	0.14	39		L
Chiquito 2	1.58	83	38	11	7	0.08	46		L
Aruba 28	1.55	103	102	65	5	0.05	42		L
Aruba 21	1.51	52	64	52	7	0.13	44		L
Aruba 19	1.32	21	19	13	4	0.19	63		L
Aruba 1	1.31	48	52	43	4	0.08	39		L
Keto N	1.26	109	104	79	7	0.06	41	F	L
Aruba 12	1.20	63	23	7	10	0.16	31	F	L
Natural Bridge	1.17	120	58	24	6	0.05	40	F	L
Aruba 7	1.13	110	37	11	5	0.05	71	F	L
Prins N	1.13	144	121	90	8	0.06	77	F	L
Curi	1.02	102	42	17	2	0.02	58	F	L
Daimara	1.02	187	142	106	4	0.02	54	F	L
Aruba 16	1.00	85	32	12	6	0.07	70	F	L
Aruba 3	0.94	137	30	7	7	0.05	50	F	L
di Pove di Noord	0.94	233	127	74	4	0.02	48	F	L
Dos Playa S	0.88	212	139	104	8	0.04	72	F	L
Hidden	0.80	47	15	6	9	0.19	40	F	L
Aruba 23	0.76	89	61	55	6	0.07	42	F	L
Dos Playa N	0.73	177	91	64	8	0.05	85	F	L
Aruba 4	0.72	110	51	33	6	0.05	37	F	L
Aruba 27	0.69	53	21	12	4	0.08	48	F	L
Aruba 15	0.68	182	40	13	7	0.04	80	F	L
Keto S	0.66	114	75	75	1	0.01	45	F	L
Mahoe	0.61	175	107	107	7	0.04	37	F	L
Prins S	0.60	195	87	65	7	0.04	47	F	L
Chiquito	0.54	99	35	23	6	0.06	41	F	L
Grande	0.43	46	16	13	6	0.13	70	F	

*F: Fluvial ** L: Littoral, No units for BMI

Table A.7 Morphometric data for bokas of Bonaire

Boka	BMI	Length meters	Width max meters	Width Min meters	Vertical Extent meters	Slope	Azimuth degrees	*	**
Onima N 2	3.02	39	36	11	2	0.05	35		L
Onima N	2.68	68	74	30	6	0.09	26		L
Malmut	2.66	26	22	7	5	0.19	1		L
Spelonk	2.20	80	75	32	3	0.04	23		L
Kokolishi	1.86	108	94	44	7	0.06	52		L
Kanoa	1.74	47	35	15	3	0.06	51		L
Onima	1.54	165	108	46	7	0.04	30		L
East Coast	1.33	36	24	12	2	0.06	90		L
Chikitu	1.14	207	46	9	8	0.04	58	F	L
Washikemba S	0.65	280	75	31	2	0.01	87	F	L
*F: Fluvial **L: Littoral. No units for BMI									

Table A.8 Morphometric data for bokas of Curaçao

Boka	BMI	Length meters	Width Max meters	Width Min meters	Vertical meters	Slope	Azimuth Degrees	*	**
Bergantinbai 2	4.41	66	80	22	7	0.11	92		L
Bergantinbai 1	3.96	32	45	16	8	0.25	90		L
Micro	3.42	50	37	8	7	0.14	60		L
Pistol	1.81	31	15	4	5	0.16	40		L
Labadero S	1.80	29	27	14	4	0.14	31		L
Santa Pretu	1.72	110	55	16	7	0.06	89		L
Playa	1.60	80	61	29	9	0.11	30		L
Micro N	1.44	20	12	5	6	0.30	47		L
Labadero	1.39	69	31	10	5	0.07	32		L
Labadero N	1.31	67	35	14	5	0.07	32		L
Ascension	0.90	752	236	82	6	0.01	63	F	L
Double	0.80	109	82	77	4	0.04	90	F	L
Bergantinbair	0.65	148	47	23	7	0.05	90	F	L
Wandomi	0.59	157	36	14	5	0.03	22	F	L
Plate S	0.50	52	19	14	7	0.13	34	F	L
Kalki	0.48	286	60	26	8	0.03	38	F	
Playa Grande	0.46	654	230	177	12	0.02	88	F	
Kortalein	0.46	198	38	16	11	0.06	37	F	
Un	0.45	185	34	14	10	0.05	35	F	
Braun	0.44	190	40	19	12	0.06	29	F	
Mansalina	0.43	265	37	12	12	0.05	37	F	
Djegu	0.43	238	32	10	12	0.05	37	F	
Bartolbair	0.42	620	184	130	10	0.02	70	F	
Plate	0.35	144	20	8	12	0.08	35	F	
Tabla	0.27	166	20	9	11	0.07	37	F	
Dos	0.27	202	22	9	12	0.06	30	F	

*F: Fluvial **L: Littoral. No units for BMI

Table A.9 Morphometric data for caletas

Caleta	Caleta morphology	Ents	Length meters	Azimuth Length	Widest meters	Azimuth width
1	large bay		143	114	189	32
2	bay + cenote		30	139	27	43
3	small bay		55	137	58	54
5	long-linear bay		80	147	20	62
6	beach		47	132	76	41
7	long-linear bay		34	27	11	107
8	long-linear bay		59	133	9	48
10	small bay		80	112	108	32
16	small bay		47	120	99	24
17	beach		53	123	41	39
Abejas	bay + cenote	1	30	147	47	59
Chacalal	bay + cenote	2	171	125	137	46
Cubera	large bay		103	140	67	54
Manati	long-linear bay	1	127	120	9	211
Nonec	bay + cenote		34	139	70	54
Pulpo	beach		726	121	939	30
Rio Xcaret	long-linear bay		126	153	42	49
Sandtrap1	bay + cenote		17	110	18	200
Sandtrap2	bay + cenote		28	115	53	208
Sandtrap3	bay + cenote		33	126	37	215
Sandtrap4	bay + cenote		18	121	22	200
Tankah	large bay		394	118	367	210
Under-the-Bridge	bay + cenote		42	135	22	66
Valet	long-linear bay	1	225	192	193	108
Xaac	large bay		230	127	198	217
Xel Ha	long-linear bay	9	708	137	102	233
Xpu-Ha	long-linear bay		297	131	151	258
Yal Ku	large bay	1	338	127	206	172
Dos Pisos	beach	2	115	123	41	37
Yal Ku Chica	large bay	1	161	109	39	216

APPENDIX B
CAVE MAPPING STANDARDS

B.1 Quintana Roo Cave Mapping Project Standards

Compiled by Peter Sprouse

The goal of this project is to produce detailed, accurate cave maps of dry caves in Quintana Roo using methods that can facilitate integration of maps between various groups. This can involve resurveying, but our goal should always be to make ours the last survey that will ever be needed.

Record only the instrument and tape readings. Don't write down LRUD distances, as they are not utilized. Concentrate instead on sketching to scale and orientation. Use of a protractor and ruler is imperative. Sketching scale is 1/8"=1m.

List station names completely (i.e. "AB123"), and on a single line. Split line data can produce errors in interpretation. Instrument back sight readings are desired. Use a slash to indicate foresight/back sight (i.e., 171/351)

Sketch complete floor detail; there is a symbol for everything so there is no excuse for blank space between passage walls. Blacken in the interior of columns in sketches so that they can be distinguished easily. There is need for floor detail outside the dripline in the collapses as remote sensing imagery will be used for that. Sketch the outline, or depression contour, of the sinkhole collapses. Sketch cross sections in addition to the plan view, and profiles of main passages and entrance passages. Because Quintana Roo caves are mazy, try to survey areas thoroughly as they are traversed. Don't shoot past any junctions, place a station at each one. There are many entrances in these systems, try to give a name to each one.

Number and mark all stations on the rock with marker and with labeled flagging, and try to place them on the wall, ceiling, or big boulders. Stations on the floor will get

trampled. Rather than picking a station prefix randomly, get one from the Walls data manager. Examine the line plot and working map of assigned areas. Give it to a team member and have them locate all existing stations in order to facilitate tie-ins. Don't resurvey any passages, always tie in to the nearest station. The pdf files of existing cave maps and survey note copies can be uploaded to smartphones and used as guides during the survey and for route finding.

B.2 Cave Research Foundation Survey Standards

1. Each day the survey team will calibrate the instruments on the compass calibration course.
2. Survey stations will be marked with flagging tape – stations labels will be written on the tape with a sharpie
3. Back sites will be taken at each survey station. In situations where it is not possible to take a back site, double front sites will be acceptable. Front and back sites should agree within plus or minus 2 degrees for compass and one degree for inclinometer. Readings should be read to the nearest half degree.
4. Taped distances are read to the nearest tenth of a foot or meter.
5. Each set of survey notes will have a cover page which includes the following information:
 - a. Date of survey
 - b. Name of surveyors and survey duties
 - c. Compass Calibration information

7. After the survey trip also include:
 - a. Survey designations and tie-ins used
 - b. Total surveyed passage
 - c. Label each page with page number in the form of page X of total# of pages.
 - d. Sketchers name, cave and survey date should be noted on each page.
8. Data sheets should be filled out neatly and legibly. If the data sheets are not pre-printed, clearly label each data column. Always use a + or – in each of the inclination readings. Always write the distances out to one decimal place.
9. A north arrow and bar scale will be included on every sketch page.
10. Sketches should be plotted with a protractor and ruler to scale at 20 feet/inch unless otherwise noted by instructor.
11. Survey stations should be clearly marked with a dark dot or triangle. Label the station outside of the passage sketch.
12. Sketches should be done in plan and profile view with cross sections at every station. Location of cross sections should be noted as well as direction of view.
13. Sketches should be done with enough detail to show the significant features of the passage.
14. Passage dimensions should be either estimated (if passage is less than 80 feet wide) and measured if the passage is greater than 80 feet wide. If you can't tell how wide the passage is, then measure the dimensions. All dimensions should be determined facing up-survey.
15. SAFETY FIRST! CAVE SOFTLY. All cave surveying should be done in as careful a manner as possible as to not negatively impact cave passages. Survey stations should be labeled discretely and if at all possible placed on natural, easily identifiable features

(though they should NOT be put on speleothems.) The survey team should try to minimize the footprints that they make while mapping the cave passage.